UNIVERSIDAD DE MÁLAGA
Departamento de Química Analítica

Ion and Photon Emission in Laser Ablation Processes of Energetic Materials in Condensed Phase

TESIS DOCTORAL

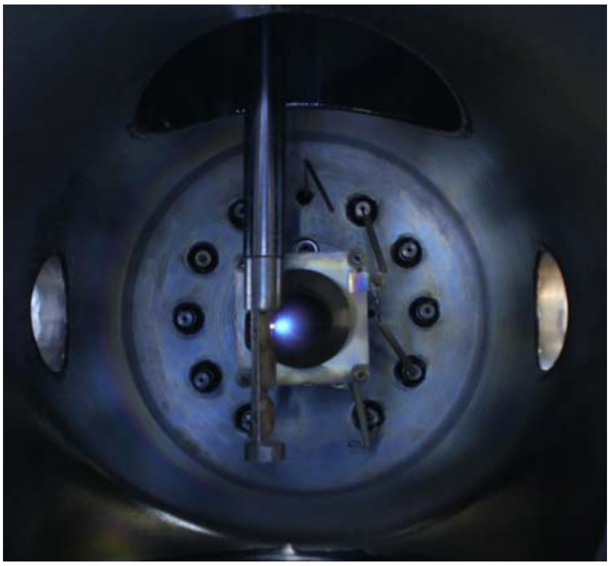

Tomás Delgado Pérez

Málaga, 2013

AUTOR: Tomás Delgado Pérez

http://orcid.org/0000-0003-2034-2844

EDITA: Publicaciones y Divulgación Científica. Universidad de Málaga

UNIVERSIDAD DE MÁLAGA

DEPARTAMENTO DE QUÍMICA ANALÍTICA

UNIVERSIDAD
DE MÁLAGA

Ion and Photon Emission in Laser Ablation Processes of Energetic Materials in Condensed Phase

TESIS DOCTORAL

Tomás Delgado Pérez

Málaga, 2013

Ion and Photon Emission in Laser Ablation Processes of Energetic Materials in Condensed Phase

por

Tomás Delgado Pérez

José Javier Laserna Vázquez
Catedrático de Química Analítica
Universidad de Málaga

José Miguel Vadillo Pérez
Profesor Titular de Química Analítica
Universidad de Málaga

Memoria presentada para optar al grado de Doctor en Ciencias (Químicas)

Tomás Delgado Pérez

Málaga, 22 de mayo de 2013

José Javier Laserna Vázquez, Catedrático de Química Analítica de la Universidad de Málaga y **José Miguel Vadillo Pérez**, Profesor Titular de Química Analítica de la Universidad de Málaga,

CERTIFICAN

Que el presente trabajo titulado **Ion and Photon Emission in Laser Ablation Processes of Energetic Materials in Condensed Phase** ha sido realizado por Don **Tomás Delgado Pérez** en los laboratorios del Departamento de Química Analítica bajo nuestra dirección, reuniendo a nuestro juicio los requisitos necesarios para optar al grado de Doctor en Ciencias (Químicas), por lo que autorizamos su presentación.

Málaga, 22 de mayo de 2013

Javier Laserna

Agradecimientos

En primer lugar quería agradecer al Laboratorio Láser de la Universidad de Málaga (UMA) el haberme dado la oportunidad de desarrollar este trabajo de investigación en sus instalaciones y contar con los medios necesarios y el soporte de los profesionales que lo conforman, hoy además grandes compañeros. Especialmente quiero agradecer a Javier Laserna y a José Miguel Vadillo su implicación y la gran ayuda que me han prestado durante la investigación llevada a cabo como directores de tesis.

Mención especial a la Consejería de Innovación, Ciencia y Empresa de la Junta de Andalucía, dentro del Proyecto de Excelencia “Análisis de discriminación forense y confirmación de explosivos mediante técnicas espectrométricas de excitación focalizada” al que ha estado vinculado este doctorado y que ha permitido su financiación.

Durante el desarrollo de esta tesis doctoral, más allá de las personas que han dirigido formalmente mi investigación, he tenido la ocasión de trabajar cerca de muchas otras personas como ya he comentado, y a ellas quiero también mostrar aquí un sincero agradecimiento. Son muchos los compañeros con los que he compartido tiempo en el laboratorio y ratos de ocio fuera de él. Los comienzos no son fáciles, y por ello quiero agradecer a Jose y Helena el haberme acompañado en esos primeros pasos como investigador. Querría agradecer también a mis vecinos de laboratorio Fran y Salva su amistad, el estar siempre dispuestos a echarme una mano cualificada y compartir conmigo muchas e interesantes conversaciones, ya fueran de ciencia o no tan científicas. Asimismo, quería agradecer la espontaneidad y los buenos ratos que hemos compartido a los caseteros Jorge e Inma. A Diana, siempre servicial y atenta conmigo. Y en esta etapa final, gracias a Marina y a Irene, con la que he redescubierto el café y el interés por la física, y gracias a Patricia, por sus palabras de ánimo y sus buenos consejos. Un lugar especial debo reservar a Xavi, al que tengo un gran aprecio como persona e investigador y al que agradezco su valiosa ayuda; y a Ángel, cuya filosofía de vida me ha aportado una gran sabiduría vital y cuya visión científica siempre ha hecho replantearme mis conclusiones, suponiendo una mejora continua en el trabajo diario.

No querría olvidar a todas aquellas personas dentro del grupo que de una manera u otra han seguido de cerca mi evolución y se han preocupado por guiarme en el camino correcto, además de mis tutores. Para Mari Carmen, Luisa, Carmen y Javier Ruiz, vaya este agradecimiento.

Por supuesto, debo estar muy agradecido a aquellas personas que durante todos estos años en mi vida cotidiana me han demostrado su cariño y me han dado ánimo en todo momento, y que me ayudaron a desconectar de la intensidad del laboratorio. Para mis buenos amigos portuenses y malagueños vayan estas palabras. Y como no podía ser de otra forma, el hueco más grande y especial lo guardo para mi familia. Gran parte del mérito se lo otorgo a mis padres, a mis hermanos y a mis hermanas, por confiar en mí. A mis suegros y mi cuñada Sandra, por estar siempre ahí.

A todos nuevamente gracias por la calidad humana que me habéis demostrado.

Sin embargo, en el fondo sé que este trabajo se lo debo íntegramente a Azahara. Estuviste siempre unida a mí en los momentos bajos. Gracias por la empatía, la paciencia y el amor que has demostrado, por ser mi mejor amiga, mi mayor crítica, mi gran confidente y compañera, y por enseñarme a buscar el cristal adecuado con el que mirar las cosas en cada ocasión.

“Verba volant scripta manent”

Caio Titus

Contents

Objectives

The study about ionization and fragmentation processes of organic energetic materials by means of laser ionization time-of-flight mass spectrometry was proposed with the objectives listed below:

- To design an ionization system by laser excitation with a fine control of the energetic and extraction conditions of ionic species that allows a suitable desorption and ionization of the organic compound of interest.
- To achieve a better understanding about the energetic channels taking place during the ions formation in the energetic desorption regime and, therefore, to obtain an improvement in both the comprehension of phenomena governing the acquired signal and the analytical quality of the technique.
- To find out the ionization thresholds of ionic species and to study the kinetics of fragmentation followed by the molecules up to the complete atomization.
- To obtain a *modulated* mass spectrum in order to acquire both useful molecular information for identification purposes and, on the other hand, atomic information that lead to fundamental aspects related to the dynamics of the fragmentation process.
- To assess the analytical capabilities of the technique for forensic identification by generation of LIMS spectral library in order to discriminate organic compounds of different nature.

Simultaneous studies about emission from laser-induced plasma by LIBS and generated ions by LIMS over solid-phase organic nitro aromatic explosives are suggested with the objectives listed below:

- To design a system allowing simultaneous ion/photon detection from species in the expanding plume at ultra-high vacuum environment over solid-phase high energetic compounds obtaining reproducible signals with analytical quality.
- To establish the adequate experimental conditions and ablation regime capable of generating a plume containing significant amount of excited atomic and diatomic species to be detected by optical emission spectroscopy without excessive bond breaking that may compromise the mass spectrometry detection of large molecular fragments.
- To carry out time- and spatially-resolved studies of the identified emission species while the ions are simultaneously extracted to a time-of-flight mass spectrometer.
- To detect differences in behaviour under laser ablation processes for TNT and its precursors (DNT and MNT): molecules with similar structures but very different physical properties.
- To know the kinetic behaviour for atomic and molecular species of interest present in the plasma during its generation, expansion and extinction, monitoring the changes with time-resolved LIBS.
- To evaluate the advantages of performing this type of analysis using both techniques at a time and the complementarity of information granted for such analytical signals.

The direct analysis of three dinitrotoluene isomers by LIMS and both high vacuum LIBS and atmospheric LIBS techniques over solid-phase samples are proposed with the following objectives:

- To prove the capabilities of laser-plasma based techniques as LIMS and LIBS for isomers identification.
- To find out experimental conditions for which the collected information allows the discrimination between isomers.
- To establish discrimination criteria on the basis of signal intensity ratios resulting from acquired spectra in the appropriate energetic regime.

The analysis of laser-induced plasmas of high energetic nitro compounds by optical emission spectroscopy at different atmospheric conditions is suggested, pursuing the following aims:

- To understand the fundamental chemical processes involved in the laser-induced breakdown of high energetic nitro compounds using optical emission spectroscopy.
- To assess the influence of the surrounding ambient on the kinetics and generation pathways of excited atomic and molecular species in the plasma plume using different energetic and pressure regimes.
- To use mass spectrometry as a support for LIBS spectra interpretation, verifying the simultaneous presence of species of interest.
- To propose possible and preferential reactions in the fragmentation pathways of the analyzed nitro explosives based on spectral features for different experimental conditions.

A controlled pressure level experiment with LIBS over organic aromatic compounds is brought up with the goals present below:

- To explore the influence of pressure level on the kinetics of excited atomic, ionic and molecular species in the plasma plume.
- To perform temporal and spatially resolved spectroscopy in order to study the characteristics of laser-induced plasma and to have a better knowledge of plasma expansion dynamics.
- To understand the way in that air pressure affects the kinetics of different excited species characteristics of organic aromatic compounds inside the generated plasma.
- To find out the pressure conditions for which the spectral features of organic compounds become enhanced.

The analysis of laser-induced plasmas of selected high energetic organic molecules into different gas environments was suggested with the following purposes:

- To evaluate the way that the molecules in buffer gas contributed to the emission signal intensities in the time-integrated LIBS spectrum in order to identify the main formation channels of excited atomic species and molecular fragments during the laser ionization process.

- To assess possible variations of the chemistry of the plume depending on both the nature of buffer gas interacting with generated plasma and pressure level inside the ionization chamber for the same ablated sample.

Resumen

Los procesos implicados en la interacción láser-materia son de gran complejidad y se encuentran interrelacionados, por lo que para llegar a una aproximación real y a una total compresión de los fenómenos involucrados se requiere de un estudio multidisciplinar profundo asistido por técnicas de análisis de superficie, principalmente por técnicas analíticas espectroscópicas. Estos mecanismos físico-químicos que tienen lugar en la interacción del haz láser con el sólido dependerán de aquellos parámetros relacionados con la radiación láser, como son la densidad de energía, longitud de onda, duración del pulso, etc., y de las propiedades físicas del material (ópticas, mecánicas y de tipo termodinámico). Los mecanismos han sido estudiados en profundidad a lo largo de los años, pero aún no han sido íntegramente razonados ni modelados por completo.

La interacción láser-materia es un fenómeno fundamentalmente basado en procesos térmicos y fotoquímicos. Como consecuencia de la incidencia del láser, y dependiendo de la dosis final de energía recogida por el material, se llevarán a cabo diferentes procesos a nivel tanto microscópico como macroscópico. Mientras que a irradiancias relativamente bajas los procesos dominantes, y que tienen lugar de forma secuencial, son el calentamiento y fusión del material, seguido de una suave desorción y una posterior ionización de las partículas, a irradiancias elevadas dominan los procesos de evaporación súbita del material y una eyección del material que derivan en la formación final de un plasma o gas ionizado de elevada temperatura cuya *nube* o *pluma* se expande a gran velocidad en el espacio.

El comienzo o umbral de la eyección masiva de material, acuñado con el término *ablación* de forma generalizada, se puede definir como la densidad de energía crítica suficiente para el sobrecalentamiento de la capa superficial hasta el límite de su estabilidad termodinámica. El hecho de que los procesos de interacción que conllevan a la ablación sean tan dependientes de la naturaleza de la muestra hace que la formación del plasma en el caso de los compuestos de naturaleza orgánica sea mucho más compleja que en el caso de metales u otro tipo de materiales inorgánicos. En el caso de compuestos orgánicos, su ablación y posterior formación del plasma suponen una serie de procesos de fragmentación molecular y recombinación no existentes en metales, que dependerán de forma sustancial de la duración del pulso láser y de la densidad total de energía depositada en dicha superficie.

Por todo lo dicho, el modelado del proceso de ablación implica el estudio de una serie de eventos clasificados en dos etapas: por un lado el calentamiento de la muestra por la interacción inicial con el pulso láser, y a continuación, la formación del plasma con su consiguiente expansión en el medio. También habrá que tener en cuenta el efecto de atenuación por *apantallamiento* o *shielding* que tiene lugar una vez que el plasma ha sido formado y se está expandiendo, debido a la absorción de la radiación láser incidente por parte del propio plasma.

La aplicación de la ablación láser para fines analíticos ha sido amplia en los estudios de materiales inorgánicos, incluyendo metales, semiconductores o incluso cerámicos. No cabe duda de que los láseres constituyen una fuente de alta energía muy versátil para llevar a cabo procesos de atomización, excitación e ionización del material ablacionado, y además sus parámetros de operación pueden ser fácilmente controlados. Sin embargo, su aplicación en el análisis de materiales orgánicos es aún un campo bastante inexplorado. No obstante, los progresos conseguidos en el conocimiento del proceso de ablación y las mejoras en la aplicación de métodos espectroscópicos han llevado a la reciente publicación de trabajos acerca de la ablación y caracterización de materiales orgánicos mediante láser. En el caso de la espectroscopía de plasmas inducidos por láser, las mejoras obtenidas han permitido la aplicación de esta técnica prometedora en aplicaciones orgánicas como caracterización de plásticos, aplicación en defensa nacional en la detección de explosivos y minas, aplicación forense con identificación de cantidades traza de residuos orgánicos, salud pública en la detección de sustancia tóxicas y contaminantes orgánicos en el ambiente. Incluso se ha podido analizar material biológico, a pesar de la dificultad que supone el muestreo a escala submicrométrica. Finalmente, hay que destacar los estudios llevados a cabo en los últimos años sobre caracterizaciones espectroscópicas de la dinámica y cinética de expansión del plasma.

En casos específicos, como es el del análisis por espectrometría de masas a fluencias por encima del umbral de formación de plasma, o el de la deposición pulsada por láser (PLD), la ablación es llevada a cabo a vacío en atmósferas inertes debido a requerimientos operacionales, factor que previene la interacción del material ablacionado con las especies procedentes del gas ambiental. Y es que la naturaleza del gas de fondo que está en contacto con la muestra irradiada, así como el nivel de presión en dicho medio gaseoso, juegan un papel decisivo en la formación y dinámica de expansión del plasma. Cuando la ablación láser se lleva a cabo en entornos de presión reducida o en presencia de gases diferentes al aire ambiental, las tasas de ablación del material se ven también directamente afectadas.

El creciente interés en el análisis de plasmas inducidos en condiciones atmosféricas distintas a las terrestres está basado en su aplicación a la exploración espacial, ya que las características de emisión de dichos plasmas se ven mejoradas cuando éstos son generados a presiones por debajo de la atmosférica y el tiempo de vida de las especies iónicas es mayor. Estas mejoras son observables en términos de mayor intensidad de las señales y mejor relación señal/ruido, así como una reducción considerable de la intensidad de base o fondo. Esto es debido a que el plasma se expande en un medio menos denso, que reduce el efecto de apantallamiento del propio plasma frente a la radiación incidente y por tanto da lugar a un aumento de la ablación de la muestra. Además, la presión reducida hace que la duración del plasma se vea incrementada ya que el enfriamiento del plasma mediante transferencia de energía hacia un entorno menos denso sea más lento. De esta forma, se han llevado a cabo numerosos estudios acerca de los efectos que la composición del medio atmosférico tiene sobre los parámetros físicos de la pluma, las características de la emisión resultante, así como en las tasas de ablación que se obtienen en cada caso. Las propiedades físicas del gas de fondo, tales como su densidad o su conductividad térmica, juegan un papel crucial en la ablación láser y las cinéticas de formación y expansión del plasma.

Como ya se ha mencionado, los plasmas generados por la acción de fuentes láser u otro tipo de fuente de excitación se pueden caracterizar por técnicas analíticas espectroscópicas, especialmente por métodos ópticos. Entre ellos, la espectroscopía de emisión se define como un método analítico basado en la luz emitida por las especies excitadas en una llama, en un plasma, en un arco eléctrico o una chispa, generados mediante un estímulo eléctrico o térmico. Por consiguiente, las especies son creadas y luego analizadas en un medio gaseoso de alta energía que constituye una fuente de vaporización-atomización-ionización-excitación del material.

En el trabajo desarrollado y descrito en la presente memoria se ha empleado como herramienta para el análisis de los plasmas inducidos por una fuente láser la técnica de espectroscopía de emisión *Laser-Induced Breakdown Spectroscopy* (LIBS), que tiene una gran aplicación en la detección e identificación de todo tipo de materiales. Dicha técnica se basa en la generación de microplasmas de elevada temperatura como consecuencia de la incidencia de un pulso láser intenso de muy corta duración sobre la superficie del material y la consecuente ablación de una pequeña cantidad de dicha muestra. El plasma se expande rápidamente a velocidades mayores a la del sonido y las especies excitadas constituyentes de la muestra generan emisiones ópticas características en su relajación a estados de menor energía. La luz emitida por el plasma es recogida mediante sistemas ópticos de colección y detección y la composición elemental de la muestra puede ser determinada de forma directa a partir de estas emisiones representativas de su composición. Este factor hace de LIBS una potente herramienta analítica para la discriminación elemental. Asimismo, LIBS posee una notable versatilidad y sencillez, además de una serie de ventajas adicionales que la hacen ideal para un amplio rango de aplicaciones donde se persiga encontrar de manera rápida y a tiempo real la composición química elemental de materiales de distinta naturaleza y en diferentes condiciones atmosféricas.

Por tanto, los procesos implicados en la ablación del material, en la formación del plasma y finalmente en el análisis composicional de dicho plasma definen el escenario en el que LIBS se desarrolla. Desde el punto de vista del principio básico de la técnica, la investigación de todos los fenómenos relacionados directamente con la generación del plasma y su evolución debe seguir avanzando para que la técnica pueda seguir evolucionando en prestaciones y ampliando el rango de aplicaciones.

El análisis de compuestos orgánicos por espectroscopía de emisión tiene ciertas desventajas si se compara con muestras de naturaleza inorgánica. Las interferencias que tienen lugar debido a la interacción del material ablacionado en la pluma con la atmósfera del entorno son significativas y deben ser tenidas muy en cuenta. Además, las tasas de ablación son superiores en la mayoría de los casos para estos compuestos, y a veces requieren de una preparación previa para transformarlos a un formato de análisis más adecuado a la técnica.

El principal desafío en el análisis de compuestos orgánicos o de naturaleza biológica mediante espectrometría de emisión radica en el hecho de que éstos están formados por las mismas especies elementales (C, O, N y H), y las emisiones correspondientes a estos elementos básicos están siempre presentes, proporcionando una base común en la mayoría de los materiales orgánicos. Además, a partir de los procesos de fragmentación y recombinación en la pluma se forman especies di-atómicas, que son detectadas como bandas espectrales de emisión. Las principales especies moleculares que se forman son CN y C_2, además de otras como OH, NH y CH.

Estas especies atómicas y moleculares generadas tras la ablación del compuesto orgánico pueden sufrir interferencias con especies provenientes de la atmósfera cuando el análisis es llevado a cabo en presencia de aire, como ocurre en la mayoría de las aplicaciones LIBS. La interacción del plasma con el aire del ambiente da lugar a nuevas especies di-atómicas, como CN, y éstas van a contribuir adicionalmente a la intensidad total de las emisiones recogidas en el espectro.

El plasma es un sistema transitorio y no homogéneo en el espacio, por lo que los estudios espectroscópicos de resolución temporal a lo largo de la vida del plasma junto con los de resolución espacial a lo largo de la dirección de expansión de la pluma son de gran valía en la caracterización de orgánicos y en la identificación de aquellas especies que proceden de la muestra y aquellas otras que resultan de las reacciones entre el aire del ambiente y las especies ya excitadas del plasma. Los diferentes orígenes de las especies emisoras se traducirán en comportamientos cinéticos también distintos. Además, este tipo de estudios también da lugar a un mayor conocimiento de la dinámica de expansión del plasma y la evolución de su composición con el tiempo.

También son un recurrente tema de investigación y de discusión las posibles rutas de fragmentación seguidas por las diferentes especies en la pluma, y son muchos los factores que tienen influencia en la reactividad de la pluma, como el nivel de fluencia, la longitud de onda de la radiación empleada y la duración del pulso, la presión y el tipo de atmósfera presente en el sistema, entre otros.

En el régimen energético por debajo del umbral de formación del plasma, el haz láser enfocado sobre la superficie del material puede dar lugar a la ionización del material por transferencia de energía a partir del calentamiento del sólido. En el caso del análisis mediante láser de compuestos orgánicos, la adquisición de información molecular en este régimen energético será factible mediante técnicas de espectrometría de masas a partir de la vaporización del material. Esto no será posible para regímenes de mayor energía, ya que la cantidad de energía depositada en la muestra supone una fragmentación excesiva en la molécula. Además, también será posible obtener información de tipo atómico. Es éste el motivo por el que gran parte del trabajo mostrado en esta memoria se centra en dicho régimen energético de trabajo para el análisis de compuestos orgánicos, utilizando para ello la técnica de espectrometría de masas de tiempo de vuelo por ionización láser. Con este método se obtendrá preferentemente información molecular del compuesto a partir de su fragmentación, ya que una menor irradiancia minimiza las tensiones térmicas inducidas por el láser. Este hecho constituye una gran ventaja en comparación con otras técnicas de análisis que presentan limitaciones en el análisis de orgánicos, como son LA-ICP-MS ó GD-MS. En función de la energía puesta en juego se podrá superar el límite el umbral de formación de plasma dando lugar a distintos regímenes de interacción. El espectro LIMS obtenido a partir de la excitación con láser de un compuesto orgánico será, por tanto, muy sensible a las variaciones en la dosis de energía absorbida por el mismo, de forma que experimentará variaciones cuantitativas y cualitativas debido a los diversos procesos de fragmentación que va sufriendo la molécula. Es por esto que las especies contenidas en el plasma y su aparición en el espectro dependerán de las condiciones específicas de excitación.

Desde un punto de vista general, el análisis directo de muestras en fase condensada mediante espectrometría de masas es llevado a cabo habitualmente en la investigación de materiales, en la industria de semiconductores, en biomedicina, y en estudios medioambientales, debido a sus excelentes capacidades para la detección de elementos traza. En dichas técnicas analíticas de espectrometría de masas, las partículas de la muestra son ionizadas y conducidas a un analizador de masas o *espectrómetro*, donde son separadas y detectadas por el sistema de detección. Cuando la técnica espectrométrica está basada en una ionización provocada por la interacción de un haz láser de determinada energía y longitud de onda con la muestra y consiguiente vaporización de la misma, adquiere el nombre de *Laser Ionization Mass Spectrometry* (LIMS), que proporcionará información de la composición elemental e isotópica de la muestra sólida.

La conjunción entre el láser como fuente de ionización y la espectrometría de masas da lugar a esta potente herramienta para el análisis elemental. La técnica será capaz de caracterizar un plasma inducido por láser, determinar el rendimiento iónico, la formación de *clusters*, así como velocidades de escape y distribución de especies. De esta forma es posible llevar a cabo análisis multi-elementales con gran rapidez sobre sólidos *bulk*, como metales, aleaciones y muestras geológicas (como rocas y minerales).

La técnica podrá ser combinada con diferentes tipos de analizador. Cuando éste es un espectrómetro de tiempo de vuelo (TOF), la técnica toma el nombre de *Laser Ionization Time-of-Flight Mass Spectrometry* (LI-TOF-MS), que será la utilizada en esta investigación. Las especies iónicas podrán ser identificadas gracias a sistemas de detección fotográficos o eléctricos.

La espectrometría de masas junto a la excitación láser en el análisis de muestras orgánicas ha demostrado ser muy válido, a pesar de que en origen su principal aplicación fuera el análisis de muestras sólidas inorgánicas. Un claro ejemplo es la detección y caracterización de compuestos orgánicos de alto contenido energético. La técnica posee la ventaja de una elevada sensibilidad y selectividad en la identificación y cuantificación de cantidades traza con un rápido muestreo y sin la necesidad de etapas previas complicadas de preparación de muestra. Además, la contribución de la espectrometría de masas a la investigación sobre productos de descomposición y detonación de sustancias explosivas ha cobrado una considerable importancia para la química forense, y supone un gran apoyo para la comprensión de las rutas de fragmentación de las moléculas madre. En este sentido, los fenómenos que tienen lugar durante la ignición y combustión de este tipo de materiales son susceptibles de ser estudiados a partir de un análisis controlado basado en los principios de la espectrometría de masas.

En cuanto al estado de agregación del material, en el pasado se han desarrollado muchos estudios en fase gas mediante espectrometría de masas sobre explosivos y compuestos vinculados a explosivos (ERCs) con láser de nanosegundo, pero sólo unos pocos lo han realizado sobre fase sólida, la mayoría utilizando pulsos ultracortos de femtosegundo. Un ejemplo de ionización láser con pulsos de nanosegundo son los estudios llevados a cabo sobre las rutas de fragmentación de nitroaromáticos mediante radiación láser ultravioleta.

La metodología LIMS permite un rápido examen de muchos tipos de muestras sin la necesidad de procesos tediosos de preparación como en GC-MS. Esta flexibilidad es compartida con técnicas vibracionales como Raman o FTIR, pero la sensibilidad de LIMS es significativamente superior. Además, LIMS está capacitada para el análisis de muestras en estado sólido, característica que no es viable para otras metodologías más económicas y sencillas, como las asociadas a las técnicas comentadas anteriormente.

Por tanto, LIMS constituye una alternativa válida para el análisis inmediato de tipo atómico y molecular y cuyas capacidades analíticas son independientes del estado físico de la muestra. Además, es independiente de las propiedades magnéticas y eléctricas del material, haciendo posible el análisis en sólidos conductores, semiconductores y dieléctricos.

La aplicación de técnicas de espectrometría de masas y óptica en la detección, identificación y discriminación de explosivos orgánicos así como de otros compuestos orgánicos peligrosos para la salud y el medio ambiente ha constituido tradicionalmente una opción para una rápida respuesta química y una caracterización semicuantitativa o cuantitativa de estos compuestos. Estos métodos han experimentado un avance espectacular en las últimas décadas en cuanto a sensibilidad y adaptabilidad instrumental. En el caso del análisis de compuestos orgánicos con elevado contenido en energía, éste siempre ha constituido un área de gran interés debido a la química que va asociada a la energía interna de estos compuestos. Las reacciones de descomposición térmica son especialmente importantes para las sustancias explosivas, y el estudio de las cinéticas asociadas y los mecanismos de ruptura de la molécula suponen un aspecto fundamental en su caracterización. Además de su identificación mediante técnicas analíticas, un siguiente paso lo constituye la detección de residuos de explosivos tanto a nivel local como a nivel remoto, campo en el que LIBS se ha convertido en una herramienta forense extremadamente útil.

En los últimos años ha sido posible la integración de sensores para la adquisición a tiempo real y simultánea de información multielemental y/o molecular de la muestra a partir de su muestreo mediante un mismo evento láser. En este sentido, el análisis coincidente de iones y fotones puede ser de gran ayuda en el estudio fundamental sobre los eventos transitorios que tienen lugar en la formación del plasma inducido por láser de materiales de distinta naturaleza (análisis de la química en la pluma) así como en el estudio de la dinámica de la pluma en su proceso de expansión en el espacio. Un ejemplo de esto lo constituye el estudio llevado a cabo para los compuestos orgánicos de interés mediante un sistema experimental combinado LIMS-LIBS descrito en la presente memoria.

En la ablación de compuestos orgánicos, la gran cantidad de energía requerida y que es depositada en la muestra va a originar la rotura de enlaces que provoca la pérdida de la información molecular en el espectro final, es decir, que la presencia de fragmentos moleculares de elevado peso molecular será poco probable. Por ello, en el análisis en coincidencia de iones y fotones en orgánicos es de vital importancia establecer unas condiciones experimentales (principalmente energéticas) adecuadas para poder generar un plasma que contenga una cantidad representativa de especies excitadas sensibles a su detección mediante espectrometría de emisión óptica, pero a la vez que no permitan un excesiva fragmentación molecular que pueda comprometer la detección por masas de los fragmentos iónicos. Es por ello que en la mayoría de los casos las condiciones óptimas para la detección en uno y otro caso no serán coincidentes.

En la presente memoria se ha llevado a cabo, en primer lugar, un estudio de los procesos de ionización y fragmentación de materiales energéticos orgánicos mediante espectrometría de masas de tiempo de vuelo por ionización láser (LI-TOF-MS). El objeto del trabajo se basó en conseguir un mayor conocimiento acerca de los fenómenos implicados en la formación de especies iónicas a diferentes regímenes energéticos a partir de la excitación con láser de la muestra, además de obtener una mejora en la señal espectral y, por tanto, en la calidad analítica de la técnica. Para ello se contó con un sistema robusto de control sobre las condiciones energéticas y sobre la extracción de especies iónicas, que permitió una adecuada desorción e ionización del material orgánico de interés. En el estudio además se obtuvieron los valores de fluencia umbral para las diferentes especies iónicas y los valores óptimos para los parámetros temporales de extracción que permitieron obtener de forma modulada información preferentemente atómica (importante para aspectos fundamentales relacionados con la dinámica del proceso de fragmentación) o preferentemente molecular (útil para propósitos de identificación forense).

Se demostró, así mismo, la capacidad analítica para identificación forense de la técnica con la monitorización de iones moleculares característicos de compuestos nitroaromáticos. Así mismo se elaboró una librería de espectros LIMS para compuestos orgánicos de diversa índole que figura como anexo en esta memoria.

A continuación se realizaron estudios en coincidencia óptico-masas a partir de la señal de emisión del plasma generado procedente de la ablación de la muestra orgánica recogida por un sistema LIBS, y de la señal iónica procedente de las especies cargadas presentes en la pluma mediante el sistema LIMS, respectivamente. En este caso, para lograr la simultaneidad en las señales, el régimen energético debe superar el umbral de formación de plasma. El estudio se llevó a cabo de nuevo a partir de compuestos orgánicos nitroaromáticos en fase condensada y en un ambiente de alto vacío, de forma que fuera posible la detección de los iones en el espectrómetro de masas. En estas condiciones evitamos las interferencias que supone la presencia de una atmósfera gaseosa.

Se obtuvo una señal analítica reproducible y de calidad aceptable gracias a que se establecieron unas condiciones experimentales tales que permitieron la generación de un plasma con una abundancia de especies excitadas suficiente como para poder ser detectadas por el sistema óptico sin provocar una excesiva fragmentación molecular, y así permitir la monitorización correcta de las especies iónicas de interés con alto peso molecular en el espectro de masas. Esto se consiguió tras un exhaustivo control de las condiciones energéticas y temporales en la adquisición de ambas señales.

Se comprobó la existencia de un gran paralelismo en el comportamiento experimentado durante la ablación por la molécula de TNT y la de sus precursores, DNT y MNT, observando la evolución de las señales analíticas recogidas con la variación de la energía: patrones de fragmentación y señales de emisión obtenidos en cada caso.

Así mismo, se evaluó el nivel de coincidencia o grado de paralelismo entre especies neutras monitorizadas mediante emisión óptica y las especies iónicas detectadas en el espectrómetro de masas, tanto atómicas como las moleculares. Para ello se observaron las variaciones de intensidad que experimentaban dichas señales a medida que aumentaba el nivel de energía del pulso láser. De esta forma se pudo monitorizar los umbrales de energía, los momentos de máxima concentración en la pluma y el momento de extinción para cada especie.

A continuación, y una vez evaluadas las ventajas de llevar a cabo este tipo de análisis usando ambas técnicas simultáneamente, el método se aplicó en el análisis directo de tres isómeros del compuesto DNT en fase sólida, llevando a cabo por un lado el análisis mediante LIMS, y por otro, el análisis por LIBS, tanto a alto vacío como a presión atmosférica, con el objetivo de evaluar las capacidades de estos métodos basados en la desorción/ablación por láser en la identificación de compuestos orgánicos con analogías de tipo composicional y estructural. Para ello se optimizaron los parámetros experimentales de adquisición para que la información recogida permitiera la discriminación entre isómeros a partir del establecimiento de criterios basados en las intensidades relativas de las señales ópticas y másicas características del compuesto en el régimen energético requerido en cada caso.

Tras este análisis se prosiguió con el propósito de dar algo más de luz en la química que se desarrolla en el plasma de nitro compuestos de carácter explosivo mediante LIBS. De esta forma se pretendía estudiar cómo afectaban las condiciones energéticas y de presión atmosférica a las rutas de formación de especies excitadas en el plasma. Para ello, el estudio se valió de la espectrometría de masas como técnica de soporte en la interpretación de los espectros ópticos, verificando la presencia de especies que potencialmente podían participar en las rutas propuestas de fragmentación de los compuestos estudiados.

A partir de aquí se aparcó la espectrometría de masas y nos centramos exclusivamente en estudios basados en LIBS. En primer lugar se realizó un experimento a presión controlada sobre el explosivo nitro aromático TNT para explorar la influencia de la presión y, por consiguiente, de la densidad del entorno, en el desarrollo del plasma, llevando a cabo espectroscopía resuelta en el tiempo y en el espacio para monitorizar la evolución en la dinámica de expansión del plasma. Para ello se siguieron las cinéticas de las especies atómicas, iónicas y moleculares de emisión características de la molécula explosiva, así como del hidrocarburo policíclico aromático pireno como molécula apoyo para fines comparativos. Con ello se perseguía, por un lado, vislumbrar en un mayor grado la forma en que la presión de aire participa en dicha cinética de generación del plasma en compuestos orgánicos de alto contenido energético y, al mismo tiempo, identificar en qué condiciones ambientales la respuesta óptica recogida por el detector da lugar a las mejores características espectrales desde el punto de vista analítico.

Por último, la ablación láser se llevó a cabo en presencia de atmósferas de distinta naturaleza, tanto gases reactivos como inertes, y se estudió cómo éstos interaccionan con el plasma y participan en la química de la pluma. Se evaluó la forma en que estos gases de fondo contribuyen a las señales de emisión en los espectros LIBS integrados en el tiempo para así poder identificar las rutas más favorables de formación de especies de emisión características en cada caso y aquellas otras que quedaban inhibidas.

Figure Captions

Chapter 1. Introduction

Figure 1.1. Scheme of energetic regimes in laser-matter interaction.

Figure 1.2. Schematic diagram of the MALDI process.

Figure 1.3. Scheme of the microscopic interactions during the heat transfer process. Reproduced from [Marla, D., 2011].

Figure 1.4. Scheme of particle distribution after laser-solid interaction in (a) high vacuum and (b) low-pressure gas ambient. Adapted from [Lin, Y. et al., 2010].

Figure 1.5. Different type of plasmas depending on electron density and average electron energy (electron temperature for plasmas in equilibrium). Adapted from [Gordillo, F. J., 2008].

Figure 1.6. (Left) Cold plasma of air, generated by a CC electric discharge at low pressure simulating plasmas in the Earth's ionosphere. (Right) Cold plasma generated by pulsed laser deposition of an Ag with an excimer laser for the synthesis of nanostructured materials. Reprinted from [Gordillo, F. J., 2008].

Figure 1.7. Scheme of the interdependence of phenomena in laser induced plasmas. Adapted from [Marla, D. et al., 2011].

Figure 1.8. Two-dimensional Cu plasma images at different pressures produced using 50 μJ femtosecond laser pulses. Reprinted from reference [Yalcin, S. et al., 2004].

Chapter 2. Experimental

Chapter 3. UV Laser Ionization Time-of-Flight Mass Spectrometry on Nitro Aromatic Explosives in Condensed Phase

Figure 3.13. Mass spectra (0-200 amu range) of 2,4,6-TNT obtained with 213 nm laser pulses. Extraction pulse width was set to 1000 ns. Extraction delay was set to 400 ns. Pressure in the analyzer was $5.0 \cdot 10^{-6}$ mb. Each data set is formed by accumulation of 100 pulses.

Figure 3.14. Mass spectra (0-70 amu range) of 2,4,6-TNT obtained with 266 nm laser pulses. The extraction pulse width was set to 400 ns; The extraction delay was set to 0 ns. Pressure in the analyzer was $5.0 \cdot 10^{-6}$ mb. Each data set is formed by accumulation of 100 pulses.

Figure 3.15. Evolution of specific low m/z species with increasing fluence level for TNT sample. Laser radiation, 213 nm.

Figure 3.16. Dependence of LIMS signal intensity with fluence level for TNT hydrocarbon fragments m/z 61^+, 62^+ and 63^+ formed in the fragmentation process of the molecule using UV 213 nm pulses as excitation source.

Figure 3.17. Dependence of the ion signal with fluence for selected ion fragments.

Figure 3.18. Dependence of LIMS signal intensity from 2,6-DNT sample with amplitude of extraction voltage. Intensities were normalized to the maximum value. Temporal conditions for the measurements: width extraction pulse, 400 ns; delay extraction pulse, 0 ns. Accumulation 100 acquisitions.

Figure 3.19. Time-of-flight mass spectra of 2,6-DNT irradiated with 213 nm laser beam under different extraction width conditions. The extraction delay pulse and the fluence value were set at 200 ns and 1.96 J/cm^2, respectively.

Figure 3.20. Mass spectra of 2,6-DNT irradiated with 213 nm laser beam under different extraction delays conditions. The extraction width pulse and the fluence value were set at 800 ns and 1.96 J/cm^2, respectively.

Chapter 4. Laser-Induced Plasma Spectroscopy of Nitro Aromatic Explosives. Understanding Fragmentation Processes Using Ion-Photon Coincidence Measurements

Figure 4.1. Ion/photon coincidence detection scheme.

Figure 4.2.a) Time-resolved emission intensity of collected light from 2,6-DNT plasma. The gate width for each measurement was 10 ns. b) Time-evolution of integrated LIMS

signal from irradiation of 2,6-DNT sample. The extraction pulse width was set in 800 ns.

Figure 4.3. (a) Mass spectra (0-80 amu range) and (b) emission spectra (250-900 nm range) of TNT acquired in coincidence at fluence values from 1 J/cm^2 to 7.1 J/cm^2.

Figure 4.4. (a-e) Coincidental LIMS-LIBS signals of atomic and molecular species versus fluence level for 2,6-DNT; (f) variation of $C_2H_2^+$ and NO^+ species from LIMS spectra versus fluence level for 2,6-DNT. Intensities were all normalized to the maximum value.

Figure 4.5. Detail of the CN emission spectra at different base pressures with 266 nm laser pulses at fluence of 3 J/cm^2.

Figure 4.6. UV wavelength region of LIBS TNT spectrum at high fluence value (10.2 J/cm^2). Gate pulse width, 10 μs; gate pulse delay, 30 ns.

Figura 4.7. Coincidental LIMS-LIBS carbon signals versus fluence level for TNT sample. Intensities were all normalized to the maximum value.

Chapter 5. Discrimination of Dinitrotoluene Isomers in Condensed Phase by Laser Ionization Time-of-Flight Mass Spectrometry and Laser-Induced Breakdown Spectroscopy

Figure 5.1. Coincidental LIMS-LIBS spectra obtained for 2,3-DNT using 266 nm UV radiation. Measurements were performed at vacuum pressure using (a) low fluence condition (2.4 J/cm^2) (b) high fluence condition (9.7 J/cm^2).

Figure 5.2. Electron Impact Spectrum of 2,3-DNT molecule from NIST data base.

Figure 5.3. (a) LI-TOFMS spectra of low-mass range for analyzed DNT isomers. (b) Peak intensities for the main low-mass fragments in LI-TOFMS spectra of DNT isomers. Peak signals at m/z 24, 51 and 63 are scaled x5 for better comparison. Fluence value, 2.4 J/cm^2. Accumulation of 100 acquisitions.

Figure 5.4. LIMS spectra of dinitrotoluene isomers obtained after ionization with nanosecond 266 laser radiation. Average 100 pulses. Fluence value, 2.4 J/cm^2. Delay in extraction, 500 ns. (a) 2,3-DNT, (b) 2,6-DNT, (c) 2,4-DNT.

Chapter 6. Pathways for Production of Emitting Species in the Laser-Induced Plasma of Organic Explosives

Chapter 7. Analysis of Influence of Pressure on Dynamics of Laser-Induced Plasma Expansion for Nitro Aromatic Explosives by Time and Spatially-Resolved Studies

Figure 7.1. Images of trinitrotoluene and pyrene plasmas at different pressure levels, (a) 1000 mb; (b) 10 mb; (c) 1 mb; (d) $1 \cdot 10^{-5}$ mb. Fluence, 12.7 J/cm^2.

Figure 7.2. LIBS spectra of trinitrotoluene and pyrene plasmas at different pressure levels. Fluence, 12.7 J/cm^2.

Figure 7.3. Normalized intensities of main emitting species depending on the air pressure level for (a) trinitrotoluene and (b) pyrene. (c) Comparative of net intensities of C_2 ($\Delta\upsilon$=0) molecular band for both samples, depending on the air pressure level.

Figure 7.4. Time-resolved studies for (a) molecular C_2 band ($\Delta\upsilon$=0) and (b) atomic H_β emitting species with pressure variation on pyrene sample.

Figure 7.5. Time-resolved study for C_2 (molecular), C(I) (atomic) and C(II) (ionic) emitting species at 0.001 mb from pyrene sample.

Figure 7.6. (a) Time-resolved evolution of main emitting species from TNT LIBS spectra (pressure 10 mb) (b) Time-resolved evolution of specific CN band (388.3 nm) from trinitrotoluene LIBS spectra at different pressure levels. Gate width, 10 ns; Resolution, 20 ns.

Figura 7.7. Spatially resolved LIBS spectra in the direction of expansion of (a) pyrene and (b) TNT plasma plumes. Pressure, 1 mb. Each spectrum corresponds to the sum of 50 consecutive shots. Experimental conditions: λ 266 nm; Fluence, 12.7 J/cm^2.

Figure 7.8. Spatial variation of signal intensity for C, N, O, H, CN and C_2 in (a) pyrene and (b) TNT. Experimental conditions: λ 266 nm; Fluence, 12.7 J/cm^2; Pressure, 1 mb; Sum of 50 consecutive shots. Intensity for C(I) emission line was multiplied by 10^2 factor for comparison.

Figure 7.9. Spatially & time-resolved studies for molecular C_2 and CN species with pressure variation on pyrene sample. Data were acquired at different distances from the surface (a) 6 mm (b) 3 mm (c) 0 mm.

Figure 7.10. Evolution of mass ablated depending on analysis pressure for TNT sample. Laser wavelength, 266 nm. Energy pulse, 3 mJ.

Chapter 8. Insights on the Acting Role of Background Gas in the Formation Pathways of Emitting Species in Laser-Induced Plasmas of High Energetic Nitro Compounds

Figure 8.1. Time-resolved study of CN molecular emission band $\Delta\upsilon=0$ (388.3 nm) collecting the plasma core at 10 mb air pressure for TNT sample. Gate width pulse, 10 ns. Fluence, 12.5 J/cm^2.

Figure 8.2. LIBS spectra for DNT sample using 266 nm and 1064 nm laser radiations and acquired at (a) air pressure, (b) low vacuum pressure, 0.2 mb, and (c) high vacuum pressure, $4.0\cdot10^{-5}$ mb.

Figure 8.3. Intensity ratios between two transitions of both CN ($\Delta\upsilon=0$) and C_2 ($\Delta\upsilon=0$) emission bands as a function of air pressure and oxygen pressure for TNT.

Figure 8.4. Intensity ratios between two transitions of both CN ($\Delta\upsilon=0$) and C_2 ($\Delta\upsilon=0$) emission bands as a function of air pressure for TNT and pyrene.

Figure 8.5. LIBS TNT spectra acquired in different atmospheres. Fluence, 12.5 J/cm^2. Pressure, 100 mb.

Figure 8.6. LIBS pyrene spectra acquired in different atmospheres. Fluence, 12.5 J/cm^2. Pressure, 10 mb.

Figure 8.7. LIBS PETN spectra acquired in different atmospheres. Fluence, 12.5 J/cm^2. Pressure, 100 mb.

Figure 8.8. Net intensities of main atomic and molecular emission species of (left) TNT and (right) PETN as a function of pressure level in different atmospheres: (a) oxygen; (b) nitrogen; (c) air. Fluence, 12.5 J/cm^2. Nitrogen net intensities are multiplied by a x10 factor for a better comparison.

Figure 8.9. Detail of spectral widening of H(I) emission line (656.3 nm) as a function of oxygen pressure in UV-LIBS analysis of TNT. Fluence, 12.5 J/cm^2.

Figure 8.10. Set of LIBS TNT spectra for different H_2 pressure values. Top spectrum was taken at unknown H_2 pressure, but in the range between 10-50mb. Fluence, 12.5 J/cm^2

Figure 8.11. Comparative study concerning the variation of CN emission signal as a function of both air and hydrogen pressures for (a) TNT; (b) PETN. Fluence, 12.5 J/cm^2.

Figura 8.12. Set of LIBS TNT spectra for different Ar pressure values in the range between $5.0\cdot10^{-5}$ mb and 50 mb. Fluence, 12.5 J/cm^2.

Figura 8.13. Set of LIBS TNT spectra for different He pressure values. Top spectrum was taken at unknown He pressure, but in the range between 10-50 mb. Fluence, 12.5 J/cm^2.

Figura 8.14. Net intensities of main emission bands corresponding to molecular species (top) CN and (bottom) C_2 from TNT LIBS spectra as a function of pressure level for different buffer gas. Laser wavelength, 266 nm. Fluence, 12.5 J/cm^2.

List of Tables

Chapter 1. Introduction

Chapter 2. Experimental

Chapter 3. UV Laser Ionization Time-of-Flight Mass Spectrometry on Nitro Aromatic Explosives in Condensed Phase

Chapter 4. Laser-Induced Plasma Spectroscopy of Nitro Aromatic Explosives. Understanding Fragmentation Processes Using Ion-Photon Coincidence Measurements

Chapter 5. Discrimination of Dinitrotoluene Isomers in Condensed Phase by Laser Ionization Time-of-Flight Mass Spectrometry and Laser-Induced Breakdown Spectroscopy

Chapter 7. Analysis of Influence of Pressure on Dynamics of Laser-induced Plasma Expansion for Nitro Aromatic Explosives by Time and Spatially-Resolved Studies

Chapter 8. Insights on the Acting Role of Background Gas in the Formation Pathways of Emitting Species in Laser-Induced Plasmas of High Energetic Nitro Compounds

CHAPTER 1

Introduction

1.1. INTRODUCTION

The work of J. J. Thomson about cathode rays from electrical discharges in gases and his discovery of the electron in 1897 deserved the Nobel award in physics in 1906. His contribution to the knowledge of the structure of atoms was more than remarkable and thus helped to clarify the nature of the plasmas. The first attempt to give an overview on physics of gas discharges was owed to Johannes Stark with his book *Elektrizität in Gasen*, published in Germany in 1902.

In 1922, the American scientist Irving Langmuir proposed the Greek word *plasma* (meaning “formed or molded”) to denote the ionized gas medium that contained electrons, ions and neutrals similarly to the fluid medium carrying all the corpuscular material in blood.

Studies on plasma physics were developed continuously during the 20th century and were very close to the magnetic fusion energy research. By the end of the 1960's decade, the empirically developed russian *tokamak* configuration (a device using a magnetic field to confine plasma in the shape of a torus in order to obtain the fusion of plasma particles) began producing plasmas with promising parameters. **[Shafranov, V. D., 1966][Fisch, N., 1978][Dolan, T. J., 1982].** At the end of the 20th century, fusion break-even had nearly been achieved in *tokamak* **[Braams, C. M., 2002]**, and international agreement was reached in the early 21st century to build the

International Thermonuclear Experimental Reactor (ITER), a break-even *tokamak* designed to produce 500 megawatts of fusion output power.

Simultaneously with the fusion effort, there has been an equally significant and extensive study of *space plasmas* since the late 19th century **[Kivelson, M. G., 1995]**. This research was greatly stimulated when it became possible to use spacecraft to make *in situ* plasma measurements of the Earth's magnetosphere (space that extends up to a distance of approximately 65,000 km from Earth's surface in which charged particles are controlled by Earth's magnetic field) **[Appleton, E. V., 1932]**, the solar wind, and the magnetospheres of other planets **[Ratcliffe, J. A., 1972][Nefedov, A., 2003].** It was concluded that space plasmas often behaved in a manner qualitatively similar to laboratory plasmas, but at a larger scale **[Melrose, D. B., 1986]**.

The use of plasmas for space propulsion applications was developed since the 1960's. Plasma thrusters are now in use on some spacecrafts and are under serious consideration for new and more ambitious spatial designs. After that, in the late 1980's a new application of plasma physics appeared: the *plasma processing*, especially important for the electronic devices industry; and in the 1990's studies emerged on *dusty plasmas* **[Shukla, P. K., 2002],** that is electrically charged dust grains immersed in a plasma acting as additional charged particle species. Different physical behaviour happens in the plasma due to different size and mass of the dust particles **[Barkan, A., 1996][Bellan, P. M., 2004].** At the same time, there has also been investigation of *non-neutral plasmas* for incompressible hydrodynamics studies and also applied to the storage of large quantities of positrons **[Surko, C., 1989]**.

In addition to the mentioned activities it is well known that there have been continuing investigations of industrially relevant plasmas such as arcs, plasma torches, and laser plasmas in many areas principally based in processing, testing and the design of new materials.

1.2. ENERGETIC REGIMES IN LASER-MATTER INTERACTION

The physical processes of the laser-solid interaction are highly complex and interrelated. They depend not only on the laser parameters, e.g. power density, wavelength, pulse duration, and spot size, but also on the material's physical properties, e.g. absorption properties, morphology, homogeneity, and melting and boiling points. The mechanisms involved in the laser-solid interaction have been studied extensively, but they are still not fully understood. However it can be controlled and highly reproduced to enable analytical measurement capabilities.

Thus, laser-matter interaction is a phenomenon essentially based on thermal and photonic processes. As a consequence of the laser pulse, and depending on the total energy reaching the sample surface, different phenomena will occur in a microscopic or macroscopic level. Whereas at low irradiance, heating and melting surface following a soft desorption and ionization are the main sequential events, the high irradiance regime is dominated by the evaporation of the material and an extensive fragmentation with the final formation of the expanding plasma cloud **[Vertes, A. et al., 1989].** On the other hand, it is clear that the processes taking place in the laser-matter interaction depend on the nature of the sample, and therefore, the plasma formation in organic compounds is much more complex than that from metals.

The modeling of ablation process involves the study of various complex phenomena (see Figure 1.1). The ablation event can be categorized into two stages: *laser-target interaction* and *plasma formation* (with subsequent shielding of the incoming radiation).

In the laser-target interaction, the ablation of the material is carried out, so that the target is heated by laser radiation and then vaporizes.

A number of models for laser heating of the target describe this heat transfer on a macroscopic scale by considering the Fourier heat conduction equation with the energy deposited by the laser as the source term. These models consider the instantaneous conversion of laser radiation into heat and they are accurate for pulse durations above the nanosecond range. As the pulse duration decreases from nanoseconds to picoseconds, and finally to femtoseconds, the modeling approach changes significantly. Under such instances, the modeling of the laser heating of the target has been done by considering microscopic interactions of the laser radiation with the target material.

On the other hand, the interaction of the ablated material in the plasma with the incoming radiation has been described in the literature considering various absorption mechanisms by the plasma **[Neamtu, J. et al., 1999] [Zhang, D. et al., 2005] [Singh, R. K. et al., 1990 A] [Chen, Z. et al., 2005] [Rozman, R. et al., 2008] [Aghaei, M. et al., 2008]**. The models differ for different range in the wavelength of the incoming radiation, IR **[Fang, R. et al., 2007]** and UV **[Fang, R. et al., 2008]**. Some models present not only the ablation phenomenon but also describe the plasma evolution, its interaction with the incoming radiation and its expansion after pulse termination. The investigations on plasma plume, its interaction with the laser and its expansion have also been carried out using hydrodynamic models, Monte Carlo simulations, and a combination of both. **[Itina, T. E. et al., 2002] [Itina, T. E. et al., 2003].**

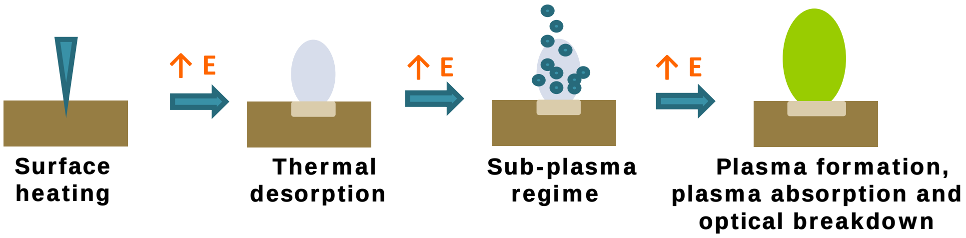

Figure 1.1. Scheme of energetic regimes in laser-matter interaction.

1.2.1. LASER DESORPTION. MALDI

Laser desorption of solids is one of the most important analytical applications in laser ablation, including the characterization of organic compounds. It has been extensively used in the analysis of metabolites and other biomolecules.

Under desorption regime, MALDI (matrix assisted laser desorption/ionization mass spectrometry) is the reference technique for laser-based analysis. Its arrival was one of the most important advances in the use of laser for analytical purposes and nowadays it becomes one of the most powerful instrumental techniques **[Bouchonnet, S. et al., 1992]**. The technique achieves a soft ionization assisted by the addition of a matrix (organic compounds as nicotinic or ferulic acids) where the analyte is dissolved, helping in the reduction of the energetic contribution of the laser. In this sense, the necessary presence of a matrix compound in order to achieve an efficient energy transfer turns into a limitation of this method. In fact, laser desorption done without the addition of a matrix implies an important challenge for analytical chemistry. Another disadvantage in MALDI is the critical step of sample preparation that usually requires wet manipulation of the samples, including the selection of a proper matrix in the correct concentration **[Demeure, K. et al, 2007]**.

In MALDI-MS, the matrix is mixed with the analyte solution in a molar excess in the order of 10000:1. The matrix absorbs efficiently a large amount of laser radiation energy in a very short time and greatly increases its temperature, and as consequence, transfers it to the sample molecules in a controlled manner allowing desorption of even macromolecules as intact gas-phase ions (see Figure 1.2). After the desorption step, ionization of analyte molecules takes place by gas phase proton transfer reactions and partially by photoionization or ion-molecule reactions. Therefore, information obtained through this experimental approach is mostly limited to molecular one. On the contrary, atomic analysis using MALDI is rarely used and it is usually assisted by other techniques like LA-ICP-MS. Moreover, metallic and, in

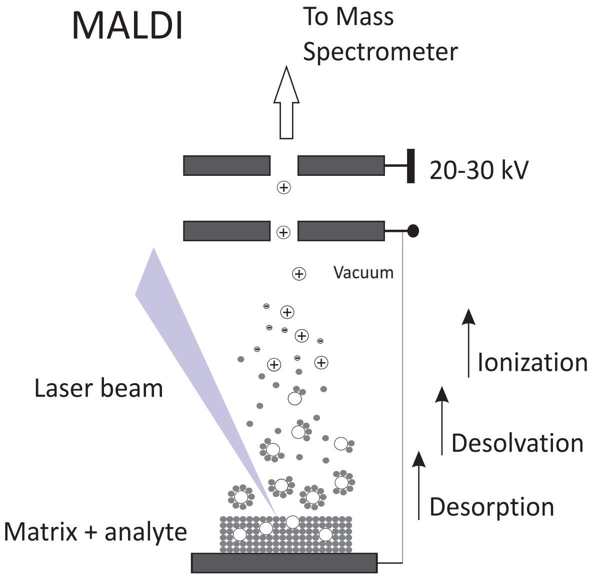

Figure 1.2. Schematic diagram of the MALDI process.

general, inorganic targets are far beyond the applicability of the technique, and are better analyzed by LIMS or LA-ICP-MS.

A number of laser systems are used in MALDI applications emitting at UV or IR wavelengths, but laser irradiance required is much lower than in LA-ICP-MS or LIMS applications. Experimental parameters affecting the MALDI process, such as laser frequency, pulse length, spot size, and fluence dependence have been recently reviewed **[Dreisewerd, K., 2003].**

1.2.2. SUB-PLASMA FORMATION REGIME

The sub-plasma energetic regime lies between desorption, where negligible mass transfer occurs, and ablation regimes. In this intermediate energetic condition, ionization of the material can be achieved by thermal heating of the solid when a laser beam is focused on its surface, while keeping the laser fluence below the plasma formation threshold. In the laser sampling of organic materials, the acquisition of molecular information by mass spectrometry techniques from vaporized material in this sub-plasma regime will be feasible (not possible at higher energetic regime) besides adding all the atomic information (not possible at desorption regime). For this regime, the amount of analytical work found in literature is scarce. We focus on this work regime in the analysis of nitro aromatic organic compounds using laser ionization mass spectrometry (LIMS) in order to obtain preferentially molecular information.

If the amount of energy deposited on the sample is not enough to reach the plasma formation threshold, the damage in sample surface will be significantly reduced **[Vadillo, J. M. et al., 2005]**. In the analysis of organic materials, sample damage consequences may be evaluated from two different points of view: permanent damage done to the surface and transformations underwent by the molecules under analysis. When the damage is permanent, a crater left by the laser may be measured. However, a significant reduction of the sample damage under sub-plasma threshold conditions is found **[Tellez, H. et al., 2008]** since the lower irradiance applied to the sample minimizes the thermal stress induced by the laser. Consequently, molecular fragmentation may appear. In the case of LIMS technique, this fact represents an advantage, when comparing with the limited features of the organic analysis in LA-ICP-MS or LIBS techniques. **[López-Moreno, C. et al., 2006][De Lucia, F. C. et al., 2007]** Additionally, as no carrier gas is needed, Ar-related interferences, that limit the LA-ICP-MS and GD-MS analysis, are not present. As a limitation, quantification in LIMS is hard to accomplish, as it is in many other MS techniques. This quantification is difficult not only as a consequence of fractionation **[Russo, R. E. et al., 2000]**, but also as a consequence of the different ionization degree within the constituents of the plume.

1.2.3. PLASMA FORMATION REGIME

When laser radiation is incident on a solid surface, a part of it gets reflected, while the rest penetrates into the material and gets absorbed by it. The absorbed radiation heats up the material, leading to its melting and evaporation. This process of removal of the material from the target is called *laser ablation*. The laser ablation process can be categorized to occur in two stages. In the first stage, laser energy is absorbed by the target leading to an increase in its temperature. In the next stage, when the temperature reaches the vaporization temperature, the ablation initiates and the material vaporizes, which forms a plasma plume above the target surface. The plume further interacts with the incoming laser radiation absorbing a part of it, thereby shielding the target surface.

Thus, the modeling of the laser ablation process involves consideration of two main phenomena. First, the laser heating of the target: this leads to prediction of target temperature and ablation rate. Second, the radiation absorption by plasma plume, and its direct influence on the ablation rate due to radiation shielding. In the following subsections, various models characterizing the two phenomena are briefly described.

1.2.3.1. MODELS ON LASER HEATING OF TARGET

Only a portion (1−R_m) of the incoming laser radiation penetrates into the target surface, where R_m is the reflectivity of the target surface. In the case of metals, values for R_m are typically important. However, in the case of organic samples, the portion of reflected radiation in most cases becomes very small. The absorbed portion gets continuously attenuated as it propagates inside the target material. As a result, the radiation intensity decreases exponentially with depth (x) inside the material as described by the Beer–Lambert law given by **[Baeri, P. et al., 1979][Wood,R. F. et al., 1981]**,

$$I_m(x) = (1 - R_m) I_0 e^{-\alpha_m x}. \qquad \textbf{(Eq. 1.1)}$$

where α_m is the absorption coefficient of the target. The heat transfer can be considered to be one-dimensional, along the depth.

From a macroscopic perspective, the laser heating of the target can be modeled by neglecting the microscopic interactions between the photons and elemental particles in the structure. The heating process can be considered to occur in a single step, where the radiation on the target leads to the rise in its temperature. The process can be modeled using the Fourier heat conduction equation, with a source term representing the radiation heating, given by **[Joseph, D. D. et al., 1989][Kim, W. S. et al., 1990],**

$$C\frac{\partial T}{\partial t} = \nabla \cdot (K \nabla T) + S, \qquad \textbf{(Eq. 1.2)}$$

where *S* is the laser heat source term and refers to heat generation per unit volume **[Baeri, P. et al., 1979]**. The above equation assumes heat transfer to occur instantaneously by diffusion, i.e. heat propagation at infinite speed. This model is also referred to as parabolic one-step (POS) model. However, this assumption is subject to question for heat transfer with ultrashort pulse duration. Under such conditions, researchers have modified the POS model by considering the heat propagation to occur at a finite speed, i.e., wave-type heat propagation, given by **[Qiu, T. Q. et al., 1994],**

$$C\frac{\partial T}{\partial t} = -\nabla \cdot \mathbf{Q} + S, \qquad \textbf{(Eq. 1.3a)}$$

$$\tau_e \frac{\partial \mathbf{Q}}{\partial t} + \mathbf{Q} = -K \nabla T. \qquad \textbf{(Eq. 1.3b)}$$

The nature of the above equations is hyperbolic and hence, the model is referred to as hyperbolic one-step (HOS) model. Though the model takes into account the relaxation time associated in the process, it does not consider the microscopic interactions of photons, electrons and phonons. The study of the microscopic interactions is very essential for modeling the laser heating process for ultrashort pulses **[Marla, D. et al., 2011]**, but especially in metals. In this case, when photons impinge on the metallic surface, a portion of them are absorbed by the electrons in the conduction band. Consequently, electrons moving freely in the metal lattice get excited, increasing their kinetic energy and interacting among them. Upon absorption, the electrons increase their temperature and collide with the lattice phonons, transferring energy to them. Further, the phonons interact among themselves until equilibrium is established. Therefore, there are other models taking into account microscopic interactions between particles, giving rise to two-step models. The parabolic two-step (PTS) model takes into account the electron-phonon thermalization, while it considers this process to occur instantaneously **[Anisimov, S. I. eT al., 1974].** On the other hand, the model referred to as the hyperbolic two-step (HTS) model improved the PTS model by accounting for the electron and phonon relaxation times **[Chen, J. K. et al., 2003]**. However, both two-steps models neglect the electron heating time by photons. All the above four models can be interrelated based on the pulse duration, relaxation times, and the thermalization time (as shows Figure 1.3).

Chen and co-workers **[Chen J. K. et al., 2003]** observed in metal films that the four models predict different temperature profiles for small pulse durations, while all of them converge as the pulse duration increases. In addition, they found out that the one-step models predicted a higher temperature as compared to the two-step models.

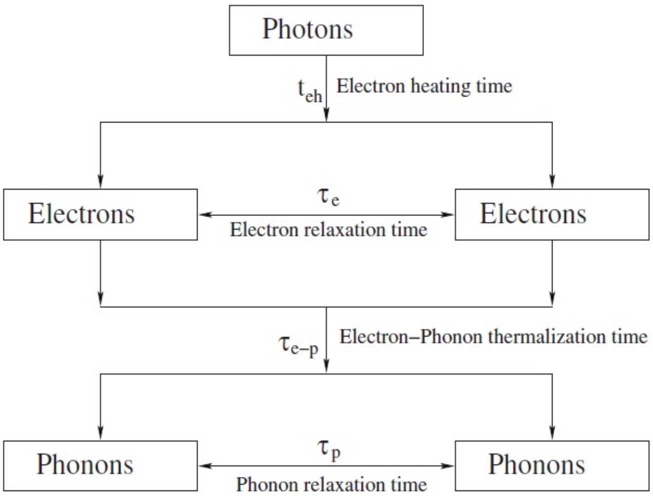

Figure 1.3. Scheme of the microscopic interactions during the heat transfer process. Reproduced from [Marla, D., 2011].

Thus, they concluded that for nanosecond pulses, the laser heating process can be adequately modeled using POS model and for smaller pulses, the process can be modeled using the PTS model.

1.2.3.2. MODELS ON LASER ABLATION

The ablation process involves complex heat transfer mechanisms and shielding effect. Hence, the ablation models must consider all of these phenomena.

In an elementary model for ablation in metals, **[Singh, R. K. et al., 1990]** a simple energy balance consideration was used to predict the amount of material ablated per pulse. In this model, the energy deposited by the laser beam is equated to the energy needed to vaporize the surface, conduction losses in the target and the absorption losses by the plasma, as given by,

$$(1-R_m)(E-E_{th}) = \Delta x(\rho_m C_p \Delta t + L_{ml}), \qquad \textbf{(Eq. 1.4)}$$

where Δx represents the depth of ablation and E_{th} represents the losses due to conduction as well as by radiation shielding. The model helps predict the average ablation rate as a result of a single incident pulse.

Most of the researchers has modeled the ablation phenomenon for pulses of nanosecond duration using POS equation (Eq. 1.2) as a governing equation of heat transfer to predict the temperature variation in the target followed by melting, vaporization and consequently, the ablation rate.

As a result of ablation, the top surface of the sample undergoes a downward movement. Peterlongo and co-workers **[Peterlongo, A. et al., 1994]** develop a model taking into account the energy loss due to the evaporation of the target material and consequent movement of the top surface boundary. The POS model has been modified as below:

$$c_p\rho_m\frac{\partial T}{\partial t} = \nabla\cdot(K\,\nabla\,T) + c_p\rho_m\left.\frac{\partial x}{\partial t}\right|_{x=0}\frac{\partial T}{\partial x} + S. \qquad \textbf{(Eq. 1.5)}$$

Bulgakova *et al.* **[Bulgakova, N. M. et al., 2004]** have further modified the model to include the latent heat of fusion and, Stafe *et al.* **[Stafe, M. et al., 2007]**, besides considering the material removal by vaporization, also considered the removal of the molten material due to the plasma pressure.

All the above models do not consider shielding of the laser radiation due to plasma formation which plays a crucial role in the ablation process. Zhang *et al.* **[Zhang, D. et al., 2005]** developed a model of the ablation phenomenon in two separate stages; one prior to vaporization and the other, after vaporization takes into account the plasma shielding effect. Considering this, the model modified the intensity term in the POS heating model (Eq. 1.2). In the first stage, the intensity of the radiation inside the target has been described by Eq. 1.1 while in the second stage, the intensity term has been modified to account for shielding effect as given by,

$$I_m(x) = [(1-R_m)I_{inc}\exp[-(\alpha_{\mathrm{IB}} + \sigma_{\mathrm{PI},n}N_n)H] + (1-R_{pl})I_{pl}]e^{-x/\delta_m}. \qquad \textbf{(Eq. 1.6)}$$

In the above equation, the radiation shielding by plasma has been considered to be due to *Inverse Bremsstrahlung* (IB) and *Photoionization* (PI) mechanisms (further described in next sections). Since the plasma temperature is high enough to heat the top surface of the target, it has also been accounted in the total intensity of the radiation irradiating the top surface by the additional term $(1-R_{pl})I_{pl}$.

It was concluded **[Fang, R. et al., 2007]** that the effect of plasma shielding is prominent only at high laser fluences (>3 J/cm^2). It is due to the formation of a dense plasma that shields the incoming radiation, while the effect is negligible at low laser fluences.

1.2.3.2.1. FEATURES OF LASER ABLATION IN VACUUM AND LOW PRESSURE BACKGROUND GAS

For LIMS, the ion source is operated in vacuum or low pressure ambient gas environment. Many experiments and theoretical simulations have been carried out in the past decade in an effort to understand the processes in more detail.

Ions generated in the nascent erosion plasma expand freely into a vacuum with kinetic energies ranging from several eV to thousands of eV; the energies are typically much lower for neutral species **[Buchsbaum, A. et al., 2008]**. Angular distributions of the ejected particles have been fit to an approximated $\cos^n\theta$ function **[Amoruso, S. et al., 1999][Torrisi, L. et al., 2001][Laska, L. et al., 2003]**. Generally, *n* depends on the laser fluence and ambient conditions and it is lower when the plasma propagates into an ambient gas where multiple collisions occur, which results in a broad angular distribution **[Willmott, P. R. et al., 2000].** The processes of plume expansion into an ambient gas are quite complicated and elusive. These processes involve the scattering and cooling of ions **[Lin, Y. et al., 2009]**, the formation of shock waves **[Wen, S. B. et al., 2007]** and recombination processes **[Laska L., et al., 2003]**. The presence of background gas causes impedance in the adiabatic expansion of plasma plume into the surrounding ambient. A shock wave is formed on the contact surface where the compressed gas layer meets the ablated plume, and the ablated species propagation is slowed; the plasma temperature also decreases, which sustains the recombination process. The schematic diagram of particle distribution after laser-solid interaction in high vacuum and low-pressure ambient is shown in Figure 1.4.

Regarding net values for characteristic parameters of plasma plume, the temperature can reach up to about $6\cdot10^4$ K with irradiance on the order of 10^9 W/cm^2 in vacuum conditions at about 10 to 20 ns after laser impact and then drops drastically **[Bogaerts, A. et al., 2003]**. At 1 atm of ambient gas pressure, the plume density reaches the highest value (more than 10^{26} m^{-3}) at the front of the plume, in contact with the background gas **[Bogaerts, A. et al., 2006]**.

The plume velocity increases near the front of the plume. In vacuum conditions, this is a free expansion with a velocity of $2\cdot10^4$ to $2.5\cdot10^4$ m/s; however, in a background gas, the plume expansion is retarded to a much lower velocity of $2\cdot10^3$ m/s and shorter plume length **[Bogaerts, A. et al., 2004]**. The expansion dynamics in a vacuum were confirmed later by experimental results in which the angular distributions of ions were also determined **[Bleiner D. et al., 2007]**.

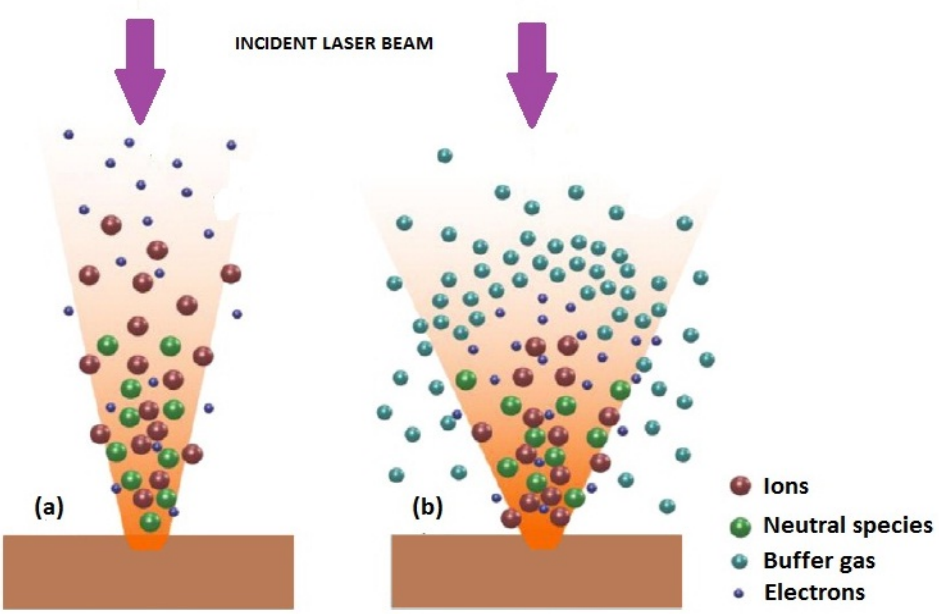

Figure 1.4. Scheme of particle distribution after laser-solid interaction in (a) high vacuum and (b) low-pressure gas ambient. Adapted from [Lin, Y. et al., 2010].

The angular distribution studies found that ablated ions were highly directional, and an empiric validation of the Lorentzian distribution function was performed as follows for the fitting of the angular distribution instead of the $\cos^n\theta$ function that is normally used:

$$f(\theta) = f_0(\theta) + \frac{A}{\pi}\left(\frac{\varphi}{(\theta - \theta_c) + \varphi^2}\right), \qquad \textbf{(Eq. 1.7)}$$

where θ is the off-axis angle, θ_c is the location of the peak, φ is the spread of angular distribution, $f_0(\theta)$ is the background offset and finally A is the integral of the distribution.

1.2.3.2.2. NATURE AND PLASMA TYPES

One of the particularities of plasmas is that is a conductor medium. At macroscopic scale plasmas are, however, electrically neutral. A first classification of type of plasmas may attend to the thermal equilibrium, i.e. if average energy of the plasma is the same for each type of particle that form it. In the case of plasmas inside the stars or analogous in Earth (thermonuclear plasmas in controlled devices for nuclear fusion) all particles in the plasma have similar average energy **[Gordillo, F. J., 2008]**.

Gas particles in a high ionized plasma can acquire individual kinetic energies presenting a particular distribution that fits to a Maxwell-Boltzmann function. A well-accepted statistical expression to count microstates that correspond to a particular macrostate (valid for both classic statistics as Maxwell-Boltzmann and quantum statistics as Bose-Einstein and Fermi-Dirac), is presented below:

$$P = \frac{N!}{n_1!n_2!n_3!}, \qquad \textbf{(Eq. 1.8)}$$

where *N* is the total of particles ($N = n_1+n_2+n_3...$) distributed in the different energy levels (E_1, E_2, E_3…) allowed in a particular instant. Considering an isolated system, the total energy remains constant ($U = E_1n_1 + E_2n_2 + E_3n_3$…). The probability of a particular macrostate is proportional to the number of possible distributions of the particles (microstates) in the available energy levels for a fixed total energy U. Due to collisions in the system, distribution of particles is continuously changing and number of particles in each level (n_1, n_2, n_3…) can fluctuate around the equilibrium values without macroscopic effects. Thus, it can be assumed that there is a more probable distribution of particles into the different levels for each macroscopic state of the system, *P*. The determination of the maximum of this distribution function is based on the hypothesis that all energy levels are equally accessible to all particles in the system.

The result in the calculation of the maximum of the *P* function so that number of particles and total energy of the isolated system keep constant is:

$$n_i = \frac{N\exp\left(\frac{-E_i}{kT}\right)}{Z} \qquad \textbf{(Eq. 1.9a)}$$

$$Z = \sum \exp\left(\frac{-E_i}{kT}\right) \qquad \textbf{(Eq. 1.9b)}$$

where *T* is the temperature of the system in statistical equilibrium, *k* is the Boltzmann constant and *Z* the partition function. These expressions are only valid in the case of non-degenerate of energy states E_i.

Plasmas inside the stars possess a high proportion of ionized particles, being the number of electrons and ions similar to that of neutral particles. These are also called *hot* or *thermal plasmas* (10^7-10^9 ºC). Another type of hot plasma, with specific industrial applications, is generated at higher pressures (up to 133 mbar) and gets temperatures between 10^4-10^5 ºC. Plasma torches for surface treatments or plasma lamps generated by high intensity discharges for streetlights or lights are examples of such a type of plasma.

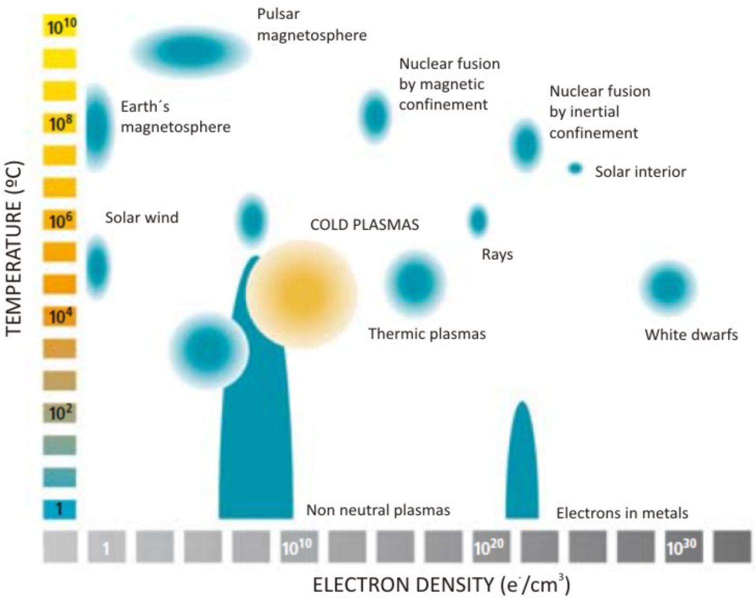

Figure 1.5. Different types of plasmas depending on electron density and average electron energy (electron temperature for plasmas in equilibrium). Adapted from [Gordillo, F. J., 2008].

When the gas pressure is low or the voltage applied to the discharge is quite high, electrons in the plasma acquire, in the time interval between collisions with other particles in the plasma, a kinetic energy value higher than the energy value associated to the random thermal motion of neutral particles (atoms and molecules) in the plasma. This implies a certain deviation out of the thermal equilibrium of plasma, since electrons, ions and neutral particles have different average kinetic energies.

Non-thermic plasmas, known also as cold plasmas are characterized by the fact that temperature of weightier species (neutral and ionic particles) is close to ambient temperature (25-100 ºC). Temperature of electrons, in contrast, is much higher ($5.0 \cdot 10^3$-10^5 ºC). This type of plasma is usually generated at low pressure (down to 133 mbar) in reactors with diverse geometry using DC discharges, RF, microwaves or pulsed discharges systems. It exists special types of cold plasmas created with discharges called corona and dielectric barrier which are generated at atmospheric pressure by using pulses in the range of 10^{-6} s and 10^{-9} s. In such a discharge, very energetic electrons are released and due to the shortness of the pulses, electrons barely have time to exchange energy with their surroundings. Thus, a large temperature gradient between electrons and heavy species in the plasma is established. Density and electron temperature cover broad ranges. Thus, the electron density can reach 10^{25} e^-/cm^3, i.e. it even exceeds the concentration of electrons in metals.

A remarkable characteristic of cold plasmas is that they contain a large number of high-energy diverse species which activate physical and chemical processes difficult

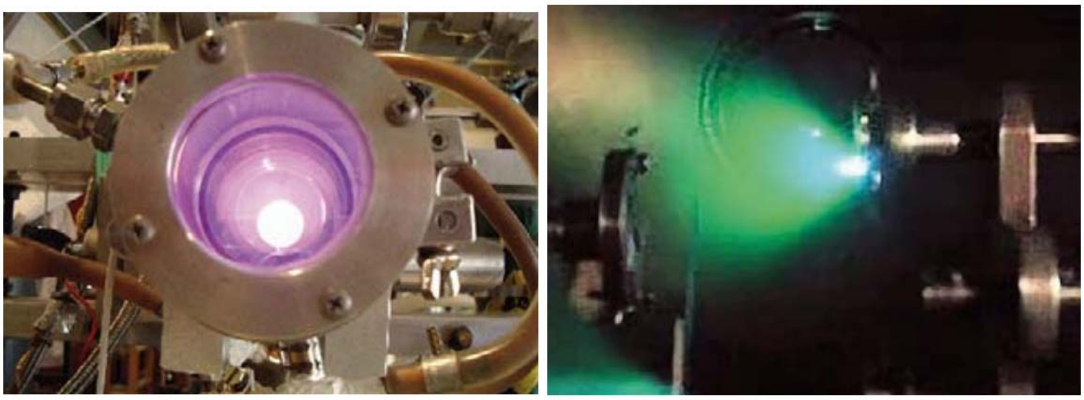

Figure 1.6. (Left) Cold plasma of air, generated by a CC electric discharge at low pressure simulating plasmas in the Earth's ionosphere. (Right) Cold plasma generated by pulsed laser deposition of an Ag with an excimer laser for the synthesis of nanostructured materials. Reprinted from [Gordillo, F. J., 2008].

to obtain in ordinary chemical environments. Among these species we can find photons in the visible and ultraviolet spectral range, charged particles (as electrons and ions), highly reactive neutral species, such as free radicals or oxygen, fluorine and chlorine atoms, excited atomic and molecular species, excimers (electronically excited molecules without a stable ground state) and monomers.

Chemistry on cold plasmas could be homogeneous (if reactions are carried out in gas phase) or heterogeneous (if plasma interact with a solid surface or a liquid).

1.2.3.3. PLASMA EXPANSION

The expansion of plasma vapor can be characterized into two phases **[Neamtu, J. et al., 1999]**:

(1) The ionization and plasma-heating phase in the presence of laser pulse, for $t<t_p$,

(2) The recombination phase corresponding to plasma cooling and relaxation after pulse termination, for $t>t_p$, where t_p is the duration of laser pulse.

There are a few models that describe the plasma expansion in presence of ambient gas **[Callies, G. et al., 1998][Gusarov, A. V. et al., 2000][Harilal, S. S. et al., 2003][Volkov, A. N. et al., 2008][Aghaei, M. et al., 2008]**. Nevertheless, the equations presented below belong to models pertaining to plasma expansion in vacuum.

Most of the models use hydrodynamic plasma expansion based methods to characterize the plasma. The basic assumption underlying this fact is that the plasma behaves as a continuum fluid. Thus, the plasma expansion is described by the Euler equations of hydrodynamics, expressing the conservation of mass, momentum and energy as **[Bogaerts, A. et al., 2003]**,

$$\begin{aligned}
&\frac{\partial \rho_{pl}}{\partial t} = -\frac{\partial(\rho_{pl} v)}{\partial x}, \\
&\frac{\partial(\rho_{pl} v)}{\partial t} = -\frac{\partial}{\partial x}(p + \rho_{pl} v^2), \\
&\frac{\partial}{\partial t}\left[\rho_{pl}\left(E + \frac{v^2}{2}\right)\right] = -\frac{\partial}{\partial t}\left[\rho_{pl} v\left(E + \frac{p}{\rho_{pl}} + \frac{v^2}{2}\right)\right] \\
&\qquad + \alpha_{pl} I - \epsilon_{rad},
\end{aligned} \qquad \textbf{(Eq. 1.10)}$$

where ρ_{pl} is the average density of the plasma vapor. In the above equation, the product of laser intensity I and plasma absorption coefficient α_{pl} gives the local laser energy absorption, which represents the laser heating of plasma. The factor ϵ_{rad}

represents the plasma plume energy loss per unit volume per unit time by Bremsstrahlung radiation.

To solve the system of conservation equations, two additional equations of pressure and internal energy have been usually considered **[Bogaerts, A. et al., 2003].** These are,

$$p = (1 + x_e)N_{pl}k_bT, \qquad \textbf{(Eq. 1.11)}$$

$$\rho_{pl}E = N_{pl}\left[\frac{3}{2}(1 + x_e)k_bT + IPx_i\right], \qquad \textbf{(Eq. 1.12)}$$

where N_{pl} is the average number density of the plasma species; and χ_e and χ_i are fraction of electrons and ions.

In order to account for the continuous production of plasma as a result of ablation, the authors have also considered a linear time dependent variation in plasma density and pressure during the pulse on-time. After the pulse termination, the number of plasma constituents was considered to be constant and the expansion was considered to be adiabatic.

Anisimov *et al.* **[Anisimov, S. I. et al., 1993]** used the above equations to model the plasma expansion process after termination of a pulse. As the pulse on-time is very small compared to the characteristic time of gas expansion, the authors have considered the initial expansion to be small and assumed the ablated material to be distributed into a half-ellipsoid shape above the target surface. The base cross-section of the ellipsoid plasma was assumed to be same as the beam cross-section and its transverse length was predicted considering the acoustic velocity of the plasma top surface. These dimensions were considered to be the initial dimensions of the plasma for the period after pulse termination.

In addition to above models, there are certain models which consider the plasma expansion in a background gas. Rozman *et al.* **[Rozman, R. et al., 2008]** used hydrodynamic equations similar to Eqs.1.10-1.12 to account for the effect of the background gas. They accounted for the pressure variation in the plasma due to the ambient gas, neglecting the chemical interaction between the ambient gas and the expanding plasma.

During the initial stages of plasma expansion, the densities are high and hence, the assumption of using the hydrodynamic theory to describe such expansion process may be justified. But as the plasma expands, its density decreases continuously. At distances far away from the target, the assumption of plasma being a continuum fluid can be subjected to question.

Some models assume that ablation occurs at a uniform rate and plasma concentration increases linearly with time. However, it is known that the effects of plasma shielding reduce the ablation rate. Therefore, it may be more appropriate to predict the ablation rate and use it in the further modeling of the plasma generation.

In addition to this, the plasma has been considered to have an uniform absorption coefficient at any given time. However, the high density near the surface of the target suggests that the absorption coefficient is higher in this region as compared to the region far away from the target surface. The absorption coefficient can be improved by considering it to be a function of the plasma density.

On the other hand, most of the researchers model the plasma expansion by equating it to an ideal gas. A wide error in the validation of results observed by Singh *et al.* **[Singh, R. K. et al., 1990]** is an indication that the behavior of plasma during the expansion process is not that of an ideal gas. Also, the issue that the plasma recombines to form a neutral gas during the expansion after the pulse termination, has not been addressed adequately. Though a qualitative validation has been reported by a few authors, quantitative agreements are not available. The plasma expansion needs to be modeled better, perhaps by including the charged particle nature of the plasma, where a PIC-MC (particle-in-cell Monte-Carlo) model may work better **[Marla, D. et al., 2011].**

The scheme in Figure 1.7 summarizes the phenomena that occurs in the complete process: shielding, ablation, plasma formation and plasma expansion. The plasma formation leads to shielding process and, in turn, to a decrease in ablation rate and therefore, a decay in the generation of new plasma by thermionic effect of the target. However, the radiation absorbed by the plasma during shielding also increases the thermal energy of the plasma and thereby, the expansion velocities of the plasma also increase. This leads to a decay in the plasma density and finally, in a reduction in shielding. Hence, it can be concluded that the four phenomena are mutually interdependent. The modeling of such a process should, therefore, be carried out by integrating all the phenomena, rather than classifying them and analyzing separately **[Marla, D. et al., 2011].**

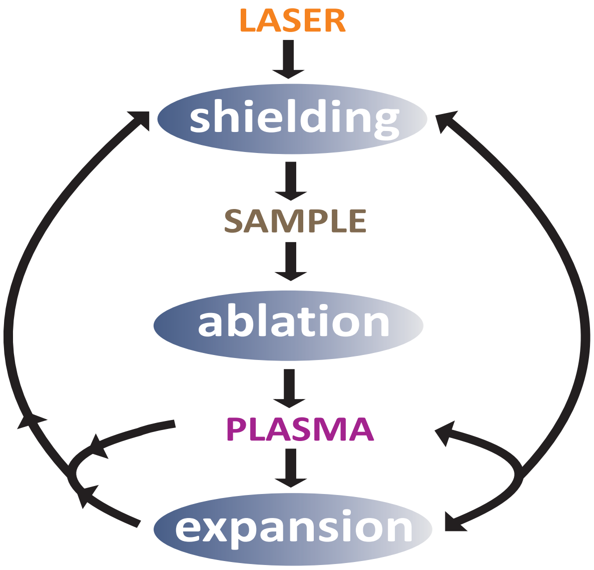

Figure 1.7. Scheme of the interdependence of phenomena in laser induced plasmas. Adapted from [Marla, D. et al., 2011].

1.2.3.4. PARAMETERS AFFECTING LASER INDUCED PLASMA FORMATION

The formation of laser-induced plasmas and their characteristics are strongly influenced by the laser operating conditions, i.e., laser wavelength (λ), pulse duration (τ), and energy reaching the sample (E). In addition, nature of the impinged material, nature of surrounding atmosphere and pressure in the medium play important roles in both the formation and the expansion of the plasma plume. The effects of these factors have been extensively discussed in the literature with the final goal of characterise the plasma as much as possible **[Aragon, C. et al., 2008][Gornushkin, I. et al., 2010][Konjevic, N. et al., 2010].**

Next sections will be focused on the particular effect that each input variable has on the parameters of the resulting plume.

1.2.3.4.1. INFLUENCE OF TARGET

Recent research on binary matrixes in air **[Aguilera, J. A. et al., 2009]** revealed the existence of a weak matrix effect that leads to a variation of physical plasma parameters, as only metallic samples were considered. Variation of plasma parameters was larger for materials having bigger differences on their physical properties. This was supported by other studies **[Viskup, R., 2009]**, as different formats featured by targets strongly influenced the processes occurring at the surface of the treated material. Hence, plume dynamics as well as particles ejected from the irradiated material seem to depend on the degree of target compaction. In this sense, recent experiments for metallic alloys **[Labutin, T. A. et al., 2009]** concluded that differences in plasma properties were caused by their different composition which induced changes in hardness of the material. It has been also proved that the ablated mass is in inverse proportion with hardness. Finally Schmit *et al.* **[Schmitz, T. A. et al., 2010][Schmitz, T. A. et al., 2011]** gave new experimental insights into the characteristics of atmospheric-pressure ablation of molecular solids by means of analytical MALDI applications, studying the early processes, material release and formation/expansion of hemispherical shock waves, in ablation of different common MALDI matrixes.

1.2.3.4.2. INFLUENCE OF LASER PARAMETERS

Laser radiation is likely the most important variable affecting the characteristics of the plasma. The effects take place during its interaction with the impinged sample and, then, with the plasma plume itself. In general, photons are coupled within the available electronic or vibrational states in the material depending on its wavelength. During this coupling, the material is heated to a determined temperature depending on the mechanism of laser-matter interaction, and the onset of ablation (either thermal or photochemical) occurs if the irradiance is above a particular threshold. Once the plasma plume is generated, its density may impede partially or entirely the way of laser radiation towards the sample surface, depending on the laser wavelength and pulse length. Consequently, just a fraction of the energy radiation is transferred from the laser pulse to the material.

1.2.3.4.2.1. LASER WAVELENGTH (λ)

From detailed studies about the effect of laser wavelength on plasma parameters can be extracted general trends and conclusions. In the case of metallic samples it was observed that using any laser wavelength in the ablation of the target, electron temperature and density decrease along the direction of plume propagation due to the rapid conversion of thermal energy into kinetic energy, in such away that the plasma expands and thermalize by transferring the energy to its surroundings **[Hanif, M. et al., 2011]**.

In general, the different absorption rate between nanosecond UV and IR radiations leads to different propagation behaviour of the produced plasmas from ablated metals **[Ma, Q. et al., 2012]**. In the study of Al targets using argon as background gas at a pressure of 1 bar it was noticed how for UV ablation the background gas is principally evacuated by the expansion of the vapour plume, and in the case of IR ablation, the background gas is effectively mixed to the ejected vapour during at least hundreds of nanoseconds after the initiation of the plasma. As a consequence, higher temperature and electronic density were observed for UV ablation than for IR ablation. These parameters confirm the existence of hotter, confined Al plasma for UV ablation, whereas for IR ablation, a larger axially extended Al vapour plume with a better homogeneity is observed. Such observations suggested descriptions by laser supported combustion wave and by laser-supported detonation wave for the propagations of plasma produced by UV and IR lasers, respectively.

Regarding the effect of type of radiation on mass ablation rate using nanosecond Nd:YAG lasers, results found that this parameter at the wavelength of 266 nm is an order of magnitude higher than at 1064 nm **[Mao, X. L. et al., 1998 A][Mao, X. L. et al., 1998 B]**. This is attributed to stronger plasma shielding and a higher target reflectivity at IR wavelengths, leaving less laser energy available for target evaporation. The same authors also reported a lower fluence threshold for mass ablation, and a more controlled ablation rate, at shorter wavelengths **[Russo, R. E. et al., 2000].** According to an empirical formula **[Fabbro, R. et al., 1982]** based on experiments for laser wavelengths at 1064, 532 and 266 nm, the mass ablation rate varies with $k^{-4/3}$, hence longer wavelengths correspond to a reduced mass ablation.

Studies about the effects of different type of laser source on plasmas **[Campos, D. et al., 2010][Harilal S. S., 2011]** noticed several outstanding differences in the features of the plumes. The major differences involved the spatial−temporal evolution of electron density and regarding the hydrodynamic expansion of the plasmas. When 1.06 µm Nd:YAG (6 ns) and 10.6 µm CO_2 (30 ns) lasers were used, the analysis of craters created confirmed a larger mass ablation rate for Nd:YAG plasmas compared to that produced with CO_2 lasers. A significant difference in electronic temperature between CO_2 plasmas and Nd:YAG plumes was also observed. When single-pulse plasmas generated using 1.06 µm Nd:YAG laser were compared with dual-pulse plasmas (reheated by a 10.6 µm CO_2 laser) **[Coons, R. W. et al., 2012]**, results concluded that the Nd:YAG-CO_2 laser combination improved the sensitivity by the effective reheating effect resulting from efficient inverse Bremsstrahlung (IB) absorption of the longer wavelength. It is thus clear that a proper choice of the wavelength allows one to produce a plume with better properties for analytical applications.

An interesting result about the effect of laser wavelength on ablation of organic materials is reported in Chapter 8 of the present memory.

1.2.3.4.2.2. LASER PULSE DURATION (τ)

Regardless their duration, laser pulses usually reach the required conditions for ablation of the sample when the rate of energy deposition greatly exceeds the rate of energy redistribution and dissipation, thus resulting in extremely high temperatures in those regions where energy absorption occurs. Nevertheless, as a consequence of the different mechanisms of energy dissipation in the sample, differences in pulse duration result in fundamental differences of the ablation process. Indeed, interaction of nanosecond (ns) pulses with materials is substantially different from that of femtosecond (fs) pulses since the rate of energy deposition is significantly shorter in the latter case. Thus, for ns pulses, the material undergoes transient changes in the thermodynamic states from solid, through liquid, into a gas ionized or plasma state. Furthermore, energy in the first stages of laser pulse goes into both the ablation of material and the generation of the plasma, and the remaining part of the pulse heats the plasma instead of interacting with the target. In the case of ultrashort laser pulses, at the end of the laser pulse, only a very hot electron gas and a practically undisturbed lattice are found **[Fortes, F. J. et al., 2013]**.

The effect of laser pulse duration on laser induced plasma emission, electron density and plume temperature has been extensively studied. When pulses of 50 ps and 10 ns were compared at a fixed laser fluence, and hence, different laser irradiance **[Rieger, G. W. et al., 2003]**, calculations with a plasma ablation model showed that in the initial plasma, both temperature and electron density are found to be significantly higher for the 50 ps pulse, because of the higher laser irradiance. However, at later times, not much difference is observed between the pulses of 50 ps and 10 ns, and it seems that the plasma characteristics then depend on the total energy deposited, and not on the pulse duration. In addition, it was experimentally observed how the plume expansion velocity increases drastically for picosecond pulses compared to nanosecond pulses **[Borchert, H. et al., 2005]**. However, other studies compared laser pulses of 500 fs, 5 ps and 270 ps of a Ti:sapphire laser at very high irradiance (at constant fluence), and the measured excitation temperature for large delay times was found higher for the longer pulses, whereas electron density was found to be independent from laser pulse duration **[Le Drogoff, B. et al., 2004]**.

On the other hand, investigation performed on the effect of laser pulse duration on the ablation rate **[Mao, X. L. et al., 1998 A][Mao, X. L. et al., 1998 B]** showed that shorter pulses gave rise to more efficient laser ablation. The mass ablation rate for ps-pulses was found an order of magnitude higher than for ns-pulses, which was attributed to different mechanisms. In the ns-pulse range, thermal vaporization processes governed whereas non-thermal mechanisms take place when picosecond pulses are used. Hence, in the nanosecond regime there seems to be more energy lost in the sample by thermal dissipation, and less energy is converted to ablated mass. The important role of laser−plasma interaction during the plasma evolution when using a relatively long pulse is underscored. Moreover, plasma shielding is more predominant for long laser pulses.

When the plasma plume is generated from metallic plates immersed in water using different ns pulse widths **[Sakka, T. et al., 2009]**, a minimized damage and efficient heating of the plume was observed for long pulses due to the direct absorption of the later part of the pulse. Thus, long ns pulses were more favorable for this laser application due to the relatively slow heating of the plasma, causing a larger and less-dense plume and, consequently, fairly intense and less broadened emission lines.

1.2.3.4.2.3. LASER PULSE ENERGY (E)

Ablation and plasma formation are largely affected by the laser pulse energy, closely connected with pulse duration. In fact, laser energy is one of the most important parameters modifying the response of the target. In laser ablation, the energy per unit area that can be delivered to the target is more important than the absolute value of E. Thus, the primary energy-related parameters influencing the laser−matter interaction are usually termed either as fluence (energy per unit area, J/cm^2) or as irradiance (energy per unit area and time, W/cm^2). Experimental determination of fluence or irradiance requires a careful evaluation of the spot size over which the laser beam is focused. However, despite that change on focusing distance introduces a degree of flexibility in the energy frame to be able to reach identical fluence/irradiance levels, the experimental conditions brought into play are not equivalent, since plasma plumes generated using different pulse energies and focusing distances show a spatial and temporal scaling **[Fortes, F. J. et al., 2013]**.

Typical irradiances for laser ablation range from 10^8 to 10^{10} W/cm^2. Below these values, neither melting nor boiling is occurring **[Bogaerts, A. et al., 2005]**. Above this irradiance level, different processes, like phase explosion, may become important. In the model by Chen and Bogaerts **[Bogaerts, A. et al., 2005]**, increasing the laser irradiance will increase the target heating, melting and boiling. Also, plume expansion velocity and temperature, ionization degree and both ion and electron densities in the plume will increase. As a consequence of all these increasing parameters, plasma shielding in the plume will also get more significant.

Regarding some suggesting investigations about the effect of laser irradiance on physical parameters of plasmas, it was observed the trends followed by temperature and electron density with variation of laser energy pulse. In a general way, both parameters underwent an increase with the raise of the irradiance using IR nanosecond pulses in air at atmospheric pressure onto metallic targets **[Luo, W. F. et al., 2010]**. Furthermore, spatial evolution of these plume parameters in the axial direction above the target surface was observed. Hence, density is highest near the target surface and decreases at larger distances from the origin due to the recombination processes between species. On the other hand, temperature slightly decreases at the periphery of plasma due to the higher radiative cooling at this area and the rapid conversion of thermal energy into kinetic energy. Also close to the target surface the temperature is lower because of thermal conduction from the plasma toward the target. Investigating the influence of laser irradiance on the early stage structure and dynamics of induced plasmas from metallic samples **[Cirisan, M. et al., 2011]** it was observed how at high irradiance values (using IR nanosecond radiation) the plume, containing more ablated matter and having higher internal energy, is capable of pushing the surrounding air far enough in order to expand into a hemispherical shape. However, at lower irradiances, the ablation plume has less energy, so its expansion in the radial direction prevails over that in the longitudinal direction, so the plume core remains close to the sample surface, having a flatter shape.

It is worth to mention that energy density is one of the key parameters in the studies performed in this memory regarding laser ionization and ablation processes of hazardous organic compounds by means of both mass and optical spectroscopy.

1.2.3.4.3. INFLUENCE OF SURROUNDING GAS

The consequences of using reduced pressure and atmospheres of different nature on acquired emission signals from laser-induced plasmas of organic compounds are further discussed in chapters 7 and 8 of the present memory.

Laser ablation and plasma formation performed in reduced pressure environments as well as in gases other than air imply significant differences on dynamics of the plume and mass ablation rates. The interest in the analysis of induced plasmas in other atmospheric conditions different from such in Earth has increased in recent years especially for its application in space exploration. In fact, emission from induced plasmas have presented enhanced features and improved ablation when studies were performed at pressures below atmosphere **[Iida, Y., 1990]**. Specifically, these enhancements in emission spectroscopy are an increase in spectral intensity, spectra signal-to-noise ratio, spectra resolution and more uniformed ablation craters. Improvements are generally observed using any laser pulse duration. However, it seems that only lasers with longer pulse lengths can take advantage of lower pressures for ablation purposes **[Effenberger, A. J. et al., 2010]**. The majority of photons from femtosecond lasers reach the surface of the target before the laser plasma develops, while with the nanosecond pulse lasers, a significant portion of the photons are able to interact with the expanding plume. At reduced pressures, plasma generated with a nanosecond pulse is expanding in a less dense atmosphere, which results in a reduced plasma shielding and an increased sample ablation **[Delgado, T. et al., submitted A]**. However, if the pressures are reduced under a critic value, then plasma confinement is lost and emission tends to degrade. In the case of using a femtosecond laser, there is little plasma shielding, so another processes must be considered for the spectral enhancement observed at reduced pressures **[Margetic, V. et al., 2000][Yalcin, S. et al., 2004].**

During LIBS plasma expansion, energy is lost to the surrounding atmosphere. This loss of energy reduces the lifetime of the laser plasma. Therefore, reducing the pressure increases the lifetime of the plasma. On the other hand, the use of background high-pressures in emission spectroscopy experiments implies plasmas with too much density and the consequent increment in plasma shielding, so a lack of spectral intensity and signal-to-noise ratio is observed **[Arp, Z. A. et al., 2004]**.

Extensive research has been carried out in order to providing a further insight into the effect of atmospheric composition in plasma physical parameters, the features of plasma emission as well as mass removal during ablation process **[Mao, X. L. et al., 1993][Lee, Y. I. et al., 1997][Aguilera, J. A. et al., 1999][Vors, E. et al., 2008][Delgado, T. et al., submitted B].** The physical properties of background gas (ionization potential, thermal conductivity, density, etc.) have a decisive role in laser ablation, plasma formation and plume expansion stages. As example, helium as background gas may be useful by improving emission response due to its high thermal conductivity **[Lee, Y. I. et al., 1997]**. The higher the thermal conductivity, the more rapidly a plasma will cool, which leads to a shorter plasma lifetime.The more the details of what occurs in the LIBS plasma are understood, the easier it will be to optimize emission detection systems for extreme environments and applications requiring high resolution and signal-to-noise ratio **[Effenberger, A. J. et al., 2010].**

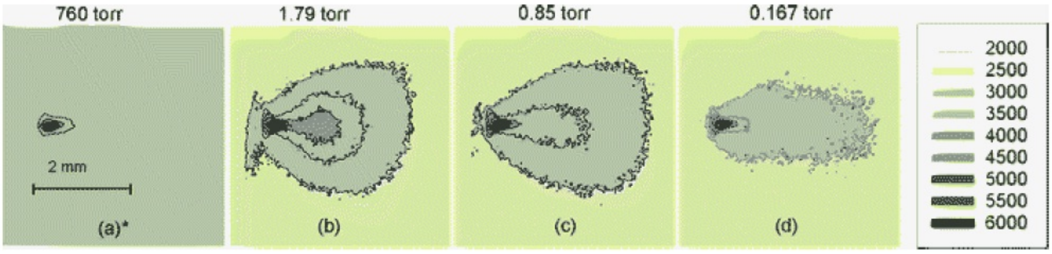

Figure 1.8. Two-dimensional Cu plasma images at different pressures produced using 50 μJ femtosecond laser pulses. Reprinted from reference [Yalcin, S. et al., 2004].

1.2.3.5. LASER ABSORPTION IN THE PLASMA

In ambient air, the plasma created due to ablation shields the target surface by absorbing a part of incoming laser radiation. It is well-known that the absorption is strong at distances very close to the target surface, where densities of the plasma species are very high. At larger distances from the target surface, the plasma is more permeable to the incoming radiation. This is because the densities of the plasma constituents decrease as the plasma expands. Moreover, there is a continuous addition of plasma species into the region close to the surface due to the ablation process, while the ions move out of the top surface due to expansion **[Singh, R. K. et al., 1990 A]**. This closer region can be assumed to be of constant thickness throughout the process, where the densities of the plasma constituents are almost uniform. Precisely due to the different nature of species forming the plasma (electrons, ions, and neutral atoms), the absorption of the radiation inside the plasma occurs by different mechanisms. There are two dominant mechanisms by which the radiation is absorbed by the plasma: inverse Bremsstrahlung (IB) and photoionization (PI) processes. Absorption of photons by free electrons in the plasma is described by IB mechanism **[Singh, R. K. et al., 1990 B]**, while absorption by excited ions and neutral atoms is described by PI mechanism **[Neamtu, J. et al., 1999]**. Mie absorption, a less dominant mechanism, which involves absorption by clusters formed due to condensation of supersaturated vapor inside the plasma, has also been reported. If α_{IB}, α_{PI} and α_{Mie} are the absorption coefficients associated with IB, PI, and Mie mechanisms, respectively, then the total absorption coefficient of plasma α_{pl} can be expressed as,

$$\alpha_{pl} = \alpha_{IB} + \alpha_{PI} + \alpha_{Mie} \qquad \textbf{(Eq. 1.13)}$$

Assuming that the attenuation of laser by plasma in region closer follows the Beer–Lambert law, the intensity of the radiation at the bottom of the region can be estimated as the intensity of radiation reaching the top surface of the target as follows **[Zhang, D. et al., 2005]**,

$$I_0 = I_{inc} \exp(-\alpha_{pl} H) \qquad \textbf{(Eq. 1.14)}$$

where I_{inc} is the intensity of the incident laser before shielding and H is the dimension of the plasma perpendicular to target.

As far as the relative importance of the three absorption mechanisms is concerned, recent studies **[Rozman, R. et al., 2008]** showed that the Mie absorption is dominant at low fluences, which is due to the high condensation rate that occurs at low temperature. The PI absorption mechanism has a major influence at high fluences. This is because at high plasma temperatures, vapour atoms become thermally excited and the PI mechanism becomes prominent. Of the three absorption mechanisms, IB has the least influence at low wavelength of the incident radiation. This is because the absorption coefficient for IB process is inversely proportional to the frequency of laser radiation. However, the IB mechanism becomes prominent at higher wavelengths **[Fang, R. et al., 2007]**.

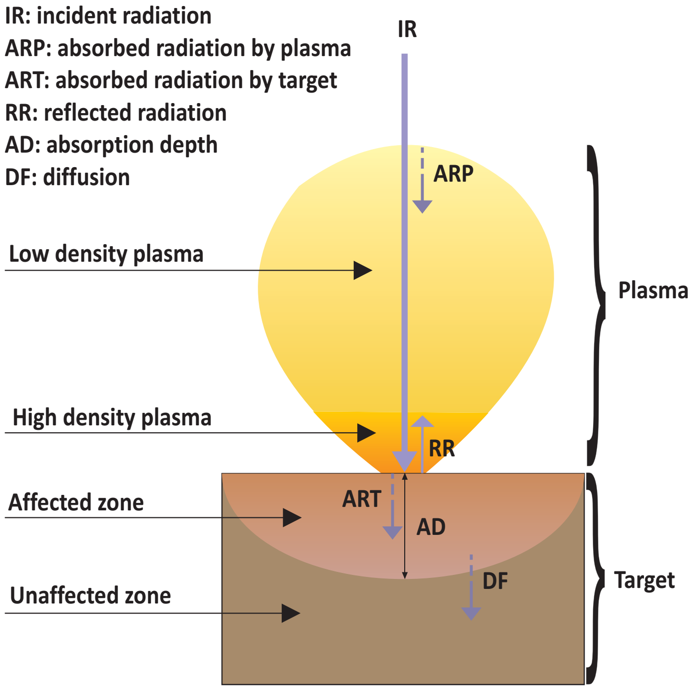

Figure 1.9. Scheme of the interaction of laser with plasma and sample surface. Adaptation from reference [Singh, R. K. et al., 1990 A].

1.3. FUNDAMENTALS OF LASER ABLATION IN ORGANICS

Interaction laser beam-sample surface is highly dependent on physical characteristics (optical, mechanical and thermodynamic properties) of the sample materials as it was presented above. Therefore, the plasma formation of organic compounds is largely different than that from metals. In the late 1960's and early 1970's Mumma and Vastola **[Vastola, F. J. et al., 1968][Vastola, F. J. et al., 1970]** investigated the laser-induced ionization of both inorganic and organic solids, followed by others who investigated also the interaction between laser radiation and organic compounds **[Minsek, D. W. et al., 1990].** Most recently, microscopic mechanisms in laser ablation of organic solids were studied in detail including the influence of parameters in the ejection of material and the plume expansion **[Zhigilei, L. V. et al., 2000].** Regardless the sample type, the cloud of ablated material (consisting of excited or ground-state neutrals, electrons and ions) moves away from the surface in all directions but preferentially along the target normal. However, in the case of organics, laser-matter interaction leading to ablation and plasma formation involves chemical processes of fragmentation and recombination more complex than those in metals. In fact, information on microscopic mechanisms and the nature of the laser-induced processes at the submicron scale is still under study.

The mechanisms and parameters responsible for ejection of ablated material in organics were found to have a strong dependence on the rate of the laser energy deposition**.** Two different irradiation regimes were differentiated in the laser ablation and damage of organic materials: *stress confinement* and *thermal confinement* **[Zhigilei, L. V. et al., 2000].** The conditions for both confinement regimes as well as some of the qualitative aspects of thermal and mechanical mechanisms of laser ablation are roughly understood. In this sense, the short time of the energy deposition in laser ablation of organic solids is critical.

When the laser pulse duration is shorter than the time of dissipation of the absorbed laser energy by thermal conduction, the condition is commonly referred to as *thermal confinement* **[Zhigilei, L. V. et al., 1999].** Thus, pulse duration in the regime of *thermal confinement* is usually shorter than the time needed for gas phase bubble formation and diffusion in the process of heterogeneous boiling **[Miotello, A. et al., 1999]**. As a result, the absorbing material can be overheated far above the boiling temperature, turning a normal surface evaporation at low laser fluences into an explosive vaporization at higher fluences **[Zhigilei, L. V. et al., 1997]**. An onset of massive material removal, or ablation, is defined in this case by the critical energy density sufficient for the overheating of the surface layer up to the limit of its thermodynamic stability. It has been predicted (based on thermodynamic considerations) that phase explosion results in a spontaneous and homogeneous decomposition of the expanding plume into a two-phase system of gas-phase molecules and liquid droplets **[Kelly, R. et al., 1999].** This decomposition proceeds through the formation of a transient structure of interconnected liquid clusters and individual molecules and leads to fast cooling of the ejected plume. In the absence of photochemical decomposition, that involves a direct photodissociation of the molecular bonds and could be dominant in the deep ultraviolet, an explosive vaporization is likely to be a major mechanism of ablation of organic materials at sufficiently high laser fluences **[Tsuboi, Y. et al., 1998].** There are, however, a significant number of experimental observations suggesting that ablation can be initiated at the energy densities much lower than those required for boiling and vaporization. A plausible explanation for the onset of cold laser ablation has been proposed based on consideration of photomechanical effects caused by laser-induced stresses **[Dingus, R. S. et al., 1991][Venugopalan, V., 1995].**

When the laser pulse duration is equal or lower than the time needed to initiate a collective motion of molecules within the absorbing volume of irradiated material, the laser heating takes place at nearly constant volume conditions, causing a high thermoelastic pressure accumulation. This condition is usually referred to as *inertial* or *stress confinement* **[Itzkan, I. et al., 1994].** In the regime of *stress confinement*, lower threshold fluence for the onset of laser ablation and damage is observed. Thus, the energy density needed for material removal is well below the one for vaporization. The energetically efficient material ejection is attributed to photomechanical effects driven by the relaxation of high thermoelastic pressure that builds up in the absorption region under the conditions of stress confinement. Laser ablation in this case proceeds through void nucleation and growth which eventually lead to disintegration and ejection of large **[Webb R. L. et al., 1997]** and relatively cold pieces of material. At laser fluences close to the ablation threshold, the mechanical fracture is localized at a certain depth under the surface that is defined by the balance between the tensile stresses that are increasing with depth and the decreasing thermal softening due to the laser heating. At higher laser fluences material can lose its integrity over a larger surface region **[Zhigilei, L. V. et al., 2000]**.

The evidence discussed above suggests a strong dependence of the threshold fluence on the onset of ablation, the parameters of the ejected plume, and the character of the damage done to the target on the balance between the thermal and mechanical processes induced by laser irradiation.

1.4. SPECTROSCOPY OF LASER-INDUCED PLASMAS

Plasmas generated by the action of laser sources or other excitation sources in a controlled system can be characterized by spectroscopic analytical techniques, especially by optical methods **[Hollas, J. M., 1987][Broekaert, J. A., 2002]**. A brief review about atomic emission spectroscopy and the fundamentals on molecular spectroscopy are presented below.

1.4.1. FUNDAMENTALS OF ATOMIC EMISSION SPECTROSCOPY

Spectroscopy is the measurement and interpretation of electromagnetic radiation absorbed, scattered or emitted by atoms, molecules or other chemical species. These phenomena are associated to changes in the energetic states of the different species, and due to each species possess characteristic energetic states, the spectroscopy can be used to identify them.

Emission spectroscopy can be defined as an analytical method based on the light emitted by excited species in a flame, an induced plasma, an arc discharge or a spark generated by a thermal or electric stimulus. Therefore, the species are generated and analyzed in a high-energy gas medium which constitutes a vaporization-atomization-ionization-excitation source.

Excited atoms or molecules at high energy levels can fall down to lower energy levels emitting radiation (emission or luminescence). In the case of excited atoms by means of a high-temperature energy source, the emission of light is commonly called *atomic* or *optic emission* (Atomic Emission Spectroscopy, AES) whereas when atoms are excited directly by light the method is called *atomic fluorescence* (Atomic Fluorescence Emission, AFE).

Therefore, radiant energy emitted when the analyte returns to lower states give us information about its nature (qualitative) and concentration (quantitative). Results of analysis are normally showed as a spectrum where emitted radiation is sketched with the variation of frequency or wavelength.

The main factors determining the intensity of emission in AES are the energetic distribution of excited levels, the probability of emission and absorption transitions, the atomic absorption coefficient and the characteristic of atomization cell.

In the case of plasma in a *closed* system, i.e. in thermodynamic equilibrium, distribution of excited states is described by the Boltzmann low:

$$n_q / n_0 = (g_q / g_0) \exp(-E_q/kT) \qquad \textbf{(Eq. 1.15)}$$

where n_q is the number of species in excited state, n_0 is the number of species in fundamental state, g_q and g_0 are statistical weight of the corresponding levels, E_q is the excitation energy of state q, k is the Bolzmann constant and T is the absolute temperature.

The resulting atomic lines in emission spectrum corresponding to allowed transitions present a natural width corresponding to the lifetime of the excited state (τ). The full width at half height of the line (FWHM) in frequency terms is given by,

$$\Delta\upsilon_N = 1/2\pi\tau. \qquad \textbf{(Eq. 1.16)}$$

However, different mechanisms in the plasma can cause a higher spectral widening. Thus, *Doppler effect* is due to the dynamic of emitting atoms and their velocity in the direction of light collection whereas *Stark* and *pressure widening* are caused by local electric fields and impacts of charged particles in the system, respectively. Stark widening is the most common effect in laser-induced plasma spectroscopy since plasmas of high electronic density are usually created.

1.4.2. FUNDAMENTALS OF MOLECULAR EMISSION SPECTROSCOPY

When an atom or a molecule absorbs or emits a photon of energy *hv,* it makes a transition from a state with energy E_1 to another state with energy E_2. Energy conservation requires that,

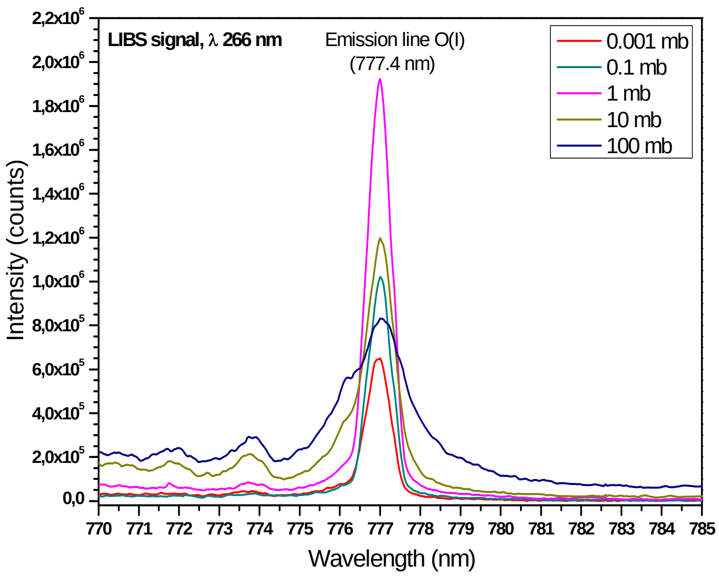

Figure 1.10. Detail of spectral widening in O(I) emission line (777.4 nm) due to pressure effect in UV-LIBS analysis of DNT.

$$hv = E_1 - E_2 \qquad \textbf{(Eq. 1.17)}$$

The states involved can be discrete, bound states with sharply defined energies. In this case, the transition takes place at an equally sharply defined frequency v. In a spectrum such a transition shows up as a sharp line at the wavelength $\lambda=c/v$. Frequently, wavenumbers $V=1/\lambda$ are used instead of wavelengths λ or frequencies v.

Atomic emissions are normally associated to a unique transition between two electronic levels. However, molecular emissions are generally more complex since molecules have additional internal degrees of freedom, and their states are not only determined by the electronic states but also by the geometrical arrangement of the nuclei and their movements, so transitions are multiple between a group of energetic levels corresponding to the ground and excited states of the molecule **[Demtroder, W., 2005]**. First, molecules possess more electronic states than atoms. Second, the nuclei in the molecule can vibrate around their equilibrium positions. Finally, the molecule as a whole may rotate around axes through its center of mass. Therefore, for each electronic molecular state there exist a large number of vibrational and rotational energy levels. Figure 1.11 shows the schematic visualization of the energy levels of a diatomic molecule.

Molecular spectra can be categorized as follows:

- Transitions between different rotational levels for the same vibrational (and electronic) state lead to pure rotational spectra with wavelengths in the microwave region ($\lambda \approx$ 1 mm to 1 m).
- Transitions between different rotational levels and in different vibrational levels of the same electronic state lead to vibration-rotation spectra in the mid-infrared with wavelengths of $\lambda \approx$ 2-20 μm.
- Transitions between two different electronic states have wavelengths from the UV to the near infrared (λ = 0.1-2 μm). Each electronic transition comprises many vibrational bands corresponding to transitions between the different vibrational levels of the two electronic states involved. Each of these bands contains many discrete rotational lines with wavelengths λ or frequencies $v=c/\lambda$ given by,

$$hv = (E_2^{el} + E_2^{vib} + E_2^{rot}) - (E_1^{el} + E_2^{vib} + E_2^{rot}), \qquad \textbf{(Eq. 1.18)}$$

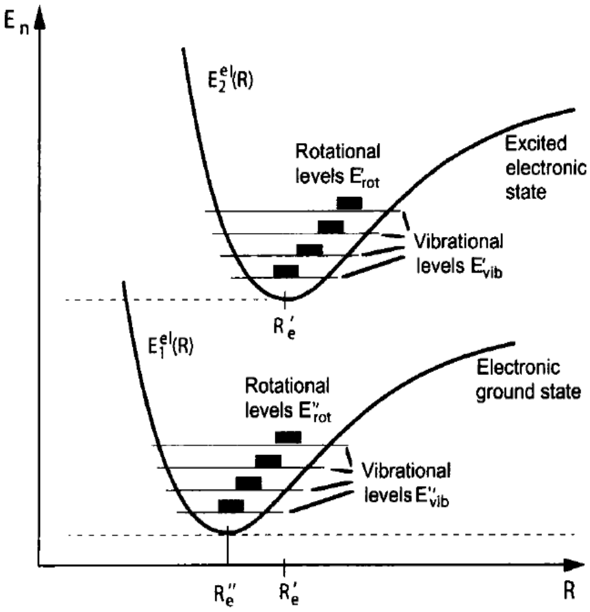

Figure 1.11. Schematic visualization of the energy levels of a diatomic molecule. Reprinted from [Demtroder, W., 2005].

as required by energy conservation (see Figure 1.11). As an example, Figure 1.12 shows a broadband emission spectra of an organic high energetic compound (2,6-Dinitrotoluene) in the visible spectral range acquired by LIBS technique at atmospheric pressure. The different vibrational bands corresponding to molecular emission systems C_2 Swan and CN Violet and the discrete rotational lines at characteristic wavelengths are indicated. As commented before, these two molecular emission systems are the most important in emission spectroscopy of organic compounds:

- C_2 Swan System ($D^3\Pi g \rightarrow A^3\Pi u$): this molecular bands system was discovered by W. Swan in 1856. It is one of the oldest observed and assigned molecular electronic spectra **[Johnson, R. C., 1927]** and its appearance is due to the electronic transition $D^3\Pi g \rightarrow A^3\Pi u$. The most intense emission is detected at 516.5 nm (band head of *Δv=0* sequence (0,0 mode)). The complete system is showed in Table 1.1. The presence of this band in emission spectra is directly related to the presence of insaturations in the structure of the molecule.

- CN Violet System ($B^2\Sigma \rightarrow X^2\Sigma$): The violet system of molecule diatomic CN corresponds to radiative transitions between the $B^2\Sigma^+$ and $X^2\Sigma^+$ electronic state at 3.32 eV and 0 eV, respectively. It is present in most of the plasma sources containing hydrocarbon and nitrogen in mixture for a temperature between 2000K and 6000K **[Kovacs, I., 1969].** The strongest emission is normally observed at 388.2 nm and corresponds to the band head of $\Delta v=0$ sequence (0,0 mode). Again, the complete system is detailed in Table 1.1.

The analysis of a molecular spectrum is usually difficult. It provides a wealth of information, however. Whereas the rotational spectra yield the geometrical structure of the molecule, the vibrational spectra give information on the forces between the vibrating atoms in the molecule, and the electronic spectra tell us about the electronic states, their stabilities, and their electron distributions. Line-widths can, under suitable experimental conditions, give information on the lifetimes of excited states or about dissociation energies. The complete analysis of a spectrum with sufficient spectral resolution provides a great deal of information on a molecule. Therefore, it is worthwhile to put some effort into the complete interpretation of a molecular spectrum.

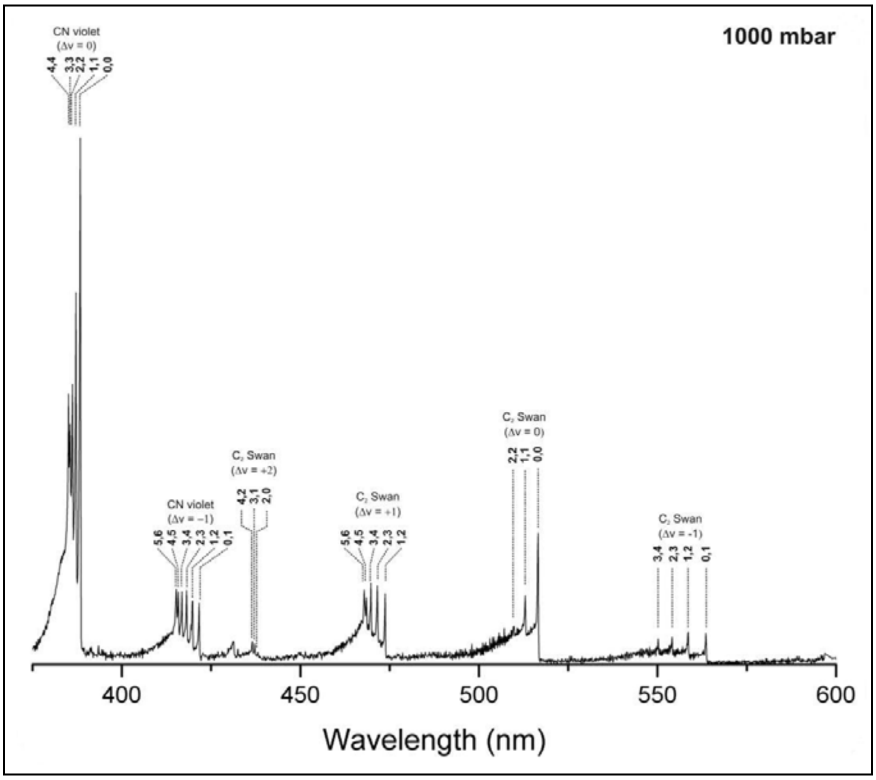

Figure 1.12. LIBS spectra of 2,6-Dinitrotoluene acquired at atmospheric pressure using a Nd:YAG (5 ns, 100 mJ) laser emitting at 1064 nm.

Table 1.1. Nomenclature of main emission spectral bands identified by LIBS for nitro organic compounds. Exact values for λ emission from [Pearse, R. W. B. et al., 1976].

Molecular band	System	Identification	λ emission, nm
C_2	$(D^3\Pi g \rightarrow A^3\Pi u)$	v´= 4, v´´= 2	436.5
		v´= 1, v´´= 0	473.7
		v´= 0, v´´= 0	516.5
		v´= 0, v´´= 1	563.5
		v´= 1, v´´= 3	612.2
CN	$(B^2\Sigma \rightarrow X^2\Sigma)$	v´= 2, v´´= 1	358.6
		v´= 0, v´´= 0	388.3
		v´= 0, v´´= 1	421.6
NH	$(A^3\Pi - X^3\Sigma^-)$	v´= 0, v´´= 0	336.0
		v´= 1, v´´= 1	337.0
OH	$(A^2\Sigma^+ - X^2\Pi)$	v´= 0, v´´= 0 (Q_2)	308.9
CH	$(A^2\Delta - X^2\Pi)$	v´= 0, v´´= 0	431.4

Diatomic molecules are the simplest and more reactive in the plume, and their origin is still investigated nowadays. Due to the large amount of energy required to get the ablation of the material and generate the plasma, the presence of high molecular weight fragments in the plume is hardly possible. The fragmentation pathways followed by different resulting fragments in the plume are still questioned **[Delgado, T. et al., submitted C]**, and there are a lot of factors affecting the mechanisms of plume chemistry: irradiance level, laser wavelength and pulse duration, pressure and type of background gas, etc. An extensive work about this issue was carried out in the present memory, covering in particular chapters 3 and 6.

1.4.3. SPECTROSCOPIC TECHNIQUES BASED ON LASER ABLATION

A wide range of analytical techniques are available for the characterization of solid materials. The combined use of several of those techniques, demanding in most cases a high spatial resolution, is usually required as no single technique provides the whole description of the solid. Hence, they offer partial views in this characterization. The required information to understand the properties and reactivity of a solid surface includes the physical topography, the chemical composition, the chemical structure, the atomic structure, the electronic states and a detailed description of bonding of molecules, among others **[Vickerman, J. C., 2009]**. Multiple probes can be used for surface characterization, including fields (thermal, electric, magnetic and sonic surface waves) and particle beams (electrons, neutrals, ions or photons). These input probes lead to the emission, transmission or scattering of four particles (electrons, neutrals, ions or photons) beams that can be analyzed with a suitable detector, giving rise to that large number of characterization techniques (see Table 1.2).

Among all different types of information regarding the chemical analysis of the material, the most requested one is usually related to the elementary or atomic composition of the sample, and for this purpose we count on the help of well-established techniques such as XPS (X-ray Photoelectron Spectroscopy), AES (Auger Electron Spectroscopy) or SEM (Scanning Electron Microscopy). However, these techniques have limitations in sensitivity they can reach.

Significant benefits and capabilities are brought into practical chemical analysis with laser sampling **[Russo, R. E. et al., 1998][Becker, J. S. et al., 1992][Rusak, D. A. et al., 1998][Russo, R. E. et al., 1995].** In combination with the proper detection system, it becomes an attractive technique for the elemental composition analysis of different samples through different spectroscopic methods. Among these methods, the optical spectroscopy is particularly suited for the study of neutrals and excited species. In contrast to optical spectroscopy, mass spectroscopy and charge collection techniques allow for the investigation of charged particles in the plume and provide useful information about the ion yields of the ablated particles.

Optical spectroscopy encompasses different type of techniques that can be classified according to the type of radiation source or depending on the nature of the interaction. Another possible classification takes into account the type of information provided by the method either qualitative (such as IR or Raman spectroscopy) or quantitative information (as Atomic Emission or Atomic Absorption Spectroscopy),

Table 1.2. Summary of analytical spectroscopy techniques [Ríos, A. et al., 2013].

Non-spectroscopic optical techniques	Photon spectroscopy: techniques				Electrons and Ions spectrometry	
REFRACTOMETRY INTERFEROMETRY POLARIMETRY TURBIDIMETRY NEFELOMETRY DIFFRACTION X-RAY	MOLECULAR			ATOMIC	IONS	ELECTRONS
	ABSORPTION	EMISSION	DISPERSION	UV-V ABSORPTION UV-V EMISSION X-RAY FLUORESCENCE	MASS SPECTROMETRY (ATOMIC AND MOLECULAR)	XPS AUGER UPS
	UV-VIS IR NMR	LUMINISCENCE	RAMAN			

even offering the possibility of using it for identification purposes. Among classified as quantitative techniques, a few are based on similar principles but leading to different applications, thereby obtaining data with different features. This is the case of laser induced atomic fluorescence **[Baiocchi, C. et al., 1994][Stchur, P. et al., 2001][Butcher, D. J. et al., 2005]**, which could be included in the emission spectroscopic techniques.

In next sections, Laser Induced Breakdown Spectroscopy (LIBS) is described in detail, with especial emphasis on instrumentation and applications of the technique.

On the other hand, mass spectrometry is one of the most promising techniques for its capabilities of sensitive, precise, and accurate multielemental determinations as well as isotope ratio measurements. In recent years, mass spectrometry in the field of spatially-resolved surface analysis has also undergone a fast development and has become one of the most versatile and suitable detection techniques for the analysis of samples in condensed phase, offering ideal features such as its ultrahigh detection sensitivity, its applicability for accurate multielemental determinations, its capability for providing accurate molecular mass and structural information on both organic and inorganic analytes, as well as isotope ratio measurements **[Becker, J. S., 2000].** In next sections, the main MS techniques for the analysis of solids and surfaces are briefly introduced. Laser Ionization Mass Spectrometry (LIMS) will be described in detail, with especial emphasis on fundamentals, instrumentation and applications of the technique.

Laser desorption followed by laser ablation of a solid is one of the more important analytical applications of lasers, including the characterization of organic compounds of different nature (biochemical, polymers…). It was first described in 1962 **[Brech, F., 1962]** and both the design and performance of devices have evolved dramatically in the last half century.

Diagnostic of the formed plasma from ablated material by the action of a high energy laser pulse could be suitable via atomic emission or ion detection for the determination of the chemical species contained in the lattice of the affected material. For many analytical techniques, laser-ablation is used as a sampling method, as it occurs for LA-ICP-MS, where ablated plume is transported to an ICP torch where the whole sample is fully atomized and ionized before a detection system (Optical Emission Spectroscopy or Mass Spectroscopy) acts. In other cases, plasma formation and collection of its optical emission are the final purpose of the laser ablation, as it happens for the case of LIBS, a spectroscopic technique that joins together a surprising simplicity and high versatility.

Laser desorption and ablation regimes have cover a wide range of applications in modern spectroscopy with different approaches in last decades **[Cremers, D. A. et al., 2000][Miziolek, A. W. et al., 2006][Mao, X.L. et al., 1998][Lee, W. et al., 2004].** As the present investigation deals with laser ionization mass spectrometry and laser-induced breakdown spectroscopy, LA-ICP-MS is further briefly described, as it combines the application of the laser ablation with the ultra-high sensitivity of mass spectrometry.

In laser ablation diagnostics, in addition to the identification of the chemical composition of the irradiated material, are also of special interest issues related to the plasma formation and plume expansion, namely:

- studies about the shape and velocity of the plume at various times after the ablating laser pulse,
- spatial distribution of density and temperature at various times after the ablating laser pulse,
- the temporal and spatial variation of the plume composition.

In next sections, a detailed view of Laser Ionization Breakdown Spectroscopy (LIBS) is carried out, including the operational basis, the description of required instrumentation, and finally, presenting the main advantages and applications of the technique.

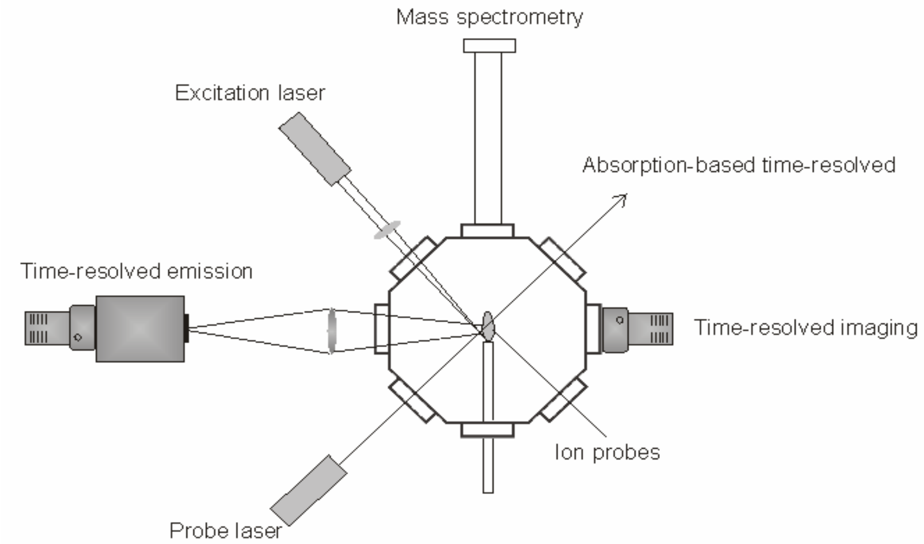

Figure 1.13. Scheme of possible emission and mass probes leading to different laser-ablation diagnostics.

1.4.3.1. LA-ICP-MS

Laser-ablation inductively-coupled plasma mass spectrometry (LA-ICP-MS) has been widely used for inorganic analysis of trace elements **[Becker, J. S. et al., 2003]** and also to perform speciation on organic samples **[Durrant, S. F. et al., 2005]**.

In LA-ICP-MS, a laser is focused on a target (normally solid) located into an ablation chamber and, as a consequence, a plasma is generated. The ablated particles are transported by a carrier gas (typically He or Ar gas) to a second excitation source, the ICP torch **[Günther, D. et al., 2003]** where they are mixed with a gas (more typically Ar) that is being ionized in the torch, forming a very high temperature plasma with a high ionization degree. Due to this heat contribution, any sample carried by the gas gets atomized. Then, the excited ions in the high-pressure torch are led to the mass analyzer under high vacuum. The ion analyzer is usually a quadrupole as there is no need of a high-mass ion detector.

LA-ICP-MS is one of the most powerful analytical techniques among available technologies. Advantages of the technique include:

- ultra-high sensitivity that allows analysis at ultra-trace levels (LOD in the order of ppb) **[Becker, J. S. et al., 2003]**,
- capability to analyze materials of different electric nature (both conductors and dielectrics),
- sample preparation methods are not required in most of the cases,
- high-velocity in the obtaining of precise results (in the order of few seconds),
- high robustness,
- possibility of in-depth analysis **[Pisonero, J. et al., 2007]** and elemental/isotopic maps with high-lateral resolution **[Zoriy, M. V. et al., 2008]**.

Due to the extremely-high ionization degree achieved in the ICP torch, ICP-MS become one of the few mass spectrometry setups with quantitative capabilities, as the high ionization efficiency greatly minimize the influence of the different ionization efficiency for many different species. When laser-ablation is used, the fractionation of the initial ablation will remain the bigger problem in quantitative analysis, and much work has been recently done to minimize it **[García, C. C. et al., 2008**]. The application of femtosecond lasers to analysis with LA-ICP-MS has improved notably the performance of the technique regarding accuracy, sensibility and lower elemental and isotopic fractionation **[Eggins, S. M. et al., 1998][Garcia, C. C. et al., 2009]**.

On the other hand, the lack of molecular information, the sample restrictions to fit the ablation chamber and the number of isobaric interferences due to the presence or Ar gas, represent the major disadvantages of the technique.

1.4.3.2. LASER INDUCED BREAKDOWN SPECTROSCOPY (LIBS)

1.4.3.2.1. LIBS FUNDAMENTALS

Laser-induced breakdown spectroscopy (LIBS) is an analytical technique based on generation of micro-plasmas by the impact of an intense laser pulse onto the material surface **[Radziemski, L. J. et al., 1989][Cremers, D. A. et al., 2000][Cremers, D. A. et al., 2006]**. A high-temperature ionized and short-lived plasma is formed at the surface of the material due to laser-induced ablation of a small amount of material. The plasma quickly expands outwards at supersonic speeds and during this time, the excited species emit characteristic optical radiation as they revert to lower energy states. Thus, the light emitted from the laser-induced plasma is collected by optical systems, and the elemental composition of the sample is directly determined from such characteristic emissions simultaneously generated by each excited species **[Cremers, D. A. et al., 2006].** This fact makes LIBS a powerful analytical tool in the elemental discrimination.

LIBS has a notable versatility and is currently being used for a wide range of applications as it satisfies a great combination of practical advantages **[Radziemski, L. J., 1994][Vadillo, J. M. et al., 2004][Fortes, F. J. et al., 2010]**:

- experimental flexibility, owing to the fact that it has no restrictions on sample size or shape
- not need of direct contact with sample
- Not need of complex methods for sample preparation in contrast to conventional methods of chemical analysis
- high sensitivity
- in situ analysis in any real environment
- real time results
- simplicity
- easy to automate,

For those reasons this spectroscopic method is ideal for the elemental analysis and chemical characterization of many materials of different nature with high analytical interest and in different surrounding conditions (air or vacuum).

However, geometry and heterogeneity of the sample, and the shot-to-shot variability are limiting factors that can affect the plasma features and, therefore, the total ablated mass. Thus, precision, exactitude and limit of detection of technique can be affected since they are largely dependent on the sample.

The LIBS analysis consists on a succession of several steps in order to obtain the spectral fingerprint of the sample, namely:

- atomization/vaporization of the sample to produce free atoms,
- excitation of atoms and
- detection of emitting light

Processes involved in the ablation of a material, in the formation of plasma and finally, in the chemical analysis of such plasma, define the scenario under which LIBS develops. Therefore, from the point of view of the basic principle of the technique, phenomena directly related to laser-matter interaction and, in addition, processes connected to laser-induced plasma generation and its evolution, could be found.

1.4.3.2.2. LIBS INSTRUMENTATION

The typical instrumentation design for LIBS is relatively simple and open, so it becomes an accessible technique of simple handling and it allows the analysis of many types of samples in different conditions. The basic elements are the laser source, the guided and focusing system, light collection system, dispersive system (spectrograph) and detector. A graphic description of the basic setup is sketched in Figure 1.14. Each component of the system used in our experiments is further described in detail in Chapter 2 of the memory.

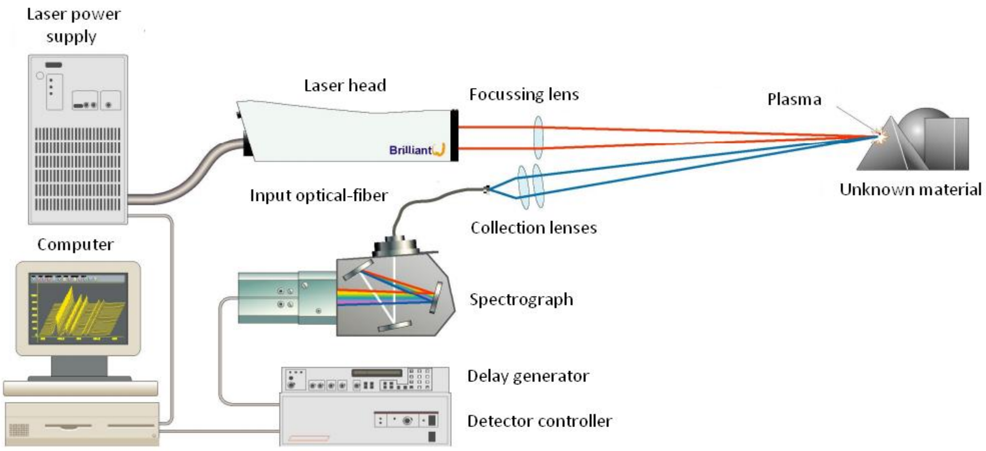

Figure 1.14. Basic scheme of a traditional LIBS setup. Reprinted from Ameasol Technology (www.ameasol.com).

In the above Figure, a laser pulse from source is focused over the sample surface by means of a focusing lens, and the plasma is immediately formed. The laser guiding can be accomplished alternatively by means of an optical fiber, adding the ability of perform remote analysis **[Davies, C. M. et al., 1995].** The optical emission of the plasma is collected and focused by means of a lens system and an optical fiber onto the entrance slit of a spectrograph. The emitted light is then separated through a diffraction grating and finally reach the detector system, typically a charge coupled device which is sometimes intensified for a better sensibility.

The output of the laser beam is synchronizes with the detector gating by either an optical photodiode or by a pulse and delay generator (PDG) which control and trigger the acquisition.

When LIBS is compared to another analytical techniques combining lasers with mass spectrometry, a few drawbacks come to light, namely sensitivity level (mainly due to the improved performance of ion detectors), and on the other hand, the absence of isotopic information.

- LASER SOURCE

The laser is used as a sampling/excitation method for analytical purposes. It was applied in analytical chemistry as early as the 1960's and offers a highly versatile energy source for atomization, excitation, and ionization **[Siegman, A. E., 1986].**

It is a source of monochromatic, one-way and highly coherent radiation. This latter property distinguishes laser from other light sources. The functioning is based on the existence of a *gain* or *active medium*, a material with properties that allow it to amplify light by stimulated emission. For the gain medium to amplify light, it needs to be supplied with energy. This process is called pumping **[Silfvast, W. T., 1996]**. The energy is typically supplied as an electrical current (a flash lamp), or as light at a different wavelength (another laser).

The most common type of laser uses feedback from an optical cavity (a chamber with a pair of mirrors on either end of the gain medium). Light bounces back and forth between the mirrors, passing through the gain medium and being amplified each time. Typically, one of the two mirrors, the *output coupler*, is partially transparent and some radiation escapes through this mirror. Depending on the design of the cavity (whether the mirrors are flat or curved), the light coming out of the laser may spread out or form a narrow beam. This type of device is sometimes called a *laser oscillator* **[Svelto, O., 1998].**

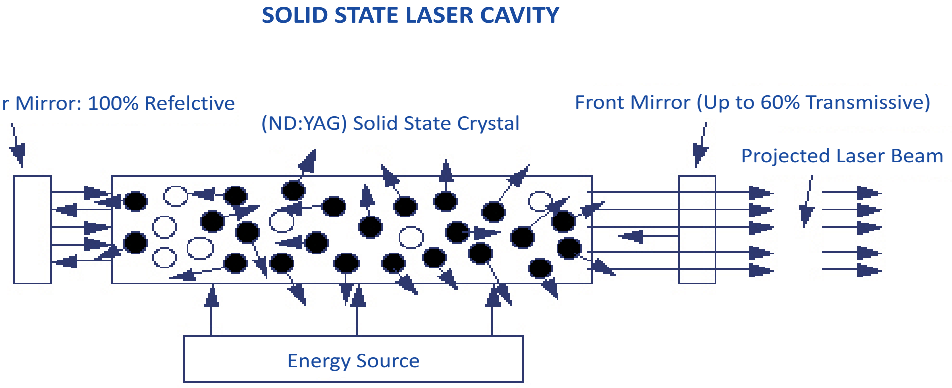

Figura 1.15. Basic scheme of mechanism of generation of a laser beam.

According to its active medium, a laser can be classified as operating in either continuous or pulsed mode, depending on whether the power output is essentially continuous over time or whether its output takes the form of pulses of light on one or another time scale. Only pulsed or modulated lasers will be able to deliver energy doses enough to generate plasmas in the surface of irradiated sample **[Csele, M., 2004]**.

Thus, many properties of the laser beam, including energy, stability, beam profile and size, pulse width, wavelength, divergence and mode of operation do influence the way the solid interacts with the laser beam. Each laser type presents a series of advantages, and some drawbacks, as well.

Nowadays, the most used laser for LI-TOF-MS is the Nd:YAG, a solid state laser with a garnet of ytrium and aluminum doped with neodimium as active medium. This laser is usually operated in combination with an electro-optic modulator or *Q-switch*, whose operation is based in the *Pockels effect*. The Pockels cell confines the laser within the optical cavity and gives origin to short pulses (duration in the range of 3-10 ns). Subsequently, the energy per pulse increases. This increasing of energy, as well as the pulse stability, can be controlled to some extent by modifying the parameters of operation of the Q-switch. Nd:YAG lasers are robust and compact laser sources requiring low maintenance, an important factor that leaded to the great adoption of Nd:YAG lasers for laser-based mass spectrometry. As a tendency in recent years, the growing adoption of solid-state mode-locked femtosecond lasers as Ti:Sapphire has led to the increasing use of this type of lasers for many laser-based spectroscopy techniques, including LIMS **[Vadillo, J. M. et al., 2004][Costache, F. et al., 2005].**

Table 1.3. Main type of laser sources depending on the emission wavelength and gain medium.

INFRARED			VISIBLE			ULTRAVIOLET		
NAME	GAIN MEDIUM	λ (nm)	NAME	GAIN MEDIUM	λ (nm)	NAME	GAIN MEDIUM	λ (nm)
Er:Glass	Solid state	1540	Ruby	Solid state	694	Argon	Ion gas	364
Cr:Fosterite	Solid state	1150-1350	Kripton	Ion gas	676.4	Nd: YAG THG	Solid state	355
HeNe	Gas	1152	Kripton	Ion gas	647.1	XeF	Gas (exciting)	351
Argon	Ion gas	1090	InGaAlP	Semiconductor	635-660	N2	Gas	337
Nd:YAP	Solid state	1080	HeNe	Gas	633	XeCl	Gas (exciting)	308
Nd:YAG	Solid state	1064	Ruby	Solid state	628	Kripton SHG	Ion gas/glass BBO	284
Nd:Glass	Solid state	1060	HeNe	Gas	612	Nd:YAG FHG	Solid state	266
Nd:YLF	Solid state	1053	HeNe	Gas	594	Argon SHG	Ion gas/glass BBO	264
Nd:YLF	Solid state	1047	Cu	Vapor metal	578	Argon SHG	Ion gas/glass BBO	257
InGaAs	Semiconductor	980	Kripton	Ion gas	568.2	Argon SHG	Ión gas/glass BBO	250
Kripton	Ion gas	799.3	HeNe	Gas	543	Argon SHG	Ion gas/glass BBO	248
Cr:LiSAF	Solid state	780-1060	DPSS	Semiconductor	532	KrF	Gas (exciting)	248
GaAs/GaAlAs	Semiconductor	780-905	Nd:YAG SHG	Solid state	532	Argon SHG	Ion gas/glass BBO	244
Kripton	Ion gas	752.5	Kripton	Ion gas	530.9	Argon SHG	Ion gas/glass BBO	238
Ti:Saphire	Solid state	700-1000	Argon	Ion gas	514.5	Argon SHG	Ion gas/glass BBO	229
			Cu	Vapor metal	511	KrCl	Gas (exciting)	222
			Argon	Ion gas	501.7	Nd:YAG FHG	Solid state	212
			Argon	Ion gas	496.5	ArF	Gas (exciting)	193
			Argon	Ion gas	488.0			
			Argon	Ion gas	476.5			
			Argon	Ion gas	457.9			
			HeCd	Ion gas	442			
			Kripton	Ion gas	416			

- OPTICS FOR LASER BEAM GUIDING AND FOCUSING

Laser radiation can be collimated/focused and redirected from the output in the laser head to the sample by means of optic elements to obtain a narrower beam and concentrate it in a very small area, accumulating a very high amount of energy in the order of gigawatts.

These optic elements are mainly mirrors, prisms and lenses that simply change beam direction and focus it. But also include elements that modify several properties of the incoming beam. This second group of elements includes polarizing crystals, beam splitters, half-wave and quarter-wave plats, telescopes, beam expanders, band filters and optical attenuators.

- LIGHT COLLECTION SYSTEM

In order to collect optimally the light emitted by plasma plume, a number of optical elements are used, namely mirrors, lens and optical fibres. They are common to mostly laser ablation setups. The light is guided though those elements towards the selective spectral system ending at the detector. It is important to minimize the number of optics in order to reduce the losses in the light transmission. Concerning optical fibres, they typically include a transparent core surrounded by a transparent cladding material with a lower index of refraction. Light is kept in the core by total internal reflection. This causes the fibre to act as a waveguide to transmit light between the two ends of the filament.

There are two choices in the observation geometry of the plasma light: orthogonal or axial observation. The most frequent is the orthogonal one in which the collection system is located so that the observation is carried out from the side or *radial* to plasma. The final position of collection element must be optimized in order to capture the maximum intensity from the source with a minimum background signal and spectral interferences **[Ríos, A. et al., 2013].** In specific optical systems, collection is centred on selected zones of interest of plasma. For this purpose, special lens and shutters can be used. For collection system based in the integration of complete radiation of plasma, a lens with high numerical aperture (range of angles over which the system can accept light) is usually used.

In the axial observation, the complete analytic signal from plasma is measured by a central axis, so position for collection does not need to be optimized. As a result, limit of detection is lower but the presence of interferences increase.

The collection with a certain angle respect to the plane of both laser incidence and plume expansion is also possible in concrete applications.

However, one of the main problems of laser induced plasma spectroscopy is the low efficient light collection due to an insufficient solid angle, so only a portion of total light emitted reaches the detector. This fact implies that the majority of results acquired by LIBS instruments are limited to specific zones of plasma selected for the study.

- DISPERSIVE SYSTEM

Plasma image is normally focused in the entrance slit of a dispersive system housed into a spectrograph. The radiation is then dispersed in its different wavelengths by a prism or a grating and finally focused by a set of lens and mirrors on the photoelectronic detector**.** Dispersive elements are based in diffraction-interference phenomena so as certain λ will be dissipated (destructive interference) whereas other λ will be promoted (constructive interference). Thus, they allow the observation of several λ at the same time along a unique spatial direction (mono-dimensional spectrum).

A prism disperses the light when it passes thorough surfaces of different diffraction index so each wavelength radiation follows a different optical path. In the case of a grating, the incident light is dispersed by the grooves on the surface so that the wavelengths are separated based on reflection and transmission phenomena **[Loewen E. et al., 1997]**.

Figure 1.16 shows the scheme of a dispersive grating. The plate is engraved resulting in thousands of grooves which disperse the light as commented. The characteristic parameters of a grating are: the distance between grooves or grating constant *d*; the blaze angle θ; free spectral range and linear dispersion. The equation of a grating is given by:

$$2d\ (\mathrm{sen}\beta - \mathrm{sen}\alpha) = m\lambda \qquad \textbf{(Eq. 1.19)}$$

where α is the incident angle, β the reflection angle, and *m* the diffraction order. The diffraction order *m* provides the resolution power of the grating as follows,

$$\lambda / \delta\lambda = m \qquad \textbf{(Eq. 1.20)}$$

where $\delta\lambda$ is the minimum gap between wavelengths that the grating is able to separate for a certain λ. Thus, a grating with a high number of grooves per millimetre (low grating constant, *d*) will be able to separate wavelengths very close, even for first order.

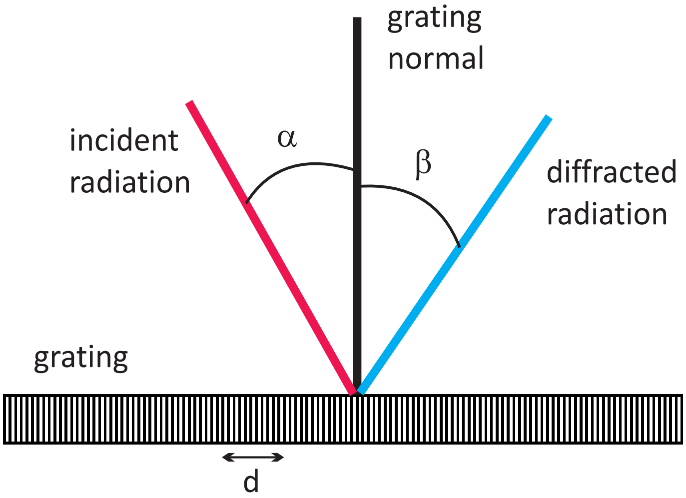

Figure 1.16. Basic scheme of a dispersive grating.

The diffraction order *m* can be positive or negative, resulting in diffracted orders on both sides of the zero order beam. The light that corresponds to specular reflection is called the zero order, and is denoted m = 0.

- DETECTION SYSTEM

Basic detection systems used in laser induced spectroscopy are photomultiplier tubes (PTM) and photodiodes (PD). They are made of photosensitive materials that are able to generate an electric current proportional to the amount of light reaching their surface. Nowadays in laboratories, the Charge Coupled Devices (CCD) are the most used devices due to advanced performance in detection. They can be found attached to an intensifier to result in intensified-Charge Coupled Devides (iCCD). They will be described in detail in Chapter 2 of the present memory.

1.5. LASER IONIZATION MASS SPECTROMETRY (LIMS)

1.5.1. INTRODUCTION TO MASS SPECTROMETRY

In 1912, as part of his exploration into the composition of anode rays, J. J. Thomson and his research assistant F. W. Aston channelled a stream of ionized neon through a magnetic and an electric field and measured its defection by placing a photographic plate in its path **[Davis, E. A., 1997]**. They observed two patches of light on the photographic plate, which suggested two different parabolas of deflection, and concluded that neon is composed of atoms of two different atomic masses or two isotopes (neon-20 and neon-22) **[Thompson, J. J., 1912][Thompson, J. J., 1913]**. This was the first evidence for isotopes of a stable element and therefore the first example of mass spectrometry, which was subsequently improved and developed into a general method by F. Aston **[Aston, F. W., 1922]** and A. Dempster **[Dempster, A. J., 1918]**.

Table 1.4 shows a record about the history of main contributions to mass spectrometry and their authors.

Mass spectrometry presents a number of advantages that make it ideal for the analysis of surfaces and solid materials:

- ability for sample identification. Unambiguous identification of almost any type of substance, from atoms to complex molecules with high molecular weight
- associated techniques can perform both qualitative and quantitative analysis
- discrimination between substances with similar structural characteristics
- high sensitivity

- universal and specific technique
- isotopic information could be extracted
- information about structures, bond energies, kinetic of molecular fragmentation, etc.
- rapid technique that could be integrated into an *in-line* analysis in real time (e. g., application on control of enzymatic and metabolic processes).

The first major application of MS is nowadays and always has been the identification of pure compounds in the field of organic chemistry and then it spread to other fields of chemistry.

Table 1.4. Schedule of main contributions to mass spectrometry.

Researcher	Date	Contribution
J.J. Thompson	1912	First mass spectrometer
A. J. Dempster	1918	Electro-ionization and magnetic focusing
R. W. Ditchburn	1929	Photoionization
E.O. Lawrence & S.M. Livingston	1932	Cyclotron
Stephens	1946	Time-of-flight analyzer (TOF)
W. Paul	1953	Quadrupole analyzer
R. J. Gomer & M. G. Inghram	1954	Field Ionization
W. C. Wiley & I. H. McLaren	1955	Advanced design of TOF analyzer
R. S. Gohlke & F. W. McLafferty	1956	Gas Chromatography/Mass Spectrometry
J. H. Beynon	1956	High resolution Mass Spectrometry
M. S. Munson & F. H. Field	1966	Chemical Ionization
M. Dole	1968	Electro-spray Ionization (ESI)
F. W. McLafferty	1973	Liquid Chromatography/Mass Spectrometry
M. Barber	1981	Fast atom bombardment (FAB)
C. R. Blakely & M. L. Vestal	1983	Thermo-spray Ionization
F. Hillenkamp & M. Karas	1985	Matrix-Assisted Laser Desorption–Ionization (MALDI)

1.5.2. THE MASS SPECTROMETER

Figure 1.17 shows the basic scheme of mass spectrometer instrument. The core of the system is the mass analyzer. Mass spectrometer works by ionizing the sample to generate charged species that are separated according to m/z ratio (where m is the ion mass in Dalton (Da) and z the number of elementary changes), obtaining the information as a singular mass spectrum showing the intensity of detected ionic current. Basically, a mass spectrometer consists of four main units,

- the ion source, which removes and then ionizes a portion of the sample,
- an extraction system which gives the ions a suitable trajectory in order to lead them towards the mass analyzer properly,
- the mass analyzer which is able to separate ions with different mass-to-charge ratio, according to a specific physical principle,
- a detection system, which measures the value of an indicator quantity and leads the calculation of abundances for each ion present in the beam.

The mass spectrometry techniques most commonly used in the characterization of solids include those listed below:

- Spark Source Mass Spectrometry (SSMS)
- Laser Ablation Inductively Coupled Plasma Mass Spectrometry (LA-ICP-MS)
- Glow Discharge Mass Spectrometry (GDMS)
- Secondary Ions Mass Spectrometry (SIMS)
- Laser Ionization Mass Spectrometry (LIMS)
- Matrix-Assisted Mass Spectrometry (MALDI)

Those techniques differ primarily on the ionization source they use. Nevertheless, they all are based in the operation of a mass spectrometer with the necessary components in order to generate, to lead, to separate and, finally, to detect the ions. Moreover, the mass spectrometry techniques listed above have as one of the main advantages the fact that the sampling is carried out directly on the solid sample with a minimum or even nonexistent sample preparation.

Although solid MS-techniques have been traditionally applied to inorganic materials, there has been an increasing focus on biological and organic analysis, especially in techniques such as SIMS, LA-ICP-MS or MALDI due to their ability to record the spatial distributions of a wide range of atoms and molecules, including pharmaceuticals, lipids, peptides, proteins, metabolites and polymers **[McDonnell, L. A., et al., 2007].**

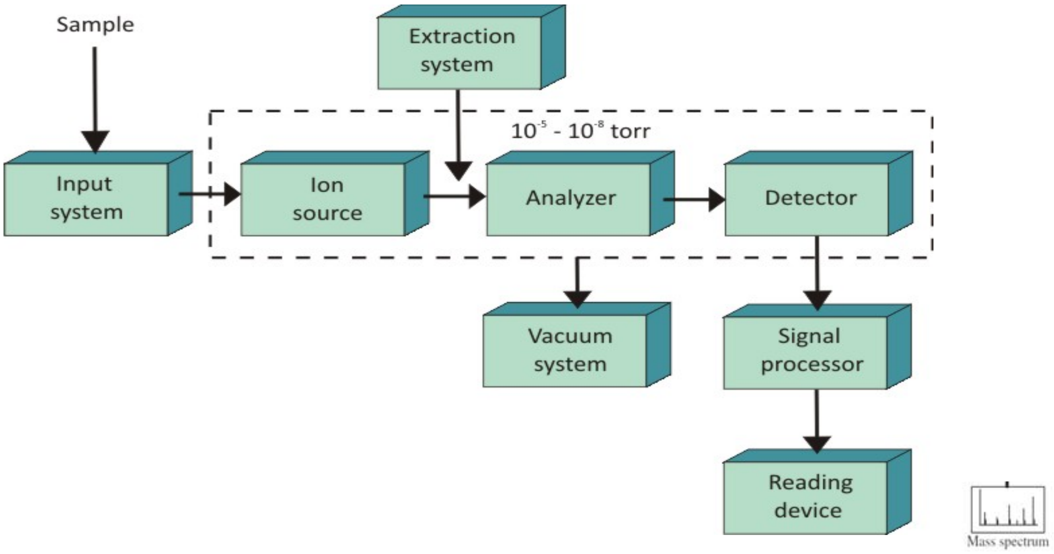

Figure 1.17. Block diagram of main components in a mass spectrometer system.

There is a wide range of analyzers in the world of spectrometry: quadrupoles (Q), magnetic sectors (EBE), time-of-flight tubes (TOF), ions traps (IT), orbitrap, as well as more complex systems by combination of the above, as the case of tandem Q-TOF. Their fundamentals are well-known and they provide different performances on spectral acquisition regarding the resolution, the sensitivity, speed of analysis, spectral range, etc. as shows Table 1.5.

We used a TOF analyzer for experiments carried out in the present research by LIMS analytical technique. This type of spectrometer presents a number of advantages which make it an excellent separator system.

In general, using one of the methods described above, ions are produced within a small enclosed space that carries an electrical charge, the ion source. All ions leaving this space are accelerated thanks to the potential gradient between the source and very closely grounded plates, producing an ion beam that can be electrostatically focused easily. Within this beam, all ions with the same charge, but different mass, will have acquired the same translational kinetic energy. When the beam passes through homogeneous magnetic or electric fields, the ions will follow different paths depending on either their momentum (magnetic field) or their kinetic energy (electric field). These two intrinsic kinematic properties form the basis of the majority of mass analyzers.

Table 1.5. Classification of mass analyzers depending on operation features.

	RESOLUTION	SENSITIVITY	MASS RANGE	SCANNING RATE
BETTER	**EBE**	**TOF**	**TOF**	**TOF**
	TOF	**EBE**	**EBE**	**IT**
	IT	**IT**	**Q**	**Q**
WORSE	**Q**	**Q**	**IT**	**EBE**

An ideal Quadrupole Mass Filter (Q) consists of four equally spaced hyperbolic rods, but for practical purposes the rods are usually cylindrical. They are connected together as two opposite pairs. A beam of ions from a source enters the longitudinal axial space between the rods and mass separation is achieved by a combination of direct current (DC) and radiofrequency (RF) fields of opposite polarities applied to the opposing rods. Under these fields, only certain ions with a given mass to charge ratio *m/z* follow stable trajectories and are transmitted through the filter **[March, R. E. et al., 1989]**.

On the other hand, the Quadrupole Ion Trap (IT) is the three-dimensional equivalent of the Quadrupole Mass Filter and the principle of operation is similar to this. A common geometry consists of two hyperbolic end cap electrodes on either side of a ring electrode. The advantage of this over the quadrupole is that the device can both store and mass-select ions through scanning of DC and RF fields **[March, R. E. et al., 1995]**.

The principle of a Magnetic Sector (EBE) separator is as follows: when a beam of ions of various m/z ratios passes through a homogeneous magnetic field they will follow different curved paths whose radii depend on the momentum of the ions; thus mass separation may be achieved. The placing of an electrostatic sector before or after the magnet improves the mass resolution in a greater extent.

The time-of-flight spectrometer (TOF) is surely the simplest method for separating ions of all and was among the earliest of mass spectrometers. Singly charged ions are extracted from a typical mass ion source and they all are accelerated through the same potential gradient towards a free drift region and so irrespective of their mass, will have the same kinetic energy. In next section will be described in detail.

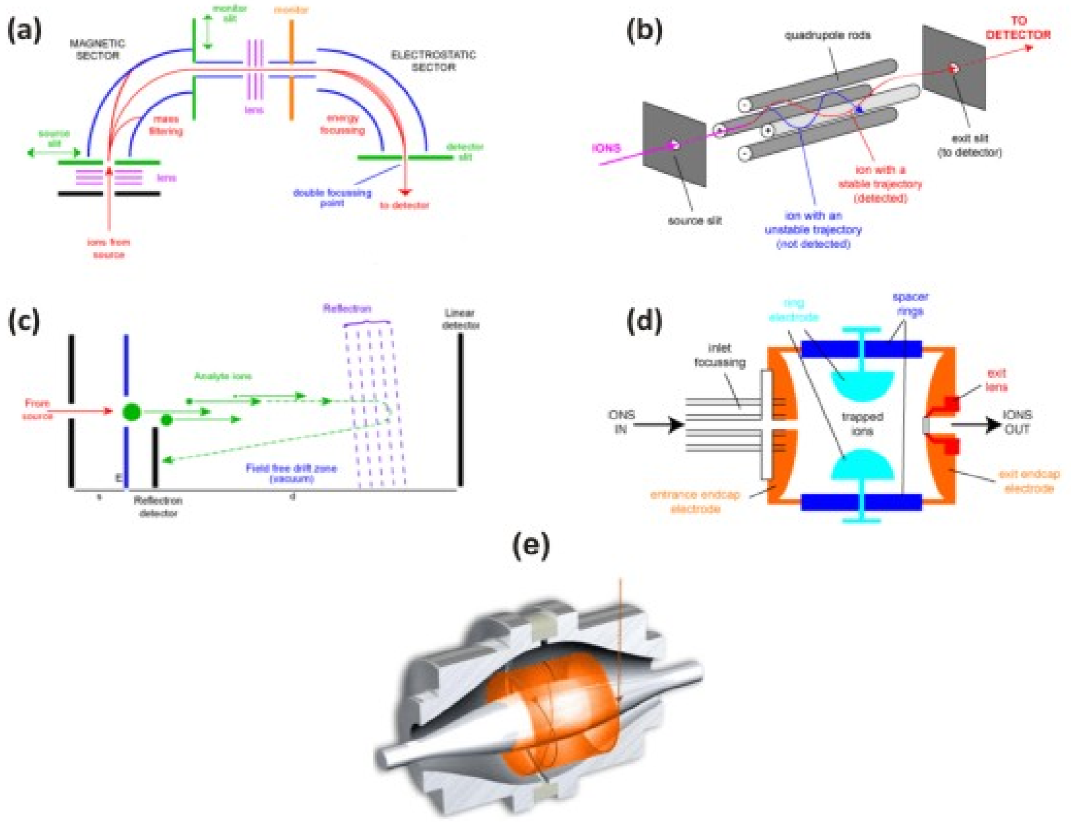

Figure 1.18. Scheme of main mass analyzers used in mass spectrometry analysis. (a) magnetic sector; (b) quadrupole; (c) time-of-flight tube; (d) ion trap; (e) orbitrap.
Reproduced from (a-d) University of Bristol (http://www.chm.bris.ac.uk/ms); (b) Thermo Fisher Scientific (http://www.thermofisher.com).

Finally, the Orbitrap was recently introduced **[Makarov, A., 2000]** providing high resolving power and excellent mass accuracy and high dynamic range **[Makarov A. et al., 2006]**. It works on the principle of an orbital trapping of ions around an axial central electrode with a purely electrostatic field. The device consists of an axial spindle-like interior electrode and a coaxial barrel-like external electrode. The electrostatic field between the two electrodes creates a quadrologarithmic potential distribution inside the trap and the trapped ions undergo rotation around the central electrode and harmonic oscillations along its length. Different ionization methods, such as MALDI or electrospray **[Makarov A., 2000][Hardman M. et Al., 2003]** have been combined with an orbitrap for the analysis of a variety of compounds, which allows the accurate elucidation of the chemical composition.

1.5.3. IONIZATION METHODS AND ION SOURCES

A number of methods are available for the generation of gas-phase organic ions and the way in which they are separated by their mass-to-charge (m/z) ratios. The major number of mass spectra has been measured using electron impact ionization (EI) **[NIST, 2005]**. This ionization method requires that the molecule of interest be volatile (or can be volatilized without decomposition) and this places significant limits on its use. Together with EI, similar ionization methods as photoionization and chemical ionization are limited to molecules of low molecular weight. Considerable efforts have been made for developing new and more versatile ionization methods suitable to non-volatile, thermally labile and high molecular weight molecules. In this sense, Fast Atom Bombardment (FAB), Electrospray Ionization (ESI) and Matrix-Assisted Laser Desorption-Ionization (MALDI) have contributed significantly to widen the use of mass spectrometry to a much broader range of molecular species.

Ion sources used in mass spectrometry are very diverse and they often depend on the final application. Among them can be found spark sources, glow discharge, laser ionization, ion or atom guns, or inductively coupled plasma sources. Different processes of vaporization and ionization that are taking place during the analysis led to distinguish between them.

Historically, ions for mass spectrometry analysis were generated by bombardment of components in gas phase samples with high energetic electrons (electronic impact source). Despite some drawbacks, this technique still has a great importance and in it is based the majority of spectral libraries. However, during the last four decades novel ion sources have been developed which offer certain advantages over classical electron beam sources, and can operate at atmospheric pressure and directly on condensed phase samples.

Normally, most commercial mass spectrometers are equipped with accessories which allow the use of several of these interchangeable sources. In Table 1.6 are listed the main ionization methods for both atoms and molecules depending on the sample state and taking into account the required pressure level.

Another classic classification distinguishes between hard or soft ion sources. Most important hard source is the electronic impact source. Hard sources transfer high energy doses to generated ions so that they are induced to excited vibrational and rotational states. Relaxation of such ions produces a large degree of fragmentation and mass spectra become complex. By contrast, soft sources such as chemical ionization and desorption produce relatively low excitation of the ions, so that short fragmentation occurs and as consequence, the spectra are simpler with fragments

Table 1.6. Methods for main both atomic and molecular ionization.

Atomic Ionization	Molecular Ionization		
	Sample Phase	**Mode**	**Pressure**
Thermal ionization Spark source Glow discharge Inductively coupled plasma Resonance ionization	Gas phase	Electron ionization	HV
		Chemical ionization	IV
		Photoionization	HV
		Field ionization	HV
		Metastable atom bombardment	HV
	Solution phase	Thermospray	LV
		Atmospheric-pressure CI	AP
		Atmospheric pressure PI	AP
		Electrospray	AP
	Solid phase	Plasma desorption	HV
		Field desorption	HV
		Secondary-ion MS	HV
		Fast atom bombardement	HV
		Matrix-assisted laser desorption	HV
HV: high vacuum; IV: intermediate vacuum; LV: low vacuum; AP: atmospheric pressure			

close to parent molecule. Both types of spectral information are useful. Simple spectra from soft sources allow an accurate determination of the molecular weight of the analyte, whereas more complex spectral models obtained by hard sources often allow its unambiguous identification. In addition, problems with volatility and/or thermal instability of many materials of interest have been largely overcome through the development of soft ionization methods, which have led to a number of techniques which favours the analysis of the sample without degradation.

1.5.4. FUNDAMENTALS OF LIMS AS ANALYTICAL TECHNIQUE

The cloud generated in the ablation process could be used as vehicle to other analytical techniques such as mass spectrometry where particles of the sample are ionized and then led to a mass analyzer to reach the detector system. Thus, mass spectrometry based on previous laser ablation of the sample allows the detection of ions generated as a consequence of the interaction of the laser beam with the sample and subsequent ablation and can provide information on elemental composition and the isotope constituents of solid samples **[Hang, W. et al., 2005][Yu, Q. et al., 2009][Brinckerhoff, W.B. et al., 2003][Watanabe, K. et al., 2003][Wang, X. et al., 2003]**. This method is called Laser Ionization Mass Spectrometry (LIMS) since it uses

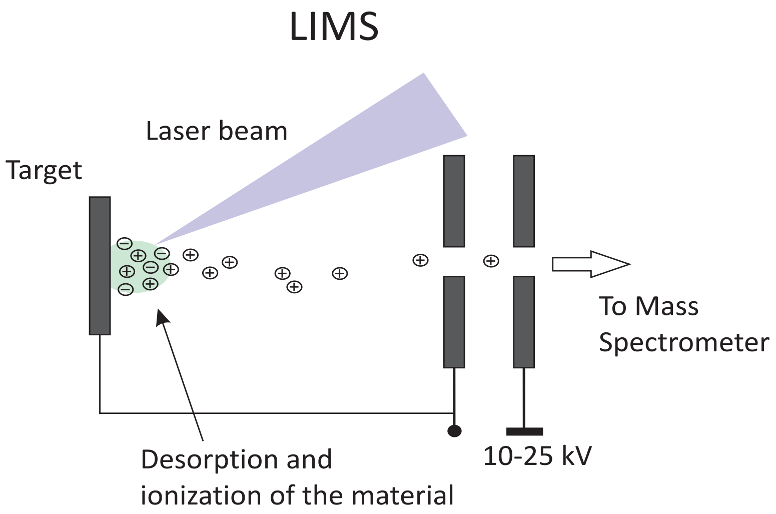

Figure 1.19. Basic scheme of laser ionization of the sample and guiding of ions towards mass spectrometer in LIMS technique [Alcántara, J. F., 2010].

laser radiation as ionization source of the sample. The technique can be combined with different type of analyzer. A classic example is the time-of-flight analyzer, so that the technique is renamed as Laser Ionization Time-of-Flight Mass Spectrometry (LI-TOFMS). The fundamentals and basic instrumentation of the technique are further described in detail.

LIMS technique is based on the atomization and subsequent ionization of vaporized material of the sample when a laser beam impinges the surface with a specific energy and a particular wavelength. All components in the target are vaporized and then ionized creating a cloud in the surrounding of the surface containing all the generated species. Depending on the irradiation level brings into play, the threshold of plasma formation will be exceeded or only a sub-plasma regime with soft desorption of the material is achieved **[Delgado, T. et al., in press D]**. The ionic species could be identified by means of photographic or electric detection methods.

The LIMS system is rather compact. The advantages provided by using a laser beam as ionization source to the technique are:

- versatility, since laser ablation becomes one of the most useful tools to produce the evaporation and ionization of many types of materials
- laser radiation is easy to guide and transport over long distances without significant loss of intensity, and the photons of the beam not disturb the electric field for ion extraction generated in the mass spectrometer source

- in a pulsed laser source, each laser pulse may provide a complete mass spectrum with very low detection limits, being necessary only small portions of sample for analysis
- it can be applied to analysis of insulator materials as well as samples with a complex geometry.

Main characteristics of the technique are listed below:

- limit of detection: 0.001 – 0.1 μg / g
- lateral resolution, 1 nm
- depth resolution, 1-100 μm
- possible depth profile studies
- no charge effects
- high selectivity and sensitivity
- large dynamic range and linear dependence of intensity signal with concentration
- moderate cost.

As disadvantages of the technique, the most notable is the absence of reference database of LIMS spectra required in studies of sample identification. Another important fact to consider is the prospective incompatibility of high vapor pressure samples with the high vacuum work regime of the instrument.

In the LIMS method, two different processes are performed when a focused laser beam irradiates the sample surface: a first stage of evaporation and atomization of removed material and after that, the ionization of those atoms, group of atoms and/or molecules generated in the previous stage. Subsequently, the separation of ions is performed using electric/magnetic fields depending on m/z ratio of species.That requires the use of a spectrometer with high mass resolution. The whole process takes place in vacuum conditions and the captured signal will depend on a number of factors including the power and wavelength of the laser beam, the physic-chemical properties of the material and the surrounding conditions.

The laser ionization may be applied to semi-quantitative analysis, and even for quantitative purposes using the appropriate standards.

In brief, LIMS technique combines speed, sensitivity and the capacity to work with samples of different chemical nature, shape or size. However the analyzed compound must be compatible with the low vacuum conditions required for mass spectrometry. Fortunately, a proper design of the mass spectrometer may allow the analysis of organic compounds with high vapor pressure without damage of the detector by means of differential pumping systems**.**

1.5.5. FUNDAMENTALS OF LI-TOF-MS

The laser induced plasma can be introduced into any kind of mass analyzer, but a TOF-MS is usually preferred because it is easily coupled with the pulsed source. LI-TOF-MS technique uses a time-of-flight analyzer (TOF) as mass spectrometer which is able to acquire a complete mass spectrum for each laser pulse applied on the sample surface, separating the collected ionic species depending on their m/z ratio, and allowing the unambiguous identification of elemental composition of the material.

Time-of-flight mass spectrometers are simple analyzers with an unlimited mass range and a sequential detection of all those ions formed in the ionization process and suitably extracted. The fundament of this analyzer lies in the fact that ions with equal kinetic energy and different m/z ratio will present different velocities and, therefore, they will take different times to go over a fixed distance. Generated ions are extracted by the application of a specific potential in the extraction electrode which supplies them with the same kinetic energy. Ions with lower mass-to-charge ratio will reach first the detector due to their higher velocity according to the equation,

$$E_k = \tfrac{1}{2}\, m\, v^2. \qquad \textbf{(Eq. 1.21)}$$

If we substitute the *m* value for the m/z ratio, then velocity of a particular ion will depend only on its mass-to-charge ratio.

$$(m/z) = 2\, E_k / v^2. \qquad \textbf{(Eq. 1.22)}$$

The time spent by a particular ion to travel across the length of the flight tube *D* is proportional to its m/z ratio and given by the equation,

$$t = [m/2zeV]^{1/2}\, D, \qquad \textbf{(Eq. 1.23)}$$

where *t* is the time-of-flight of the ion, *z* is its charge, *e* the electron charge, *V* the potential applied in the acceleration area, and *D* the length of the field-free drift region. Detection system will be able to distinguish the different ionic masses, the better the greater their separation in time (i.e., the longer the flight tube), the lower the energy dispersion of the ions generated in the source.

From the Equation 1.23, the time it takes an ion to reach the detector will vary with its m/z ratio. So, depending on this value, ions will reach the detector sequentially, sorted by their time-of-flight. A TOF analyzer is not simultaneous as the ions reach the detectors at different times. However, the time difference is so small that TOF are commonly referred as *quasi-simultaneous* or *panoramic*.

When compared to other well-known analyzers as quadrupoles or magnetic sectors, time-of-flight spectrometers present clear advantages, as such listed below:

- theoretical unlimited mass-to-charge working range
- quasi-simultaneous or panoramic operation mode since the ions reach the detector at different but very close times
- voltage scanning is not required to select the ions for detection
- momentary data acquisition
- easy to build and certain flexibility.

1.5.6. LI-TOF-MS INSTRUMENTATION

In regard to Laser-Ionization Time-of-Flight Mass Spectrometry setup, many instrumental sources combine to build a robust but complex system. Basic instrumentation to perform LI-TOF-MS includes a laser source, the optics needed to guide and focus the laser beam on the sample and specific electrodes needed to deflect the ions towards the ion analyzer and a detection system. Naturally, an ion analyzer and an ion detector are basic components. A read-out system to measure the ion current reaching the detector is also needed, as well as a pumping system to get high vacuum or ultra-high vacuum inside the chambers were ions are generated and transported. A diagram with the experimental LI-TOF-MS system is shown in Figure 2.1 in next chapter.

- LASER SOURCE AND OPTICS FOR LASER BEAM GUIDING

When the laser is focused on the sample, ions are formed and they will be analyzed and detected later. Information about these basic elements of the analytical system is presented above in section 1.4.3.2.2.

- IONIC LENSES

The ionic lenses system is intended to a proper focusing of generated ions before they enter the analyzer by applying suitable voltage values to each ionic electrode. Ion extraction from ionization area is a critical phase for any mass spectrometry analysis. In LIMS, after laser ionization process, ions tend to fly off the solid material with high kinetic energy and great spatial dispersion. In order to reduce this dispersion on direction and velocity, a set of ionic lenses are installed (see Figure 2.7 besides comments in Chapter 2) at the entrance of the tube-of-flight. By means of pulsed extraction, the resulting ion packet will be collimated and focused. After the ion optics, the analyzer will separate ions based on their m/z ratio.

- TIME-OF-FLIGHT ANALYZER

As it was commented above, Francis W. Aston, an advanced pupil of Joseph J. Thomson, designed the first velocity focusing mass spectrometer, a precursor of what would later be the time-of-flight analyzer. The first real proposal with the concept of time-of-flight analyzer was designed by William Stephens and presented in 1946 **[Stepens, W. E., 1946]**. A few years later, W. Wiley and I. McLaren improved the resolution of the instrument by adding a synchronized and delayed two-grid extraction system that made possible to make some corrections in the observed effects of uncertainty in the time of ion formation, location in the extraction field and initial kinetic energy. The basic geometry of the Wiley-McLaren configuration is shown in Figure 1.20 **[Wiley, W. C. et al., 1955].** The first commercial time-of-flight instrument was produced in the late 1950's by the Bendix Corporation. Nearly two decades later, Boris Mamyrin presented the next major improvement for the time-of-flight mass spectrometry: the reflectron. This novel device is described in detail below.

In the LI-TOFMS are possible two different configurations according to the path

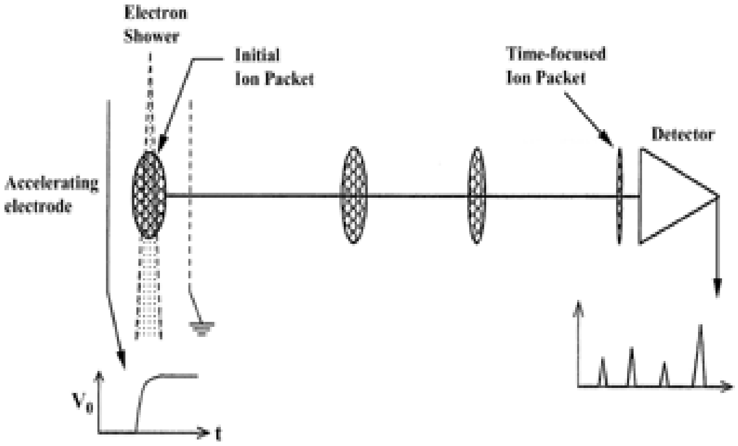

Figure 1.20. Scheme of basic geometry of the Wiley-McLaren design. Reprinted from [Wiley, W. C. et al., 1955].

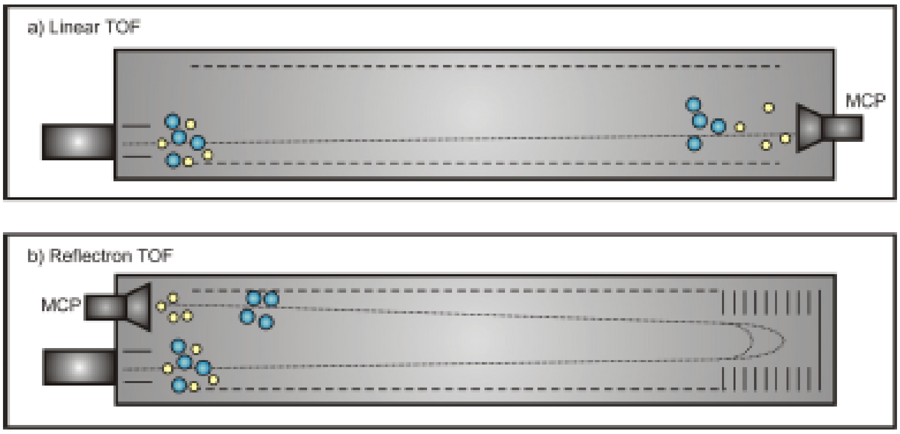

Figure 1.21. a) Scheme of Linear TOF. b) Scheme of Reflectron TOF. Reproduced from [Alcántara, J. F., 2010].

run by the ions: linear mode or no linear mode. Figure 1.21 shows a linear and a reflectron time-of-flight.

- Linear TOF. It consists of a single stage design in which ions describe a straight line through the flight tube and reach the detector situated at the end, opposite to the entrance region (Fig 1.21(a)). Ions with different m/z get separated, but little dispersion on kinetic energies among ions with identical m/z is not corrected. Typical values for accelerating voltages applied in this type of spectrometer ranging from 1 kV to 30 kV.

- Reflectron TOF. In order to improve the resolution of the system, the length of the total distance run by the ions to the detector is increased using a device called reflectron (Fig 1.21(b)). This system proposed by Mamyrin and co-workers **[Mamyrin, B. A. et al., 1973]** is able to improve the separation between ions with different m/z ratio as a result of such rise in the total path length and, on the other hand, it also corrects partially the initial dispersion among ions with similar m/z ratio (temporal spread due to the initial velocity of the ions). The reflectron (or ionic mirror) is located at the end of the tube and, by means of different parallel electrodes connected alternatively to potential sources with opposite polarity, it gets to slow first and then push the ions back focusing the beam towards the detector situated in the entrance area. Thus, the ions with similar m/z will be forced to describe different trajectories inside the reflectron flight-tube, so that the ion packet will be narrower **[Mamyrin, B. A. et al., 1973].**

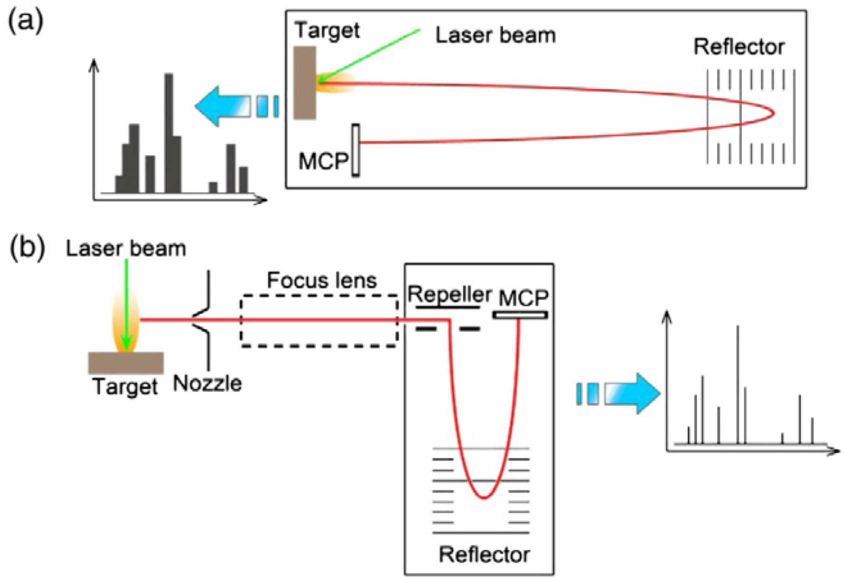

Figure 1.22. Schematic diagram of (a) on-axis and (b) orthogonal geometry laser ionization TOFMS. Reprinted from [Lin, Y. et al., 2010].

The combination of pulsed and delayed extraction with a reflectron turns a time-of-fight in one of the most powerful ion analyzers available for mass spectrometry. In this analyzer, all ions generated in the ion source and collected by the electric field of the ion optics fly through the analyzer (a field-free drift region) and reach the detector sequentially. This is a main difference with other analyzers such as quadrupoles. It should also be noted the existence of reflectron with double stage in which two separate homogeneous field regions, of different potential gradient, are used. The result is a large enhancement in resolution, in particular for ion beams with broad kinetic energy distributions.

The versatile and easy coupling between the pulsed source and TOF mass analyzer leads the possibility of different configuration geometries of the instrument. Laser ionization orthogonal time-of-flight mass spectrometer (LI-O-TOF-MS) (shown in Figure 1.22(a)) represents the traditional on-axis geometry instruments, but the orthogonal extraction technique, as shown in Fig. 1.22(b), can achieve high resolution because the broad kinetic energy distribution of the ions from the ion source has little effect on the mass analyzer.

- DETECTION SYSTEMS

The detection systems used in mass spectrometry usually depends on the mass analyzer and its applications. Among the most common ion detection systems are found the Faraday cups, the multiplier systems such as Microchannel Plates (MCP), the ion-photon conversion detectors or new cryogenic detectors. In any case, the ion detector is required to have high sensitivity, high linear dynamic range and high speed of operation.

In the special case of time-of-flight analyzer, MCP is normally the selected detector since it has suitable properties as a very fast time response, high linear range, and notable sensitivity. These features allow getting a good resolution on the signal from ions with slightly different mass-to-charge ratio. As a disadvantage, MCP detectors lack sensitivity for extremely high-mass ions that impinge the conductive surface of the plate with less speed. Details on MCP detector are included in Chapter 2.

Cryogenic detectors can also be used with TOF analyzers and present many advantages compared to other mass spectrometry detectors. Specially, cryogenic detectors are suitable to be used after a time-of-flight analyzer since they keep high sensitivity for huge ions **[Frank, M., 2000]**. In cases where TOF analyzers are used and ions are too heavy for the MCP detector to be sensible enough, cryogenic detectors operating at extremely low temperatures (near 0 K) are used.

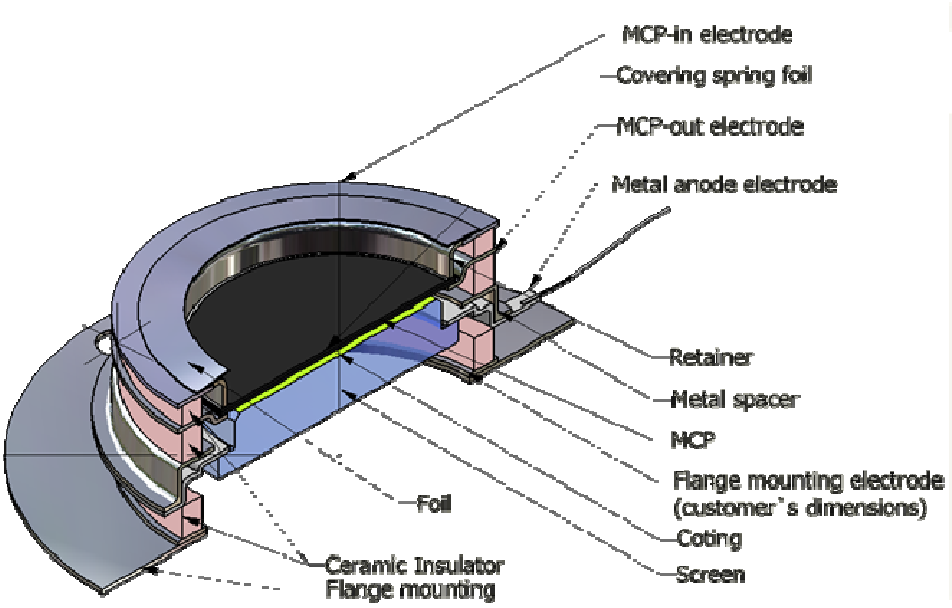

Figure 1.23. Schematic diagram of multichannel plate detector (MCP). Reproduced from [Del Mar Photonics (www.dmphotonics.com)].

- VACUUM INSTRUMENT

Reduced pressure becomes an essential requirement for a suitable operation in any mass spectrometer in order to establish a collision-free environment that allows mean free paths larger enough to charged particles. Depending on ionization source and the type of detector in the system, vacuum requirements will vary to the level of high-vacuum (around 10^{-5}mb) or ultra-high vacuum (around 10^{-8} mbar). In this sense, the established ambient conditions enable to disregard collisions in the system. Mean free path λ for an ion at a certain pressure level can be calculated with the expression:

$$\lambda = \frac{kT}{2^{1/2}\sigma P} \quad , \qquad \textbf{(Eq. 1.24)}$$

where *k* is the gas kinetic constant; *T* the temperature in the system; σ the effective section or collision probability and *P* the pressure level. Thus, λ is inversely proportional to pressure level and no dependent of the temperature.

Vacuum pumps are usually classified considering the way they operate:

- Primary pumps: they work directly against atmospheric pressure by throwing the exhausted gas to it and, as a result, by reducing the pressure inside the system. These pumps are called *primary* because they can operate autonomously without being connected to an additional pump. They can achieve reduced pressure down to 10^{-3}mb. This category includes rotary pumps (needing oil to operate) as the more extended type. Membrane pumps do not require oil to operate but vacuum level achievable is limited in the order of a few mbar.
- Secondary pumps: they require to be connected to primary pump in order to operate since they can not discharge directly into the atmosphere. First type of secondary pump used was the diffusion pump. They have no moving components, but they are getting abandoned due to the back stream of oil to the system. Turbo molecular pumps are nowadays the most used. This type does not use any oil, and represent a clean alternative to work in ultra-high vacuum conditions. It consists on a set of joined plates that spins at speeds as high as 75,000 rpm (comparable to thermal velocity of molecules). The successive collisions of gas molecules with static (stators) and mobile (rotors) plates give rise to momentum transference. They achieve a vacuum as low as 10^{-8}mb (comparable to diffusion pumps).

- Tertiary pumps: their proper operation is subject to the support of a secondary pump (connected in turn to a primary pump). Sputter-ion pumps are the prototype of tertiary pumps and they typically are fitted to turbo molecular pumps to discharge. Main advantages of this type include the absence of any moving parts, the no requirement for any oil and a long life-time expectation. This system achieves a vacuum down to 10^{-12} mbar.

1.6. APPLICATIONS OF LIBS/LIMS FOR ORGANIC EXPLOSIVES AND PAHs

Application of optical and mass spectrometric techniques on the detection, identification and discrimination of organic explosives as well as other hazardous organic compounds as pollutants has been a traditional approach for fast chemical response and focused on the semi quantitative and quantitative characterization of these materials. Methods have undergone a spectacular improvement in the last decades in sensitivity and adaptability of the instruments.

Recently, the integration of two sensing technologies in a hybrid sensor for the simultaneously acquiring, in real time, of multi elemental and molecular information from the same laser pulses irradiating the organic samples is possible as the case of the successful combination of LIBS with Raman spectroscopy, presented as an alternative for the detection of explosives **[Moros, J. et al., 2010 A][Moros, J. et al., 2010 B].** In this sense, ion-photon coincidence measurements could be of interest in the study of

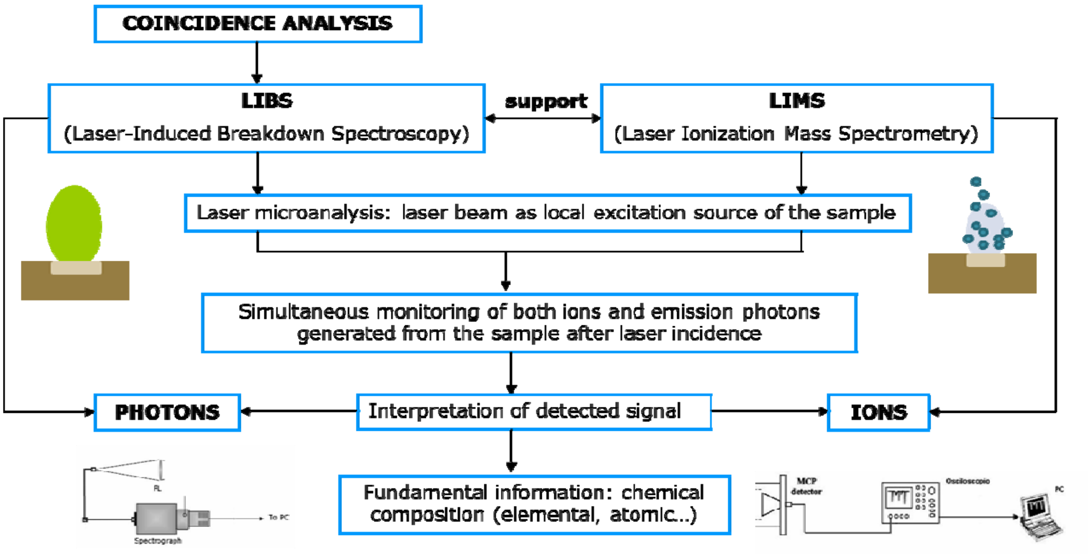

Figure 1.24. Schematic diagram of coincidence ion/photon analysis.

fundamental information about transient events occurring in laser induced plasmas of such materials (plume chemistry) as well as dynamics of the plasma plume. This has been carried out by means of a combined LIMS-LIBS experimental system in the analysis of energetic materials **[Delgado, T. et al., 2013 E]**. Figure 1.24 sketches the principle of the hybrid system.

1.6.1. SAMPLES

1.6.1.1. HIGH ENERGETIC ORGANIC COMPOUNDS

In general terms, *explosives* are reactive substances that contain a great amount of potential energy capable of producing detonation instead of combustion. A detonation implies a chemical reaction that consume the oxygen contained in the material with the subsequent release of gases which quickly expanding and the generation of high amount of energy as heat. Therefore, explosives are independent of oxygen in the surrounding in their process of detonation.

The first explosive artificially manufactured was black powder, a mixture of vegetal carbon, sulphur and potassium nitrate, with high content in oxygen.

The suitability of an explosive substance for a particular use is based on its physical properties: sensitivity to initiation, velocity of detonation, stability, etc. The different behaviour of explosives in the ignition is explained on the basis of relative rates of the corresponding energetic reactions. Thus, an explosive is classified as a low or high explosive according to its rate of burn: low explosives burn rapidly (or deflagrate), while high explosives detonate.

- **Low explosives**

The decomposition of the explosive material is propagated by a flame front which moves slowly through the explosive material (velocity of sound is not exceeded), in contrast to detonation. Hence, the initiation is performed by means of classic chemical mechanisms (thermo-kinetic activation).

- **High explosives**

The decomposition of the explosive is propagated by an explosive shock wave traversing the explosive material. The shock front is capable of passing through the high explosive material at supersonic speeds, typically thousands of metres per second. Due to such high reaction rates, these are very powerful explosives.

From the point of view of their sensitivity, explosives are divided in two main groups: primary or secondary explosives.

- **Primary explosives**

They have very low activation energy (by means of impact, heat or friction) and the amount of energy released in the detonation is generally low as well, but they are considered as highly dangerous and are desensitized for handling. In most of the cases the heat of explosion is around 400cal/kg.

- **Secondary explosives**

They present moderate activation energies and high powerful in the explosion, in the order of gigawatts. Heats of explosion are normally higher than 1000 kcal/kg. This category includes typical nitro organic explosives as TNT, RDX, PETN, HMX, TNP, etc. These compounds own a number of nitro groups joined to carbon atoms in the molecular structure by bonds C-NO_2 that provide to the molecule high detonation power and high degree of instability due to weakness in bonds between O and N atoms.

- **Tertiary explosives**

This group included exclusively ANFO substances, consisting of ammonium nitrate and fuel-oil. They present a very low sensitivity.

In the wide range of energetic materials, a special group of organic compounds of high interest and extensively studied are formed by nitroaromatic explosives.

Most organic nitroaromatic explosives have oxidant and oxidizing constituents within the same molecule. The juxtaposition of atoms C, H and O is intermolecular and they remain separated due to the presence of N atoms which do not participate in the explosive reaction. Gas nitrogen is liberated in the exothermic explosion.

The most widely used military explosive is 2,4,6-trinitrotoluene (TNT). It is a nitro-derivative of toluene, a hydrocarbon derived from coal tar. Its main features include low melting point, stability, low sensitivity to impact, friction, shock and electrostatic energy, and its relatively safe methods of manufacture. The addition of oxygen-rich products to TNT can form mixtures with enhanced explosive power. A typical group of by-products of industrial 2,4,6-trinitrotoluene (TNT) include isomers of trinitrotoluene, dinitrotoluene, trinitrobenzene, and dinitrobenzene.

Characterization and origin identification of explosives is important in forensic analysis of post explosion residues. In addition to the type of explosive used in a bombing, the investigators would like to know its country of origin and, especially, its manufacturer. Each manufacturer produces explosives with characteristic differences in the type and amount of by-products, impurities, and additives, depending on the purity of the raw materials and solvents used and the type of manufacturing process, thus resulting in a characteristic profile of by-products, organic impurities, and additives.

The production process of TNT **[Yinon, J., 2004]** includes toluene formation from benzene and methanol, followed by three steps of nitration: from toluene to mononitrotoluene (MNT), to dinitrotoluene (DNT), and finally, to 2,4,6-trinitrotoluene (TNT). Nitration is carried out in the presence of nitric and sulphuric acid, followed by crystallization in alcohol or water, and washings with sodium sulphite. The three steps of nitration can be carried out as batch processes or as a continuous process.

Most widely accepted techniques for detection of traces of explosives, e.g. ion-

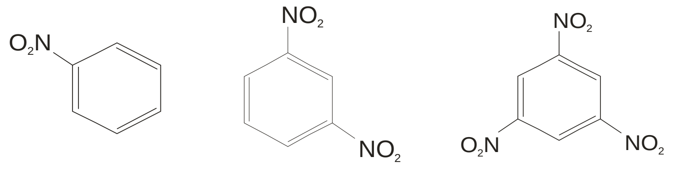

Nitrobenceno (NB) 1,3-Dinitrobenzene (DNB) 1,3,5-Trinitrobenzene (TNB)

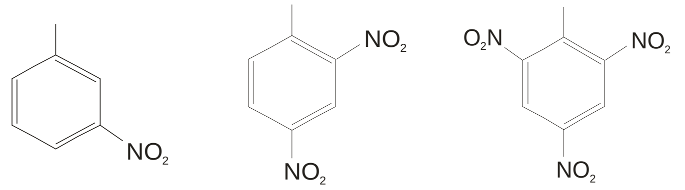

3-Nitrotoluene (MNT) 2,4-Dinitrotoluene (DNT) 2,4,6-Trinitrotoluene (TNT)

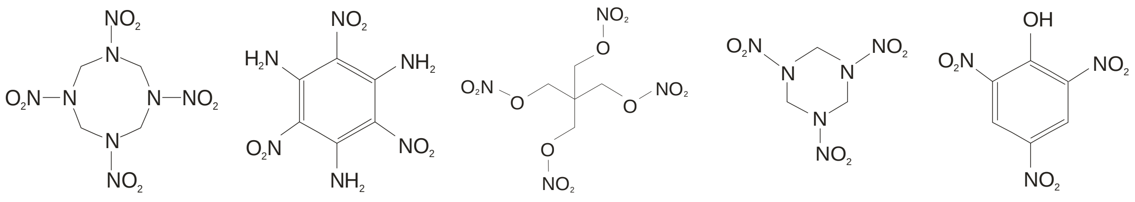

1,3,5,7-Tetranitro-1,3,5,7-Tetrazocane (HMX) 1,3,5-triamino-2,4,6-trinitrobenzene (TATB) Pentaerythritol tetranitrate (PETN) 1,3,5-trinitro-1,3,5-triazaciclohexano (RDX) 2,4,6-Trinitrophenol (TNP)

Figure 1.25. Most important nitro-organic explosive compounds.

mobility spectrometry and gas chromatography, rely on vapour detection. Unfortunately, at room temperature the vapour pressures of many common explosives are extremely small (ppb or less) and attempts to conceal the explosives by sealing them in packaging materials can reduce the vapour concentrations by up to three orders of magnitude **[Steinfeld, J. E., 1998]**. Thus, those techniques are partially limited and the development of alternative analysis methods seems to be necessary. In this direction, mass spectrometry in ambient conditions is a new promising field very useful and with a fast growth that provides mass spectra of high sensitivity directly from surfaces at atmospheric pressure by means of atmospheric ionization sources. Among these ionization techniques are Desorption Electrospray Ionization (DESI), Direct Analysis in Real Time (DART), Plasma-Assisted Desorption Ionization (PADI) and Extractive Electrospray Ionization (EESI) **[Takats, Z. et al., 2004][Cooks, R. G. et al., 2006].**

1.6.1.2. POLYCYCLIC AROMATIC HYDROCARBONS (PAHs)

In addition to explosive compounds, many other organic substances have been extensively studied and closely controlled by spectroscopic techniques as in the case of polycyclic aromatic hydrocarbons (PAHs), mainly due to its high toxicity and risk for the environment and human health.

PAHs present characteristic UV absorbance spectra. The absorbance bands are unique for each ring structure. This is particularly useful in the identification of PAHs by UV-VIS molecular absorption spectroscopy. On the other hand, most PAHs present fluorescence properties and emit characteristic light wavelengths when they are excited. The extended pi-electron electronic structures of PAHs lead to these spectral features. Thus, Fluorescence Spectroscopy (including Laser-Induced Fluorescence) is the spectroscopic technique most used in the determination of such compounds on water, soil or aerosols.

The PAHs molecules consist of fused aromatic rings with no heteroatoms or substituents in their structure **[Fetzer, J., 2000]**. PAHs may contain four-, five-, six-, or seven-member rings, but those with five or six are most common. They could be present in oil, coal and tar deposits, and they are produced as by-products of fuel burning (whether fossil fuel or biomass). They also can be found even in cooked foods **[SCF(EC), 2002]**. Moreover, they are also found in the interstellar medium, in comets, and in meteorites and are a candidate molecule to act as a basis for the earliest forms of life **[Tielens, A. G., 2008].** Thus, studies concerning decomposition pathways followed by such molecules as well as their behaviour during ionization process become of great interest.

1.6.2. APPLICATION OF LIBS IN THE ANALYSIS OF ORGANIC EXPLOSIVE COMPOUNDS

Laser ablation for analytical purposes has been extensively applied in studies of inorganic materials, including metals, semiconductors or even ceramics **[Günther, D., 2005]**, but its application to analysis of organic compounds is still largely unexplored. However, recent progresses in laser ablation and spectroscopy techniques have led to novel analysis of organic samples of different nature. There are progressively more works about ablation and characterization of polymeric substrates by the application of techniques as Pulsed Laser Deposition (PLD) **[Kordás, K. et al., 2001][Weber, I. T. et al., 2005][Mominuzzaman, S. M. et al., 2008]**, or concerning the fabrication of new organic material with the help of Laser-Induced Forward Transfer (LIFT) **[Fardel, R. et al., 2007]**. In the case of Laser-Induced Breakdown Spectroscopy (LIBS), that uses the light emitted from a laser-generated microplasma to determine the composition of the sample on the basis of elemental and molecular emission intensities **[Cremers, D. A. et al., 2006]**, the improvements carried out have allowed the application of this promising technique in organic applications as plastics characterization **[Anzano, J. M. et al., 2000],** homeland defense (landmines **[Harmon, R. S. et al., 2006]** and explosives **[De Lucia, F. C. et al., 2003][Lopez-Moreno, C. et al., 2006]**), forensic (trace of explosive or organic materials **[De Lucia, F. C. et al., 2007][Lazic, V. et al., 2011],** public health (toxic substances **[Portnov A. et al., 2003]** and pharmaceutical products **[St-Onge, L. et al., 2002]**, or environment (organic wastes **[Moench, I. et al., 1997]**). Even more complicated than organic materials, biological materials such as bacteria have also been analyzed by LIBS **[Baudelet, M. et al., 2006 A][Baudelet, M. et al., 2006 B].**

Also notable is the publication of researches on fragmentation routes of molecules in the plume and studies about the spectroscopic characterization of organic plasmas **[Sovová, K. et al., 2010]**.

The challenge for organic or biological material analysis by emission spectroscopy lies in the fact that the materials to be analyzed are composed of the same elemental substances. In the process of laser ablation, atomic emission lines corresponding to four basic elements, C, O, N, and H are always present and provide the common basis of the most organic materials **[Baudelet, M. et al., 2007]**. Moreover, from recombination processes in the plume, molecular species are also formed which are detected as spectral emission bands. Main molecular species present in plasmas from organic compounds are CN and C_2, but other characteristic diatomic species can also appear in a minority way: OH, NH and CH, among others. However, they are rarely reported.

On the other hand, detection and identification based on atomic oxygen and nitrogen or their diatomic compounds can suffer from interferences with emission from ambient air when measurements are carried out in open atmosphere. Chemical reactions also can occur between laser-induced plasma and ambient gas, leading to diatomic compounds such as CN. Therefore, atomic as well as molecular species produced after ablation due to interaction between plasma and ambient gas can additionally contribute to the total intensities of specific plasma emission lines **[Lucena, P. et al., 2011].**

Regarding the field of explosives detection, the ability of LIBS to provide rapid multi-element microanalysis of bulk samples (solid, liquid, gas, and aerosol) in the parts-per-million range with little or no sample preparation has been widely demonstrated **[Song, K. et al., 1997][Rusak, D. A. et al., 1998][Sneddon, J. et al., 1999][Winefordner, J. D. et al., 2004][Pasquini, C. et al., 2007]**. LIBS technique holds particular promise for the detection and identification of explosives because of its intrinsic capability for minimally destructive, in situ, real-time detection and analysis of a broad range of chemical species. The ability of LIBS to detect trace amounts of materials with a single laser shot is especially important for residue detection, because the first shot can ablate all or most of the residue.

Moreover, the analysis of organic compounds with high energetic content has been always an interesting task due to the chemistry associated to their internal energy **[Adams, G. F. et al., 1992]**. Thermal decomposition chemistry is fundamentally important in the explosives field, and the determination of the kinetics and mechanism of this breakdown process remains a fundamental aspect of their characterization **[Cohen, R. et al., 2007].** Apart from their analysis and once the identification has been performed, next step is the detection of explosive residues for both local and remote detection, a field where LIBS has become a very useful and suitable forensic tool. **[Mullen, C. et al., 2006][Jennifer, L. et al., 2008][Jennifer, L. et al., 2009][Lucena, P. et al., 2011][Moros, J. et al., 2010 A].**

On the other hand, a considerable amount of literature has been published about the application of LIBS to the detection of explosive residues regarding methods to improve the sensitivity and selectivity of the technique as the use of chemometric tools, double-pulse arrangements, resonant LIBS, and the use of ultrashort laser pulses. Other strategies have been designed to improve the discrimination of explosives from non-explosive substances **[Lazic, V. et al., 2012][Fernández-Bravo, A. et al., 2012].** Concerning the analysis of explosive residues, selective sampling and analysis of explosive residues on solid surfaces has been successfully tested. The field of forensics can greatly benefit from the analytical performance of LIBS, in particular from the single-shot LIBS approach due to the often small sample size available for analysis.

In addition to LIBS, a lot of spectroscopic methods are been used in the explosive detection including Ion-Mobility Spectroscopy, Terahertz Spectroscopy, Raman Spectroscopy, and Cavity-Ring Down Spectroscopy.

Besides the analysis for detection or identification of organic compounds, LIBS has been widely used in the characterization of plasmas coming from samples of different nature, due to its many advantages as analytical technique. Plasma is a spatially inhomogeneous and transient system, so temporally and spatially resolved spectroscopy stands as an efficient tool to carry out this type of researches in order to obtain a better knowledge of plasma expansion dynamics and to study the physical properties of its emission.

1.6.3. APPLICATION OF LIMS IN THE ANALYSIS OF ORGANIC EXPLOSIVE COMPOUNDS

Direct analysis of solids by Laser Ionization Mass Spectrometry has been widely used in materials research, the semiconductor industry, geology, biomedicine, and environmental research for its excellent ability to determine trace elements. Lasers offer a highly versatile energy source for atomization, excitation, and ionization and laser parameters can be easily controlled to adjust the condition of ionization source. The combination of laser ionization and mass spectrometry makes it a powerful tool for elemental analysis. Mass spectrometry is capable of characterizing the laser plasma to determine the ion yield, cluster formation, and both angular and velocity distribution. The high laser irradiance one-step ionization LIMS, is specialized for rapid multi-elemental analysis, and this system shows great potential for the analysis of bulk solids, e.g. metal, alloy, and geological samples.

Although the primary application of mass spectrometry together with laser excitation is the trace analysis of metals and alloys, further LIMS has demonstrated to be versatile enough in the analysis of organic materials. An excellent example is the detection and characterization of organic compounds with high energetic content

[Mullen, C. et al., 2009]. The technique shows as clear advantage the significant improvements in sensitivity and selectivity in the identification and quantification of trace amounts with a fast sampling and avoiding tedious methods of sample preparation **[Tönnies, K. et al., 2001]**. Moreover, the contribution of mass spectrometry on studies of decomposition and detonation products has become considerable importance in forensic chemistry, helping greatly to the understanding of fragmentation pathways of parent molecules **[McMillen, D. F. et al., 1997][Kosmidis, C. et al., 1994]**. In this sense, a number of remarkable phenomena during the ignition and combustion of energetic materials are likely to be studied by means of coordinated analysis based on mass spectrometry fundamentals.

Concerning the physical state of the material, in the last years many studies have been carried out in gas phase by laser photo-ionization of explosives and explosive-related compounds (ERCs), but only a few have been reported for condensed phase (mostly using ultrashort (fs) laser pulses) **[McMillen, D. F. et al., 1997][Mullen C., et al., 2006 A][Mullen C., et al., 2006 A].** An example of laser ionization with nanosecond pulses is the study of fragmentation routes for nitrobenzene and nitrotoluene, recently studied by UV laser radiation **[Kosmidis, C. et al., 1994] [Galloway, D. B. et al., 1993].**

Therefore LIMS is considered as a trade-off tool for rapid atomic and molecular analysis whose analytical capability is independent from the state of aggregation of the matter **[Sisoev, A. A. et al., 2002].** Moreover, it is independent of the electric and magnetic properties of the solids, making possible the analysis of conductive, semiconductive and dielectric solids. Multielemental and simultaneous analysis of major, minor and trace elements with a wide dynamic range of up to 10^9 in any kind of solid can be easily done **[Becker, J. S. et al., 2003].** These advantages, added to the non-existence of moving parts inside a TOF, explain the use of LIMS even for extraterrestrial analysis in solar-battery powered instruments **[Brinckerhoff, W. B., 2005].**

CHAPTER 2

Experimental

2.1. INTRODUCTION

The basic experimental setup used to carry out the experiments included in next sections will be described in detail in this chapter. Further in successive chapters, modifications or improvements implemented in the configuration will be indicated in case of each particular experiment.

First of all, it is necessary to differentiate between the instruments required for the acquisition of mass spectra (LI-TOF-MS) and those used to obtain the optical emission signal from the generated plasma (LIBS). These two independent analytical systems were connected and synchronized conveniently in order to work simultaneously with both techniques and therefore to be able to acquire coincidental measurements in real time, obtaining spectral mass data and optical emission information from the same laser event.

In last section of this chapter it will be presented the connection between both acquisition systems to carry out the development of *analysis in coincidence* experiment.

2.2. LI-TOF-MS SYSTEM

The time-of-flight analyzer, core of the LI-TOF-MS system, was purchased from *R.M. Jordan (Mountain View, CA, USA)* and has been conveniently modified in many of its different parts (ionization chamber, ionic lenses, sample insertion system, etc.). This fact facilitated to carry out the appropriate adjustments or to adapt new parts to the experiment if necessary. The equipment worked under high vacuum regime and, therefore, it required a powerful pumping system to keep a stable pressure level within both the analyzer and the ionization chamber.

The time-of-flight mass spectrometer used in the development of this research had a pulsed Nd: YAG laser as excitation source, conveniently focused on the sample surface object of analysis. In all cases the sample was located inside a stainless steel vacuum chamber where ionization occurred, and it was fixed to an aluminium sample holder with double-sided adhesive tape. Sample was then subjected to a vacuum level enough to ensure the correct running of the detection system.

When the laser beam comes into contact with the solid surface of the sample, a series of physical phenomena, described in detail in the previous chapter, takes place, and the generated ionic species will characterize the material in question. Such ions are extracted from the ionization zone by applying an electric potential from an extractor electrode with negative polarity, and then the positively charged ion beam passes through an ionic lens system which will accelerate and focus the beam suitably before entering into the tube of flight, where the beam will find the field-free region. As the ions travel through this region, they are separated according to their mass-to-charge ratio (m/z) in such a way that ions with less m/z ratio will acquire larger speed and therefore, they will hit first the microchannel plate detector. Once they arrive to the detector, and after the collision of each ion with the first plate, a first electron is released and it generates a cascade of secondary electrons by successive collisions on the walls of the microchannels forming the active area of the plate, thus resulting in the amplification of the signal when such electrons reach the anode.

The signal is transferred to a digital oscilloscope whereby the mass spectrum is monitored. Finally, the data is transferred to the computer for further processing and storage using the software designed for this purpose **[Vadillo, J. M. et al., 2005][Alcántara, J. F. et al., 2008].**

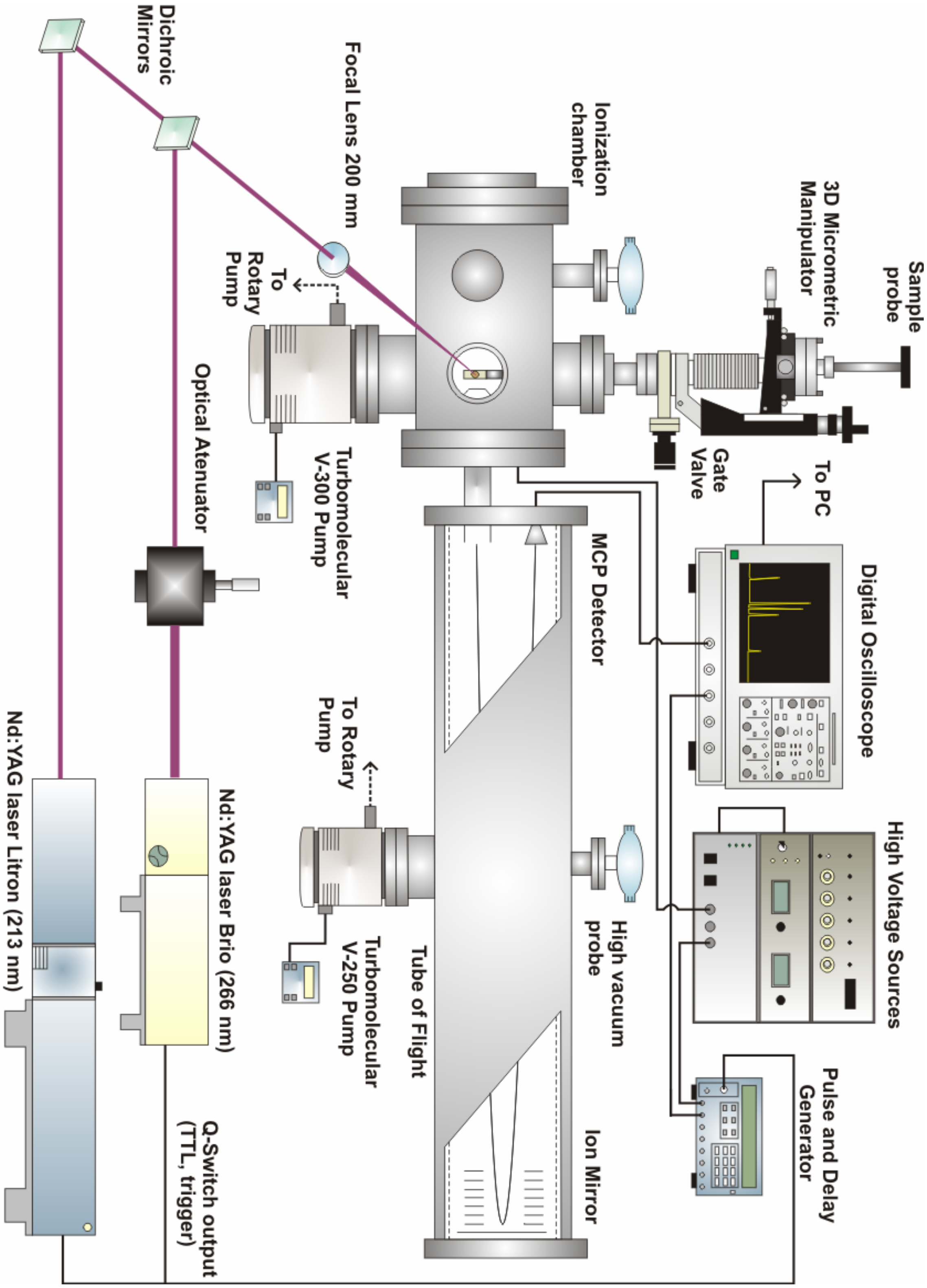

Figure 2.1. General diagram of the experimental setup used for LI-TOF-MS analysis.

In next section of the present chapter the main elements that make up the LI-TOF-MS system will be described in detail for greater understanding of its operation. Figure 2.1 shows a general scheme of the equipment that will complement the further description.

2.2.1. IONIZATION SOURCE

The laser as a source of ablation and excitation of the species contained in the sample is common in all performed studies. The dose of energy per pulse, the repetition rate, the beam profile and spot size, besides the type of cooling and power supply are the main laser parameters that affect their mode of operation and make to a certain laser suitable for a specific application.

The laser sources used in the development of the research are presented here:

- Nanosecond pulsed Nd:YAG laser *Quantel* model *D31Brio*. It emits at the fundamental 1064 nm wavelength. By means of the appropriate harmonic generator crystals and dichroic mirrors, the second (532 nm) and fourth (266 nm) harmonics are also arranged, being this latter the mainly output radiation used in the different performed analysis. The maximum output power for the fourth harmonic was 12 mJ according to specifications. The specified laser pulse width was 4.4 ns.

- Nanosecond pulsed Nd: YAG laser *Litron* model *NANO-T-250-10*, which emits at the fundamental 1064 nm wavelength. With the corresponding harmonic generator crystals and dichroic mirrors, the second (532 nm), third (355 nm), fourth (266 nm) and fifth (213 nm) harmonics are also available. The maximum output power for the latter 213 nm radiation was 12 mJ according to specifications. The specified output pulse width was 4 ns in this case.

Laser pulse energy was controlled thanks to variable attenuators that allowed continuous variation of the energy per pulse without causing distortions in the beam spatial profile due to thermal lens effect in the laser rod.

In the experiments carried out with *D31 Brio laser,* an external attenuator *Newport 935-3/5-OPT* was used, which allowed a precise control on the doses of radiation reaching the sample, and whose operation is based on Fresnel reflection principle. It uses a pair of counter-rotating crystals with wedge shape to reduce the energy of the beam due to a reflection phenomenon with a negligible deviation of the optical path of the beam at the output of the system. It is crucial to operate the laser at its maximum flashlamp voltage and at a fixed value for delay in Pockels cell or Q-switch in order to keep constant the whole system, and therefore, the laser output energy. In this case, the optimum delay value was 140 μs that allowed working at maximum output energy for laser source. To get this, it is required this type of attenuation system for the control of energy and thus, the resonator and the laser beam output does keep stable pulse to pulse. In the case of SHG (Second Harmonic Generator, 532 nm), the adjustment was performed through the use of the phase-matching screw by tuning the crystal angle. But for the FHG (Fourth Harmonic Generator, 266 nm), the non-linear crystal is operated by temperature control so the phase-matching was obtained by adjusting the temperature by the potentiometer, reaching the optimum temperature of 81ºC. In such conditions, the refraction index does not change at all. The optimization of voltage of the potentiometer was carried out at a repetition rate (frequency) of 2 Hz and the results are showed in Figure 2.3.

In the case of *Litron NANO-T-250-10 laser*, the attenuator is built in the instrument between the oscillator and the external module of harmonic generators.

The optimum value for electro-optical modulator is also set (130 μs) in order to assure the laser stability. The harmonic generator crystals have all a thermal control system and once the temperature reaches 100 °C, it remains constant during the lasing process.

On the other hand, and in order to achieve a suitable guiding and focusing of the beam towards the sample surface, a dichroic mirror and a focal lens were used. The dichroic mirror reflects only the radiation of interest and removes the residual radiation by transmission whereas the quartz plane-convex focal lens with 200 mm focal length and diameter of 1" was situated in the optical path and it focused the beam on a small area so that the fluence level was enough to reach the desorption regime and to generate ions when sample was irradiated.

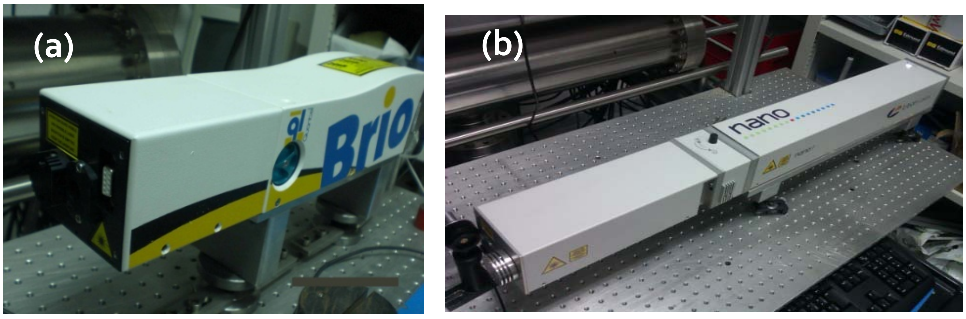

Figure 2.2. Ionization laser sources. (a) Brio D31 (b) Litron T-250-10.

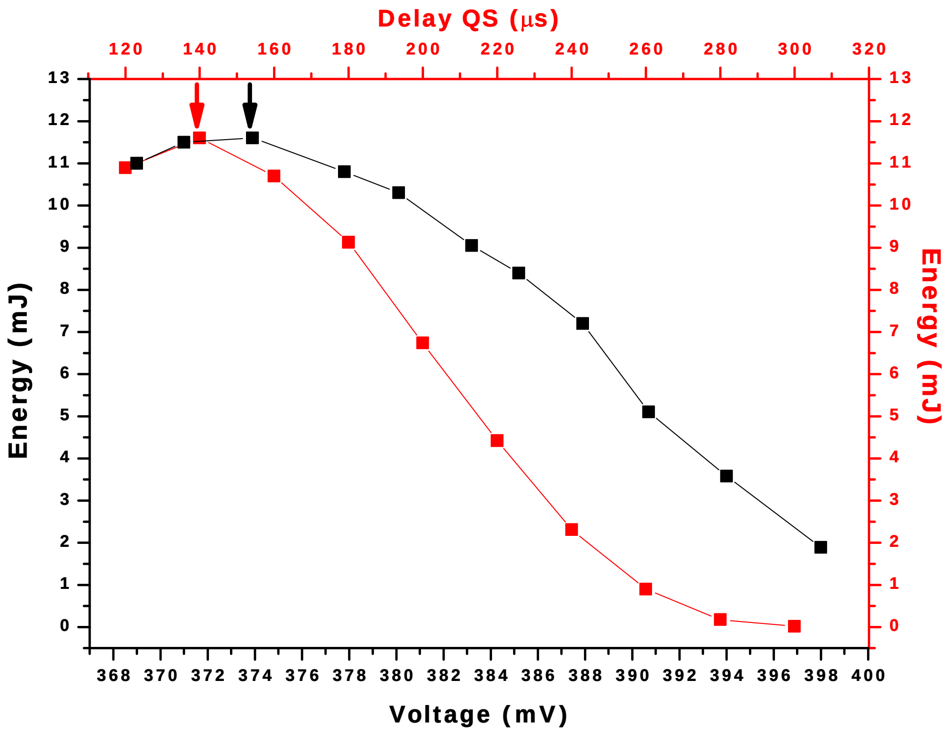

Figure 2.3. Operating voltage and delay Q-Switch optimization for FoHG laser Brio.

Table 2.1. Main characteristic of laser sources

Laser	Brio D31	Litron NANO-T-250-10
Fundamental radiation	1064 nm	1064 nm
Maximum output energy (1064 nm, F 10 Hz)	100 mJ	250 mJ
Harmonics	532, 266	532, 355, 266, 213
Optimum DQS	140 μs	130 μs
Width pulse	4.4 ns	4 ns
Spot beam area	3,5 mm	6,35 mm
Beam profile	Gaussian	TEM^{00} (plane) / Multimode (gaussian)

2.2.2. VACUUM SYSTEM

High vacuum regime must be set in both the ionization chamber and the TOF analyzer in order to allow the transference of ions from the ionization region to the detector without collisions in their trajectory. The mean free path of the ions must be at least 2 times longer than the length of the tube, since that is the total distance covered by such species in the reflectron mode operation. To achieve this, the presence of turbomolecular pumps is required in order to evacuate the air out of the internal volume of the system. In our case, two pumps *Varian* model *V-300 (300 L/s)* and model *V-250 (250 L/s)* were installed, which reached a rotational speed of 56 krpm in the operation regime. The first one was installed under the ionization chamber joined to it, whereas the second one was placed attached to the flight tube. Under pressure conditions achieved with them, the free path of ions is significantly higher than the minimum value required. This parameter can be calculated using the equation 1.24 indicated in Chapter 1 of this memory, where λ represents the mean free path, k is the kinetic gas constant, T is the temperature, σ correspond to effective section or collision probability, and P symbolizes the pressure level.

The molecules in gas phase coming from the interior of the system will collide against the suitably positioned rotor blades of the turbomolecular pump which rotates at high speed, receiving an additional component of velocity in vertical direction. Each of the secondary pumps is connected to another rotary pump *Varian* model *MDP12*. These primary pumps are necessary for the proper evacuation of the secondary pumps, and they maintained constant the vacuum level by expelling the air directly to the atmosphere. In that way the vacuum level reached inside the analyzer was down to $1.0 \cdot 10^{-7}$ mb. This low pressure value is measured using a special probe for high vacuum systems as *Bayard-Alpert* model *571* from *Varian*, located at the midpoint of the flight tube through a lateral access port. On the other hand, the primary vacuum level was measured by a thermocouple sensor installed in the pre-chamber circuit used for in-advance sample introduction. This initial vacuum existing in the pre-chamber ($1.0 \cdot 10^{-3}$ mb) was generated by means of a third rotary pump *Edwards 8 two stages* model *BS2212*. The pre-chamber housed the sample prior to come into contact with the high vacuum environment inside the ionization main chamber.

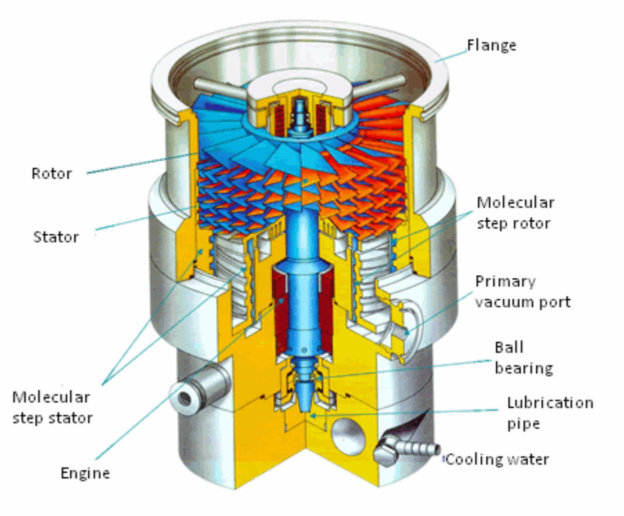

Figure 2.4. Cross section of a turbomolecular pump. Adapted from MILKA.

2.2.3. IONIZATION CHAMBER

The ionization chamber is a compartment made of stainless steel with multiple access ports which is able to operate in ultra high vacuum regime. It is attached to the flight tube through a flange *CF150* in one of the lateral ports. A spatial restriction causes a gap of around one order of magnitude between the vacuum level inside the chamber and that existing inside the flight tube. Thus, pressures better than $1.0 \cdot 10^{-6}$ mbar inside the chamber are always used. This parameter was measured by another *Bayard-Alpert* probe from *Varian* model *571* installed in a port on the top of the chamber using a flange *CF35*. The main upper port was mainly used for the sample insertion device specifically designed to control the sample holder, whereas the lower port was used for connecting the turbomolecular pump *V-300* through a flange *CF150*.

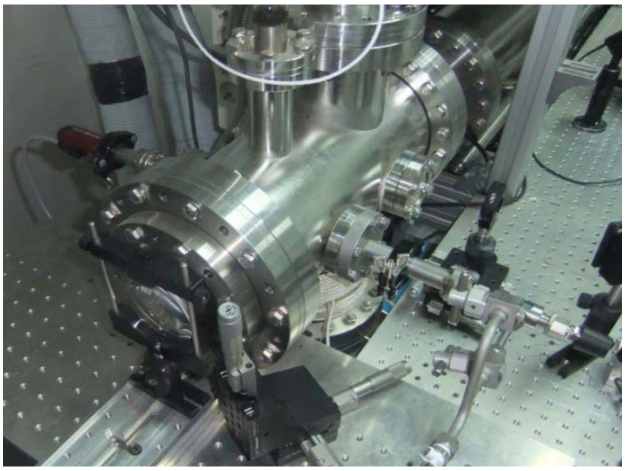

Figure 2.5. Upper view of the ionization chamber.

The other lateral port has adapted a flange *CF100* with a *UV FSVP* window which allows transmission of light in the UV region up to 200 nm, and it was used for visual inspection of the interior of the chamber and also to carry out the plasma optical collection in those experiments where the optical emission signal was collected.

There are also several additional auxiliary ports in the front and rear of the chamber. In one of them a *TPR Pirani sensor 280* was adapted with a flange *CF35* capable to measure the pressure level inside the chamber in the range between 10^{-4} mb and atmospheric pressure. Finally, in another port, a needle valve was adapted using once again a flange *CF35* for precise control of air leak in the system.

2.2.4. PRE-CHAMBER AND SAMPLING PROBE

For the insertion of the samples into the ionization chamber and in order to speed up their interchange, a pre-chamber already developed in our laboratory **[García, C. C. et al., 2003]** was used into which the sampling probe was placed manually. After closing the vent valve and isolate the compartment from the atmosphere, vacuum from a primary vacuum is applied into the pre-chamber by means of the corresponding rotary pump *Edwards BS2212*. When pressure has stabilized into the compartment (around $1.0 \cdot 10^{-3}$ mb), the pre-chamber is let to keep in contact with the main chamber by opening a guillotine valve that kept separated both sections, and the sample was placed in the final position for the analysis. The system had a 3D micrometric manipulator with four degrees of freedom, allowing movement of the sample in the three axes of space (X, Y, Z) and rotation on itself (θ). The micrometer for Z axis control allowed a total displacement of 100 mm, whereas micrometers in X and Y axes allow a shift of 20 mm.

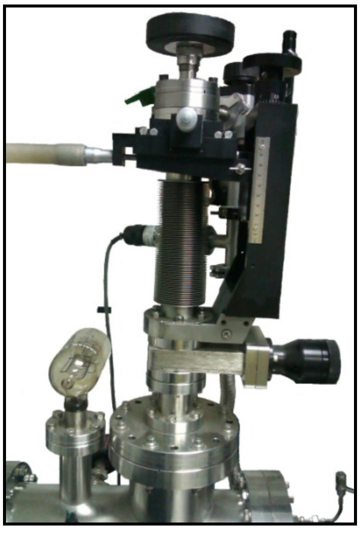

Figure 2.6. 3D micrometric manipulator and pre-chamber.

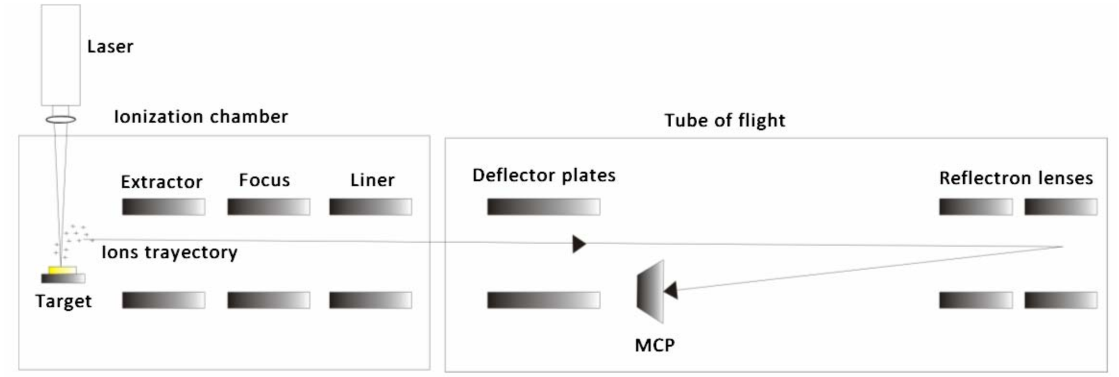

Figure 2.7. Distribution of ionic lenses (electrodes) for the guiding of ions from ionization point to detection system.

2.2.5. IONIC LENSES

The ionic lenses of the system have the function of extraction, focusing and acceleration of generated ions in the laser ionization process. It consists of several electrodes and grids to which different voltages are applied. Such voltages were modified with the purpose of optimizing the final detection of ionic species. For the application of these voltages on the electrodes, several associated potential sources were available: a source *ITAR* model *D-803-R* to supply electric energy to the lens train in the input of the flight tube, to the lenses of reflectron and detector; another source *Demestres DG-31* supplied the voltage to the extraction electrode; and a final source *DEI* model *PVX-4150* which essentially consists of a voltage switch that allowed to pulse the electric potential applied to the electrode extractor. In Table 2.2, optimized values for the voltages applied to each of these lenses or electrodes and their physical location on the system are showed.

Table 2.2. Optimized voltage values in electrodes used for guiding the positive ions toward the detector.

Electrode	***Ubication***	***Voltage***
Extractor	Ionization Chamber	-1250
Liner	Ionization Chamber	-1075
Focus	Ionization Chamber	-205
Deflectors	Input of Flight Tube	-960
Reflectron 1	End of Flight Tube	-50
Reflectron 2	End of Flight Tube	+405
Detector	End of Flight Tube	-3010

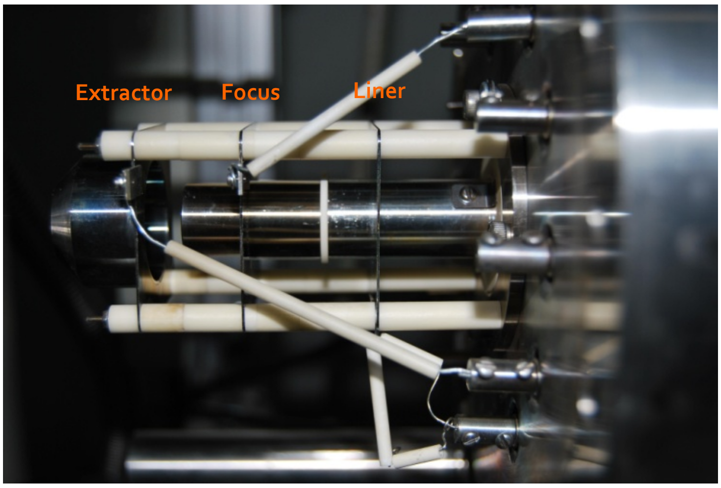

Figure 2.8. Ionic lenses into the ionization chamber.

The configuration for ion extraction used in the experiments was orthogonal. The laser entered into the vacuum chamber in a direction perpendicular to the axis of the flight tube (extraction axis) through a front window, and the beam impinged the sample orthogonal to its surface as well.

After passing through the grid of the extraction electrode, the liner and focus electrodes were in charge of accelerating and focusing the ion beam in a suitable way, and then the deflector plates modified the trajectory of the beam in order to impinge on the reflectron lenses with the appropriate incidence angle. The ions were repelled by the reflectron and finally they reached the detector in the other side of the tube.

Figure 2.7 indicates the location of all the electrodes of LI-TOF-MS system whereas the photograph in Figure 2.8 shows the appearance of the lenses situated into the chamber joined to the entrance of the analyzer.

2.2.6. TIME-OF-FLIGHT ANALYZER WITH REFLECTRON

Once the ions have travelled through the focusing lens after leaving the ionization chamber, they pass through the deflector plates which redirect the ions towards the reflectron placed at the end of the tube with a suitable angle, being subsequently pointed back towards the detector. The achievement of reflectron was developed by Mamyrin in 1973 **[Mamyrin, B. A., 1973]** so the non-linear trajectory for ions was established for new time-of-flight analyzer thereafter. Thus, the use of the reflectron gets to improve the resolution of the analyzer by increasing the distance covered by the ions, allowing better separation between them and correcting the small velocity dispersion of ions with the same mass-to-charge ratio, due to the initial dispersion at the time of their generation, making these packages of ions narrower.

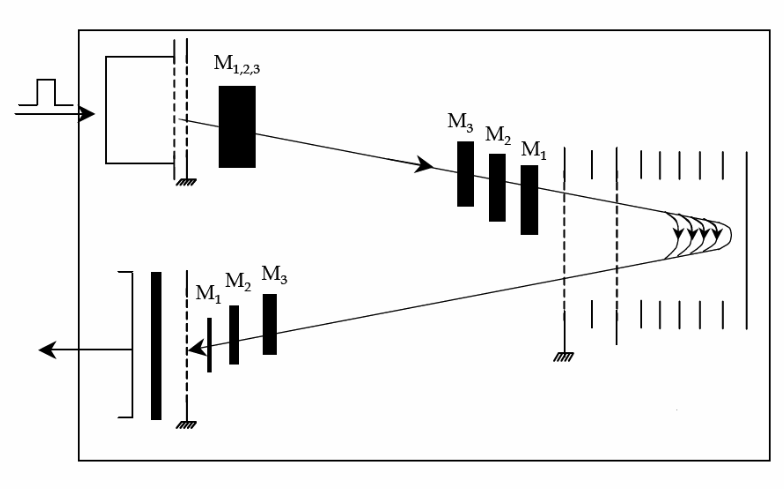

Figure 2.9. Basic scheme of operational fundament of a reflectron-TOF analyzer.

In the application of the LI-TOF-MS as a technique of analysis, it is necessary to calibrate the mass range of the analyzer in order to assign an accurate m/z value to an ion whose flight time has been measured. This aim requires obtaining the time-of-flight of at least two ions with known mass-to-charge ratio. A mathematical parabolic fit is performed with the time-of-flight times obtained for such selected peaks of the standard samples and their mass-to-charge ratios, by means the time-of-flight equation:

$$m/z = a\, t^2 + b, \qquad \textbf{(Eq. 2.1)}$$

where t represents the time-of-flight of the ion; and a and b are the fit constants to calculate in the resolution of the system.

2.2.7. DETECTION SYSTEM (MCP)

A suitable detector for the LI-TOF-MS system must have a fast response time besides a high gain value and good efficiency in the conversion. In this way, detection with excellent temporal resolution can be achieved. The detector installed in our system is a three units microchannel plates (MCP) with *Chevron* configuration that operates in positive mode. This type of detector is incorporated in the most of time-of-flight spectrometers, and the multiplication of electrons takes place into their microchannels. The first plate of the detector is operated at -3000 V, but it can be operated up to -3300 V. Such voltage is applied from the potential source and due to safety reasons it was never operated above -3150 V. The second plate is always at the 54.5% of the first MCP voltage, and the third works at 9.1% of the initial voltage. Each

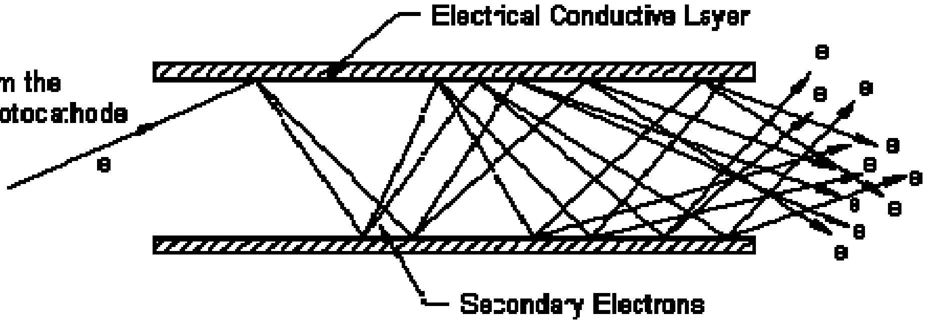

Figure 2.10. Process of multiplication of electrons in a MPC.

plate has a diameter of 18 mm and a thickness of 0.5 mm, whereas the channels have a diameter of only 10 μm, with spacing between channels of 12 μm and a resistive coating. After the collision of an ion with enough energy with the walls of the first microchannel plate, a first electron is released and this generates more electrons by colliding with the walls of the channels. The collisions in cascade result in a current of electrons reaching the anode, which is made of steel and is always connected to ground, causing the signal amplification (see Figure 2.10). Beyond the anode collection, signal is transferred to a digital phosphor oscilloscope (DPO) using a cable with an impedance of 50 Ω, which ends in a *Bayonet Neill-Concelman* (BNC) connector. As the efficiency of the detection strongly depends on the kinetic energy of the ions (not noticeable at low mass range but easily observable in the case of working with macromolecules), **[Wenzel, R. J., 2005]** the MCP has a grid connected to ground voltage so that ions get accelerated before hitting the MCP surface. This allowed for greater signal gaining, estimated around 10^6 in the present case.

2.2.8. DATA ACQUISITION AND PROCESSING SYSTEM

The electronic elements in the experimental system associated to the capture and display of the signal were mainly two: the DPO and the software linked to storage and post-processing of the signal.

- **DIGITAL PHOSPHOR OSCILLOSCOPE**

The acquisition of the mass signal was accomplished with a four-channel DPO *Tektronix* model *TDS5054B* (see Figure 2.11). This device was responsible for capturing the electrical signal and displaying it as mass spectrum. As main characteristics, the DPO had a 500 MHz bandwidth capable to work at a sampling rate of 5 Gsample/s. The digitization of the signal allowed obtaining the full mass spectrum for each ions pulse,

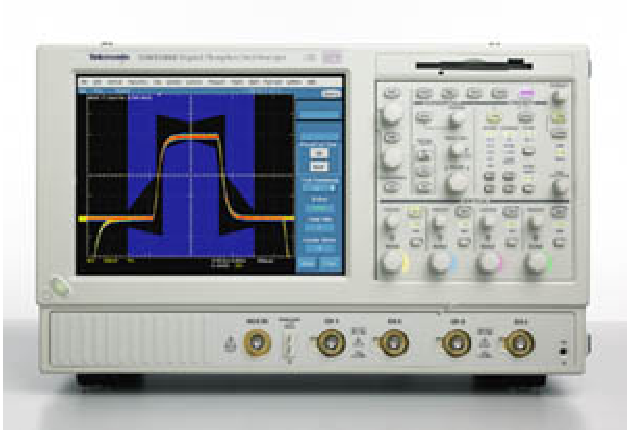

Figure 2.11. Digital Phosphor Oscilloscope Tektronix TDS5054B.

showing the intensity data (voltage) versus time-of-flight of ions present in the sample. In the spectrum, ions of equal mass originated a peak and the corresponding time for that ion is provided by the maximum of peak value.

Spectral resolution was calculated by dividing the time-of-flight of the ion measured at the point of peak maximum intensity and the full width of the peak measured at half of its maximum high (FWHM).

- **SOFTWARE**

All the information is then processed by three different software interfaces: TekScope^{TM} , MATLAB^{TM} and OriginPro 7.5.

The oscilloscope includes an integrated CPU with specific software developed by *Tektronix* (TekScope^{TM}). An interface allowed the control and manipulation of the every single parameter of the instrument in real time for the acquisition, monitoring and proper storage of signal. The device had the ability of acquiring through the four independent input channels simultaneously.

The most interesting tool of this software was the *Fast Frame* acquisition mode, which can acquire kinetic series with a limited number of events in response to a certain trigger signal. The resultant waveforms were saved in the RAM memory of the computer. This powerful tool allowed to perform many of the experiments described in this memory.

The post-processing data work was assisted by MATLAB^{TM} software application. Some MATLAB^{TM} routines were designed and adapted to carry out the rapid and orderly compilation of data coming from the output of *TekScope* files, as well as to carry out the computation of the resolution and calibration of the analyzer. When the routine is running, it prompts the user for some information about the data to be

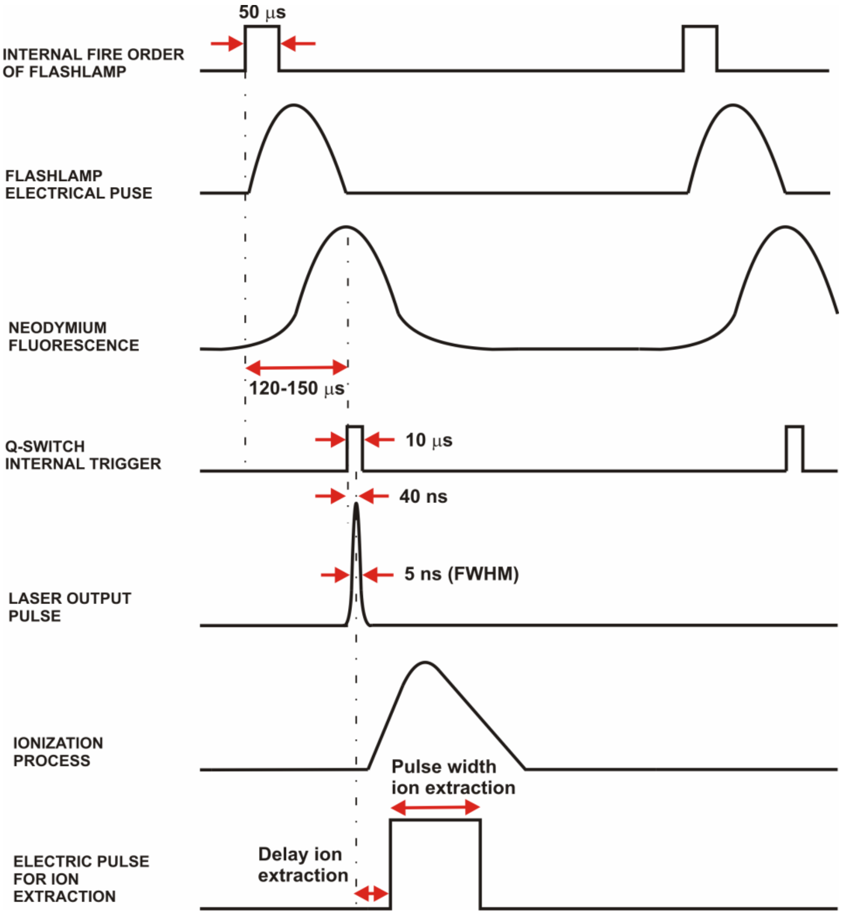

Figure 2.12. Timing diagram for the synchronization between laser pulse event and the extraction of ions pulse through the PDG. (FWHM: Full width at half maximum).

processed. The use of these scripts implied the reduction of time required for the processing of data considerably. On the other hand, subsequent math processing data work for analysis and interpretation of results was carried out with software OriginPro7.5.

2.2.9. ADDITIONAL ELECTRONIC DEVICES

To start the acquisition of mass spectra after sample ionization, a TTL pulse coming from output laser Q-switch was used as trigger signal of the system, and this signal was sent to a pulse and delay generator (PDG) *Stanford Research Systems* model *DG535*. This device made possible the delay in the ion extraction step. The PDG sent two signals: one went to the oscilloscope to start the acquisition, and the second one was sent to the pulsed potential source which controls the delay in the application of the voltage pulse at the extraction electrode. A timing diagram about the synchronization between the shot of the Q-switch laser, the activation of PDG and the opening of pulsed potential source is shown in Figure 2.12.

2.3. LIBS SYSTEM

The experimental system used in the development of optical emission experiments by laser-induced plasmas spectroscopy basically consisted of an optical system for light collection from plasma plume generated in the irradiation of a sample and a spectrograph with an optical ICCD detector. The collected light was then scattered and recorded by means of the detector so that such signal was transformed into a digital emission spectrum.

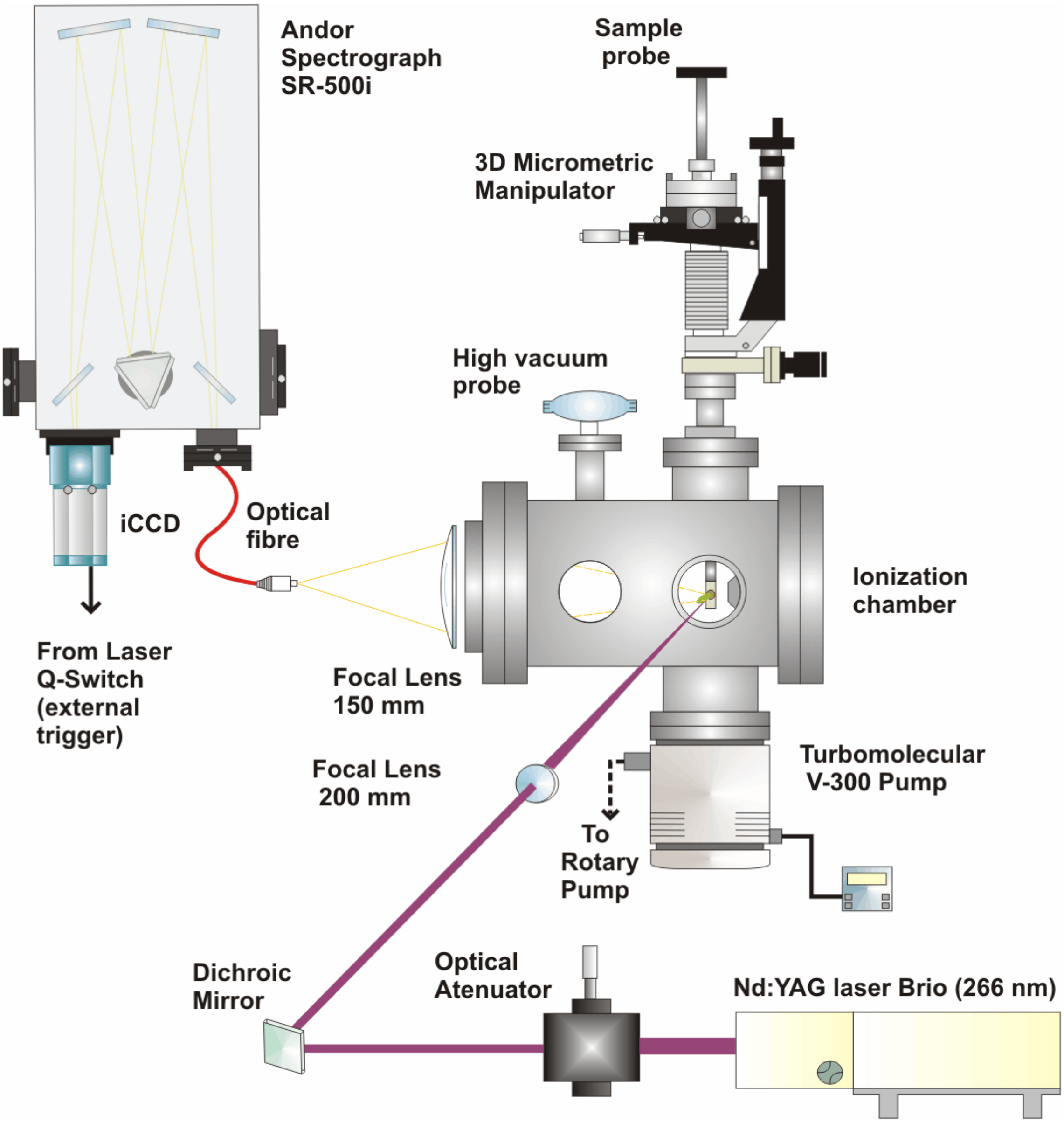

Figure 2.13. Basic scheme of LIBS experimental configuration.

2.3.1. OPTICAL COLLECTION SYSTEM AND SPECTROGRAPH

The emitted light from plasma generated in the ablation of a specific sample was collected sideways and orthogonal to the expansion direction of the plume, as can be observed in Figure 2.13. A quartz plane-convex lens with a diameter of 3" and a focal length of 150 mm was used for collecting the light. The lens was situated outside and next to the lateral quartz window of the chamber. It covered most of the window area so that almost all the light coming from the plasma plume was collected. Then, the plasma image was focused on the end of a fibre optic *Avantes FC-UV600-2* with a core diameter of 600 μm that led the light to the entrance slit of the spectrograph *SR-D1-500i Andor*, equipped with a intensified charge-coupled device (ICCD) camera *iStar Andor* model *DH734-18F-03*. The spectrograph had a focal length of 500 mm, and was equipped with 3 diffraction gratings inserted in a turret with 600, 1200 and 2400 lines per mm respectively, with an accessible spectral coverage of 45 nm, 20 nm and 12 nm respectively, and maximum values for resolution of 0.19 nm/pixel, 0.106 nm/pixel and 0.044 nm/pixel for each of them. Therefore, the end of the fibre optic was connected by means of a SMA connector to the front input port of the spectrograph, setting a gap of 20 μm for the entrance slit. The dimensions of the device are shown in Figure 2.14.

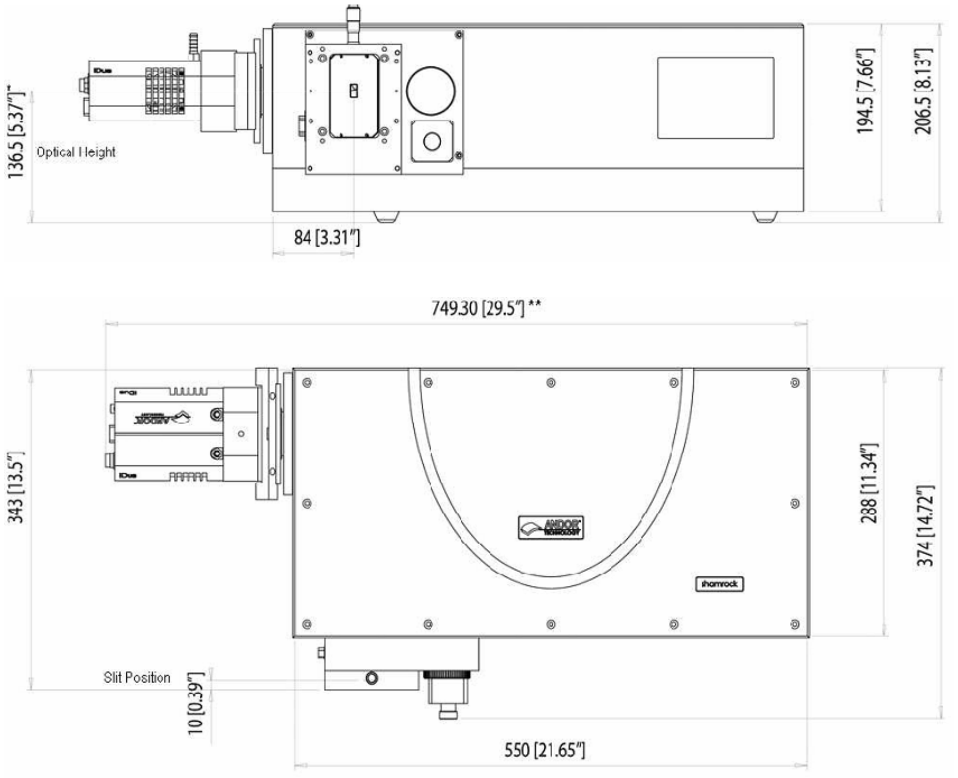

Figure 2.14. Plan of spectrograph SR-500i-D1 and intensified CCD DH 734-18F-03 from Andor.

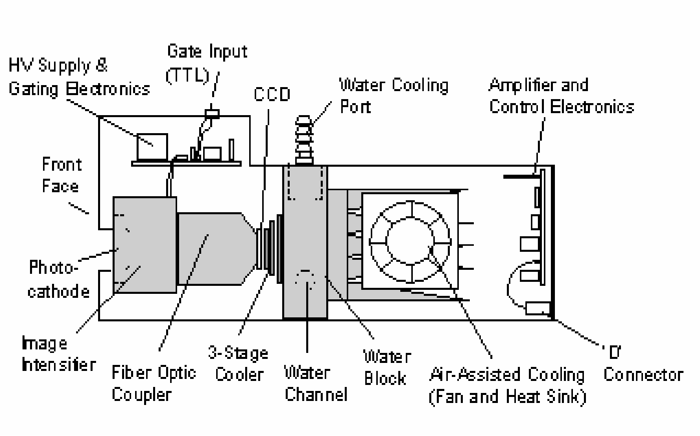

Figure 2.15. Sectional simple view of intensified CCD camera.

2.3.2. INTENSIFIED CCD

The collected light, after being scattered in the spectrograph, is detected by an intensified CCD camera *Andor* model *DH734-03-18F*, which is coupled to one of the output ports of the spectrograph (see Figure 2.15). The camera includes two basic elements namely the image intensifier and the CCD. The latter is attached to the intensifier by means of a high efficiency fibre optic coupler. Moreover, the device includes the cooling system and the gating electronics.

An image intensifier is a device that amplifies the intensity of an image. Adding an image intensifier to a CCD gives two main advantages: a higher sensitivity (single photon events can be detected) and ultra fast shuttering. There are three major elements in the image intensifier: the photocathode, the microchannel plate (MCP) and the output phosphor screen. The properties of these three components determine the performance of the device. Thus, as can be seen in Figure 2.16, the image intensifier consists of an evacuated tube with a front window which has a photocathode coated on its inside surface. When a photon strikes the photocathode, an electron is emitted towards the microchannel plate by an electric field. The combination of the input window and photocathode determines the spectral response of the image intensifier: the input window usually determines the lower wavelength limit and the photocathode the long wavelength response.

The microchannel plate has a high potential across it (500 to 1000 V) so that the emitted photoelectron will cascade down the channel producing secondary electrons and exiting as a cloud of electrons. The cloud is finally accelerated and strikes a phosphor coating on the inside of a fibre optic exit window. By increasing the voltage

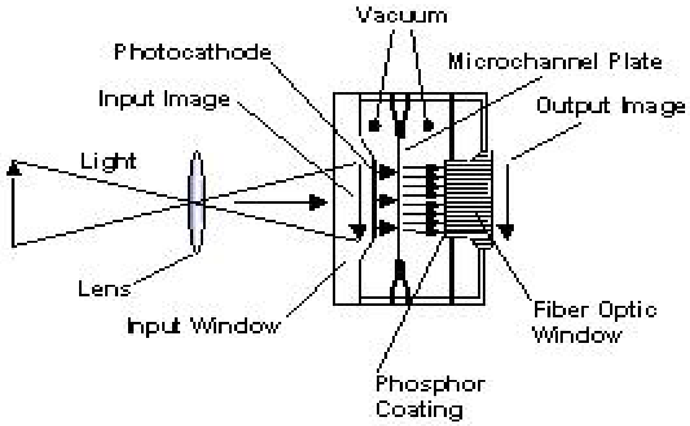

Figure 2.16. Elements of an Image Intensifier.

across the microchannel plate, the gain is increased and hence the signal reaching the CCD sensor is amplified. This MCP gain is variable through a range of 0 to 255.

The function of the phosphor on the exit window is to convert the incident electron pattern into a visible light pattern that can be detected by the CCD. For best efficiency, it is important that the emission of the phosphor is matched to the response of the CCD. The output fibre optic of the image intensifier is coupled to the CCD via a fibre optic reducer (which reduces the size of the image before it falls on the CCD). The high efficiency of fibre optic coupling is important because it means that the image intensifier can be operated at lower gains, which results in better dynamic range and linearity. This is why ICCDs have replaced Intensified Photodiode Arrays (IPDAs) as the detector of choice.

A Charge Coupled Device (CCD) is a silicon-based semiconductor chip bearing a two-dimensional matrix of photo-sensors, or pixels. This matrix is usually referred to as the image area. The pixels are often described as being arranged in rows and columns: the rows running horizontally and the columns vertically.

Finally, the iStar's detector head incorporates a Digital Delay Generator (DDG) inside. A trigger pulse from either an internal or an external source activates the DDG, so as it can control the intensifier tube for gating applications.

The main technical features of ICCD are listed below:

- Matrix of 1024 x 1024 active pixels in CCD-chip.
- Total active area 13.3 x 13.3 mm.
- Diameter of intensifier, 18 mm.

- Maximum spectral range, 115 nm – 920 nm
- Maximum delay time from external trigger signal to the opening of intensifier tube, 35 ns.
- High sensitivity (single photon) and ultrafast shuttering up to 1.2 ns.
- Thermo-electric cooling system
- Digital delay generator integrated in the detector head.

2.3.3. TRIGGERING AND GATING

The experiments carried out with LIBS system were triggered by a TTL pulse coming from the laser source as occurred with the LI-TOF-MS system previously described. The output of the Q-Switch process marked the beginning of the acquisition sequence and sent out the order to switch the ICCD that worked in slave mode by operating in external trigger mode. The laser QS trigger output was linked by a BNC connector to the external trigger input at the back of the iStar detector head by a SMA connector.

2.3.4. SOFTWARE

The Andor Solis^{TM} software allowed us to configure the system so that the application software interfaces correctly with its hardware environment: spectrograph setup, shutter control, temperature control, etc. Moreover, it facilitated us the control and handling from the computer of the main parameters related to the input signal: timing parameters (gate delay, gate width, exposure time…), signal acquisition mode, resolution and amplification of signal, etc. Next, the main timing parameters to take in account are described:

- Gate pulse width: it is the length of time that the intensifier tube is switched (or gated) on. Optical signal falls on the CCD sensor during this time.
- Gate pulse delay: it postpones the time that the gater switches on the intensifier tube, in order to synchronize the opening of the tube with an optical pulse.
- Exposure time: it is the period during which the CCD collects light prior to readout.

In most of the experiments described in this memory, the *step & glue* acquisition mode was used. Each of the acquired LIBS spectra were composed of overlapping spectral windows of 45 nm approximately to obtain a final spectral coverage of 240-900 nm. For each spectral window, accumulation of a set of laser pulses was acquired to reach satisfactory signal-to-noise ratio. The collection geometry was also orthogonal to the plume expansion direction and sideways. The dispersion grating of 599 lines/mm was usually selected for the acquisition of time-integrated plasma measurements. Samples were moved during analysis with the micrometer stage in order to expose new fresh surface after each laser shot. Intensity was integrated from band heads in the case of signals from molecular species whereas the maximum height of peak of discrete lines was used for atomic and ionic species. In both cases net (background subtracted) signals were considered.

2.3.5. EXPERIMENTAL SET-UP CONFIGURATIONS

In this section, it will be described the different variations or additions performed in the experimental setup throughout the experiments detailed in the memory. The purpose of gathering together all the experimental configurations here is to give a standing point of reference when a given experiment is being presented in next chapters.

2.3.5.1. CONFIGURATION FOR *COINCIDENTAL ANALYSIS*

The LI-TOF-MS system was joined to LIBS system in order to get a combined analytical technique for the simultaneous monitoring of emission LIBS and mass LIMS signals from samples in condensed phase and irradiated by a pulsed laser.

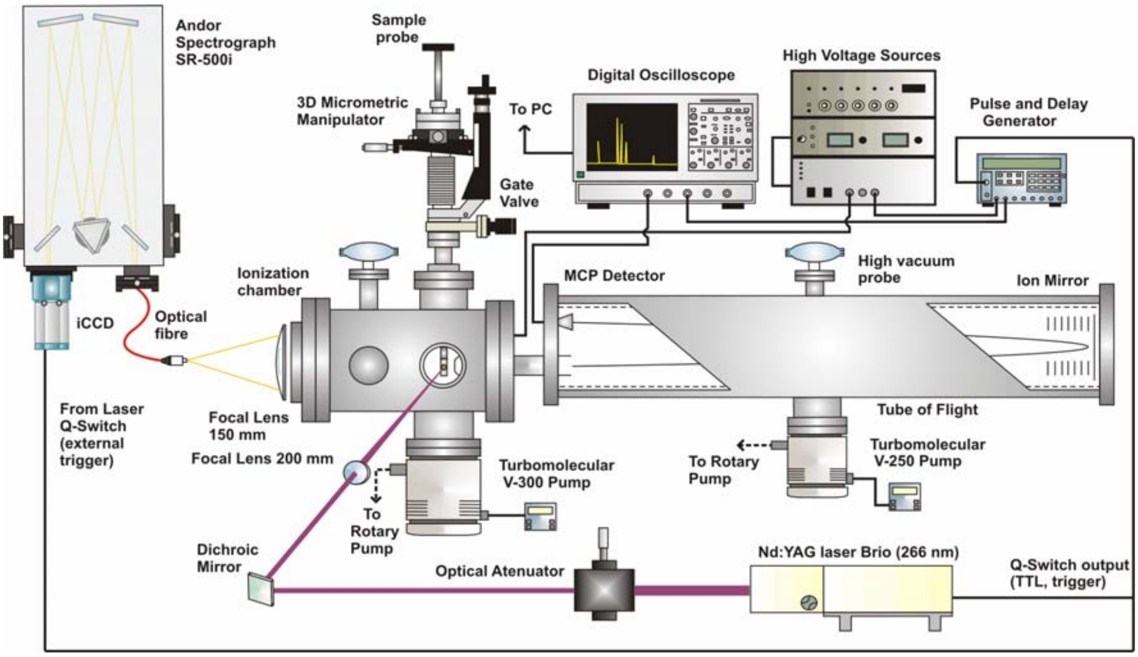

Figure 2.17. Experimental setup for coincidental analysis.

Both systems for emission signal collection and for ions detection were synchronized by means of the pulse and delay generator (*PDG Stanford Research System DG535*, 5 ps delay resolution). The trigger signal from the laser reached the PDG and from here was simultaneously delivered to the pulsed voltage source (that actives the MCP detector and the extraction electrode) and the aperture of ICCD camera. A general view of the coincidence set-up is shown in Figure 2.17.

2.3.5.2. CONFIGURATION FOR *ANALYSIS OF INFLUENCE OF PRESSURE ON DYNAMICS OF LASER-INDUCED PLASMA EXPANSION*

The experimental configuration was optimized to obtain high-resolution spectra from time-integrated plasma and to carry out time-resolved and spatial-resolved analysis.

For a precise control of air leak in the system and to assure a stable environment for analysis, a needle valve was attached to an auxiliary port of the chamber. Moreover, pressure into chamber was real-time monitored by means of a single gauge pirani system whose pressure probe was installed in another additional port of the chamber.

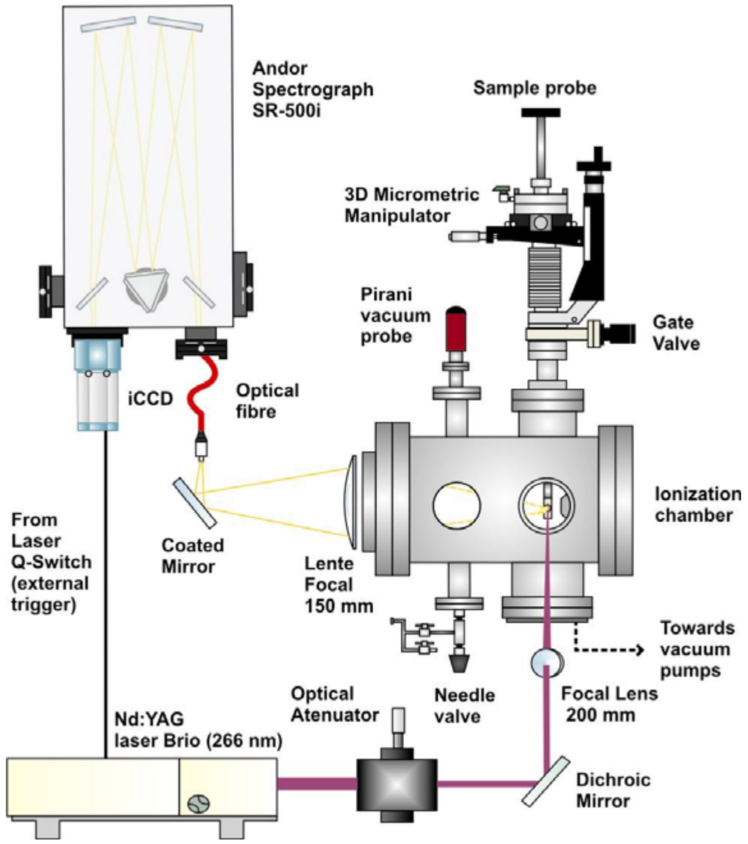

Figure 2.18. Setup for analysis of influence of pressure on LIBS response.

For the collection of emission light, a UV coated mirror was interposed in the optical path after the focal lens in order to improve the configuration of the collection of the plasma image due to spatial impediments of our experimental system. A three-stage positional system was installed with a micrometric manipulator with spatial control in the three axes (X, Y, Z) for fixing the head of the optical fibre to performed spatial-resolved analysis of the plasma plume expansion.

2.3.5.3. CONFIGURATION FOR *ANALYSIS OF INTERFERENCE OF BACKGROUND GAS ON LASER-INDUCED PLASMAS*

The system is similar to the previous configuration but a needle valve was installed in order to introduce the buffer gases in the chamber and create atmospheres of different nature. Moreover, a few additional changes were carried out in the experimental configuration:

- The isolation of the analysis chamber from the time-of-flight spectrometer and the MCP detector, and from turbomolecular and primary oil pumps with gate valves.

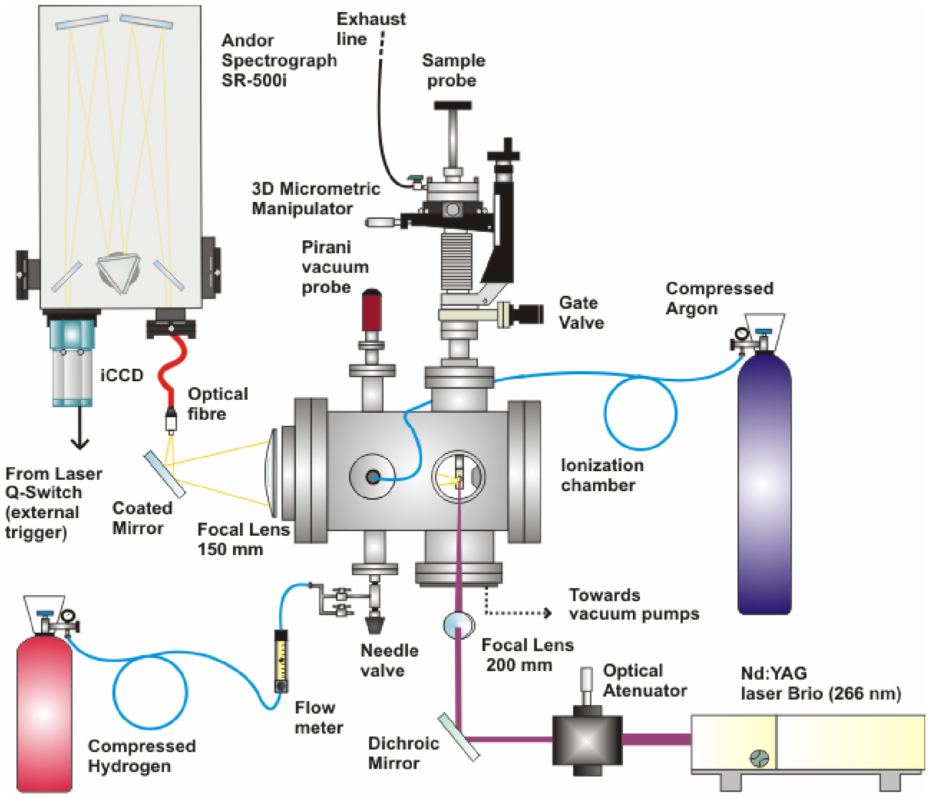

Figure 2.19. Setup for analysis of influence of buffer gas on LIBS response.

- The addition of an evacuation system with an exhaust line outside the laboratory and a new inlet line for Argon (purge gas) to remove the background gas from the internal volume of the chamber.
- The elaboration of a specific procedure to work with hydrogen gas in laser ablation trials.

CHAPTER 3

UV Laser Ionization Time-of-Flight Mass Spectrometry on Nitro Aromatic Explosives in Condensed Phase

3.1. SUMMARY

Analysis of explosive compounds represents an interesting field of work due to its obvious social relevance. Direct laser ionization allows the analysis of these high internal energy compounds without sampling or preparation procedures. We have studied nitro-aromatic compounds to understand their mass spectra when they are directly ionized in the condensed phase, different from the gas-phase studies commonly conducted. Thus, laser ionization time-of-flight mass spectrometry of high energy density materials has been performed using a nanosecond quadrupled Nd:YAG laser. No matrix assistance was used. Fine control of the laser energy allowed the study of the fragmentation processes from values close to the ionization threshold to ones where atomic-only mass spectra were recorded. The influence of the variation of extraction conditions on the recorded mass spectra was investigated. For low extraction width pulses, ions with low m/z values were mainly observed, whereas, at higher widths, higher mass fragment ions were also detected while the total ion current was maintained. Therefore, the mass spectra can be modulated to obtain mass spectra containing molecular or atomic information. The onset of ion generation for the different fragment ions was also studied, yielding information that can help to understand the processes involved in the fragmentation pathways of the molecule and in the dissociation mechanisms. Two sampling procedures allowed the prospective use of LIMS as a screening technique for nitro-aromatic-based highly energetic explosives.

3.2. INTRODUCTION

Laser ionization mass spectrometry represents a happy marriage for condensed-phase analysis where ions generated as a consequence of the interaction of the laser beam with a sample (usually of inorganic nature) are led to a detector in order to obtain information about the chemical composition **[Vertes, A. et al., 1993][Lubman, D. M. et al., 1990]**. In the field of elemental (atomic) or molecular analysis of solid samples, different works have proved the extraordinary capabilities of LIMS that combines speed, sensitivity, good lateral and in-depth resolutions in the sub-micrometric regime **[Garcia, C. C. et al., 2003][Huang, R. et al., 2011]**. When it comes to molecular compounds, the direct (matrix-free) or matrix-assisted laser-based desorption techniques **[Hillenkamp, F. et al., 2007]** are also of interest due to their universality and analytical power. If the elucidation of a detailed mechanism in any ionization technique always represents a difficult task, the problem appears way more complex when it implies the direct ionization of condensed phase. The complexity relies in the two different sequential processes that must occur: the movement of sample molecules or atoms from a condensed phase into gas phase and the subsequent transformation of those molecules into ions. In order to be fully understood diverse approaches different that the simple generation of mass spectra under a variety of experimental conditions are needed **[Alcántara, J. F. et al., 2008 A][Alcántara, J. F. et al., 2008 B].**

One of the main advantages of laser mass spectrometry for condensed phase analysis is the capability to work with samples of different chemical nature and the lack of limitations with sample shape or size. Moreover, this technique provides improvements in selectivity and sensitivity for the identification and quantification of trace material with rapid sampling and without complicated techniques for the analyte preparation **[Tönnies K. et al., 2001]**. The only consideration to be accounted is the vacuum compatibility of the compounds to be analyzed with the high vacuum conditions required for mass spectrometry. Luckily, a proper design in the mass spectrometers allows the analysis of compounds with high vapour pressure without damage of the detector by means of differential pumping systems. However, significant lack of sensitivity is concomitant.

The analysis of energetic compounds has been always an important task due to the interesting chemistry associated to their high internal energy **[Adams, G. F. et al., 1992].** Thermal decomposition chemistry is fundamentally important in the explosives field, and the determination of the kinetics and mechanism of the thermal decomposition remains a fundamental aspect of their characterization. Laser ionization of many explosives and explosive-related compounds (ERCs) in gas phase has been studied using nanosecond laser pulses **[Ledingham, K. W. D. et al., 1995] [Marshall, A. et al., 2005]**. An example is the fragmentation pathways of nitrobenzene and nitrotoluene isomers that have been discussed by nanosecond UV laser studies **[Kosmidis, C. et al, 1994][Galloway, D. B. et al., 1993]**. Laser-based mass spectrometry has proved itself to be rather versatile in the characterization of these families of compounds **[Mullen, C. et al., 2009]**. Moreover, the use of mass spectrometry in studies of the products of decomposition and detonation of explosives has been of considerable importance for forensic chemistry, as it helped to understand the chemical fragmentation pathways which lead to the dissociation of the parent molecules **[McMillen, D. F. et al., 1997][Kosmidis, C. et al., 1994]**. Additionally, explosives detection represents a complex field where analytical chemistry has to face the forensic problem of analyzing the residues of explosive compounds once the explosion has taken place **[Marshall, M. et al., 2009]**. Conventional analyses are based on well-defined sampling procedures and further confirmatory analysis by chromatographic techniques and tandem mass spectrometry **[Yinon J., 2007]**. However, the availability of direct analysis techniques for previous screening performed directly on the condensed-phase samples provides several benefits as the reduction of sample manipulation, and limiting in the sources of contamination. In the situation of a possible positive detection, specific confirmatory techniques may be directly applied, redounding in a significant save in resources, samples and time.

In this way, several underlying phenomena in the energetic of ignition and combustion of energetic materials are susceptible to a focused and coordinate research assault based on mass spectrometry. Most of commented works have been performed on gas phase, achieving extraordinary sensitivity and excellent mass resolution. However, no atomic information is achieved, focussing their efforts to the generation of mass spectrum with the best molecular information as possible to understand the fragmentation pathways or to obtain direct identification of the compounds from the molecular peak. Very few works have been published about this subject for condensed phase, and most of them using femtosecond laser **[McMillen, D. F. et al., 1997][Mullen, C. et al., 2006 A][Mullen, C. et al., 2006 B].** There is a trend in the last years in the seeking of ionization sources with the capability to provide molecular and atomic mass spectra of solid samples with the same source. Normally, this task implies the modulation of the source into two switchable low/high energy modes (as it happens in laser desorption/ablation or SIMS), or the recording of temporally resolved signal where different species may be found at specific times as it occurs in glow discharges.

In the particular case of nitro-related compounds, their fast dissociative states in the neutral excited state have been always considered an inherent difficulty as the parent ion and high mass fragments were not visible in the recorded mass spectra **[Mullen, C. et al., 2006 B]**. In this sense, femtosecond excitation has been always proposed as the only alternative to overcome the commented problem in gas-phase. However, condensed-phase ionization may involve a larger number of processes than those involved in gas-phase photo-ionization that changes completely the scenery of the ionization.

The recording of mass spectra at increased controlled fluences and adjustment of best temporal extraction conditions allowed the establishment of the ionization threshold for the different desorbed ions of the molecule, the generation of atomic/molecular mass spectra, and a major knowledge about the ionization processes and possible fragmentation pathways involved. Under these premises, a detailed study of the condensed-phase analysis of nitro-aromatic compounds via nanosecond laser ionization was performed with the purpose of understanding the effect of different experimental parameters on the resultant mass spectra in the aim of finding the best excitation conditions for direct surface time-of-flight mass spectrometry of the samples. Finally, optimization of the parameters for acquisition of molecular information allowed the identification of the organic compound from characteristics fragment in mass spectra.

3.3. DESCRIPTION OF ANALYZED MATERIALS

In the present study, different nitro aromatic energetic compounds were selected for the analysis. Specifically, an organic homologous series was chosen, namely 2,4,6-trinitrotoluene (2,4,6-TNT), one of the most powerful energetic materials, and its precursors, 2,6-dinitrotoluene (2,6-DNT) and 4-mononitrotoluene (4-MNT). All these molecules are generated from toluene nitration, only differing in the chemical structure regarding the number of nitro groups associated to the aromatic ring. This fact involves pronounced differences in their physical properties, especially the volatility. The undeniable analytical interest concerning the chemical decomposition chemistry of these high energy compounds has been already featured in previous sections.

The organic explosive 2,4,6-TNT is a stable solid compound obtained from the nitration of toluene. Its features of high stability, high power and low melting point make it highly flexible and easy to use and, therefore, very attractive for armed groups. It is mainly used as explosives in shells, bombs and mines. Due to its considerable oxygen deficit, this compound is often mixed with other substances of high content in oxygen, as ammonium nitrate to form Amatol. Some types of *ammonal* own TNT in their composition, which is usually used in detonator capsules. For TNT, vapour pressure is two orders of magnitude lower than that for DNT and five lower than that for MNT. Therefore, TNT was analyzed at high vacuum regime without operational problems, different from its precursors (see Table 3.1).

There are no natural sources of DNT, which is also manufactured by nitration of toluene, producing a mixture of 2,4-DNT (~ 80%), 2,6-DNT and small quantities of other four DNT isomers. Small quantities of the DNT isomers are also produced as by-products in the manufacturing of 2,4,6-TNT **[Akhavan J. et al., 2004]**. 2,6-DNT is less powerful than TNT, and do not produce as much -NO as TNT does, what has limited the number of analytically-oriented work using it. However, the *orto* geometry of its NO_2 groups is quite similar to TNT, turning it an excellent model molecule to study its direct laser desorption in condensed phase and the energetic channels involved in its decomposition. As it happens in TNT, the NO_2 groups in positions 2 and 6 in 2,6-DNT are twisted out of the plane due the inductive, resonance and steric effects between them, assuming a non-planar position with respect to the phenyl ring. This fact decreases the conjugation to the phenyl ring and its stability with respect to the almost coplanar 2,4-DNT **[Steinfeld, J. I. et al., 1998][Adams, G. F. et al., 1992].**

In regard to commercial MNT, it normally consists on oily liquid mixture of two isomers, 2-MNT and 4-MNT. It is a component of certain explosives for blasting and smokeless gunpowder.

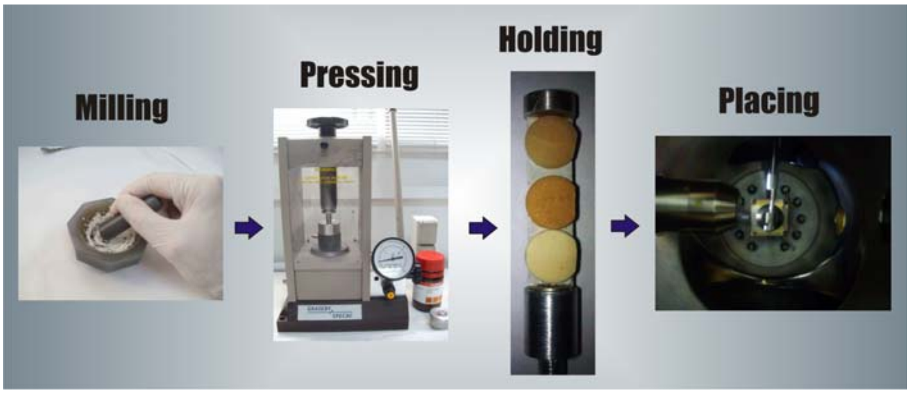

Figure 3.1. Samples preparation steps for LIMS analysis of organic compounds.

The 4-MNT and 2,6-DNT samples were both purchased from *Sigma-Aldrich* company in the form of yellowish powder with a purity of 99%. Due to the high vapour pressure of the 4-MNT and 2,6 DNT, the pressure in the ionization chamber could not be lower than $1.0 \cdot 10^{-4}$ mbar. The analysis was performed thanks to the differential pumping that kept the detector below 10^{-6} mbar during data acquisition. On the other hand, TNT was obtained from National Department of Defence as small flakes. The solids were ground in an agate mortar to reduce the grain size and facilitate subsequent pelleting. Pellets of 2 mm thickness and 10 mm in diameter were prepared by weighting 0.4 g of the different compounds and pressing the sample at 2.5 tons for 15 minutes in a small commercial press. Non especial drying was required before grinding, as long as the sample is kept in a relatively dry and fresh environment. For direct sampling from surfaces, conductive tape consisting of an aluminium foil with an electrically conductive acrylic-based pressure-sensitive adhesive backing was used. The resulting ground powder was deposited onto the tape without any additional pressing. The low likelihood of initiation/detonation by accidental of the compounds allowed risk-free handling of the samples.

Table 3.1. Physical properties of TNT homologous series, [Chen, P.C., 2003][Schramm, E., 2008].

	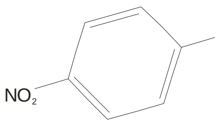	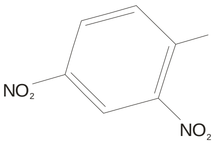	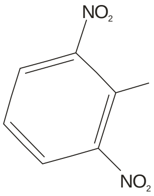	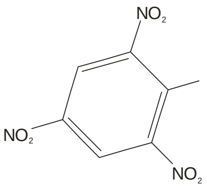
	4-MNT	**2,4-DNT**	**2,6-DNT**	**2,4,6-TNT**
Meeting point (ºC)	53-54	71	66	80.1
Boiling point (ºC)	238.3	300	285	240 (decomp)
Flashpoint (ºC)	106	207	207	167
Vapor pressure (kPa, 25ºC)	4.0 x 10^{-3}	3.1 x 10^{-5}	9.3 x 10^{-5}	7.7 x 10^{-7}
Molecular formula	$C_7H_7NO_2$	$C_7H_6N_2O_4$	$C_7H_6N_2O_4$	$C_7H_5N_3O_6$
Molecular mass	137.1	182.1	182.1	227.1
Heat of formation (kcal · mol^{-1})	7.4	4.7	9.6	12.3
Ionization potencial (eV)	10.59	10.3	10.1	9.46

3.4. EXPERIMENTAL

In the preceding chapter, Figure 2.1 sketched the most relevant elements of the instrument used for LIMS experiments. The system has an ionization chamber where the sample was housed at a high vacuum environment. The chamber was coupled to the time-of-flight mass analyzer by a reduced diameter tube between them so that ions travelled through it. Two pulsed Nd:YAG lasers emitting in the ultraviolet region were employed as ionization sources, and their characteristics are described in the chapter 2 of this memory. The laser beam was focused onto the sample in the direction perpendicular to its surface, and the ions produced from the irradiated spot on the target surface were immediately accelerated and extracted by a potential fall of -3 kV before going into the field-free drift tube.

Voltage values for the laser flashlamps (discharge lamps) and the delay in Pockels cell were adjusted to their optimum values in order to obtain maximum pulse to pulse stability. In the case of laser *Brio*, the value was set at 140 μs for the laser Q-Switch and potentiometer voltage that controlled the temperature of the 4th harmonic crystal was set at a value of 374 mV. In the case of laser *Litron*, the Q-Switch was set at 130 μs. Laser pulse energy was controlled using a variable attenuator that allowed continuous variation of the energy per pulse without causing modifications in the beam spatial profile **[Vadillo, J. M. et al., 1999]**. Finally, the detector output fed a 500-MHz four-channel *Tektronix model TDS5054B* Digital Phosphor Oscilloscope to monitor and storage the signal. In most of the measurements, series of 100 spectra associated to 100 laser events were captured in specific acquisition conditions, taking special care in the recording of all spectra under identical excitation and focus conditions.

3.5. RESULTS AND DISCUSSION

The irradiation of the sample with the laser beam yields a number of ions that can be sorted and detected in the mass spectrometer. In the condensed-phase ionization, the laser impinges the sample generating a significant pool of neutrals that could be directly photo-ionized by non resonant absorption from their ground state in gas-phase. To check the extension of this process in our experiment, the laser beam was redirected so that it passed close to the surface of a 2,6-DNT pellet. As the sample is constantly vaporizing, it is expected that the UV photons find a high population of DNT molecules in gas phase in the vicinity of the sample surface available for direct absorption. No evidence of ion formation was found even at the maximum fluence achievable by our experimental setup. Thus, all the ions generated after direct laser irradiation of the sample must be exclusively attributable to those formed as a consequence of the laser-matter interaction. The lack of ions directly generated by gas-phase photo absorption does not imply the absence of these photo-mechanisms in the solid combined with thermal-induced processes. Considering the fluence values in our experiment, two-photon absorption process would be possible (higher order of absorption is ruled out due to the fluence regime). In the case of 2,6-DNT, its ionization potential (10.1 eV) **[Schramm, E. et al., 2008]** cannot be reached by absorption of two 266 nm photons (9.30 eV). However, a combined photo-thermal mechanism can be considered for ion generation in our sample where the thermal energy of the expanding plume could supply such defect of energy. Additionally, at higher laser fluence values, electron generation in the focal volume may induce electron ionization like mechanisms with extensive fragmentation. In the case of 213 nm radiation (5.80 eV), the absorption of two photons exceed the ionization potential of 2,6-DNT as well as the rest of analyzed nitro-aromatic molecules (see Table 3.1) so ionization of the molecules is undergone directly.

3.5.1. Comparative study between LIMS and EIMS as mass spectrometry analytical techniques in the analysis of TNT homologous series

In the present section we compare the mass spectra acquired by our LI-TOFMS system and the mass spectra taken from the NIST data base by Electron Impact Mass Spectrometry (EIMS) of the TNT homologous series compounds. LI-TOFMS spectra were recorded in order to include them in the LIMS spectra library, with the purpose of using this database as analytic tool in the forensic analysis and identification of materials in solid phase from post-explosion scenarios. This type of samples could contain different explosive substances not detonated in residual quantities.

The EIMS technique consists on the bombardment of the sample (previously vaporized using high vacuum and a heat source) with a high velocity flow of electrons. During this process, the substance loses some electrons and gets fragmented, giving rise to different ions, radicals and neutral molecules. Charged fragments are then led by means of an ion accelerator towards a curved analyzer tube subjected to a strong magnetic field, and finally they are led to a collector-analyzer which collects the impacts of such ions according to their mass/charge ratio.

As shown in Figure 3.2, there is a significant match between the two, considering the differences between electron ionization performed in the gas-phase under well-controlled conditions, and the complexity and variety of mechanisms occurring in direct laser ionization in the condensed-phase. The direct link between the

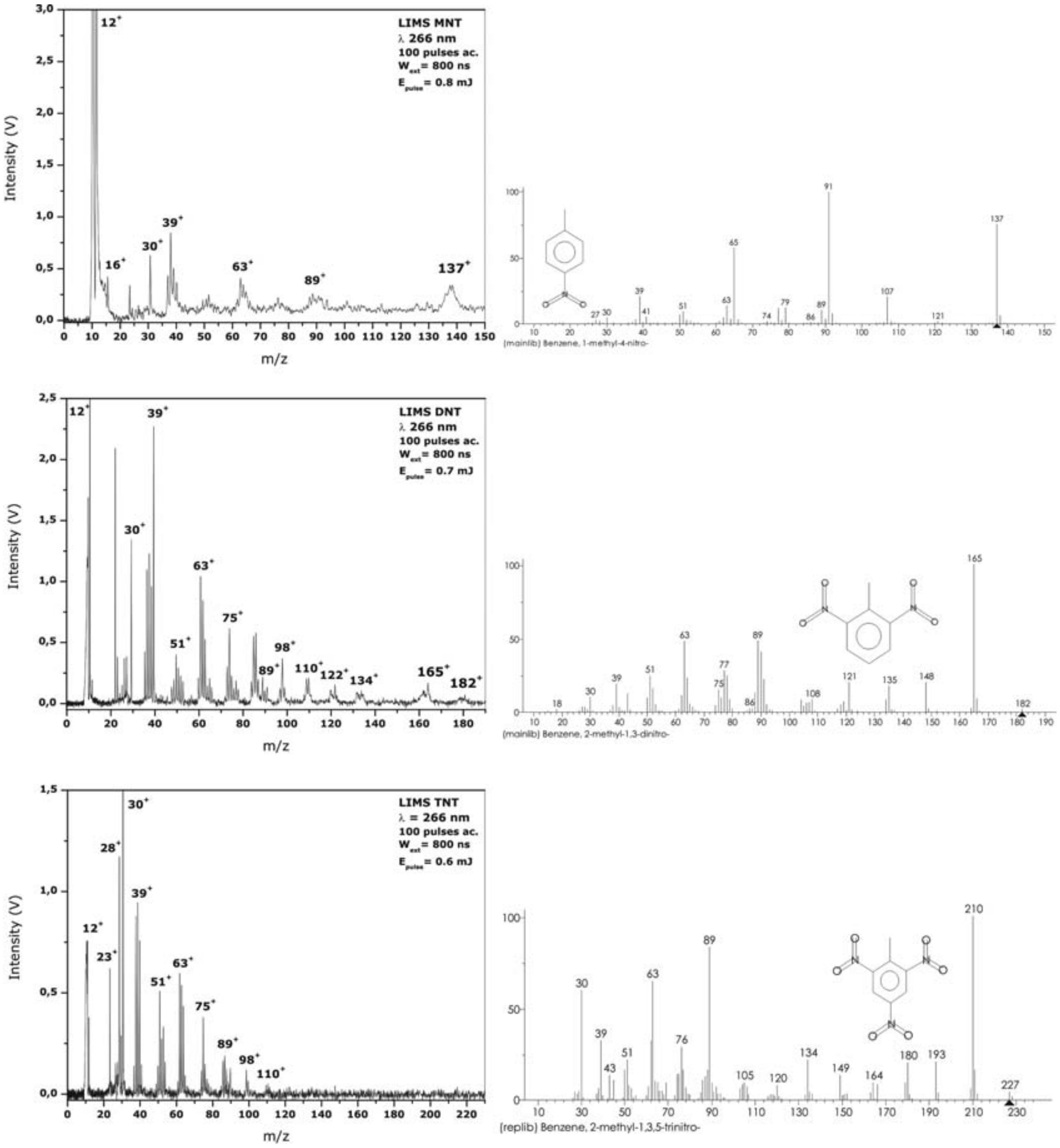

Figure 3.2. Comparison of representative nanosecond LI-TOF mass spectra and 70 eV electron ionization NIST mass spectra of MNT (top), DNT (middle) and TNT (bottom) molecules. Selected spectral features have been indicated.

chemistry in the gas phase and the reactions taking place in the condensed phase is complex. The final mass spectrum is a convolution of the early chemistry at the time scale of the laser-matter interaction and a variety of secondary reactions **[Knochenmuss, R. et al., 2003 B]** that further degrade the parent molecule. The laser-driven ignition process and the time scale over which our measurements are taking place allow secondary mechanisms to occur that will enrich the final spectrum with additional features closely related to those occurring under detonation conditions showing the products of decomposition caused by the action of laser pulse irradiation.

We thus consider that direct ionization in the condensed phase coupled to TOFMS represents a remarkable tool in the understanding of the chemistry of high energetic materials.

The acquisition of an acceptable resolution LIMS spectrum appearing the characteristic high mass fragments of the molecule was particularly complex in the case of MNT. Firstly, the pulse energy level required for the onset of the ionization was very close to such that produced the complete atomization of the molecule. On the other hand, the high pressure vapour value for MNT gave rise to a rapid vaporization of the compound and the vacuum pressure level into both the chamber and the mass analyzer approached the maximum allowed for safe operation of the detector. However, under specific conditions of extraction and energy, a number of high mass fragments coincidental with the electron impact ionization spectrum were monitored in LIMS signal for this sample, including the molecular peak at m/z 137^+, with acceptable signal to noise ratio. This parent peak identified uniquely the MNT molecule. Figure 3.2 shows a representative LIMS spectrum for MNT obtained in optimal operating conditions and the corresponding EI spectrum in normalized units.

The LIMS spectrum obtained for 2,6-DNT kept a close resemblance to its EI spectrum as the same major fragments appeared in both cases, although their relative intensities were not common at all. Hydrocarbon fragments ($C_nH_m^+$) such as $^{39}C_3H_3^+$, characteristics of studied aromatic molecules, together with $^{30}NO^+$ radical, related to the presence of nitro groups in the structure of organic molecule were identified. Furthermore, the molecular ion peak m/z 182^+ was subtly glimpsed, and the typical fragment m/z 165^+ corresponding to the loss of an -OH radical from the molecule by the known *ortho* effect was clearly observed (Figure 3.3). This fragment is indeed the main peak in the EI spectrum, and it likewise allows us to identify the molecule from its corresponding LIMS spectrum. As it is observed in the figure, several families of peaks with good resolution appeared in LIMS spectrum, which were mostly observed in the EI spectrum as well. This is the case of hydrocarbon fragments such as $^{39}C_3H_3^+$, $^{51}C_4H_3^+$,

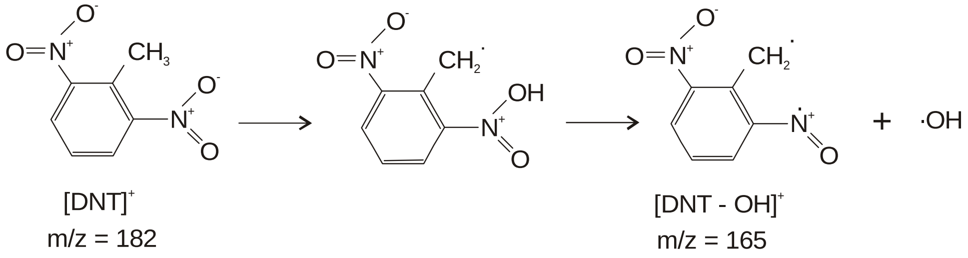

Figure 3.3. Pathway of *ortho effect* for 2,6-DNT molecule.

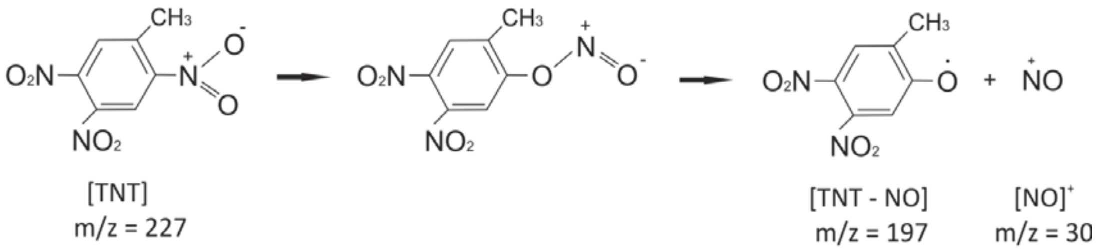

Figure 3.4. Nitro-nitrite mechanism for 2,4,5-TNT molecule.

$^{63}C_5H_3^+$, $^{75}C_6H_3^+$ and $^{89}C_7H_5^+$, which are associated to the fragmentation pathways followed by the breakage of the aromatic ring. However, the observed fragmentation pattern in both spectra is not exactly the same, especially for peaks in the high m/z range. This is a logical fact assuming that such techniques have different ionization sources and the sample is analyzed in different phase state: direct ionization on condensed phase versus bombardment on gas phase. Therefore, molecules suffer different atomization processes.

Finally, in the case of TNT, the characteristic fragments of high molecular weight present in EI spectrum, namely the parent molecular ion at m/z 227^+ and the typical fragments $[TNT-OH]^+$ at m/z 210^+ and $[TNT-2[OH]]^+$ at m/z 193^+ due to the *ortho* effect, could not be visualized in registered LIMS spectra. As can be seen in the figure, peaks with high intensity and adequate resolution were detected in the low mass range. These families of fragments are common for MNT and DNT LIMS fragmentation patterns, and consequently this feature gave us information about the aromaticity and the presence of nitro groups in the molecule, but did not identify unequivocally the TNT compound. Moreover, the presence of the same peaks at low mass range for all the three molecules indicates a similarity in the breakdown mechanism of these energetic molecules. The base peak in the spectrum is m/z 30^+, which corresponds to post-ionization of neutral NO fragment. This diatomic species can be produced either by a nitro-nitrite-type mechanism (Figure 3.4) or by a later-stage fragmentation of the products **[Bhasu, V. C. J. et al., 1991].** Obtained mass spectra prove that the loss of NO becomes faster as the number of nitro groups in the molecule increases.

Under lab-frame conditions, LIMS may be seen as a fast MS-based screening tool prior to detailed confirmatory analysis. However, our results are based on pressed pellets, a situation unrealistic under forensic analysis conditions, that implies working with surface traces of the sample, and where special sampling conditions are required. Thus, two different approaches have been investigated for the analysis of TNT that could potentially be valid for forensic analysis and allowed us to know the real influence of the method of sample preparation on the efficiency of ionization process by LIMS. In the first one, the sample is collected from the surface in powdered form **[Tellez, H. et al., 2012]** by using conductive double sided adhesive Al tape, while in the second the sample recovered from a given surface is dissolved in acetone, deposited (50 μL) on the surface of an untreated aluminium disk and allowed to dry by slow recrystallization at room temperature before analysis. Typically, the crystal sizes were ~ 2.5 mm across and ~ 0.5 mm thick **[Bhasu, V. C. J. et al., 1991]**.

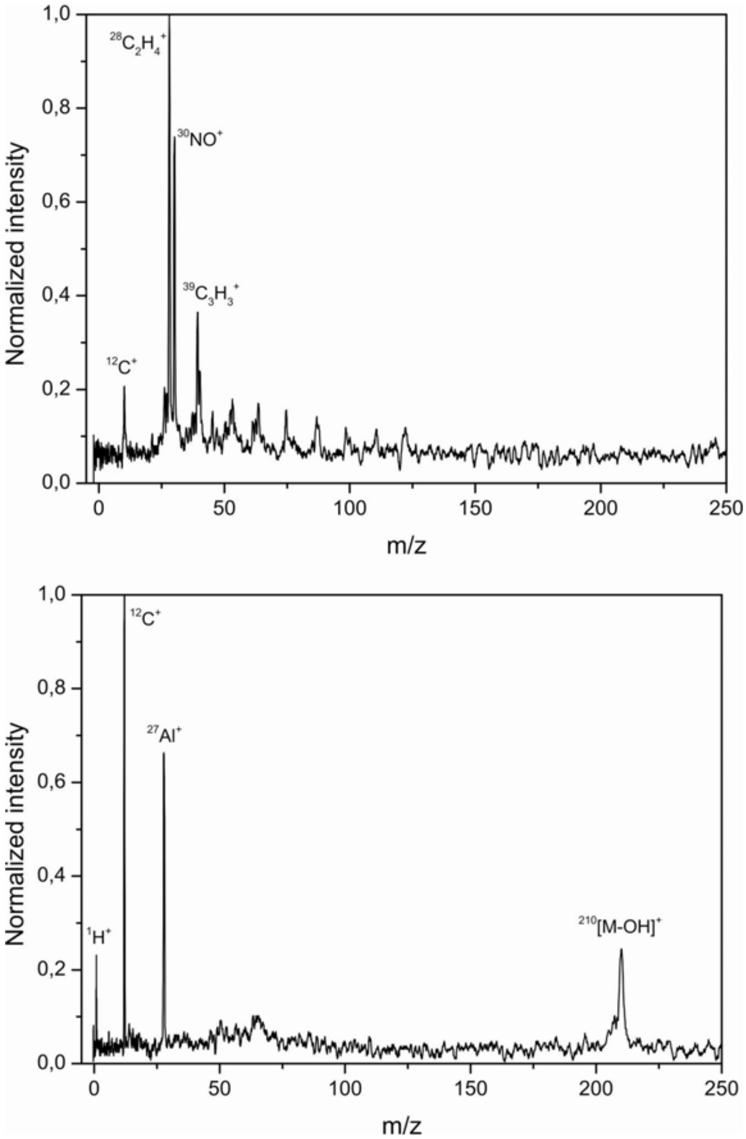

Figure 3.5. Single-shot mass spectra of TNT traces sampled on conductive double-side Al tape (top) and as a dried-droplet of acetone-dissolved residue (bottom). Laser energy: 0.8 mJ/pulse; Wavelength, 266 nm.

Figure 3.5 shows a single-shot LIMS spectrum of TNT that has been analyzed following both methods for specific energetic and extractive conditions. In this approach, the sample is not pressed but dispersed in powdered form. Thus, the laser energy required was slightly lower than that required for pellets. Figure 3.4 (top) and 3.4 (bottom) show the analysis using the Al-tape and dried-droplet procedures, respectively. As observed, in the first method, although the presence of $^{30}NO^{+}$ ion may clearly help to trigger a security protocol due to the presence of nitro-compounds, little molecular information is found. When the dried-droplet method was used, it was the $^{210}[TNT\text{-}OH]^{+}$ fragment ion that was clearly observable which allows to identify the compound unequivocally since it corresponds to the loss of an hydroxide group from the parent molecule. Moreover, the $^{27}Al^{+}$ from the substrate was also monitored. This fact was likely due to differences in efficiency of energy absorption from UV photons by TNT crystals and powder residue. Mechanical properties associated to the microstructure were also important in the behaviour of the compound in the initiation of explosion and plasma formation by laser irradiation. The fast ionization of metallic holder favours the sudden fusion and ejection of complete explosive molecules into the plume which are subsequently ionized.

Higher energies led to the absence of any signal from the explosive residue. Modifications in the extraction conditions did not produce any effect other than a loss of overall intensity.

3.5.2. Parameterization studies

Measurements performed to the parameterization of the experiment were carried out with the final purpose of studying the parameters related to the laser radiation used for the excitation and ionization of the sample and those related to the extraction of ionic species, which had a crucial influence on the studied phenomenon. Thus, the optimal conditions for acceptable resolution and signal-to-noise ratio were established.

3.5.2.1. Influence of laser wavelength on organic ionization process

As it was commented, a combination of mechanisms is involved in the generation of ionic species after irradiation of the sample. Thermal and photo absorption processes are implicated in the soft fragmentation and ionization of the molecule whereas for higher energies, electron generation lead to a further fragmentation by electron-impact phenomena. This fact was checked by performing the ionization with different laser wavelengths (1064, 532 and 266 nm). Another factor to be considered is the fluence threshold, i. e., the minimum laser fluence required to record a measurable signal. In our studies, the lowest threshold fluence was found for UV pulses. These facts can be related to a better laser absorption derived from the existence of a larger number of excitons per unit volume that increase the rate of energy pooling and ionization in the sample. The primary ions react with neutral molecules during their expansion, giving new ions that are detected as well.

The power density or *irradiance* required to ionize the organic sample with infrared radiation is higher than that using shorter wavelengths. In fact, these compounds presented a low energy absorption rate and remarkable thermal effects for the IR laser sampling. Moreover, shielding of the laser radiation by the absorbing plasma limits direct laser ablation and increases the temperature of the plasma **[Geertsen, C. et al., 1994].** This fact means a less efficient ionization process and the ablation of larger amounts of material. In this sense, electron ionization phenomena occurring in the plume favour extensive fragmentations so information predominantly atomic with low resolution was finally obtained.

The 532-nm output (photon energy, 2.33 eV) generated spectra with restricted information and still affected by extensive fragmentation as can be seen in Figure 3.6. The quality of the acquired signal is limited as well.

In the case of UV radiation at 266 nm and 213 nm, irradiance required to reach the ionization threshold was much lower due to high photon energy (4.66 eV and 5.80 eV, respectively) and the coefficient of energy absorption was much greater, resulting in an optimum coupling in the laser-matter interaction. Therefore, the plasma was formed by efficiently ionized species from a minimum amount of ablated material. In this case, phenomena of fragmentation are soft and less thermal effects take place, increasing photoionization processes. Furthermore, a precise operational control in the extension of the rupture of the molecule modulating the energy of output laser pulse was possible and molecular information along the m/z range with high resolution peak signals was obtained.

The consequences of this difference between IR and UV laser radiation are considerable and lead to a superior performance of UV laser sampling in every analytical aspect: reproducibility, matrix effects, quantification, spatial resolution and sensitivity **[Geertsen, C. et al., 1994].**

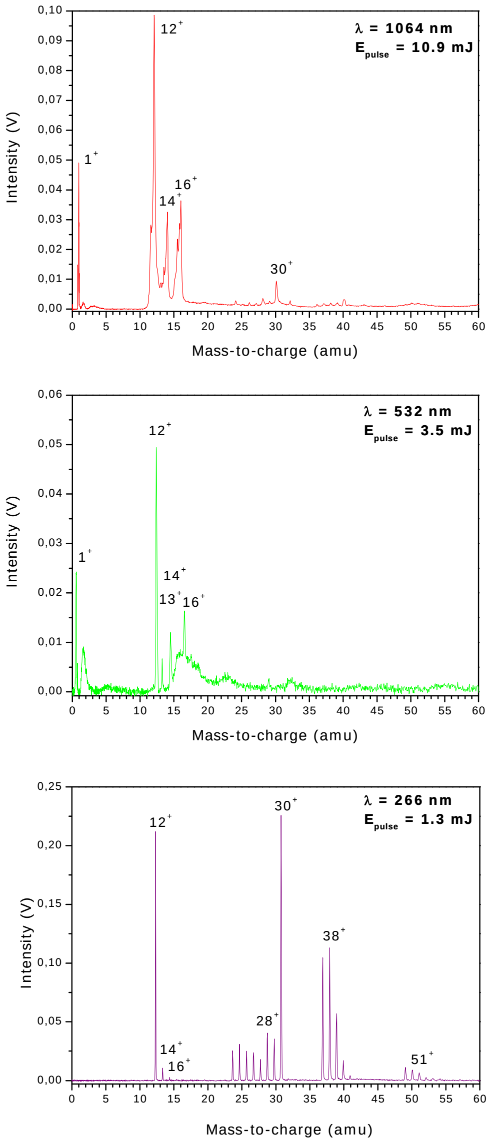

Figure 3.6. Nanosecond LI-TOF mass spectra of 2,6-DNT acquired in the low m/z range for different laser radiation wavelengths. Average 100 acquisitions.

Although the hot plume associated to the IR output did impair greatly the recording of mass spectra with molecular information due to extensive fragmentation yielding to atomic-only fragments, the acquisition of certain molecular information of low quality with IR laser excitation was possible for 2,6-DNT sample by means of a rigorous optimization of extraction and focalization conditions.

Figure 3.7 shows a comparison between LIMS spectra acquired with both UV short wavelength (266 nm) and the fundamental emission wavelength (1064 nm) of the Nd:YAG nanosecond laser *D31Brio* by setting a width extraction pulse of 800 ns. The mass spectrum obtained with infrared radiation presented very low resolution signals consisting on different bands with unresolved peaks throughout the whole mass range. However, they were coincident with characteristic fragment groups which appeared in the EI pattern spectrum of the molecule (see Figure 3.2.). In the range of low mass species ($1^+<m/z<12^+$) it was also observed a family of low resolution peaks out of mass range calibrated, and which may correspond to species doubly ionized ($^6C^{2+}$, $^7N^{2+}$ and $^8O^{2+}$) from a second ionization of ions $^{12}C^+$ $^{14}N^+$ and $^{16}O^+$. The dispersion in detection times of the ionic species was mainly owing to a deficient extraction and deflection of ion packs due to the turbulent dynamics existing in the plasma on account of the high kinetic energy of ions in the plume **[Torrisi, L. et al., 2002]**, with a poor efficiency in the ablation process with a large removal of material which avoids a proper detection.

High dispersion in kinetic energy of particles is generated when a high energetic regime is established in the system and, in consequence, both the resolution in the detector and focus factors are prejudiced. The reflectron corrects around 10% of that dispersion but, for a particular dosage of energy, the ionic mirror is not capable to focus the ions on the detector correctly. The analyzer undergoes a loss of resolution as m/z ratio of ions increase.

In Figure 3.7 it is also shown the proposed assignment for the different peaks appearing in the spectrum, linking the m/z values with possible atomic or molecular ionic species. Peaks m/z 165^+ and m/z 148^+ correspond to the loss of one or two -OH radicals off the DNT molecule, respectively, and this takes place through a reaction pathway called *ortho* effect (Figure 3.3) **[Kosmidis, C. et al., 1994][Tönnies, K. et al., 2001].**

The hydrogen atom in the hydroxide group comes from methyl group exclusively. The presence of m/z 135^+ fragment is due to the joint loss of –OH and –NO groups off the molecule, and, finally, the rest of molecular clusters are mainly typical hydrocarbon fragments $C_nH_m^+$, appearing at m/z 87^+, 75^+, 63^+, 51^+ and 39^+, among others. In order to calibrate the mass axis of spectrum, a pair of inorganic samples was used as internal standards: a foil of Pb, taking as reference the stable isotope at m/z 208^+ to establish the top of high mass range, and a foil of graphite, using atomic carbon signal to take the low mass reference at m/z 12^+. Using the expression **(2.1)**, with the values of time of flight of ionic signal from metallic standards, a parabolic fit was set, being the calibration exclusive for each temporal extraction condition.

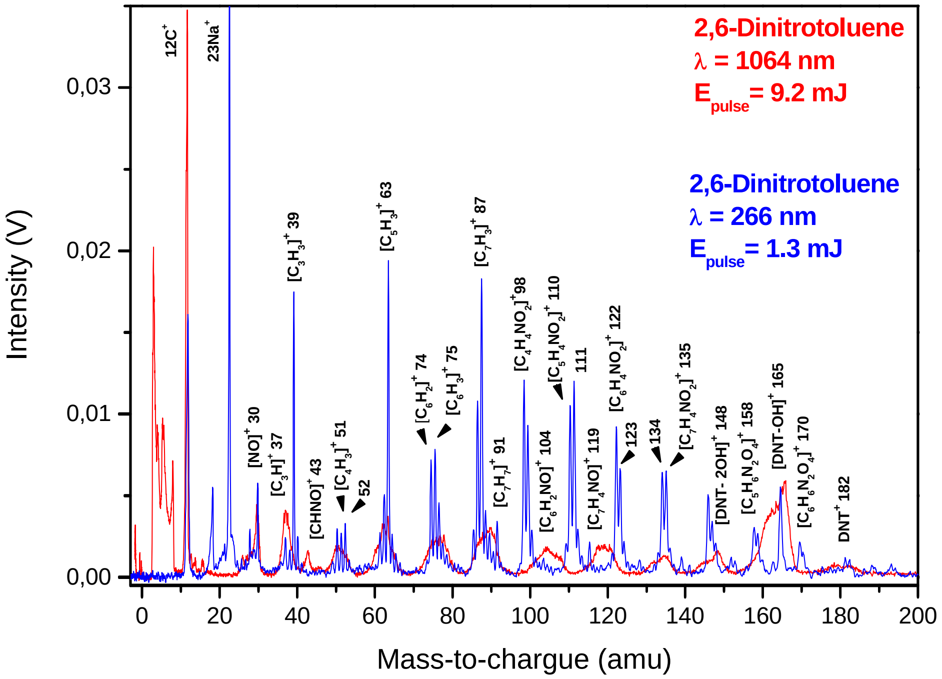

Figure 3.7. Comparison between LI-TOF mass spectrum acquired with the fourth harmonic (266 nm) and fundamental radiation (1064nm) of nanosecond Nd:YAG laser of 2,6-DNT for different energetic regime.

3.5.2.2. Influence of focalization on laser ionization process

The acquisition of a mass spectrum with high resolution and suitable signal-to-noise ratio from ionization of a specific compound using a pulsed nanosecond laser as excitation source mainly depends on the amount of energy reaching the sample besides the spot area, i.e. the irradiance value ($J/cm^2 \cdot s$). This factor is influenced by the focusing system for the laser beam and the beam profile. For this reason, a specific study was carried out to find out the best focusing conditions that would provide the most effective excitation setting.

Thus, we studied the behaviour of signals corresponding to the most significant ionic species in the 2,6-DNT mass spectrum when the local focus of laser beam and, therefore, the dimensions of the irradiated area, were varied in a wide range, keeping the value for laser output power. Energy per pulse was set at 0.4 mJ since a richer fragmentation pattern was obtained for this energetic condition in the low mass range. In this way, several fluence values were tried, changing the local position of the focal lens (FL 200mm, 1” diameter), so that the lens-object distance varied between 17 and 20 cm, owning the latter condition the minimum spot area and therefore the maximum fluence value.

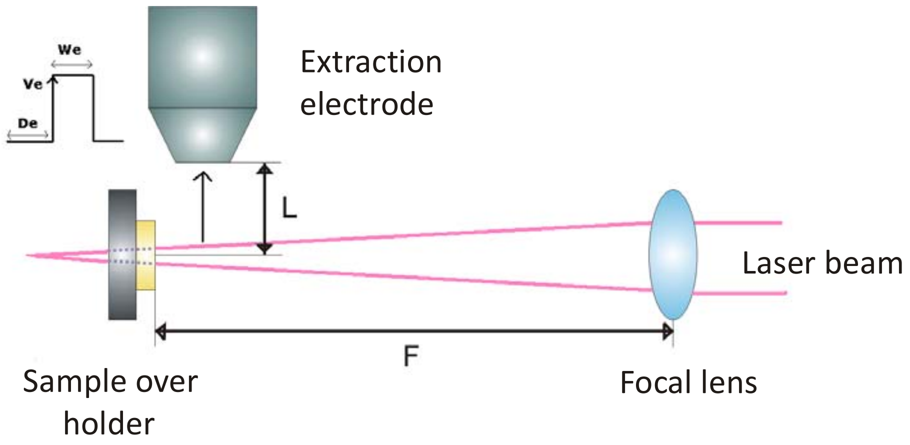

Figure 3.8. Location of organic sample fixed on the metallic holder with respect to focal lens and extraction electrode into the ionization chamber.

The sample position was the same for all the measurements, with the surface next to the extraction axis so that the distance between the centre of sample and the grating of extraction electrode remained unchanged (L = 1.5 cm). This fact made possible the direct comparison of results obtained for every tested object-lens distances (F) (see schematic diagram in Figure 3.8).

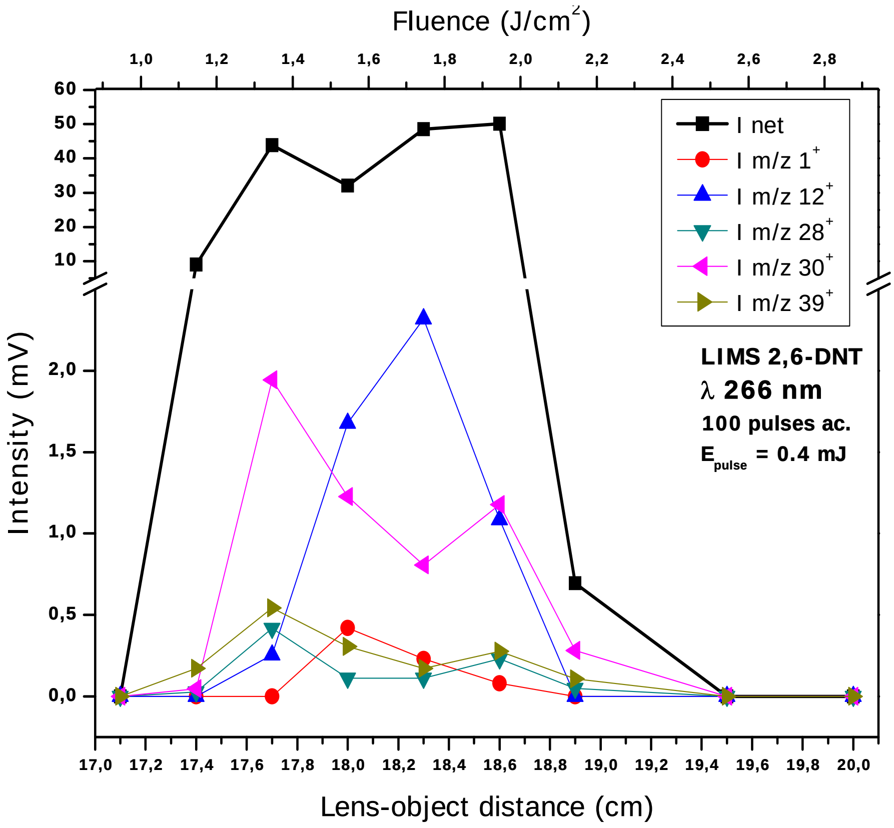

Figure 3.9. Influence of nanosecond laser beam focus in LIMS signal. UV radiation, 266 nm. Solid sample, 2,6-DNT.

Figure 3.9 shows the obtained results. Both total current from all the generated ions and net intensity for several ionic species of interest are presented versus the object-lens distance and the fluence level. Each value of intensity (measured in mV) corresponded to the sum of 100 acquisitions. From such information we concluded that focus is an especially critical parameter for the ionization of this type of organic samples, since a minimum change in the distance, and therefore, in the irradiance value, implied a notable variation in the intensity of the different signals in the mass spectrum. Not all the species presented the same intensity variation as the focus changed. Particularly notable was the different evolution for $^{1}H^{+}$ and $^{12}C^{+}$ ionic signal with regard to the rest of species (the behaviour of these species will be discussed in the next sections). However, it is also noteworthy the fact that the low mass fragments characteristic of this compound, which also appeared in the EI mass spectrum, presented a similar behaviour, keeping constant the intensity ratios between them. This is the case of $^{28}CO^{+}$, $^{30}NO^{+}$ and $^{39}C_3H_3^{+}$ species.

It was observed a fluence interval in which intensity of collected current in the detector is maximum, from 1.3 J/cm^2 to 2.0 J/cm^2, corresponding to lengths from 17.6 cm to 18.8 cm from sample to focal lens. That means that an object-lens distance of 18 cm, i.e. 2 cm behind the focal point for the lens, is the optimum for the desorption and ionization processes in the prevailing experimental conditions.

3.5.2.3. Influence of fluence on the fragmentation of organic molecules

The amount of energy reaching the sample is a key parameter in direct laser desorption/ionization. Differences of a few mJ may drastically change the information contained in the mass spectra. The laser energy per pulse can be easily controlled in our set-up, thus allowing precise calculation of the minimum laser energy required to record a measurable signal and the evolution of the ion signal with laser energy. The onset of ion generation (ionization threshold) for the aromatic compounds of studied homologous series including MNT, DNT and TNT was determined by increasing the energy per pulse reaching the sample while monitoring the time-of-flight mass spectra. Energy level was controlled by means of the variable attenuator that allowed continuous variation of the energy per pulse without modifications in the beam spatial profile. The experiment was performed using UV 266 nm radiation and starting from an energy per pulse that provide no ion signal in our TOFMS system (lower than 0.4 mJ/pulse for all the studied compounds) and was raised progressively to a maximum of 7 mJ/pulse. This maximum limit was due to excessive plasma formation in the ionization chamber that induced electrical contact between isolated electrodes. For each new energy setting, the entrance of the laser beam was blocked with an energy-meter and 100 consecutive shots were monitored to determine the average energy per pulse and the relative standard deviation (RSD) of the data. In the studied range, RSD values lower than 1% were obtained. After that, a sequence of 100 new laser pulses were shot against the sample surface and the accumulated signal was recorded for subsequent processing. Likewise, focus conditions of laser beam were kept constant so that the irradiated area of the sample surface was maintained invariable, taking this value as reference for fluence and irradiance calculations. Moreover, extraction parameters as voltage, pulse width and delay were optimized to carry out the measurements.

The obtained fluence thresholds resulted to be in a very narrow energy range. In order to calculate them, a simple criterion was established. We took as fluence threshold the minimum value whose corresponding net intensity signal registered in the detector was at least 5% of the maximum intensity value recorded for that compound. This maximum value was set by that fluence value whose resulted ionic signal started to saturate the detector.

Figure 3.10 presents the threshold energies for the analyzed compounds. The sensitivity of the detector can be prejudiced by the irregular level pressure into the chamber caused by the high vapour pressure of MNT (see Table 3.1). Its vaporization rate was considerable (around to 0.01 g/min) so that the correct extraction of ions

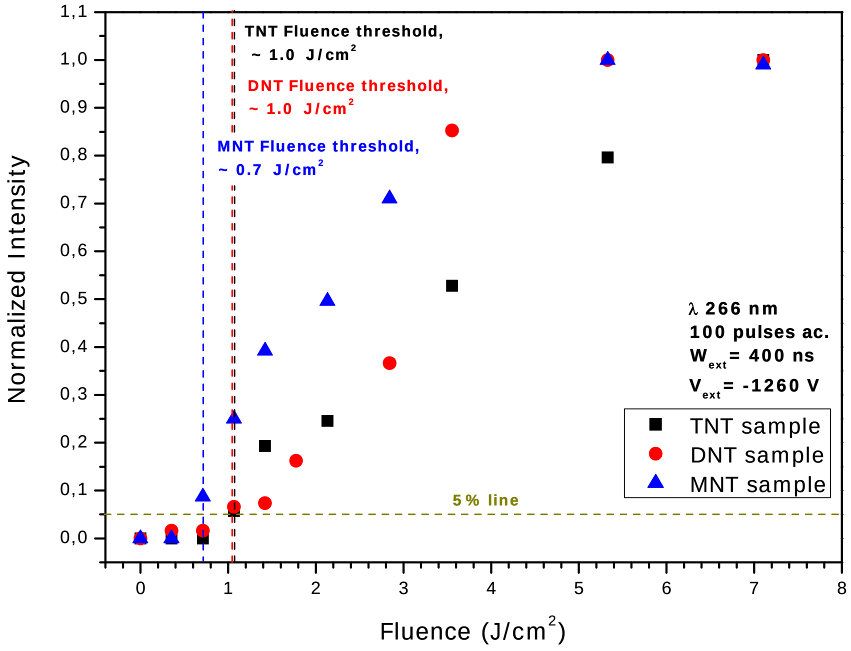

Figure 3.10. Ionization thresholds for homologous TNT series. Intensity values were normalized to the maximum intensity value registered in each energy condition.

could be affected. Its ionization threshold (around 0.7 J/cm^2) seemed to be lower than the threshold of TNT and DNT (around 1 J/cm^2), probably due to the appreciable amount of MNT in gas phase in equilibrium with the solid pellet, leaving more molecules available for ionization.

In the study of the effect of fluence in the fragmentation of organic molecules, both 266 nm and 213 nm UV radiations were used for the ionization of the samples. The estimation of beam spot at the sample surface was carried out by irradiating a piece of thermal paper with a laser pulse capable to leave a mark on it, establishing the same focus conditions fixed in the experiment, and then measuring the affected area with an optical microscope. The resultant beam diameter for 266 nm radiation was approximately 280 μm, corresponding to an area of 6.15 $\cdot$ 10^{-4} cm^2, whereas in the case of the laser beam emitting at 213 nm the final area was 9.31 $\cdot$ 10^{-4} cm^2. Characteristic of Nd:YAG laser sources were previously described in Chapter 2 of the present memory.

Short wavelengths resulted in lower thermal effects in the ablation process and a more efficient ionization, requiring less laser power to carry out the desorption due to higher energy of the photons involved in the excitation process. Both the laser output at 266 nm (E_{photon} = 4.66 eV) and 213 nm (E_{photon} = 5.80 eV) resulted in a proper signal-to-noise ratio over a wide mass range with similar resolution level. The energy losses by lack of transmission through focal lens (7-15%) and thought the quartz input window of the chamber (8-12%) were finally estimated around 15% for 266 laser radiation and 27% for 213 output. The presence of these optical elements in the laser beam path implied the correction of the measured energy values.

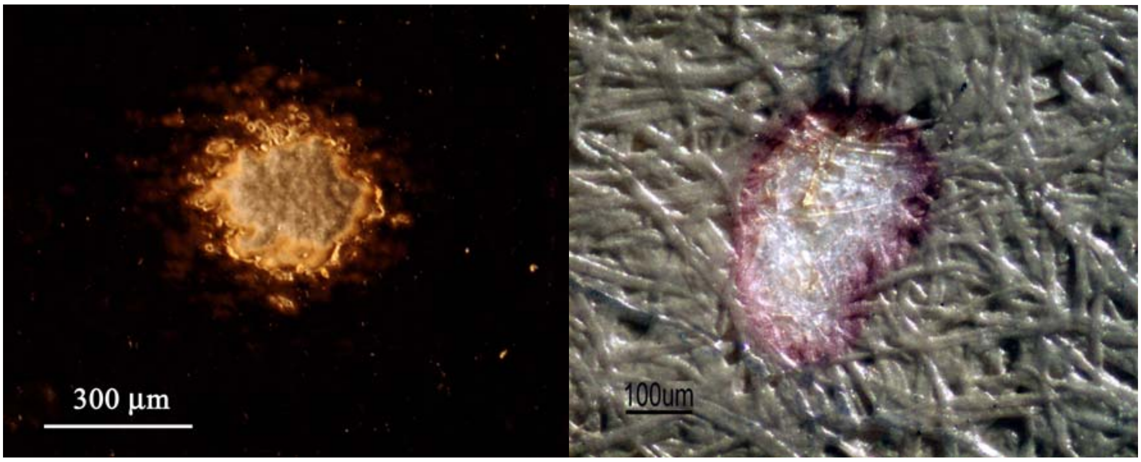

Figure 3.11. (a) Crater left by a 266 nm laser pulse with 2 mJ energy on thermal paper. (b) Crater left by a 213 nm laser pulse with 0.5 mJ energy on thermal paper.

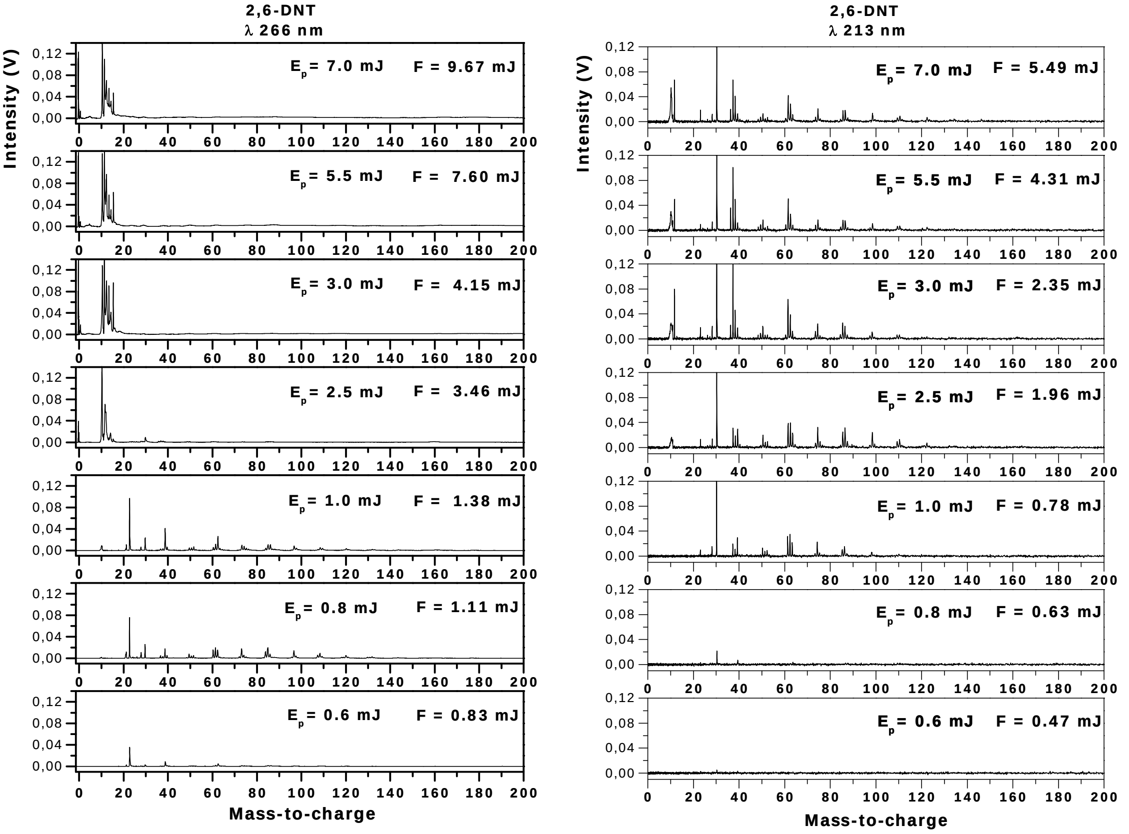

Figure 3.12. Mass spectra (0-200 amu range) of 2,6-DNT obtained with 266nm and 213 nm laser pulses at output energies from 0.6 mJ to 7 mJ. Extraction pulse width was set to 800ns.

Finally, the fourth harmonic was chosen as main laser radiation for this experiment since the available energy range allowed to perform the complete kinetic study from desorption and ionization of the heavier fragments to the total atomization of the molecule. Furthermore, the alignment of laser beam was achieved easily. Laser ablation using the 5thharmonic in optimum focal conditions did not reach the complete fragmentation of the molecule when maximum energy available was imposed (7 mJ). The energy density could be increased by reducing the spot on the sample surface, but this implied a loss of resolution in the mass signal.

The Figure 3.12 shows the described effect. The fluence was not sufficient to achieve full atomization regime when 213 nm radiation was used. For 5.5 J/cm^2 fluence value, the spectrum already showed a considerable intensity level for $^{12}C^+$ ion as a proof of ring breakage, but many of the hydrocarbon fragments and the characteristic $^{30}NO^+$ ion persisted in the plume. However, analysis with very precise energy-resolution was possible with this short UV radiation and therefore allowed us to carry out a detailed monitoring of life-evolution of certain fragments showed further on.

The same parameterization study was performed for the case of MNT and TNT molecules, identifying the rising ionic species and studying the evolution with the pulse energy level. In these cases, monitoring of a number of species including atomic, diatomic and some high mass fragments, was carried out obtaining the same behaviour as observed for 2,6-DNT.

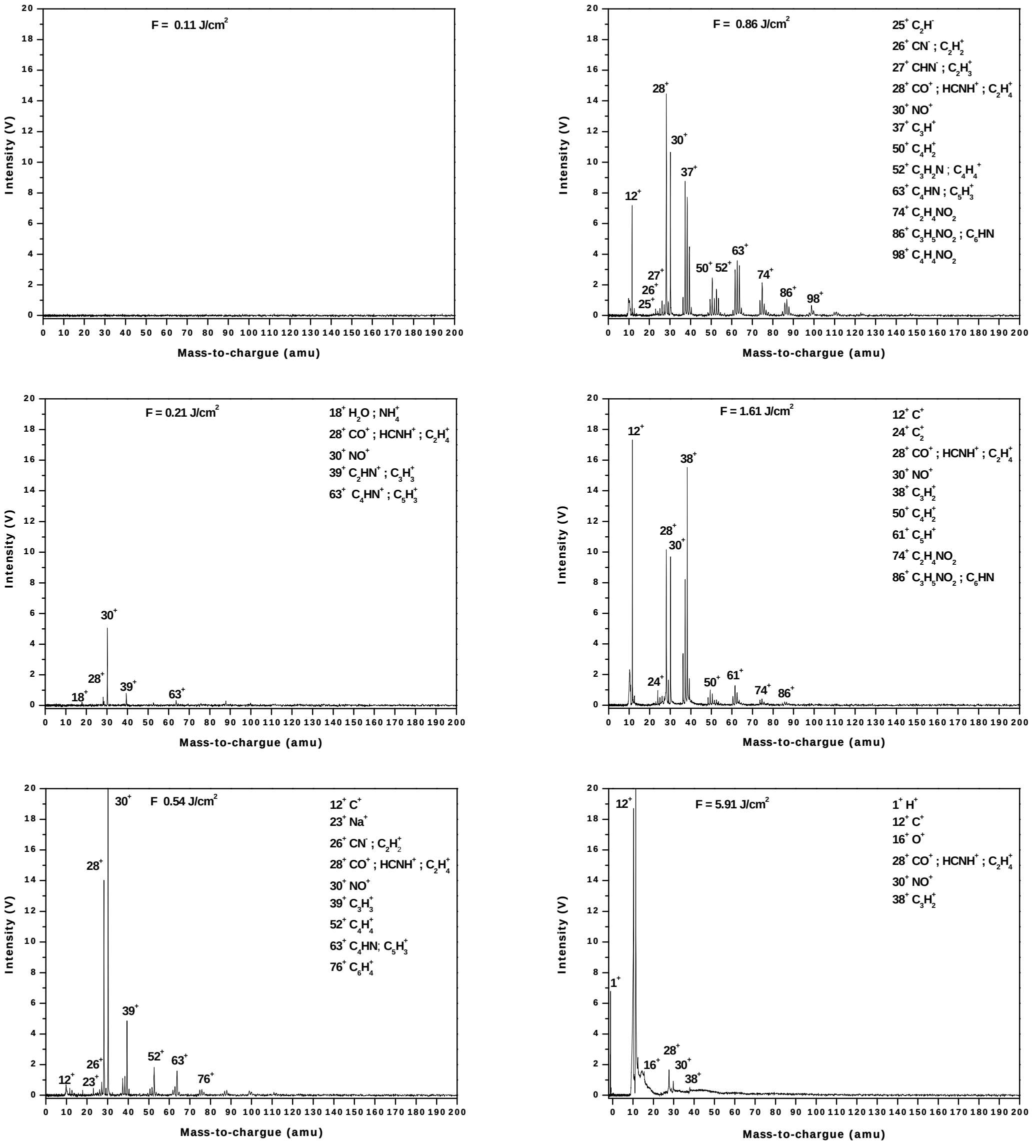

Figure 3.13. Mass spectra (0-200 amu range) of 2,4,6-TNT obtained with 213 nm laser pulses. Extraction pulse width was set to 1000 ns. Extraction delay was set to 400 ns. Pressure in the analyzer was 5.0 · 10^{-6} mb. Each data set is formed by accumulation of 100 pulses.

Results for TNT sample using 5th harmonic are showed in Figure 3.13. Mass spectra presented high resolution in all the energy range, and the assignment of different fragments was performed. A few species, namely 12^+, 28^+, 30^+, 39^+, 52^+, 63^+ and 89^+, were present in all fluence range, but no fragments higher than 98 a.m.u. were detected. Those latter four fragments ($^{39}C_3H_3^+$, $^{52}C_4H_4^+$, $^{63}C_5H_3^+$ and $^{89}C_7H_5^+$) are characteristic of TNT compound when the molecules in gas phase are subjected to electronic impact or to other ionization techniques as multiphotonic ionization with femtosecond laser. In the case of laser ionization using 266 nm radiation, a complete fragmentation of TNT molecule was observed by the onset of atomic species H^+, C^+, N^+, and O^+ when a fluence value of 3.6 J/cm^2 was supplied as shown Figure 3.14.

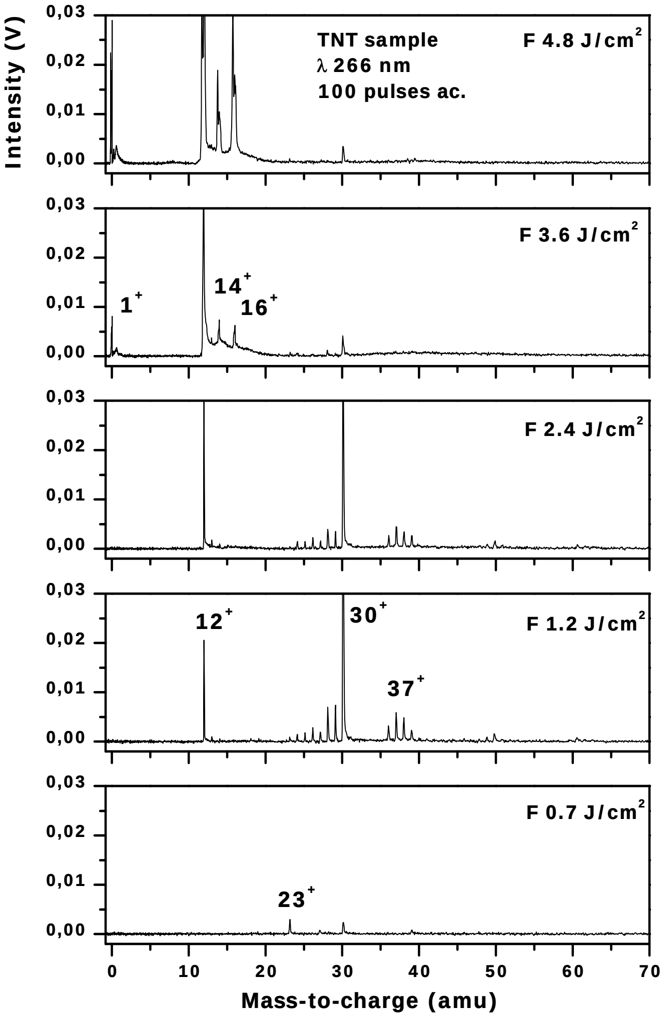

Figure 3.14. Mass spectra (0-70 amu range) of 2,4,6-TNT obtained with 266 nm laser pulses. Extraction pulse width was set to 400 ns; Extraction delay was set to 0 ns. Pressure in the analyzer was 5.0 · 10^{-6} mb. Each data set is formed by accumulation of 100 pulses.

Results of study about the evolution of LIMS signal with the variation of fluence level by using 213 nm radiation for certain characteristic fragments are showed below in Figure 3.15. Thus, it was deduced that there was a fluence value for which intensity value of each fragment was maximum. For that energy level, the different species reached the maximum population in the plume and from that moment forward, the population started to drop. As the amount of fragments declined, the atomic signals started to gain intensity, showing the intensity curve for $^{12}C^+$ a continuous increase by following an exponential fit mainly caused by the loss of H atoms from the hydrocarbon fragments. The signal corresponding to the hydrogen ionization appeared at higher energy regime, as can be observed in the spectrum obtained for the highest fluence level in Figure 3.13.

Results from LIMS signal parameterization let us to study the kinetics followed by certain groups of hydrocarbon fragments C_nH_m with similar molecular weight coming from the rupture of the phenyl ring. By increasing the fluence, fragments suffered the loss of hydrogen atoms, which were quickly transferred to other species in the medium and the amount of free protons was not enough to be detected at the beginning for mass analyzer, i.e., it was under the detection limit of the detector. Hydrogen signal was observed when the abundance of ions in the medium was high enough to be correctly extracted towards mass analyzer. In fact, for TNT molecule, H^+ ion was detectable at about 5 J/cm^2 with 213 nm radiation, when C_nH_m fragments nearly disappeared from the ionization site.

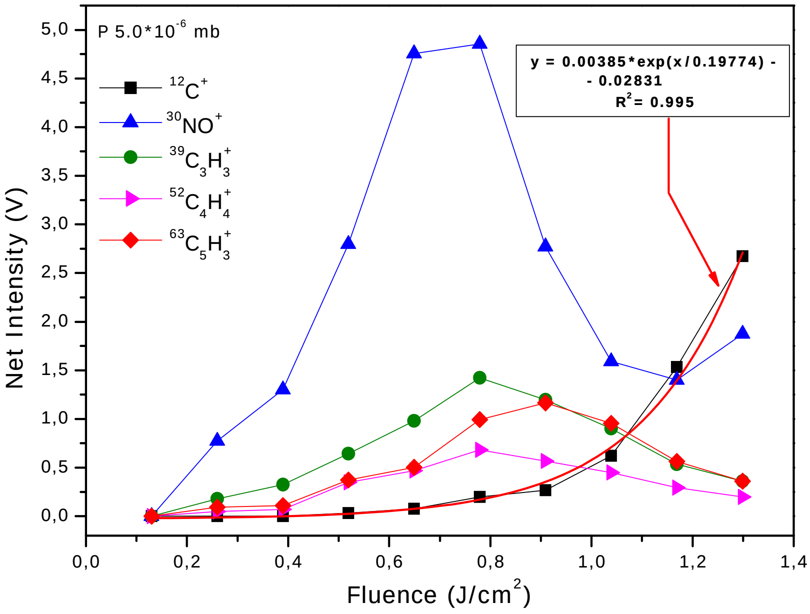

Figure 3.15. Evolution of specific low m/z species with increasing fluence level for TNT sample. Laser radiation, 213 nm.

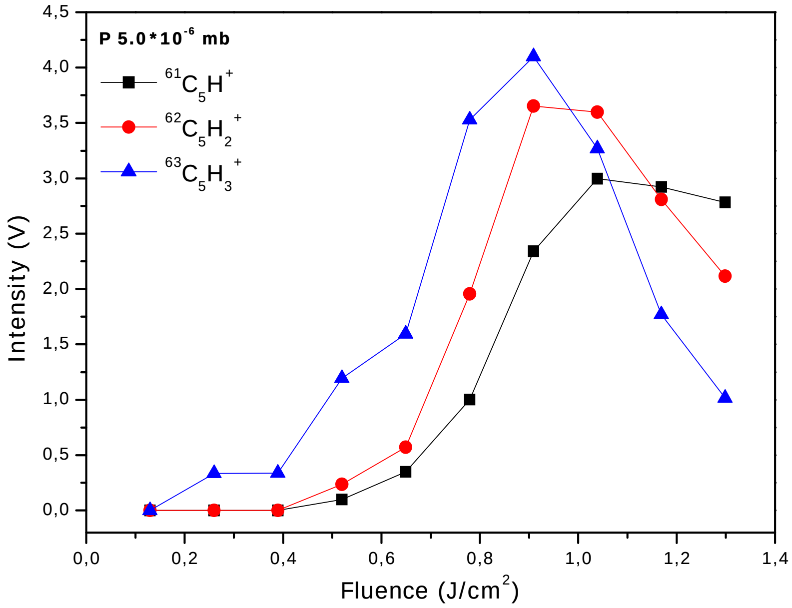

Figure 3.16. Dependence of LIMS signal intensity with fluence level for TNT hydrocarbon fragments m/z 61$^+$, 62$^+$ and 63$^+$ formed in the fragmentation process of the molecule using UV 213 nm pulses as excitation source.

In Figure 3.16 the kinetics undergone by particular hydrocarbon fragments is shown. It is clearly observed how the loss of a first proton from the cluster and then, a loss of a second proton, took place in such way that the higher fragment $C_5H_3^+$ transformed into $C_5H_2^+$ in a first step and then this new fragment transformed into C_5H^+ in a second stage. This analysis demonstrated the ability of the technique to carry out fundamental kinetic studies in the fragmentation of molecules of organic nature.

To carry out the study of the complete fragmentation of an organic and nitro aromatic molecule, the 4th harmonic emitting at 266 nm of Nd:YAG laser was used due to it allowed us to work in a wider range of fluence. 2,6-DNT was chosen as *model* molecule for the analysis. Previously, Figure 3.12 showed the changes in the recorded mass spectrum for 2,6-DNT when the energy per pulse was enough to provide measurable ion signal. Obviously, the calculated values can not be taken as absolute as to some extent there is an artefact of the instrumental detection efficiency. It was expected that low fluence would lead only to desorptive ion emission from the sample surface, while ions deeper in the material would not be released. Only when ablative phase explosion becomes widespread can a larger fraction of the available ions reach the gas phase. The early ion signal (corresponding to the surface desorption of $^{23}Na^+$) demands a minimum energy per pulse of 0.30 mJ. From 0.40 mJ/pulse, apart from the ubiquitous $^{23}Na^+$ signal, incipient ion signals corresponding to fragment ions such as $^{30}NO^+$, and groups of signals centered at m/z 39^+, 63^+, 77^+, etc, were observed. These low-mass ions correspond to $C_nH_m^+$ hydrocarbon radical cations and are not limited to specific m/z values **[Hankin, S. M. et al., 2002][Huestis, D. L. et al., 2008][Bhasu, V. C. J. et al., 1991]**. Nevertheless, they are consistent enough to be useful for identification of aromatic compounds **[Smith, R. M., 2004]**. On increasing the energy to 0.80 mJ/pulse, a well-resolved mass spectrum is observable with information in the high-mass range. As in related work, **[Tönnies, K. et al., 2001][Kosmidis, C. et al., 1994][Mullen, C. et al., 2009][Huestis, D. L. et al., 2008][Pond, B. V. et al., 2007]**, our spectra did not show signals associated to $^{46}NO_2$. This is because the short lifetime of the intermediate states involved in the generation of $^+NO_2$ (a few hundred femtoseconds) leads to rapid dissociation to generate the most stable $^{30}NO^+$ ion **[Pond, B. V. et al., 2007]**. Additional energy per pulse is required to generate the molecular ion peak. The richer spectral information obtained with increasing the energy per pulse is clearly obvious. However, greater fragmentation, visible as ions at m/z < 20, can also be seen. There is a limit irradiance level applied on the organic sample surface. Above that energetic regime, high dispersions on kinetic energy of species are generated, and this fact impairs the focus and resolution on the detector notably. Due to the balance between sensitivity, full mass-range information and fragmentation, a value of 1.3 mJ/pulse was taken as optimum value for further experiments.

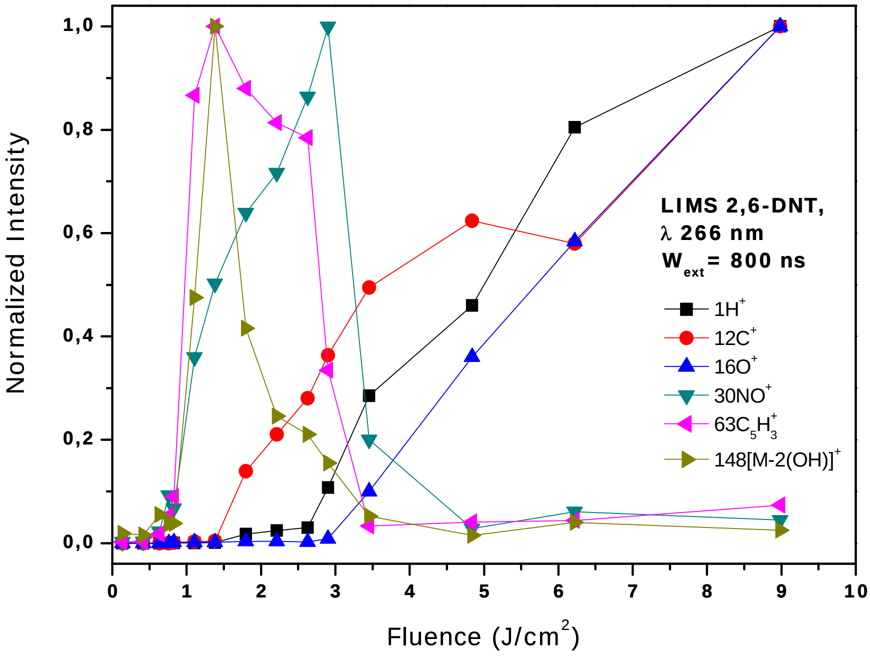

Figure 3.17. Dependence of the ion signal with fluence level for selected ion fragments.

Figure 3.17 shows the threshold for the evolution of ions of specific m/z values with increasing fluence level for $^{1}H^{+}$, $^{12}C^{+}$, $^{30}NO^{+}$, $^{63}C_5H_5^{+}$ and $^{148}(M\text{-}2[OH])^{+}$ ions. The intensity values were normalized to the maximum value for each species. The presence of $^{30}NO^{+}$, $^{63}C_5H_5^{+}$ and $^{148}(M\text{-}2[OH])^{+}$ ions at low energies per pulse is clear, with a sudden intensity increase being seen for the three peaks at about 0.8 J/cm^2. From this point, different behaviour is observed. The $^{148}(M\text{-}2[OH])^{+}$ fragment ion exhibits a maximum around 1.5 J/cm^2, and then decreases quite sharply in intensity, reaching zero at about 4.5 J/cm^2. The same behaviour was found for the $^{165}(M\text{-}OH)^{+}$ fragment ion. Meanwhile, the $^{30}NO^{+}$ signal increases up to 3.0 J/cm^2, dropping abruptly afterwards.

It is interesting to note in Figure 3.17 that all the plots modify their trends at about 1.3 J/cm^2. Depending on the monitored ion, this cut-off value corresponds to a change in the slope (as in m/z 63$^+$), the onset of ion generation (m/z 12$^+$) or the starting of the ion extinction (m/z 148$^+$). The fact that the $^{12}C^{+}$ signal (indicating the complete break-up of the phenyl ring and full fragmentation of the molecule) starts at this cut-off value supports the idea of a change in the ablation mechanism corresponding to a Coulomb explosion.

The orthogonal extraction geometry used in our experiment allows a decoupling of the initial kinetic energy of the ions resulting from their escape velocities from the solid and that energy provided by the extracting field. Even under near threshold conditions, the kinetic energy and the energy spread of the ions are large once the molecule fragments completely. Thus, the applied voltage and the pulse amplitude, length and delay with respect to the laser incidence are important parameters in orthogonal extraction that can quite dramatically modify the signal intensity of the detected ions.

3.5.2.4. Influence of extraction conditions on mass signal acquisition

In our experiments, it was observed that the ion yield was very sensitive up to changes in the amplitude of the extraction voltage. This electric potential was applied to extraction electrode located in the inlet hole inside the vacuum chamber.

Figure 3.18 shows the commented dependence of intensity signal with amplitude level. The values between -1200 V and -1300 V were set as optimum for extraction voltage since best resolution and highest intensity level were obtained. Moreover, the rest of voltage values applied to different electrodes in the system (ionic lens battery, ionic mirror and detector) were also optimized trying to get a high quality mass spectrum. Table 3.2 summarizes the set voltage values and their polarity.

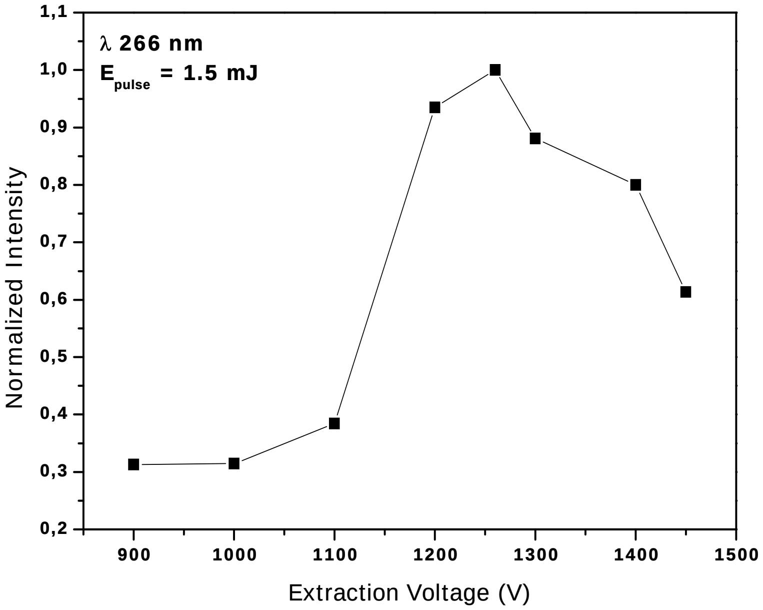

Figure 3.18. Dependence of LIMS signal intensity from 2,6-DNT sample with amplitude of extraction voltage. Intensities were normalized to the maximum value. Temporal conditions for the measurements: Extraction pulse width, 400ns; Extraction pulse delay, 0 ns. Accumulation 100 acquisitions.

Table 3.2. Optimized voltage values for the electric electrodes of the LIMS system to carry out experiments with organic samples.

ELECTRODE	VOLTAGE
E1 (extraction electrode)	-1265 V
LINER (acceleration electrode)	-1075 V
FOCUS (focus electrode)	-206 V
DEFLECTORS (deflection electrode)	-960 V
VR1 (reflectron, negative electrode)	-50 V
VR2 (reflectron, positive electrode)	+404 V
VD (voltaje in detector)	-3020 V

In addition to the adjustment of voltages, the influence of extraction time conditions on the registered signal regarding the ionic species generated in the laser ionization process was studied. Therefore, qualitative changes undergone by mass spectra were analyzed. The extraction pulse width (We), i.e. period of time on which the electric field applied to lead the ions into the time-of-flight analyzer is active, and extraction delayed time (D_e), i.e. period of time passed from the laser event until the opening of extraction electrode **[Song, K. et al., 2004]** were controlled with a pulse and delays generator (PDG). The temporal pattern of synchronization between the laser event and set values for extraction parameters in the PDG was showed in the Figure 2.12 included in Chapter 2 of the present memory.

The most significant effect was observed in the pulse width. Figure 3.19 shows the full mass spectrum at increasing pulse widths from 400 ns to 2000 ns with zero delay set for all the sequence data. For values lower than 400 ns the signal was quite unstable probably due to instabilities on the electronics of the high power switch at these low values. At 400 ns, the spectrum reveals atomic information preferentially with high peak resolution (higher than 300 units) and FWHM lower than 40 ns. That implied the peaks were resolved to spectrum baseline completely. Progressive richer high mass range information was obtained at larger extraction widths, decreasing the peak resolution in the low mass region and keeping constant the total ion current. No changes were observed when the width was increased to more than 2000 ns. The full explanation for this experimental finding still remains unclear. Initially, a simple hypothesis based on differences in escape velocities of generated ionic fragments was considered. Thus, for short extraction pulses, ionic species in the low m/z range would have time enough to be reoriented and conveniently extracted under the effect of the applied electric field due to its higher velocity, and therefore they would be efficiently deflected to the field-free region of the analyzer. On the contrary, higher m/z ions would require a longer extraction pulse in order to modify correctly their expansion trajectories based on their different momentum and pass through the extraction electrode. However, this approach does not explain the lack of signal in the low-mass range at large extraction widths (as shows Figure 3.19). Moreover, overestimating the escape velocities of the formed ions as 1 μm/ns, based on distance between sample surface and geometrical centre of the extracting electrode (15 mm in diameter) and on matrix-assisted laser desorption/ionization (MALDI) ion measurements, and considering no momentum loss during the expansion, it can be asserted that the ions will be under the effect of the orthogonal extractive grid for 7.5 ms after the laser has hit the sample. With this figure in mind, the ions should be efficiently and equally deflected to the field-free region of the analyzer with the pulse widths used. Thus, there is no explanation for the optimum interval between 400 and 2000 ns for the pulse width. A second factor to consider is the different distribution of species along the expanding cloud. The higher temperatures and electron density favour the formation of atomic species close to the surface. As long as the expansion plume takes place, secondary mechanisms in the plume leading to the generation of molecular ions, such as charge transfer, electron attachment, gas-phase cationization among others, **[Knochenmuss, R., 2003 A][Knochenmuss, R. et al., 2003 B]**, become important. The question to be solved in future studies is the understanding of the effect of the gas-phase processes on the final spectra and how the final mass spectrum is representative of the molecules and particles in the condensed phase. Regardless of this, the experimental results clearly open the possibility of obtaining modulated atomic/molecular spectra based on a simple modification in the extraction conditions, even if the mechanism is not yet fully understood. The experiment was also performed with other organic compounds and confirmed that the described phenomenon took place systematically.

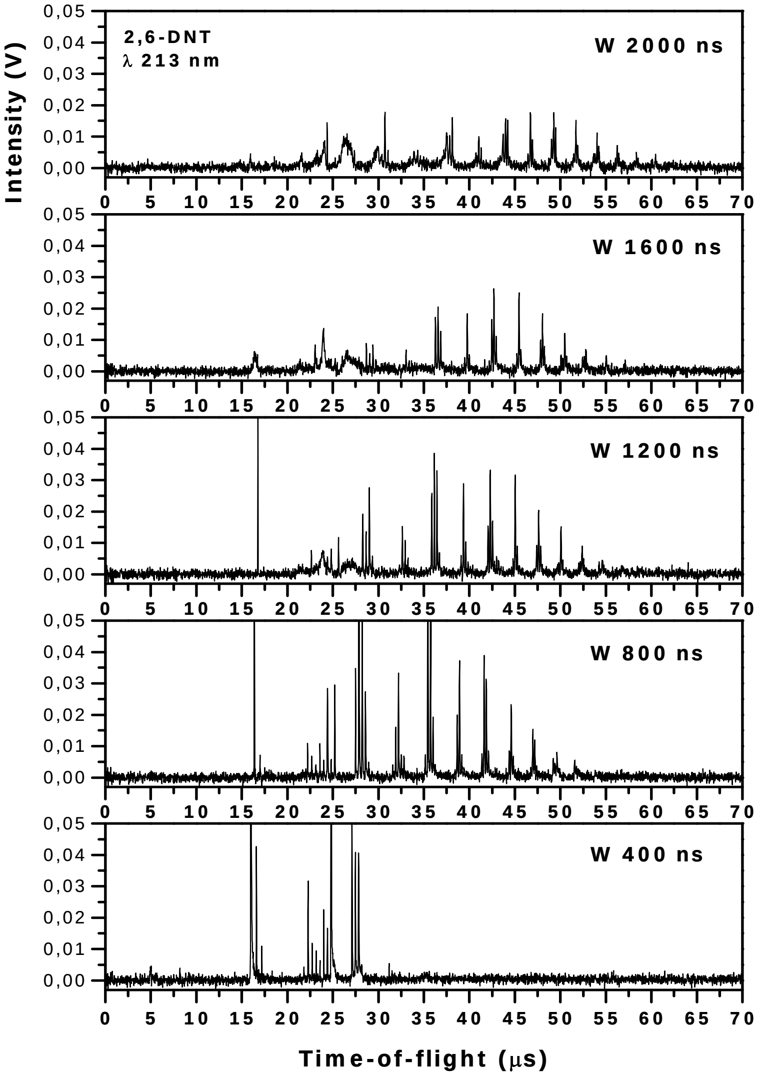

Figure 3.19. Time-of-flight mass spectra of 2,6-DNT irradiated with 213 nm laser beam under different extraction width conditions. The extraction delay pulse and the fluence value were set at 200 ns and 1.96 J/cm^2, respectively.

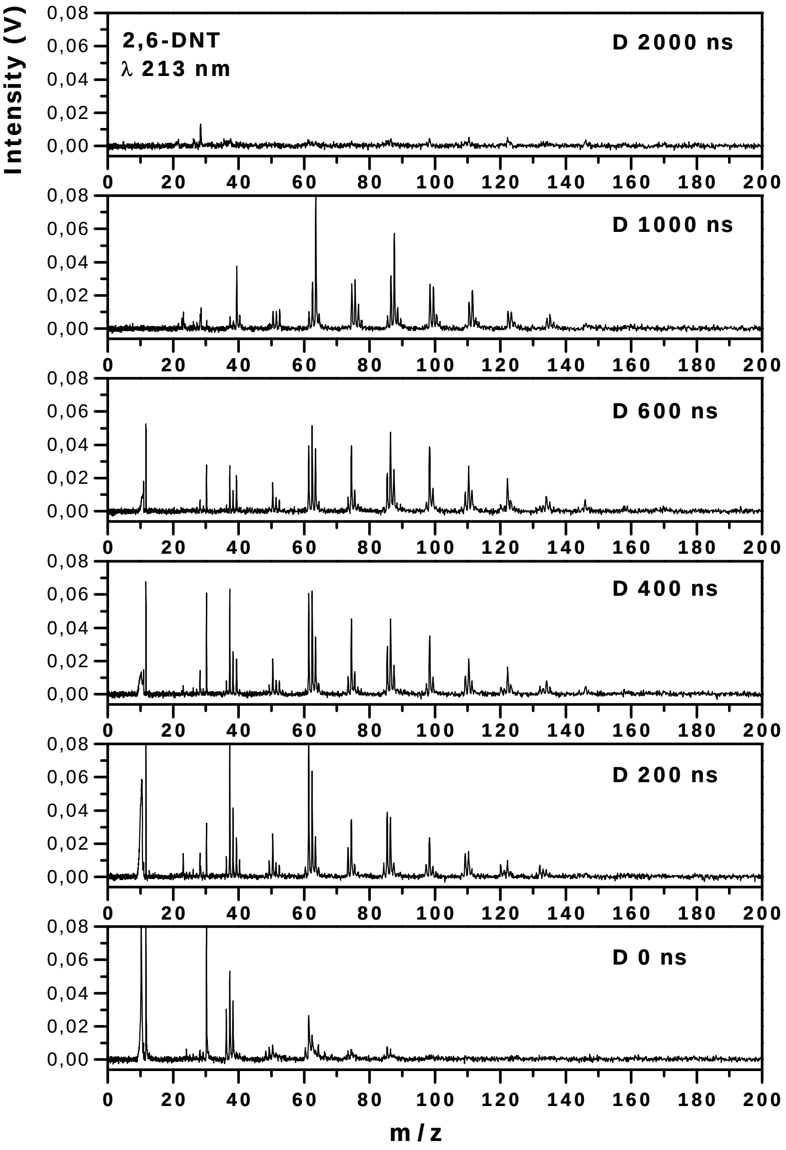

Figure 3.20. Mass spectra of 2,6-DNT irradiated with 213 nm laser beam under different extraction delays conditions. The extraction pulse width and the fluence value were set at 800 ns and 1.96 J/cm^2, respectively.

As well as studying the effect of extraction pulse width, the influence of delay time between laser pulse event and the application of extraction voltage was evaluated. Figure 3.20 shows the acquired mass spectra for given delay times (D_e= 0, 200, 400, 600, 1000 and 2000 ns). Extraction width pulse was set at 800 ns. It was observed how the ionic yield in the detector increased from 0 ns up to 400 ns so that the efficiency of species extraction grew significantly. However, for higher delay times the signal began to decline gradually with a progressive loss of resolution, particularly in the low-mass range. Therefore, the range from 0 to 400 ns as delay time gave rise to best spectral results, showing the highest resolution and the best signal-to-noise ratio.

When delay time was set close to 400 ns, extraction of ions seems to be more efficient despite a slight loss in resolution.

This effect was also confirmed for several compounds and for different extraction pulse widths, obtaining similar results.

3.5.3. Identification of organics by LIMS. Spectral Library

LIMS mass spectra acquired under optimized conditions for TNT homologous series are part of a LIMS spectral library elaborated with the purpose of serving as an analytical tool in the identification of organic compounds of interest, such as explosives or toxic substances dangerous for health and the environment. Appendix 1 includes a compendium with some of LIMS acquired spectra as a part of this collection. In the acquisition of spectra, the focus, energy and temporal extraction conditions were adjusted independently in order to obtain maximum values for intensity signal, signal-to-noise ratio and resolution.

3.6. CONCLUSIONS

Laser ionization time-of-flight mass spectra of nitro-aromatic compounds (TNT, DNT and MNT) in condensed phase have been acquired using nanosecond UV outputs from a Nd:YAG laser for one-step desorption/ionization. The performed study has demonstrated the ability of the technique to generate analyte molecular and structure-specific ions of the nitro compounds with information comparable to that obtained by electron impact ionization.

Different parameterization studies of such variables which further affect the direct laser ionization process of the sample were carried out. Thus, experimental measurements concerning the selection of the most favourable radiation wavelength, the optimization of focus conditions of laser beam onto the sample surface, and the adjustment of best temporal extraction conditions, were performed. This search for the optimal ionization conditions allowed the study of the onset of ion generation (or ionization threshold) for different fragment ions from the molecule, and a deeper understanding about changes in the ablation regime and about the energetic channels involved in the break-up of the molecule. This was discussed from changes undergone by mass spectra when energy per pulse was increased gradually. Thus, the opening of the aromatic ring in the case of 2,6-DNT molecule seems to occur at values around 1.3 J/cm^2) where a change in the ablation regime (Coulomb explosions) occurs, as indicated by the increase in the $^{12}C^+$ signal.

Results about the effect of the extraction settings on the acquired signal attracted special attention. The mass spectra underwent important qualitative changes when the extraction width pulse was varied. At short extraction widths (400 ns), a cut-off exists for high-mass ions, and the mass spectrum reveals atomic-only information. For longer width pulses (>800 ns), higher mass fragment ions are detected, while low-mass ions are reduced in intensity and resolution. These results allow modulation based on a simple modification in the extraction settings, not in the excitation conditions, opening the possibility of acquiring quasi-simultaneous atomic/molecular modulated mass spectra.

Optimization of the parameters for acquisition of molecular information allowed the identification of the organic compounds from characteristics fragments appearing in the mass spectra. In this sense, direct ionization in the condensed phase coupled to time-of-flight mass spectrometry represents a remarkable tool in the deep understanding of the chemistry of high energetic materials.

Finally, two different procedures have been investigated to detect surface traces of TNT that could be valid for forensic analysis. Their usefulness in alerting about the possible presence of a nitro-aromatic compound has been demonstrated, although additional work in determining the role played by the supporting substrate on the resultant spectra is still required.

CHAPTER 4

Laser-Induced Plasma Spectroscopy of Nitro Aromatic Explosives. Understanding Fragmentation Processes Using Ion-Photon Coincidence Measurements

4.1. SUMMARY

Coincident detection is of interest to get as much information as possible about transient events occurring in laser induced plasmas. The present work is focused on coincidental ion-photon detection of laser plasmas of high energetic organic compounds in condensed phase irradiated with UV laser pulses using an advanced instrument for simultaneous monitoring of both type of chemical species generated. The optical emission spectrum is acquired from atoms, atomic ions and diatomic molecules, whereas the mass spectrum derives from fragment ions of the molecule. These fragments result from direct ionization or may be formed through indirect pathways. Fluence-resolved experiments showed the evolution of the main optical-mass signals in the acquired spectra for a limited energetic range, showing the different stages of lifetime of plasma: the rising thresholds and extinction of the different atomic and molecular studied species, besides the breakage of the aromatic ring and the later excitation of ionic species at higher fluence level.

4.2. INTRODUCTION

Laser-matter interaction is essentially based on thermal and photonic processes, where as a consequence of laser irradiation, different phenomena occur in a microscopic or macroscopic scale. While at low irradiance, surface heating and melting following soft desorption and ionization are the main sequential events, the high irradiance regime is governed by an evaporation of the material and an extensive fragmentation with the final formation of the expanding plasma cloud **[Vertes, A. et al., 1989]**. The processes taking place in the laser-matter interaction depend on the nature of the sample, and therefore the plasma formation of organic compounds is largely different than that from metals. Regardless the sample type, the cloud of ablated material moves away from the surface in all directions but preferentially along the target normal, and consists of excited or ground-state neutrals, electrons and ions. A whole description of the plume would require the combined effort of a plethora of techniques such as mass spectrometry, optical emission and absorption spectroscopies, Langmuir probes, fast imaging and particle collectors to describe the shape and velocity of the plume at various times after the ablating laser pulse **[Aguilera, J. A. et al., 2004][Kushwaha, A. et al., 2008]**; the spatial distribution of density and temperature at various times after the ablating laser pulse **[Aguilera, J. A. et al., 1999][Aguilera, J. A. et al., 2002][Aragon, C. et al., 2004]**, or the spatial and temporal variation of the plume composition, in terms of the atoms, molecules, excited states and clusters present **[Acquaviva, S. et al., 2002 B][De Giacomo, A. et al., 2008][Galbács, G. et al., 2010]**.

Simultaneous studies of the plasma optical emission (laser-induced breakdown spectroscopy, LIBS) and the ions formed in the plasma plume (laser ionization mass spectrometry, LIMS) may provide real-time and complementary information about ion formation kinetics, fragmentation pathways, recombination mechanisms and thermo-chemical measurements in the expanding plume from ablated organic materials **[Song, K. et al., 2004]**. This advantageous ion/photon coincidence counting can also be used to search for the correlated emission of secondary ions from the same initiating excitation pulse, revealing spatial and chemical relationships. Many advantages may be found in coincidence counting as enhancing the selectivity and accuracy; establishing temporal correlation between different signals or gaining additional information from transient single events **[Sovová, K. et al., 2010]**. Furthermore, simultaneous monitoring of both spectra can provide information regarding to calculations of density of ions compared to neutrals, as well as electronic and target surface temperatures, among others **[Vadillo, J. M. et al., 2005]**.

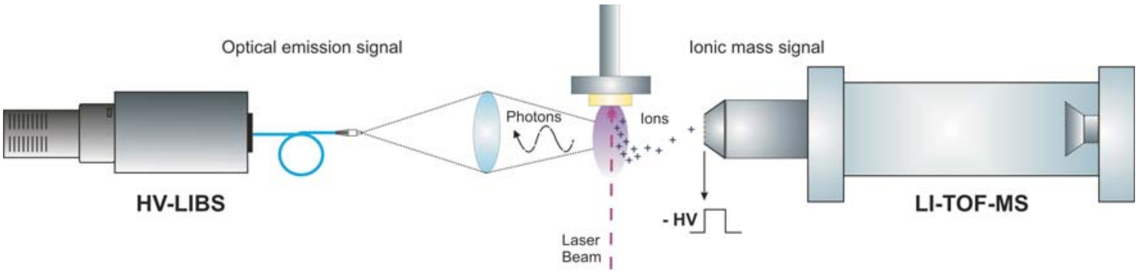

Figure 4.1. Ion/photon coincidence detection scheme.

The bibliography reveals a few references with ion/photon coincidence detection scheme in which the authors put mass information in keeping with emission signal coming from a unique plasma sampling. Sovová *et al.* **[Sovová, K. et al., 2010]** and Civis *et al.* **[Civis, M. et al., 2011]** studied the LIBS spectra emission of several high-energy explosive materials and performed mass spectrometry analysis of the neutrals generated by ion flow tube mass spectrometry (SIFT-MS). The information obtained allowed to explain fragmentation pathways and to propose mechanism of decomposition for each molecule. A similar approach was recently used by He *et al.* **[He, X. N. et al., 2012]**. The authors compared the LIBS spectra with those obtained by ambient metastable ionization (DART) of the neutrals generated with laser ionization time-of-flight mass spectrometry (LI-TOFMS) to study the effects in metallic and carbon samples. The methods described make use of charge-transfer neutrals ionization and do not deal with laser-generated primary ions. The simultaneous monitoring of photons and ions from a laser plume was described by Song *et al.* **[Song, K. et al., 2004]**, allowing the measuring of lifetime of ions inside the plasma and laser power dependence of mass resolution for solid samples. The determination of the laser fluence thresholds for ion or photon formation has been also studied **[Vadillo, J. M. et al., 2005]**, demonstrating the dependence of such value with thermal properties of the sample, and the lower energy values required for ion emission. Despite the interest for direct analysis or organics by LIBS or LIMS, there are no references dealing with their coincidence analysis.

In this work, ion/photon detection is performed over solid-phase organic nitroaromatic compounds. TNT and its precursors (DNT and MNT) were chosen as reference molecules since they represent a well-known family of organic energetic molecules with simple structures which, in suitable energetic conditions, experience an easy fragmentation that lead to the study of the dissociation pathways under different excitation techniques **[Kosmidis, C. et al., 1994][McMillen, D. F. et al., 1997][Tönnies,**

K. et al., 2001][Tanaka, G. et al., 2008][Mullen, C. et al., 2009][Sovová, K. et al., 2010][Civis, M. et al., 2011]. Moreover, their similar structures but very different physical properties lead to us to study the existence of little differences of behaviour under laser ablation process. The system has been designed to allow simultaneous ion/photon detection of the expanding plume in orthogonal direction with respect to the expansion axis of the plume. Time- and space-resolved studies of the plume can be performed while the ions are extracted to a time-of-flight mass spectrometer. At a difference of organics, the atomic/isotopic information describes completely the sample of inorganic nature. Thus, above some energy threshold and over a certain energy range, the qualitative information contained in the spectra is quite constant. The upper limit in the laser energy for the ablation process is normally determined by the saturation level of the detector or by an excessive damage of the sample. During the ablation of organics, however, an excess of energy deposited on the sample originates bond breaking and so, the complete loss of any molecular information codified in the observed spectra. Thus, for ion/photon coincidence analysis of organics, it is crucial the establishment of adequate ablation and experimental conditions capable of generating a plume containing significant amount of excited species to be detected by optical emission spectrometry without excessive bond breaking that may compromise mass spectrometry detection.

4.3. EXPERIMENTAL

The schematic diagram of the complete experimental system used in the study is shown in Figure 2.17 of the present memory. Moreover, a simple scheme of the coincidental system is exhibited in Figure 4.1. The combined analytical system made possible the simultaneous monitoring of both emission LIBS and mass LIMS spectra in order to identify the species existing in the plasma plume. Some improvements were implemented on the set-up for coincidental inorganic acquisition in order to optimize both the system for plasma light collection and the ion extraction system so that we were able to obtain reproducible spectral information from organic samples. The fourth harmonic output of a Q-switched Nd:YAG laser (*Quantel, Mod. Brio*, pulse width 4.4 ns) was used to irradiate the samples for both LIBS and LI-TOF-MS analysis. UV radiation was chosen for the study since phenomena of fragmentation are soft and less thermal effects take place as was discussed in Chapter 3 of this memory. The laser beam was focused by a 1” diameter convex lens (20 cm focal length) located outside of the vacuum chamber. The laser beam was slightly defocused in the surface of the sample to a spot size of about 280 µm for a suitable plasma formation. The maximum laser pulse energy used in the experiment was 4.3 mJ. The pulse repetition rate was set to 4 Hz during experiments.

The light emitted from the entire plasma was collected orthogonally to the plasma expansion axis and focused by means of a quartz lens of 3" diameter to an optical fibre coupled to the input slit of a 0.5 m imaging spectrometer (*Andor, Mod. Shamrock*) equipped with an intensified CCD detector (*Andor Tech., Mod. iStar*). The ICCD has a wide spectral range of 115–920 nm. A grating with 599 grooves/mm allowed a dispersion of 0.19 nm/pixel and coverage of 45 nm/spectral window. Each of the acquired LIBS broadband spectra were composed from overlapping spectral windows, to obtain a final broad range of 240-900nm. For each spectral window, 30 laser shots were accumulated to reach satisfactory signal-to-noise ratio. Detection gate delay and time of gate width can be adjusted so that the spectra can be obtained at different temporal settings after the laser pulse. They were set under 50 ns and up to 1 µs, respectively, for the temporal plasma-integrated measurements.

A reflectron-based time-of-flight mass spectrometer (TOF-MS) with lab-made modifications from the original configuration (*R. M. Jordan*, USA) in the ion optics, feedthroughs and sample entry **[García, C. C. et al, 2001]** was used in the experiments. The atomic and molecular ions are orthogonally extracted to the flight-tube spectrometer, passing through different electrodes that extract, focus and accelerate the ions by means of the application of different optimized voltages. The distance between the laser beam axis and the exit grid electrode was optimized to 1.5 cm. Then they are sequentially registered by means of an ion detector comprised of dual microchannel plates (MPC) that fed a digital oscilloscope. Kinetic series of 500 mass spectra (associated to 500 laser events) were acquired for every coincidence measurement. Care was taken to record all the spectra under identical laser excitation and focusing conditions. The electronic configuration of the system allowed the detection of positive ions only.

Both systems for emission signal collection and for ions detection were synchronized by means of a pulse and delay generator (*Stanford Research System DG535*). The trigger signal from the laser reached the PDG and it is used to drive the extraction electrode and the aperture of ICCD camera at the same time, with which temporal parameters of signal acquisition were controlled.

A summary of the values set for the experimental parameters for laser, LI-TOFMS and LIBS systems is presented in Table 4.1.

4.4. SAMPLES

2,4,6-TNT was obtained from National Department of Defence whereas 4-MNT and 2,6-DNT was purchased from *Sigma-Aldrich*. They all were prepared by compressing powders of pure compounds using a standard press machine applying a pressure of 2.5 tons. The thickness of the resulting pellets was 2 mm and they were introduced into the ionization chamber orthogonal to both flight and collection axis and facing the incident laser. They were fixed onto a metal holder by means of a direct insertion probe previously described **[Vadillo, J. M. et al., 2005]** equipped with a 3D micrometer for fine control of the position of the sample.

4.5. RESULTS AND DISCUSSION

4.5.1. Introduction

The laser radiation causes heating, desorption, fragmentation, atomization and then ionization of the material. Ionic, atomic and molecular species were identified on the basis of characteristic emission from LIBS spectra of the analyzed organic nitro aromatic compounds. On the other hand, final products of photo-chemical ionization were observed in LIMS spectra. All the results shown throughout this work were performed using 266 nm pulsed radiation, and all identified species are listed below in the Table 4.2.

Table 4.1. Optimal operating conditions in coincidental analysis at high vacuum pressure.

Mass signal acquisition		Optical emission collection		Laser operation	
Width extraction pulse	400 ns	**Gate pulse width**	≥ 1 μs	**Wavelength**	266 nm
Delay extraction pulse	0 ns	**Gate pulse delay**	20 ns	**Repetition rate**	4 Hz
Extraction voltage	-1265 V	**MCP Gain**	≥ 200	**QS-d**	140 μs
Chamber pressure	$< 1.0\cdot10^{-4}$ mb	**Collection geometry**	Orthogonal	**Energy**	0 - 4.3 mJ

Table 4.2. Identification of molecular bands along with main atomic lines in LIBS spectra and main ionic species in LIMS spectra for homologous TNT series.

Identified ions			
Species	**Mass (u.m.a.)**	**Ionization Potential (eV)**	
H^+	1	13.60[A]	
C^+	12	11.26[A]	
N^+	14	14.53[A]	
O^+	16	13.62[A]	
C_2^+	24	12.5 ± 0.05[B]	
$C_2H_2^+$	26	-	
CN^+	26	14.2 ± 0.3[C]	
HCN^+	27	-	
CO^+, $CHNH^+$	28	-	
NO^+	30	9.25[D]	
$C_nH_m^+$	39^+, 51^+, 63^+	-	
Identified atomic emission lines			
Species	**λ (nm)**	**Electronic transition**	**Excitation Energy (eV)[A]**
C (I)	247.8	$2s^22p^2$ - $2s^22p(^2P^0)3s$	7.68
C(II)	426.7	$2s^23d(^2D)$ - $2s^24f(^2F^0)$	20.95
H_β (I)	486.1	Balmer series ($2P^0$-2D)	12.70
H_α (I)	656.3	Balmer series (2S-$2P^0$)	12.08
N (I)	746.7	$2s^22p^2(^3P)3s$ - $2s^22p^2(^3P)3p$	11.99
O (I)	777.4	$2s^22p^3(^4S^\circ)3s$ - $2s^22p^3(^4S^\circ)3p$	10.74
Identified molecular emission bands			
Species	**λ (nm)**	**Electronic Transition[E]**	**Excitation Energy (eV)[F]**
OH	308.9	$A^2\Sigma+ - X^2\Pi$	-
NH	336.0	$A^3\Pi - X^3\Sigma^-$	-
CH	431.4	$A^2\Delta - X^2\Pi$	-
CN	358.6	Violet, $B^2\Sigma^+{}_u$ - $X^2\Sigma^+{}_g$, $\nu'=1$, $\nu''=0$	3.19
CN	388.3	Violet, $B^2\Sigma^+{}_u$ - $X^2\Sigma^+{}_g$, $\nu'=0$, $\nu''=0$	
CN	421.6	Violet, $B^2\Sigma^+{}_u$ - $X^2\Sigma^+{}_g$, $\nu'=0$, $\nu''=1$	
C_2	473.7	Swan, $A^3\Pi_g - X'^3\Pi_u$, $\nu'=1$, $\nu''=0$	2.48
C_2	516.5	Swan, $A^3\Pi_g - X'^3\Pi_u$, $\nu'=0$, $\nu''=0$	
C_2	563.5	Swan, $A^3\Pi_g - X'^3\Pi_u$, $\nu'=0$, $\nu''=1$	

A [Y. Ralchenko, Y. Nist Atomic Spectra Database]
B [Ibdzig, A., 1983]
C [Berkowitz, J., 1962]
D [Nakayama, T., 1959]
E [Pearse, R.W.B., 1976]
F [Abdelli-Messaci, S., 2005]

Coincidence analysis has been previously carried out in metallic targets with diverse purposes **[Song, K. et al., 2004][García, C. C. et al., 2001][Vadillo, J. M. et al., 2005]**, but as commented before, in the case of organic compounds there is limited research about this issue. For organics, laser-matter interaction leading to ablation and plasma formation involves chemical processes of fragmentation and recombination more complex than those in metals. The physical-chemical properties of the nitro-aromatic compounds, the high excitation and ionization energies of atomic species, combined with the requirement of high vacuum work regime (below $1.0 \cdot 10^{-4}$ mb) make difficult the coincidental analysis since it involves the absence of buffer gas in the surrounding of sample surface and, therefore, the absence of collisions between gas and ablated material. In consequence, the plasma plume has a low density and lifetime of plasma emission become very short, in some cases shorter than 1 microsecond. Therefore, high-resolution dispersive gratings are necessary for suitable signal collection. In the other hand, the absence of ambient air or any buffer gas in the zone of plasma formation assured that both charged particles and excited-state species in the plume came exclusively from ablated material and the subsequent collision and recombination processes in the free expansion plume.

4.5.2. Temporal parameters for signal acquisition

In both detection ways, it is possible to set the acquisition conditions to obtain signal from specific time slices and so, information about the lifetime of the detected species. Figure 4.2 shows the results obtained for 2,6-DNT at a base pressure of $1.0 \cdot 10^{-5}$ mbar that was exposed to 266 nm laser pulses at a fluence of 3 J/cm^2. For LIBS, diffraction grating was set to zero order so that non wavelength-dispersed light reached the detector. Gate widths of 10 ns were used to sketch the plot shown in Figure 4.2 (top left). As observed, the intensity of all the emitted photons falls to a 10% of its initial value just after 100 ns of laser firing. This rapid decay is due to the free expansion of the plasma and not to a loss in the collection efficiency, as the 3” diameter lens was able to collect efficiently over a wide solid angle. In order to check this effect, we affixed the end of an optical fiber (connected in one end to a pointing laser) to the sample holder. We could not observe any loss in the recorded signal during the 2.5 cm displacement in the two degrees of freedom available. Concerning the lifetime of ions presented in the plasma (Figure 4.2, top right), the minimum time resolution achievable was 800 ns to allow proper ion extraction. Delay values above 500 ns gave rise to the starting of the loss of total net intensity of current signal, dropping to 10% of its initial value after 5000 ns.

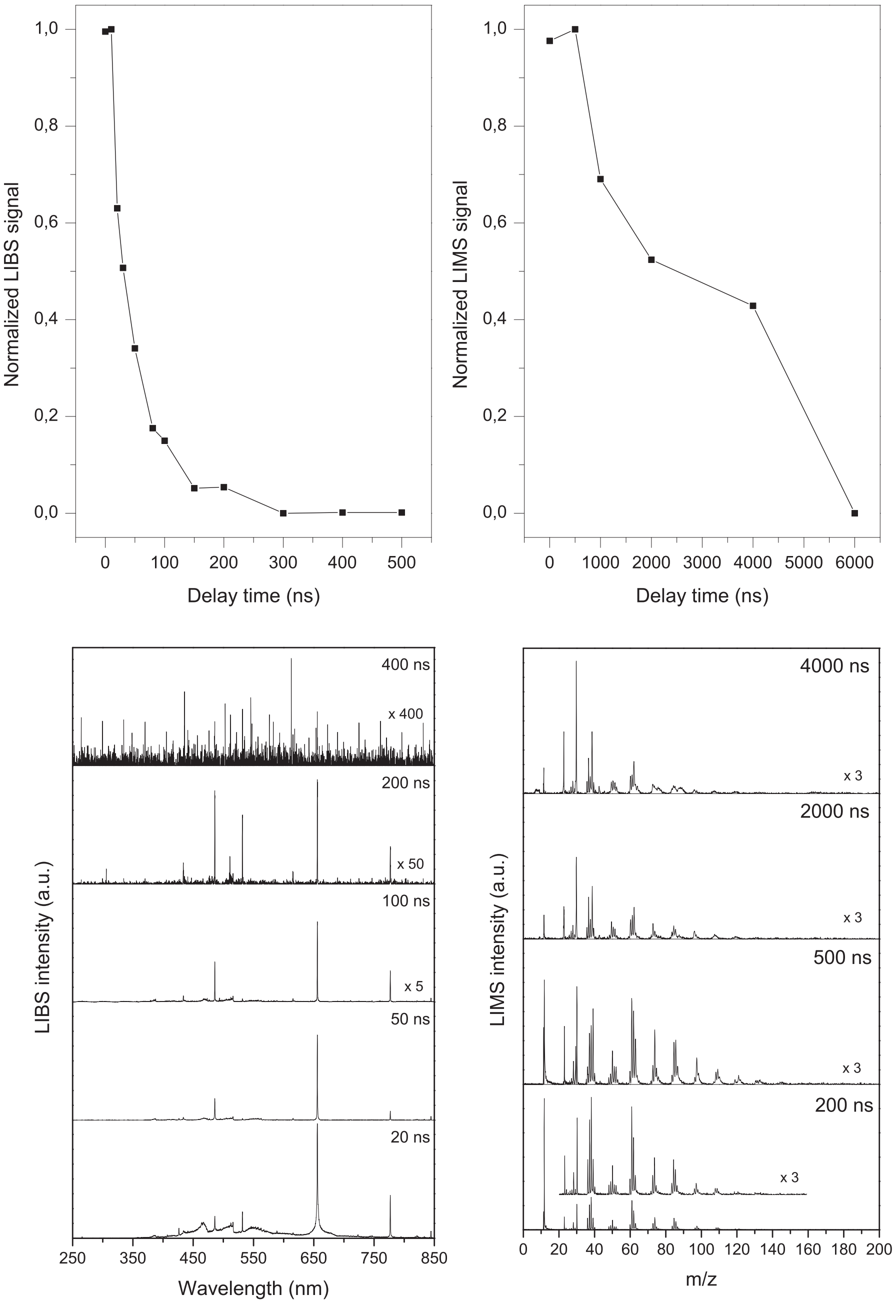

Figure 4.2.a) Time-resolved emission intensity of collected light from 2,6-DNT plasma. The gate width for each measurement was 10 ns. b) Time-evolution of integrated LIMS signal from irradiation of 2,6-DNT sample. The extraction pulse width was set in 800 ns.

The LIBS spectra at different delay times are shown in Figure 4.2 (bottom left pannel). The spectra have been shown at their maximum scales to show the falling in the overall intensity and the variation of the emission lines. At short delay times, the LIBS spectrum is mainly taken by the intense H and O atomic lines at 656.3 nm and 777.4 nm, as well as by the CN and C_2 emission at 388.3 nm and 516.5 nm, respectively. A large background contribution is observed at 20 ns, decreasing at longer delays. The same behaviour follows the contribution of diatomic emissions, reaching values close to zero at about 200 ns. From these values, atomic-only emission is found. The LIMS spectra in the 0-200 amu interval at different delay are shown in Figure 4.2 (bottom right pannel). As shown, the delay time can be increased up to 500 ns while keeping good signal-to-noise ratio and resolution. Delay values above 500 ns gave rise of the decrease of total net intensity, with some loss of resolution after 2000 ns.

After these results, a time-integrated window of 1 μs was selected for coincidental studies in order to ensure the complete capture of the plasma light. Regarding the delay time, short times were preferable (20 ns) avoiding the continuum background emission but assuring the detection of ionic emitting species in the early stages of plasma life. Regarding LIMS, taking into account the escape velocities of the species in the expanding axis, ions could be efficiently extracted within a considerable time interval. Extraction conditions which allowed obtaining higher resolution of species in the low mass range were selected due to only atomic and diatomic species were aim of study in the coincidental analysis. Delay of 0 ns and an extraction width of 400 ns yielded the best results.

4.5.3. Dependence of coincidental signal on fluence level

The amount of energy used to irradiate the sample affects significantly the resultant spectra, particularly in organics, as the observed peak pattern will change quantitatively, but also qualitatively due to molecule fragmentation. Thus, the relative weight of atomic or molecular species within the expanding plasma, or the appearance of specific signals may depend on the particular excitation conditions.

In the study of the evolution of atomic species and molecular fragments with fluence level, a similar behaviour for the three homologous series compounds was found out. Figure 4.3 shows the sequence of spectra with increasing fluence level in the case of TNT. In the studied fluence range, the acquired signal was very sensitive to slight changes in energy. The fragmentation peak pattern of the molecule was richer at 3.6 J/cm^2. Higher fluence values basically generated a marked atomic fragmentation. Below the ionization threshold (F_{th}), little photochemistry occurs and the species of interest are simply desorbed into vapour phase, but they are not ionized. Characteristic molecular ions as m/z 39$^+$, m/z 30$^+$, m/z 28$^+$, m/z 26$^+$ and m/z 24$^+$ have an ephemeral existence and they coexist in a very narrow energy range. The starting of their extinction coincides with the appearance of the atomic species H$^+$, N$^+$ and O$^+$, whose values of first ionization potential are very similar as shows Table 4.2. However, C^+ ion is visible at lower fluence values, according to its lower first ionization potential (11.26 eV). The onset of C^+ generation up to 1.8 J/cm^2 evidences the point of breakage of carbon-carbon bonds in the molecule.

In contrast, the increase of signal intensity for molecular and atomic species in LIBS spectra is progressive with fluence level. It was observed how molecular emission bands corresponding to CN and C_2 fragments emerged and became visible at low laser energy values whereas atomic species presented higher energy thresholds. This fact is due to the large different between excitation energies of molecular and atomic species as indicated in Table 4.2. Thus, as can be noted from Figure 4.3(b), higher laser pulse energy is required to excite atomic species in the plume. On the other hand, the existence of excited CN and C_2 fragments in the plasma plume and subsequent emission of molecular bands at high vacuum and from very low energy regime suggested the direct fragmentation of the aromatic molecule as the most likely generation source, in addition to the possible immediate recombination processes between native atoms in the plume. This hypothesis will be discussed later.

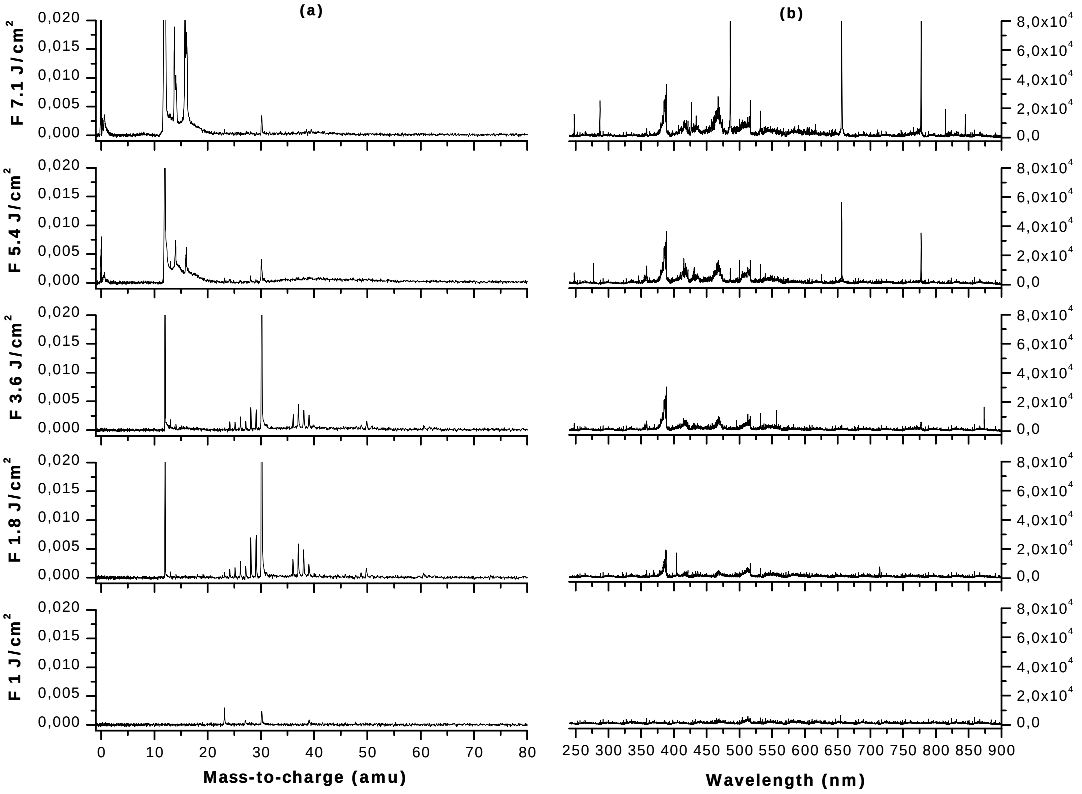

Figure 4.3. (a) Mass spectra (0-80 amu range) and (b) emission spectra (240-900 nm range) of TNT acquired in coincidence at fluence values from 1 J/cm^2 to 7.1 J/cm^2.

Figure 4.4 shows the evolution of different atomic (H, C, N and O) and molecular (C_2) signals in the expanding plasma monitored by optical emission spectroscopy for 2,6-DNT. Simultaneously, the intensity of ions in positive mode at m/z 1, 12, 14, 16 and 24 (corresponding to H^+, C^+, N^+, O^+ and C_2^+, respectively) were also detected. Moreover, in Figure 4.4(f) is showed the variation of m/z 26^+ and m/z 30^+ peaks for the same energetic range. The signal at m/z 26^+ can not be assigned to CN^+ or $C_2H_2^+$ as the resolution of our TOF system is below the minimum required to resolve their isobaric interference (2000, m/Δm). However, due to the high electronegativity of the cyanide group, it is expected a larger population as anion and only a possible minimum contribution as a cation. Therefore, the signal was attributed almost entirely to $C_2H_2^+$ ion so the LIMS-LIBS comparative study for this radical was not possible. As for NO^+ fragment (main peak in the mass spectrum at m/z 30^+ in the low fluence range), it can be produced either by a nitro-nitrite-type mechanism (the C-N-O_2 bond quickly rearranged into C-O-NO, which dissociated directly to NO) **[Bashu, V. C. J. et al., 1991]** or by the direct dissociation from parent molecule, yielding labile intermediate NO_2 groups which are in turn rapidly photodissociated into the most stable NO fragments **[Pond, B. V. et al., 2007]**. However, in our experimental conditions, main emission systems of NO molecule (located mostly in the ultra violet region) were not observable in LIBS spectra of organic nitro compounds. In fact, no references were found about NO molecular emission for this type of molecules by means of UV-LIBS detection. Therefore, the coincidental study of such species could not be carried out.

The coincidental data in Figure 4.4 were also acquired from fluence values below the ion or photons formation threshold, up to a fluence value well-above the plasma formation (7.1 J/cm^2). Due to the large variations in intensities along the fluence range, each set of intensity data was normalized between 0 and 1 for a better comparison. All signals were obtained in coincidence ion/photon detection scheme and 100 individual laser events were averaged at each energy setting. Due to the use of an optical attenuator, laser energy stability was better than 1% as measured for series of 1000 laser shots at the different energy points. Data above 7.1 J/cm^2 were not acquired due to the massive sample destruction which prevented the generation of reproducible data. On the other hand, the conductivity of the large plasma generated at such fluence values induced arcing in the adjacent electrodes, impairing a stable setting of the extraction conditions.

The signals corresponding to $^{1}H^+$, $^{12}C^+$, $^{14}N^+$, $^{16}O^+$ were recorded in the mass spectrometer, while emissions at 656.3 nm, 247.8 nm, 746.8 nm and 777.4 nm were used for H, C, N and O, respectively. A quick overview of the Figures 4(a), (b) and (c) reveals coincidence in trends for H, N and O in the ion and photon detection schemes. As expected, signals start to increase once a given fluence threshold (F_{th}) has been reached (with some differences between atomic and molecular species, as well as between compounds). Then, atomic signals rise up quite steeply right after the threshold value and follow a linear trend up to a maximum fluence value. This fact suggests an agreement in the behaviour for both emitting neutral species and ionized atomic species as energy regime changes. As observed, the fluence threshold for H and O are always lower for ion detection, while for N, the thresholds values are almost identical. The behaviour of $^{12}C^+$ was clearly different since its fluence threshold (about 1.4 J/cm^2) was smaller than those for the rest of the atomic monitored species, evidencing a clear sequence, with C being released before than H, O or N. Moreover, trends observed for both ion (C^+) and photon C(I) species were quite different. Thus, for ion detection, the signal rises up quite sharply just after the threshold value, reaching a plateau at medium fluence (about 5 J/cm^2). However, for photon detection the trend is identical as that observed for the rest of atomics, with an emission threshold value slightly lower according to its also lower excitation energy (7.68 eV). Therefore, regarding the order of species releasing, the same behaviour is observed when photons are monitored although the fluence values where the cut-off value occurs are shifted at larger fluence values.

The most striking trend was that followed by the diatomic species. Fragments $^{24}C_2^+$, $^{26}C_2H_2^+/CN^+$, $^{28}CO^+/HCNH^+$ and $^{30}NO^+$ as well as other larger molecular fragments only exist as stable ions for a narrow fluence interval and then they rapidly tend to break down as increasing the intensity of laser energy. However, emission bands corresponding to main molecular systems tends to grow up in a gradual way with energy from very low fluence values, once the excitation energies have been achieved.

Figure 4.4.(e) shows the trend followed by C_2^+ ions and C_2 excited molecules. The presence of both species in the plasma plume allowed their coincidence detection. The ionic species exhibited a sharp increase right after the threshold value, reaching a maximum near to 4 J/cm^2, and dropping from this point and decaying to zero at 6 J/cm^2. This behaviour was not observable in photon detection, where the trend was identical to that of monoatomic species. As Figure 4.4.(f) shows, the behaviour of the stable NO^+ radical and the $C_2H_2^+/CN^+$ fragments were identical to that followed by C_2^+ molecule, as the rest of ionized low mass fragments (see also Figure 3.17 in Chapter 3). Thus, it is obvious the different trend of the diatomic species monitored by mass spectrometry. The presence of CN from the emission spectra was evident, but its

appearance in the mass spectra as $^{26}CN^+$ is not clear as discussed above. On the contrary, only NO is detected as NO^+ in the mass spectrometer. The fluence thresholds for the C-containing fragments are quite similar to that calculated for C^+. However, the onset of NO^+ species occurs below 1 J/cm^2, this being the first mass fragment observable. This fact is in full agreement with the quick release of the NO_2 from the ring due to the well-known *ortho-effect* in nitroaromatics. Moreover, fluence range in which NO^+ species persists in the plume is lightly higher to that for the rest of low-mass fragments. The drop of the curve coincides with the onset of atomic oxygen which is consistent to the dissociation of the diatomic species. Another remarkable aspect in the photon detection of C_2 and CN molecules is the lower fluence threshold in comparison with that for atomic species. This fact supports the quick opening of the aromatic ring.

Behaviour observed for ionic fragments can be based on the marked difference between excitation and ionization energies for such species. In the specific case of C_2 molecule, first ionized fragments come directly from the rupture of parent compound at low fluence regime. When energy is quite enough to reach the dissociation energy for C_2 molecule (6.27 eV) **[Pradhan, A. D. et al., 1994]**, fragments turn into atoms and through different thermodynamically favoured routes at high vacuum regime, C_2 fragments are formed again and led to excited state rapidly (2.48 eV). But then they could suffer a new dissociation before reaching the first ionization potential (12.15 eV), so that generation of C_2^+ ions is not favoured at high fluence regime and as a consequence, they are not detected above a specific energy level. This phenomenon can be generalized to other low atomic fragments.

The results obtained seem to be in accordance with the dynamic of the ring opening of nitrotoluenes described in gas-phase spectroscopy, where the extensive fragmentation observed in the mass spectra after nanosecond irradiation is the consequence of the short dissociative lifetimes of the intermediate states involved in the ionization process (a few hundred femtoseconds). The presence of NO in the mass spectra of these species was attributed to rapid dissociation of the parent molecule (RNO_2) producing the NO_2 fragment, and the subsequent photon absorption from its ground state, leading to NO and O. In an overall picture, once a given fluence level has been reached the aromatic ring opens up, releasing the NO_2 groups and inducing the breaking of the structure. This fact explains the early appearance of NO^+, C_2^+ and $C_2H_2^+/CN^+$ signals (see Figure 4.4). An increased fluence produces a subsequent breakage of bonds, what generates an increase in the population of monoatomic ions in the plume. Thus, it is explainable the growing abundance of C^+ even after the C_2^+ or $C_2H_2^+$ have reached their maximum. This fact is supported by the monitoring of the emitting species, what evidences the usefulness of the simultaneous monitoring of ion and photons.

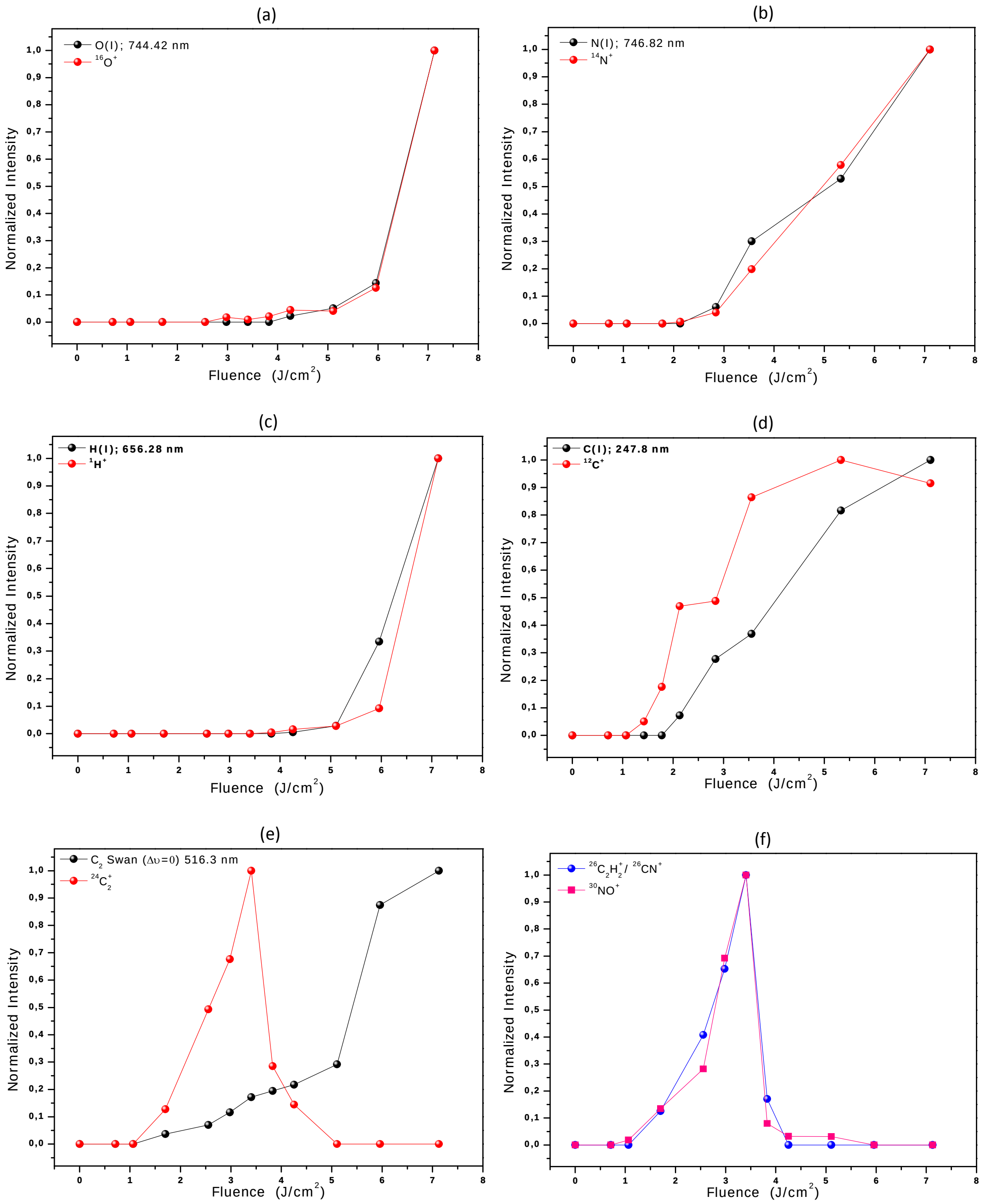

Figure 4.4. (a-e) Coincidental LIMS-LIBS signals of atomic and molecular species versus fluence level for 2,6-DNT; (f) variation of $C_2H_2^+$ and NO^+ species from LIMS spectra versus fluence level for 2,6-DNT. Intensities were all normalized to the maximum value.

In this sense, it is especially interesting the situation of the CN band emission. It has been discussed above the difficulty in assigning unequivocally the mass fragment at m/z 26^+ to CN^+ due to the most probable existence of the $C_2H_2^+$ ion. However, the existence of CN in the expanding plasma is undoubted from its optical emission spectra. Different pathways have been proposed in the literature to explain the origin of weak-intensity CN bands **[Dong, M. et al., 2011] [Ma, Q. et al., 2011] [Sovová, K., et al., 2010] [Vivien, C. et al., 1998] [Abdelli-Messaci, S. et al., 2002]**:

$$[\mathrm{MOLEC}] \longrightarrow n\mathrm{CN} + m\mathrm{C_2} + \text{other prod.} \qquad (4.1)$$

$$\mathrm{C} + \mathrm{N_2} \rightleftharpoons \mathrm{CN} + \mathrm{N} \qquad (4.2)$$

$$\mathrm{C_2H} + \mathrm{N} \longrightarrow \mathrm{CN} + \mathrm{CH} \qquad (4.3)$$

$$\mathrm{C_2} + \mathrm{N_2} \rightleftharpoons 2\mathrm{CN} \qquad (4.4)$$

$$\mathrm{C_2} + \mathrm{N} \rightleftharpoons \mathrm{CN} + \mathrm{C} \qquad (4.5)$$

$$\mathrm{C} + \mathrm{N} + \mathrm{M} \longrightarrow \mathrm{CN} + \mathrm{M} \qquad (4.6)$$

Only reaction (4.3) seems to be the best candidate under the high vacuum conditions of our experiment. Reaction (4.2) and (4.4) require the existence of N_2 in the surrounding atmosphere, what does not occur under high vacuum conditions. On the other hand, reaction (4.5) favours to the left-hand side so it should be discharged and reaction (4.6) requires the presence of N atoms in gas phase from dissociation of N_2 molecules to proceed. Reaction (4.3) needs the presence of atomic N and ring fragments to evolve. The latter is present as the aromatic ring is broken at low fluence values (confirmed by the early presence of C_2^+ and hydrocarbon fragments in LIMS spectra), but the onset of N occurs with the dissociation of the NO species at moderate fluence values (around 3 J/cm^2). Therefore, an alternative route should be responsible of the CN emission observed under that fluence value. Although it is well-known the favourable releasing of the NO_2 groups from parent molecule (as has been already commented), direct fragmentation of the molecule (4.1) and generation of diatomic structures (single bond C-C, double bond C=C and bond C-N) could occur as the breakage of aromatic ring takes place at low fluence values. Therefore, (4.1) and (4.3) are proposed as main pathways in the CN formation at first stages in the laser-induced fragmentation of nitro aromatic molecules. This fact may be seen in Figure 4.5, where a close-up in the spectral region where the CN ($\Delta\upsilon$=0) appears is shown for different pressures ranges from atmospheric pressure to 10^{-5} mbar during the laser excitation of TNT at a fluence of 3 J/cm^2. The significant presence of N_2 in the surrounding atmosphere is clearly responsible of the formation of CN up to certain base pressure.

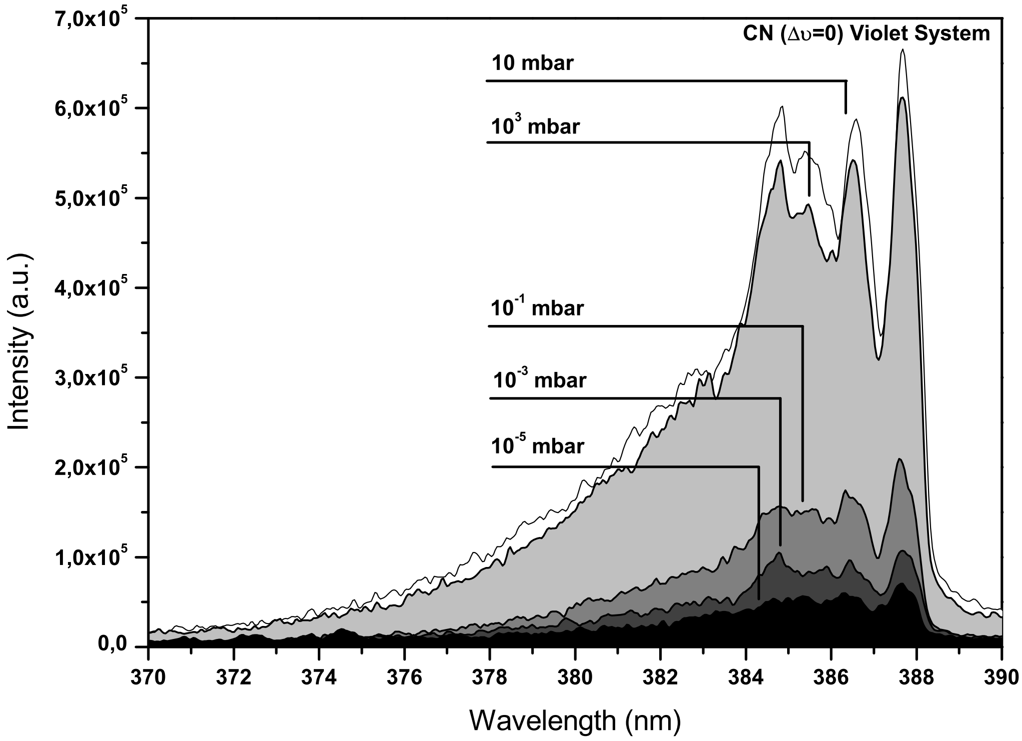

Figure 4.5. Detail of the CN emission spectra at different base pressures with 266 nm laser pulses at fluence of 3 J/cm^2.

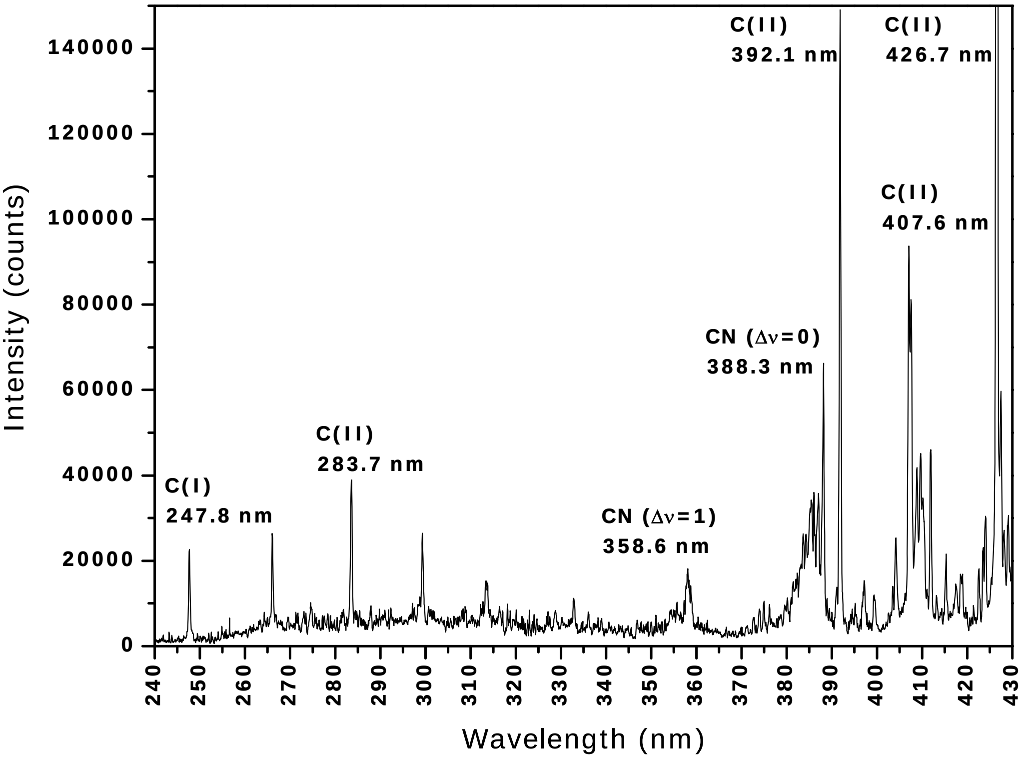

Figure 4.6. UV wavelength region of LIBS TNT spectrum at high fluence value (10.2 J/cm^2). Gate pulse width, 10 μs; gate pulse delay, 30 ns.

However, the CN band is still observable even under high-vacuum conditions.

On the other hand, in the studied high-energetic range, resolved C(II) ionic lines appeared clearly in the emission spectra of homologous TNT series. This was the only ionic emitting species detected in the induced plasma of these nitro-aromatic compounds. Fig. 4.6 shows a detail of the low-wavelength spectral range of TNT LIBS spectrum showing C(I) atomic emission line at 247.8 nm, CN emission bands ($\Delta\upsilon$=1; $\Delta\upsilon$=0) of Violet System, and C(II) ionic emission lines at 283.7 nm, 391.9 nm, 407.6 nm besides the most intense line at 426.7 nm. Once ionization potential of atomic carbon (11.26 eV) was exceeded by laser radiation and ionic species $^{12}C^{+}$ were generated in the plume, the excitation energy of ionic carbon (20.95 eV) can be achieved as increasing the irradiance level applied on the sample sufficiently, resulting in the subsequent ionic emission after relaxation.

Once more, we found out a very low fluence threshold for mass signal $^{12}C^{+}$ and a higher onset for C(I) atomic emission at 247.8 nm. All the signal intensities increased with fluence accordingly. However, as can be observed, when fluence value increases up to 6 J/cm^2, intensity of $^{12}C^{+}$ mass signal reaches a plateau and peak intensity stabilizes. This fact is probably due to further energy increase causes a decay in the efficiency of ion extraction by space-charge effects in the entrance of extraction electrode and ion current saturation in the detector with the consequent widening of mass peak and loss of resolution.

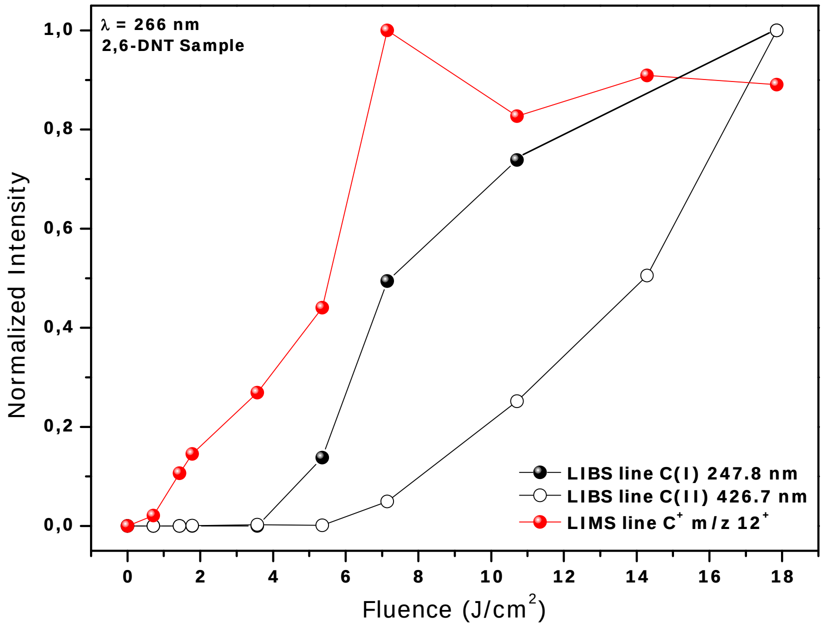

Figura 4.7. Coincidental LIMS-LIBS carbon signals versus fluence level for TNT sample. Intensities were all normalized to the maximum value.

4.6. CONCLUSIONS

In this work we have focused on the analysis of optical-mass coincidental information from solid MNT, DNT and TNT samples irradiated with UV laser pulses. These compounds presented a similar fragmentation pattern in time-of-flight mass spectra in the low-mass region and analogous features in emission LIBS spectra.

The reported fluence parameterization showed the evolution of the main optical-mass signals in the acquired spectra for a limited energetic range, showing the different stages of lifetime of plasma: the rising thresholds and extinction of the different atomic and molecular studied species, besides the breakage of the aromatic ring and the later excitation of ionic species at higher fluence level. This general behaviour recurred for all compounds of the homologous TNT series.

A good agreement between the trends of the emission and mass atomic species (H, C, N and O) was found out, indicating a high correlation between both processes in the time and energetic scales. As for molecular species, the observed trends were different for diatomic ion signals and emission of molecular bands mainly due to differences in the energetic regime of excitation and ionization processes.

Further work will focus on the coincidental analysis of different organic energetic compounds with a new configuration for mass spectrometer that leads the change of polarity in electrodes and therefore, the detection of both positive and negative ions in order to widen the coincidental study.

CHAPTER 5

Discrimination of Dinitrotoluene Isomers in Condensed Phase by Laser Ionization Time-of-Flight Mass Spectrometry and Laser-Induced Breakdown Spectroscopy

5.1. SUMMARY

The ability of laser ionization time-of-flight mass spectrometry (LI-TOFMS) together with laser-induced breakdown spectroscopy (LIBS) as a combined analytical system for ion-photon detection to establish discrimination criteria between dinitrotoluene isomers is demonstrated in the present work. Direct analysis on condensed samples were performed in high vacuum environment using a nanosecond pulsed Nd:YAG laser at 266 nm, and differences on spectral features of the compounds were studied. Results were in keeping with the relative internal energy values of the different DNT isomers for the optimized structures since 2,4-DNT (the most stable isomer) presented a lower fragmentation degree in mass spectrum and lower intensity levels for atomic emission species in LIBS measurements. Moreover, LIBS analysis was also carried out in air, and changes in the relative intensities of emitting species in the plume were further discussed.

5.2. INTRODUCTION

Trace detection of explosives and other hazardous chemicals has represented a field of considerable interest for environmental and analytical chemistry. Concretely, the use of analytic techniques based on laser ablation and ionization has demonstrated its abilities in this subject **[Mullen, C. et al., 2006 B][Martin, A. N. et al., 2007][Moore, D. S. et al., 2007][Gottfried, J. L. et al., 2008][Sheaff, C. N. et al., 2008][Gottfried, J. L. et al., 2009][Lucena, P. et al., 2011][Garcia-Reyes, J. F. et al., 2011].** In this sense, high-power laser ablation supported by certain spectroscopic detection methods becomes a very suitable technique for direct elemental analysis of many diverse solid samples. The main advantages of laser sampling are the little or no prior sample preparation, the rapid process of analysis and the chance of carrying out *in situ* analysis **[He, J. et al., 2006]**. Laser-induced breakdown spectroscopy (LIBS) is particularly suited for the study of neutral species and atoms at different excitation levels present in the plasma plume. They are generated by the local impact of a laser beam after a rapid melting and vaporization of the material followed by complex atomization, excitation and ionization processes **[Cremers, D. A. et al., 2006].** LIBS has strong advantages in the identification task of solid explosives as multi-elemental capabilities and real-time measurements in different surroundings **[Lazic, V. et al., 2009]** and inherent simplicity. Moreover, the technique has the potential for semi-quantitative analysis which avoids the need for standard preparation and calibration curve fitting procedures **[Hang, W., 2005]**. However the technique is rarely used in quantitative approaches due to limited precision and repeatability **[Ctvrtnickova, T. et al., 2010]**. Ion detection by mass spectrometry (MS) can provide useful information about charged particles in the plume, such as ion yielding from ablated particles, cluster formation, and angular and velocity distribution of species **[Lin, Y. et al., 2010]**. The ions are normally picked out from the plasma plume applying an intense electrical field **[Yu, Q. et al., 2009]**. The combination of laser ionization and MS (laser-ionization mass spectrometry, LIMS), results in a powerful tool for multi-elemental and isotope analysis of solids with very diverse physical properties (bulk or powder samples, conductors, insulators…) **[Huang, R. et al., 2010]** thanks to its high sensitivity and precision **[Lin, Y. et al., 2010]**. LIMS uses the laser irradiance for both the ablation and ionization processes jointly in a single step leading to a complex physical process **[Lin, Y. et al., 2010][Huang, R. et al., 2009].** Moreover, an added advantage is that spectra from LIMS experiences less interferences compared to spectra from other laser ablation methods as laser ablation inductively-coupled plasma mass spectrometry (LA-ICPMS) or glow discharge mass spectrometry (GDMS) **[Huang, R. et al., 2010]**. In a typical LIMS configuration, the ionic population existing in the induced plasma is led into a time-of-flight (TOF) mass spectrometer **[Lin, Y. et al., 2010]** as it is easily coupled with a pulsed source and it offers the complete elemental composition from each laser pulse **[Yu, Q. et al., 2009]**. Therefore, LI-TOFMS has become a well accepted micro analytical technique for qualitative and semi-quantitative analysis covering many fields as metallurgy, geology and biology, including the trace detection of hazardous chemicals in environmental media **[Dale, M. J. et al., 1994][Zenobi, R. et al., 1994][Boels, U. et al., 2000][Weickhardt, C. et al., 2002][Globig, D. et al., 2003]**. Besides, its application as a tool for studies of molecular ionization is of high interest. However, the complexity of the physical processes involved in laser-induced ion formation makes difficult the absolute (standarless) quantitative analysis by this method **[Dimov, S. S. et al., 1998]**.

From mass spectrometry perspective, the generation of molecular characteristic ions is a key feature in the technique's analytical ability. Moreover, unambiguous identification of precursor ions and structure-specific ions are highly desired as they are characteristic of the analyte molecules and necessary for component identification in mixtures. However, the presence of labile molecular substituents presents a critical issue to the analytical mass spectrometrist: rapid molecular dissociation of the analyte resulting in fragmentation to non-specific low mass ions and this can mean the unambiguous identification of the component analyte in the mass spectra.

According to this, the good choice of values for parameters of laser source (e.g. pulse duration, wavelength and energy level) and a correct control over them becomes a very important key in order to adjust the condition of ionization source. The dependence of laser ablation process with the laser wavelength has been extensively studied. It is generally accepted that the shorter wavelength the lower irradiance (or power of radiation per area unit) is needed to initiate the ablation of the material, and in the same way higher laser absorption, ablation rate, surface temperature, and evaporation rate are caused by lower wavelengths **[Huang, R. et al., 2009]**. On the other hand, plasma absorption is more efficient at longer wavelengths indicating intense interactions occurring between the laser beam and the expanding plume, which results in a higher breakdown extent of the molecule and larger ionization fraction in the plume **[Huang, R. et al., 2009]**.

Nitrotoluenes represent a group of nitro compounds with high energetic content used as precursors to the production of TNT, the most widely used military explosive. They also have application as intermediates for dyes and pharmaceutical manufacture. In appropriate energetic conditions, nitrotoluenes experience easy fragmentation so they are ideal molecules for dissociation pathways studies **[Kosmidis, C. et al., 1994][Bhasu, V. C. J. et al., 1996][McMillen, D. F. et al., 1997][Tönnies, K. et al., 2001][Hankin, S. M. et al., 2002][Tanaka, G. et al., 2008][Mullen, C. et al., 2009][Sovová, K. et al., 2010]**. To date, little research on the discrimination of this type of analyte in condensed phase by means of laser ablation techniques has been carried out, even with the analytical techniques proposed in this work. However, results have proved this combined analytical system becomes a good choice for fine identification analysis and provides a direct and rapid method to discriminate organic compounds differing only in the structural arrangement of the molecules.

In the present work, three dinitrotoluene isomers were selected with the aim of proving the capabilities of laser-plasma based direct analysis techniques as LIMS and LIBS for isomers identification. Under plasma formation fluence regime, the information generated is mostly restricted to atoms or small molecular fragments making complex the direct identification of isomers. Under strict control of experimental variables (mainly the laser fluence) it is possible to find conditions where the information provided allows the discrimination between isomers. The differences in the optical or mass spectrum are in accordance with the variations in internal energy of each isomer due to the relative position of the substituents in the aromatic ring.

5.3. EXPERIMENTAL

A combined analytical system (LIMS/LIBS) for simultaneous ion-photon detection was developed. A schematic view of the system is shown in Fig. 2.17, and the most relevant conditions used are summarized in Table 5.1. The system was equipped with a 3D stage for fine control of the position of the samples inside the analysis chamber. They were introduced into the ionization chamber by means of a direct insertion probe orthogonal to both ions extraction and light collection axis and facing the incident laser. They were irradiated at λ 266 nm with a 4.4 ns width pulse from a Nd:YAG laser (*Quantel, Mod. Brio*) and focused on the sample surface by means of a quartz lens with a focal length of 200 mm. The UV excitation allows gentle fragmentation of the molecule and lower thermal effects. Laser pulse energy was controlled using a variable attenuator that allowed continuous variation of the energy without modifications in the beam spatial profile. A differential pumping geometry did allow keeping the detector operating at pressures better than 10^{-6} mbar while the analysis chamber was at pressures as high as $1.0\cdot10^{-4}$ mbar. This fact was especially advantageous as the samples did exhibit high degassing rates.

The time-of-flight spectrometer was acquired from a commercial manufacturer (*R. M. Jordan Company*, Mountain View, CA, USA), but modifications of ion optics, feed troughs and sample inlets were lab-made. The ionization chamber was capable of hosting the pumping system, view ports, and additional electrical devices **[García, C. C. et al., 2001].** The atoms and molecular fragments desorbed from the solid sample and transformed into ions were accelerated by an electric field, orthogonally extracted to the reflectron flight-tube spectrometer and detected by a MCP detector. LIMS analysis was performed at variable extraction conditions (width and delay of extraction pulse) depending on the mass spectral information was required to visualize.

Optical emission from the sample was collected by an optical fibre external to the vacuum chamber connected to the entrance slit of a spectrograph (*SR-500i-D1, Andor*), equipped with an intensified CCD detector (*iStar, Andor*). The collection geometry was also orthogonal to the plume expansion direction. A dispersion grating of 599 lines/mm was used for the acquisition of time-integrated plasma spectra.

Table 5.1. Selected values for experimental parameters in coincidental analysis at high vacuum regime.

Mass signal acquisition	
Extraction pulse width (ns)	400/800
Extraction pulse delay (ns)	0/500
Extraction voltage (V)	-1260
Chamber pressure (mb)	$< 1.0\cdot10^{-4}$
Emission signal acquisition	
Gate pulse width (ns)	1000
Gate pulse delay (ns)	50
MCP Gain	150
Collection geometry	orthogonal
Laser operation	
Wavelength (nm)	266 nm
Repetition rate (Hz)	4 Hz
Energy (mJ)	0.5-6.0
Pulse width (ns)	4.4 ns

Samples were moved during analysis with the micrometer stage in order to expose a new fresh target surface after each laser shot. Emission intensity was measured in the band heads of detected signals from molecular species whereas in the case of emission lines from atomic and ionic species, the peak intensities were taken for the study. In both cases net (background subtracted) signals were considered.

5.4. SAMPLES

Three different isomers (2,3-DNT, 2,4-DNT and 2,6-DNT) were acquired from *Sigma-Aldrich* (Madrid, Spain) in the form of yellowish powders. The energetic nitro compounds were prepared following the same procedure for all the samples: equal mass of material was weighed (0.4 g) and ground in an agate mortar. The resultant powder was pressed (2.5 tons during 15 minutes) with a hydraulic press. The resulting pellets (10 mm in diameter and 2 mm in thickness) were fixed onto a sample holder and then introduced into the ionization chamber for subsequent analysis.

5.5. RESULTS AND DISCUSSION

5.5.1. Features of coincidental spectra

Initially, the most suitable values for each studied experimental parameter of both analytical techniques were selected. Extraction conditions in LIMS were adjusted to obtain the best mass information achievable by our instrument. For LIBS, collection and acquisition variables were selected in order to get an optimum optical emission signal. Fixed values for experimental variables are summarized in Table 5.1. Parameterization of energy doses per pulse was performed to study the influence of fluence level on desorption and ionization processes and on breakdown behaviour of the samples. The fluence thresholds of both ionization and optical emission were found similar for each of studied isomers. In the case of LIMS signal, the criterion taken as valid to set fluence threshold was the minimum fluence value for which signal-to-noise ratio of NO^+ ion was higher than 3 units. This fragment was taken as reference since it becomes a characteristic ion that appears early in the ionization of the molecule from the fast ionization of the neutral fragment. Moreover, in the case of LIBS signal, the value taken as fluence threshold was the minimum fluence value for which it was possible the observation of characteristic molecular emission bands with signal-to-noise ratio higher than 3 units.

The calculated fluence range of studied DNT isomers was 0.8-1 J/cm^2 for ionization threshold whereas in the case of emission threshold the value was between 1.8-2.0 J/cm^2. These fluence values directly depended on the laser parameters and on the temporal conditions of signal acquisition. However, in order to record spectra of enough quality, the excitation conditions had to be increased way over the threshold values.

Coincident ion-photon detection was applied using the combined analytical system for simultaneous monitoring LIBS and LIMS spectra in order to obtain different but additional qualitative information from the same event.

Figure 5.1 shows two pairs of coincidental spectra obtained at different energetic conditions for 2,3-DNT: 2.4 J/cm^2 (1.5 mJ/pulse) (a) and 9.7 J/cm^2 (6.0 mJ/pulse) (b), respectively. Spectra in Fig. 5.1(a) were acquired with the most favourable energetic condition to get atomic and molecular mass information from the molecule. The ion fragments were the result of direct ionization after coming off the aromatic molecule, or could occur through indirect pathways as recombination. Thus, signals from the low mass range (as the atomic ion $^{12}C^+$) to the characteristic molecular ion at $^{182}M^+$ were recorded. A complete series of fragments corresponding to the substituents groups coming off the ring and typical dissociation products of alkylated benzenes $(C_mH_n)^+$ as a result of the ladder climbing process were also observed. Moreover, the characteristic fragment m/z 165$^+$ for DNT isomers, which corresponds to the loss of a hydroxyl group formed by the hydrogen transfer mechanism (the well-known *ortho-effect,* distinctive in the decomposition of ortho-substituted nitrobenzenes) **[Jyothi, V. C. et al., 1996]** (see scheme of Figure 3.6 in Chapter 3) is clearly monitored. All these characteristic peaks are found in the electron ionization libraries of this compound, suitable for identification. However, some of the main peaks in LIMS spectra (namely, 98$^+$, 110$^+$, 122$^+$ and 134$^+$ ions) are not found in the EI spectrum (Figure 5.2), so it suggests other routes of fragmentation and recombination in the molecular ionization. Those fragments most probably correspond to hydrocarbon chains after the breakage of benzene ring that retain a NO_2 group in first nanosecond of desorption/ionization process. In such energetic and pressure conditions, these intermediate species are stable and they are captured by the extraction electrode. The observed fragmentation pattern was quite similar for all the three isomers although slight differences were observable and discussed below. On the other hand, simultaneous LIBS spectra acquired with 2.4 J/cm^2 laser pulses exhibited very low signal intensity and only main molecular bands from emission of C_2 and CN fragments with low signal-to-noise ratio were observed.

According to Figure 5.1(b), when laser pulses with a relatively high energy were used, the signal-to-noise ratio in LIBS increased since a marked enhancement of signal intensity was observed. Concretely, selecting pulses of 9.7 J/cm^2 as optimum, typical atomic and molecular emissions are clearly observed in emission spectra. Main atomic emission lines were identified as C(I) (247.8 nm and 2nd order at 495.7 nm), C(II) (426.4 nm), H(I) (H_γ 434.0, H_β 486.1 and H_α 656.3 nm), O(I) (777.2, 777.4 and 844.6 nm) and N(I) (742.4, 744.2, 746.8, 821.6, 822.3 and 868.1 nm). Peaks corresponding to H_α and O(I) at 777.4 nm besides C(II) ionic emission line at 426.4 nm, dominated the broadband spectrum. The presence of CN Violet System and C_2 Swan System emission bands suggested the formation of excited molecular fragments by means of two possible pathways: direct fragmentation of the parent molecule and different recombination routes from C and N atoms in the plume **[Lucena, P. et al., 2011]**.

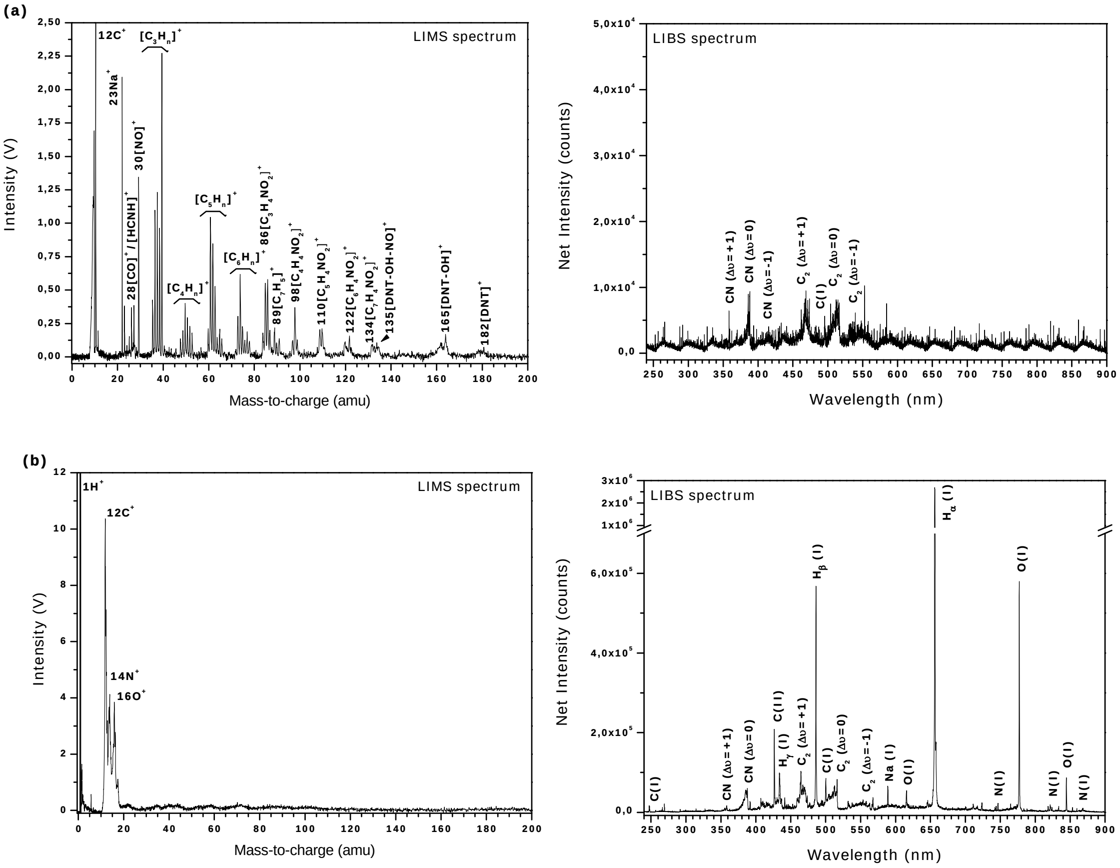

Figure 5.1. Coincidental LIMS-LIBS spectra obtained for 2,3-DNT using 266nm UV radiation. Measurements were performed at vacuum pressure using (a) low fluence condition (2.4 J/cm^2) (b) high fluence condition (9.7 J/cm^2).

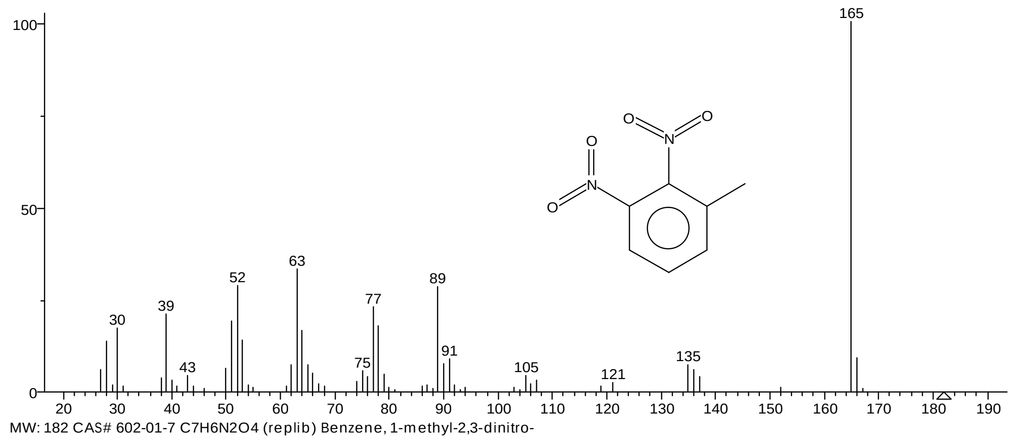

Figure 5.2. Electron Impact Spectrum of 2,3-DNT molecule from NIST data base.

Under these high energy conditions (where LIBS emission is optimum), the simultaneous acquired mass spectrum confirmed the total atomization of the compound. It is important stressing out the negative effect of an excess of dispersion in the initial kinetic energy of the generated ions by LIMS. Thus, under plasma formation conditions, the mass spectra worsen significantly their mass resolution. Only the four atomic species forming the organic compound appeared in the mass spectrum (H^+, C^+, N^+ and O^+) with significant increase in signal intensity but with deteriorated resolution owing to the space-charge effect in high density plasma in a given space and the differences in the distribution of ion velocities inside the plasma.

5.5.2. LIMS/LIBS comparative study

Figure 5.3(a) shows the low-mass region of LIMS spectra for the three analyzed DNT isomers acquired in suitable extraction conditions to get the maximum peak resolution. The fixed value for fluence was 2.4 J/cm^2. Ion signals corresponding to the diatomic fragments $^{24}C^+$ and $^{30}NO^+$, and signals related to $C_nH_m^+$ hydrocarbon fragments were clearly observed. The low-mass ions series for aromatic compounds are not restricted to specific m/z values, but they are, however, consistent enough to be helpful for identification of compounds with aromatic rings. Finally, the presence of atomic $^{12}C^+$ signal evidenced that complete fragmentation of chain is already possible in the soft imposed energetic regime. It was noticed that in the case of the 2,4-DNT isomer, the spectrum registered lower signal intensity for the main peaks as can be also extracted from Figure 5.3(b) in which variation bars are included.

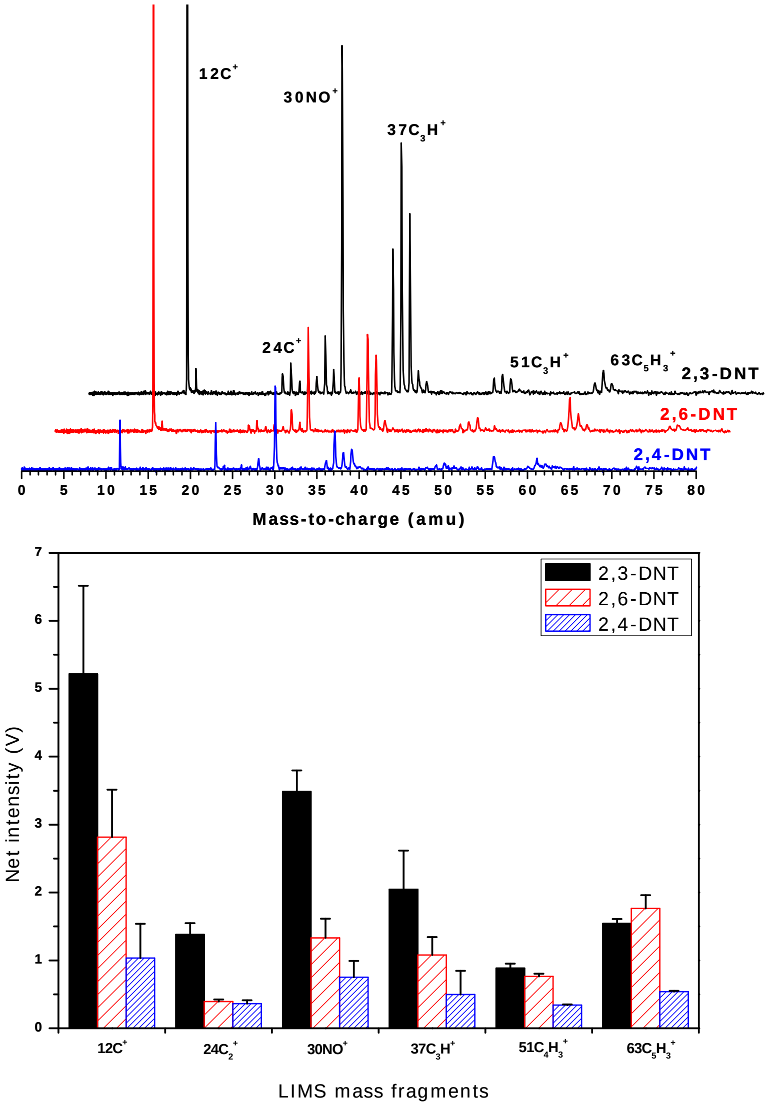

Figure 5.3. (a) LI-TOFMS spectra of low-mass range for analyzed DNT isomers. (b) Peak intensities for the main low-mass fragments in LI-TOFMS spectra of DNT isomers. Peak signals at m/z 24, 51 and 63 are scaled x5 for better comparison. Fluence value, 2.4 J/cm^2. Accumulation of 100 acquisitions.

Table 5.2. Relative energy values for DNT isomers. The most symmetric isomer, 3,5-DNT, was taken as reference level. [Tanaka, G. et al., 2008].

Isomer	**3,5-DNT**	**2,4-DNT**	**2,6-DNT**	**2,3-DNT**
Structure	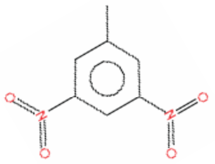	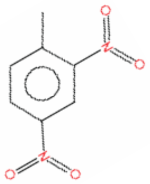	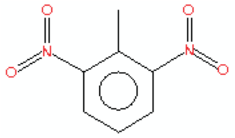	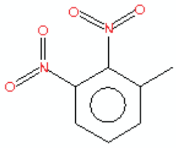
Energy (Kcal/mol)	0	2.399	7.373	10.674

The results indicated that this isomer exhibited a weaker fragmentation and thus the abundance of fragments and atomic species was lower. On the contrary, 2,3-DNT showed the most intense signal for ions up to m/z 51^+, and from that point forward, the intensities were comparable to those obtained for 2,6-DNT isomer. This information is in concordance with the relative energy values of the different DNT isomers for the optimized structures showed in Table 5.2 and related to the molecular stability derived from the relative position of their substituents. These relative energy values were assigned by Tanaka *et al.* using density functional theory (B3LYP) with the 6-31G(d) basis set that can predict the energetics of large molecular systems to within a few kcal/mol **[Tanaka, G. et al., 2008]**. With the exception of 3,5-DNT (0 kcal/mol, energy reference level), the most symmetric and coplanar isomer which does not contain a nitro group in an ortho position to the methyl group, 2,4-DNT is the next more stable isomer since one NO_2 group is also isolated from the methyl group on the benzene ring. In contrast, 2,6-DNT and 2,3-DNT own all three groups next to each other so they are the least symmetric isomers, and the most unstable ones. Due to such peculiarity, 3,5-DNT isomer (not analyzed here) can be identified easily by comparison from its LIMS spectrum owing to the lower intensity of m/z 165^+ fragment corresponding to the OH-loss since the ortho reaction occurs in a very low rate **[Tönnies, C. et al., 2001]**.

In addition to the study of mass spectra in the low m/z range, the experimental conditions were again optimized in order to acquire complete mass spectra of DNT isomers. Results are showed in Figure 5.4. Spectra are qualitatively similar among them, but it is observed how parent ion (m/z 182^+) was just visible for 2,3-DNT and 2,6-DNT, and very weakly or even absent in the case of 2,4-DNT, presenting this latter a poorer fragmentation due to the absence of several characteristic ionic species between m/z 98^+ and m/z 165^+ signals.

In the case of 2,3-DNT isomer, fragments corresponding to OH-loss (m/z 165^+) and the simultaneous OH- and NO-loss (m/z 135^+) own the highest intensities in the high m/z range of spectrum. Regarding 2,6-DNT, a peak corresponding to the loss of two OH- groups (m/z 148^+) becomes visible and it is not observable in the rest of isomers. This seems to be in agreement with the position of the substituents in the molecule due to both nitro groups are flanking the methyl group. Moreover, it also presented very intense signals at m/z 135^+ and m/z 165^+ as it was expected. Finally, and as commented before, the above fragments are weakly or no detected in the ionization of 2,4-DNT with the exception of m/z 165^+. A summary of intensities for these high-mass fragments is presented in Figure 5.5.

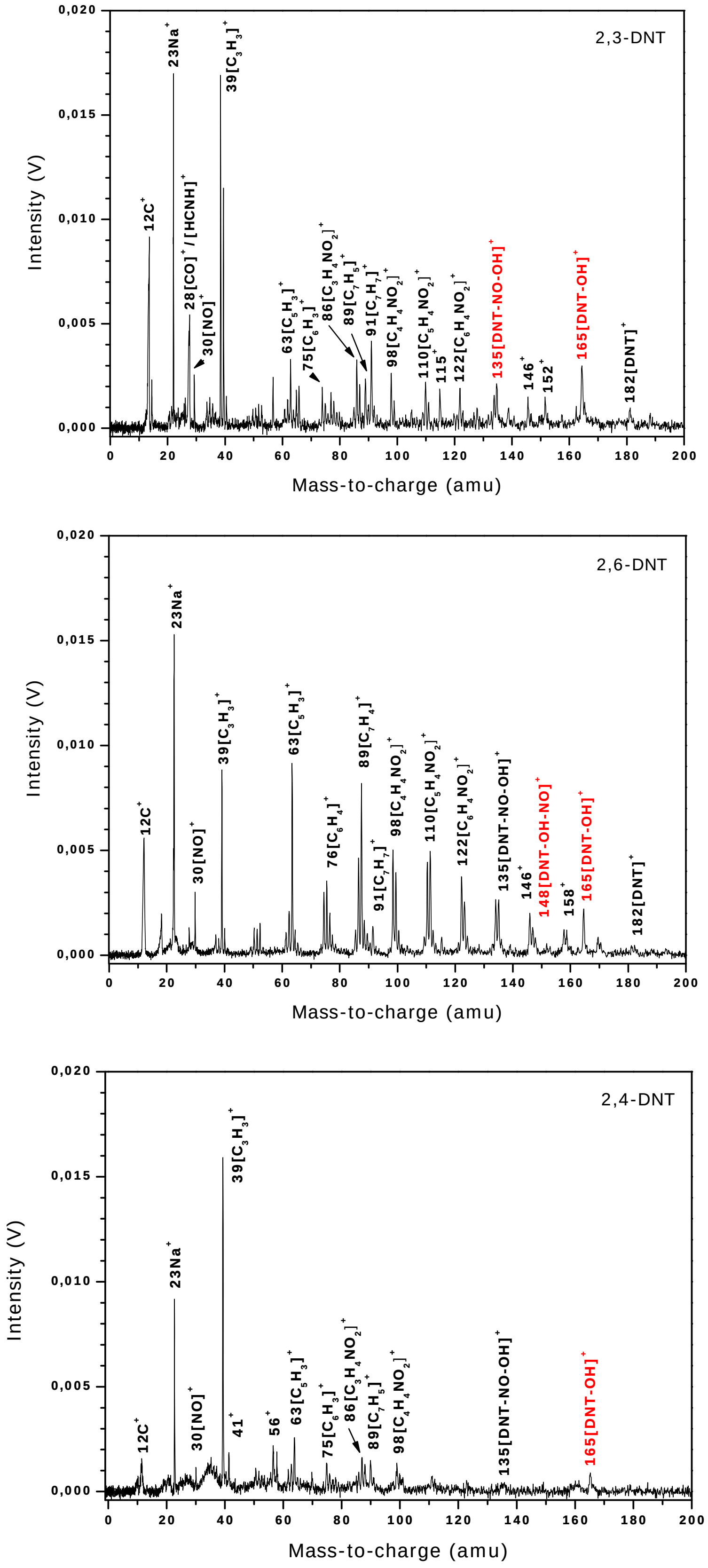

Figure 5.4. LIMS spectra of dinitrotoluene isomers obtained after ionization with nanosecond 266 laser radiation. Average 100 pulses. Fluence value, 2.4 J/cm^2. Delay in extraction, 500 ns.

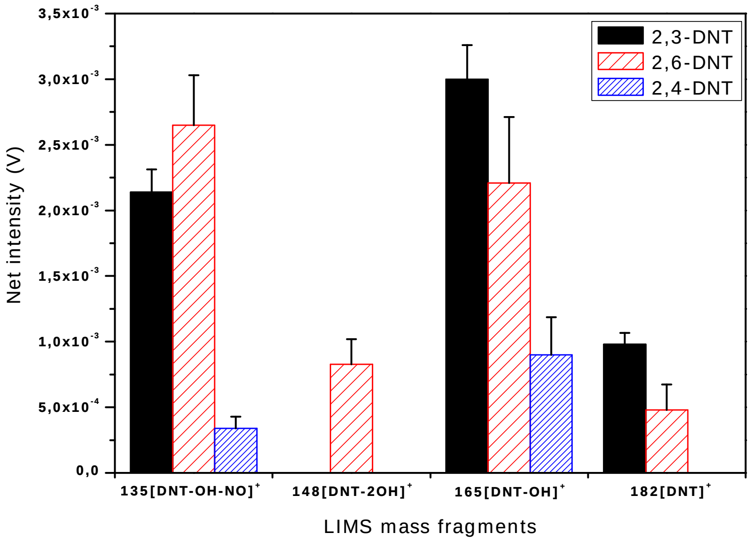

Figure 5.5. Peak intensities for the main high-mass fragments in LI-TOFMS spectra of DNT isomers. Fluence value, 2.4 J/cm^2. Accumulation of 100 acquisitions.

Thus, LIMS spectra of DNT isomers obtained from the direct ionization of sample in condensed phase have showed characteristic features so discrimination may be possible by the analysis of individual ionic signals. However, in order to support the discrimination study, an additional analysis using optical emission spectroscopy was performed.

Figure 5.6.(a) shows the net optical emission intensities for DNT isomers at high vacuum regime. The result was in good agreement with that obtained from LIMS analysis since weak atomic emission was observed for 2,4-DNT compared to that obtained for the other isomers investigated under the same energy regime, so a less atomization degree of 2,4-isomer is deduced from such result. Moreover, it is observed that 2,6-DNT and 2,3-DNT isomers are indistinguishable due to intensities of every species are similar. In addition to differences on net emission intensity of atomic lines, divergence in emission intensity of molecular bands was also found at high vacuum regime. The bands exhibited higher intensities for this isomer compared to results for 2,3-DNT and 2,6-DNT. Again this altered behaviour could be related to the spatial configuration of the molecule as well as changes in the kinetic of fragmentation and recombination of species within the plasma.

When LIBS analysis was performed at atmospheric pressure with the presence of air molecules in the surrounding of sample surface, relative intensities of emission species in the spectrum experienced significant modifications. Thus, molecular emission notably increased for all the isomers whereas atomic emission markedly

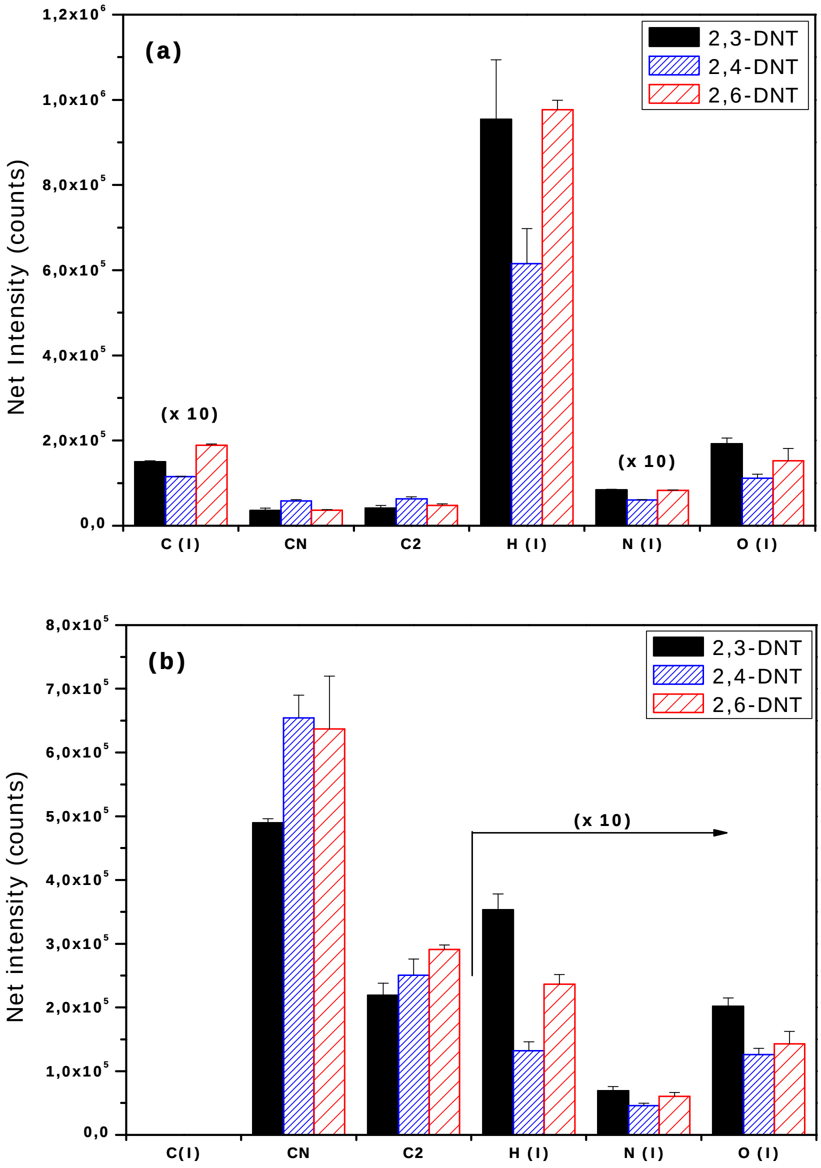

Figure 5.6. LIBS intensities for the most significant emission signals manifested in emission spectra from DNT isomers acquired with a fluence of 9.7 J/cm^2 (a) at high vacuum regime, (b) in air at atmospheric pressure.

decreased as can be observed in Fig. 5.6(b). Changes in the kinetics of plasma are induced by the increase of background pressure. Presence of air makes difficult the advance of the plume and it works as a retaining barrier that implies the confinement of plasma and therefore, a marked increase in collisions rate **[Yalçin, S. et al., 2004].** That resulted in variation of plasma properties (temperature, electron density…) and the appearance of shielding effect that avoids part of laser energy achieves the sample surface. As a result, modifications in the ablation process and plasma expansion implied notable variations in the relative intensities of emission species compared to vacuum trials. Once more 2,4-isomer presented lower atomic emission than the other isomers and, at the same time, very high molecular emission with intensities comparable to those for 2,3 and 2,6 isomers when they were irradiated at atmospheric pressure. Thus, 2,4-DNT atomic emission corresponding to H(I), N(I) and O(I) species was the lowest of three isomers, and C(I) line was even not detected in this case like many other ionic and atomic signals.

On the other hand, as can be inferred from the Figure 5.6(b), atomic emission was significantly higher in the case of 2,3-DNT while the molecular emission was visibly lower compared to the other isomers. All these features are probably related once more to the total internal energy of the molecules and its subsequent degree of stability as commented above.

In order to obtain a better comparison that allows us the univocal identification of DTN isomers from LIBS analysis, we plotted the intensity ratios between molecular and atomic signals from emission spectra acquired in both vacuum and atmospheric regimes. Results are illustrated in Figure 5.7. Shown net intensities are the addition of intensity values of the main atomic species (C, H, O and N) and the main molecular species (CN and C_2) in emission spectra. Resulting ratio for each isomer will give us univocal information about the analyzed molecule. In the case of 2,4-DNT in vacuum,

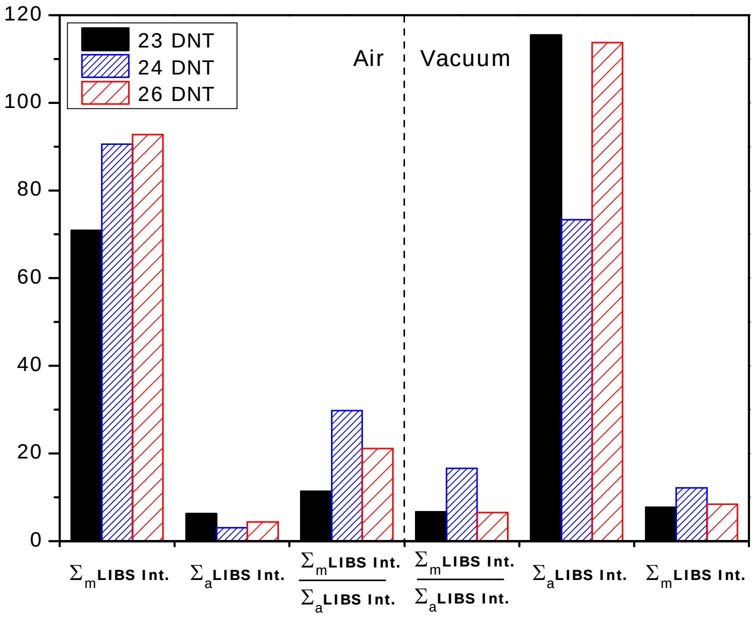

Figure 5.7. LIBS ratios from atomic and molecular emission signals of DNT isomers taken at atmospheric and vacuum pressure. Showed net intensities were divided by a 10^4 factor for a better visualization.

the molecular/atomic ratio was more than double compared to those for the other isomers, so this factor can be taken as criteria for its discrimination. The distinction between 2,3-DNT and 2,6-DNT isomers is possible only turning to the ratio calculated in atmospheric pressure. As can be noticed in the Figure 5.7, value of ratio for 2,6-DNT is twice of value of ratio for 2,3-DNT.

This kind of measurement constitutes a reference parameter to the identification and discrimination of certain organic compounds in LIBS analysis.

5.6. CONCLUSIONS

Laser ionization time-of-flight mass spectrometry (LI-TOFMS) and laser-induced breakdown spectroscopy (LIBS) have been applied to the identification of different solid-phase dinitrotoluene isomers. Our results demonstrate the relationship between the internal energy of the different isomers and the information obtained from optical and mass signals. Therefore, the capability of LIMS together with LIBS to discriminate between isomers from the analysis of the associated spectra has been demonstrated.

As a result, the statistical analysis of obtained spectral information could be taken as reference discrimination criteria for organic nitro aromatic isomers. Thus, a combination of both detection probes will be able to identify uniquely the isomeric compounds by means of an algorithm developed with coincidental information of each organic compound provided by this type of studies, but further optimization work is required before applying the approach in real case scenarios.

CHAPTER 6

Pathways for Production of Emitting Species in the Laser-Induced Plasma of Organic Explosives

6.1. SUMMARY

The influence of the surrounding ambient on the generation pathways and the kinetics of excited atomic and molecular species from high energetic nitro compounds has been studied. Two energetic molecules, TNT and PETN, were analyzed by LIBS at different pressure levels in diverse gas environments (air, N_2 and H_2). The study was completed with coincidental detection at high vacuum of both the optical emission and the mass spectra originated from the same laser event. For that purpose, samples were irradiated with UV laser pulses to generate ions and excited species that were simultaneously detected by means of a reflectron time-of-flight mass spectrometer and a gated intensified CCD, respectively.

Results from obtained emission spectra for different atmospheres have verified that pressure becomes a decisive parameter in LIBS trials affecting the kinetics and chemical composition of the plume. The evolution of the main atomic and molecular emitting species inside the plasma with the variation of pressure has been followed and possible and preferential reactions in fragmentation pathways have been suggested. Moreover, further examination of the data showed that the information offered by both techniques were complementary.

6.2. INTRODUCTION

The combination of experimental flexibility, contact-free analysis, real-time and time-resolved information with the multiplicity of analysis modes (point, scanning, depth profiling and imaging), turns laser induced breakdown spectroscopy (LIBS) the method of choice for many applications on the direct analysis of solid metal and non-metal samples **[Baudelet, M. et al., 2006 A][Osticioli, I. et al., 2008][Rodriguez-Celis, E. M. et al., 2008][Gondal, M. A. et al., 2009][Gottfried, J. L. et al., 2009][Gaudiuso, R. et al., 2010][De Lucia, F. C. et al., 2011][Vadillo, J. M. et al., 2004][Fortes, F. J. et al., 2013]**.

Laser-matter interaction is based on thermal and photochemical processes where, as a consequence of the laser impact and depending on the final energy quantity reaching the sample surface, different phenomena will occur both at the microscopic and macroscopic scale. While at low irradiance, heating and melting at the surface followed by a soft desorption and ionization are the main sequential events, the high irradiance regime is dominated by evaporation of the material and an extensive fragmentation with the final formation of a expanding plasma cloud **[Vertes, A. et al., 1989]**.

Extraction of additional information other than atomic abundance from LIBS spectra has been a clear trend in recent years, and many strategies leading to bring isotopic and molecular information while keeping the inherent experimental flexibility of LIBS are described in the literature. The possibility of performing isotopically-resolved characterization of solid samples has been demonstrated in the past **[Smith, C. A. et al., 2002]** and it is currently under continuous development **[Russo, R. E. et al., 2011][Mao, X. et al., 2011 A][Mao, X. et al., 2011 B][Cremers, D. A. et al., 2012].** On the other hand, the molecular information included in the emission spectra is of interest in the identification of organic compounds. This molecular information is basically restricted to the presence of molecular bands from diatomic species emitting in the laser-induced plasma.

The origin of molecular emissions in LIBS is of special interest as their spectral signatures are used for identification purposes in organic analysis. Considering the high pressure and electron temperature typically associated to laser plasmas and the presence of a surrounding gas (typically air), the observed spectra will be a convolution of emissions from primary reactions (fragmentation taking place after laser excitation), and from secondary reactions occurring in the plume **[Lucena, P. et al., 2011]**. Thus, it is important to establish the relative weight of the primary and secondary reactions and their variations with the experimental conditions, particularly when the analyzed compounds include C, N, O and H in their structures.

The analysis of energetic compounds has been always an interesting task due to the chemistry associated to their internal energy **[Adams, G. F. et al., 1992]**. Thermal decomposition mechanisms are fundamentally important in the explosives field, and the determination of the kinetics and mechanism involved in the breakdown process remains a fundamental aspect of their characterization **[Cohen, R. et al., 2007]**. Furthermore, the detection of explosive residues represents an active field in LIBS, where it has become a very useful and suitable forensic tool **[Mullen, C. et al., 2006 B][Gottfried, J. L. et al., 2008][Gottfried, J. L. et al., 2009][Moros, J. et al., 2010 A].**

The reason of the trend observed implies the consideration of the different phenomena taking place during laser-matter interaction besides plasma formation and further expansion at the different vacuum conditions. In the general picture of LIBS on metals in air at atmospheric pressure, recombination mechanisms do not play a significant role in the emission of the species of interest, except in the case of metal oxides. However, in the extension of LIBS to organic compounds under reactive atmospheres, the concentration of the different components of the expanding plasma into the dense and reactive atmosphere is governed by the chemical reactions occurring during the lifetime of the plume. This fact is one of the main difficulties in the interpretation of the emission from diatomic species since their emissions can be due to native bonds as well as the recombination of atomic carbon (C) or diatomic carbon (C_2) with molecular nitrogen (N_2) in the air. This problem is not restricted to organic compounds and has been also reported for ZnO and AlO signals **[Lewis, A. L. et al., 1983][Beenen, G. J. et al., 1984]**. In non-conductive materials, the energy of nanosecond laser pulses is initially transformed into electronic excitations, although subsequent energy transfer can take a variety of forms. Above the laser plasma threshold and under atmospheric pressure conditions, the ablation products are also a convolution of primary and secondary products. As the pressure is reduced, the expansion occurs in a less dense media where the fragments generated as a consequence of ring opening or releasing of some side chains may experiment electron-induced reactions leading to generation of additional molecular or atomic fragments.

With the purpose of providing a further insight into the mechanisms involved in the fragmentation pathways and consequent formation of sub-products inside the plasma plume, a number of controlled pressure experiments have been performed in this work. Two energetic molecules including explosive nitro compounds 2,4,6-trinitrotoluene (TNT) and pentaerythritol tetranitrate (PETN) were selected for the study. Moreover, different background gases were tested in LIBS measurements (air, N_2 and H_2) in order to study the interaction of the ensuing plasma from organic compound with the established atmosphere and how the kinetics and the formation channels of excited species were affected during the plasma lifetime.

6.3. EXPERIMENTAL

A scheme of the experimental set-up is shown in Fig. 2.19 of the present document. For this study, a quadrupled Nd:YAG laser (266nm, 4.4 ns pulse width) was used to irradiate the samples located in the ionization chamber of a time-of-flight (TOF) mass spectrometer. Pressure in the chamber was monitored in the 10^{-4} to 10^{3} mbar range by a *Pirani* gauge and a *Varian* ionization gauge was used to control vacuum pressure into the time-of-flight analyzer. Buffer gases were introduced in the chamber through a needle valve. Laser pulse energy was controlled using a variable attenuator that allowed continuous variation of the energy without modifications in the beam spatial profile. The laser beam was focused on the sample surface with a 1” quartz plane-convex lens (f = 200 mm) leading to a spot size of $2.77 \cdot 10^{-4}$ cm^2. Light emitted from the plasma plume was focussed by a 3” quartz planoconvex lens (f= 150 mm) onto a quartz optical fibre placed orthogonal to the plume expansion direction and connected to the entrance slit of a 0.5 m focal length spectrograph (*SR-500i-D1, Andor*) equipped with a gated ICCD detector (*iStar, Andor*) with a wide spectral range of 115-920 nm. Spectra were recorded from 250 to 900 nm with a 599 grooves/mm diffraction grating. Under these conditions, the maximum coverage was 45 nm per acquisition window. Full spectral range acquisitions were automatically obtained by successive measurements performed over 15 overlapped spectral windows (each one consisting of 30 accumulated spectra). The sample surface was continuously refreshed to avoid bias in the data as a result of different ablation conditions. The detected emission signal from molecular species was recorded in the band heads, where the emission intensities were strongest. In the case of emission lines from atomic and ionic species, the peak intensities were taken for the study. In all cases, background was subtracted from the signal.

On the other hand, mass spectra of analyzed sample were acquired in order to obtain simultaneous and complementary information by means of a time-of-flight mass spectrometer previously showed in Figure 2.17. Thus, ion fragments from the sample were extracted and accelerated in an orthogonal geometry by means of ion lenses connected to a voltage source and then guided to the time-of-flight tube operating in the reflectron mode. During mass analysis, a minimum pressure difference of one order of magnitude was kept between the ionization chamber and the flight tube by differentially pumping. A base pressure of 10^{-6} mbar was always kept to assure safe operation of the detector, whose output was sent to a 500-MHz digital storage oscilloscope. Kinetic series of 500 mass spectra (associated to 500 laser events) were acquired for every coincidence measurement. Finally, data files were transferred to a PC for storage and subsequent data processing.

2,4,6-TNT and PETN samples were acquired from National Department of Defence and prepared by compressing bulk powders using a hydraulic press machine to obtain 10 mm diameter and 2 mm thickness pellets. The samples then were fixed onto an aluminium holder that was introduced in the ionization chamber in the final location.

6.4. RESULTS AND DISCUSSION

6.4.1. Air Atmosphere

Figure 6.1 shows a typical emission spectrum of TNT obtained by laser ablation (3.5 mJ/pulse, 12.6 J/cm^2) under identical acquisition conditions (50 ns delay time, 1 ms acquisition time) in vacuum (top) and in air at atmospheric pressure (bottom). The laser fluence was chosen to provide good signal-to-noise ratio (SNR) in the atomic lines and molecular bands with reduced sample damage. The spectra have been plotted at the same intensity axis with an offset to help in the comparison. As observed, the LIBS spectrum in air at atmospheric pressure is dominated by emissions from the C_2 Swan system and the CN Violet system with weak (if detectable) signals from atomic species. Similar results were obtained for DNT, PETN and pyrene. However, the spectrum in vacuum is dominated by atomic and ionic emissions with much lower contribution from diatomic species. Initially, the significant reduction in the CN signal in vacuum might be directly attributed to the complete removal of atmospheric N from the surrounding gas, impairing the formation of CN molecules. However this fact does not satisfactorily explains the drop of the C_2 signal, as there is no direct recombination process with air components involved in its formation. On the other hand, it might be expected a progressive reduction in the molecular signals and increasing in the atomic emissions with a continuous variation in the vacuum level.

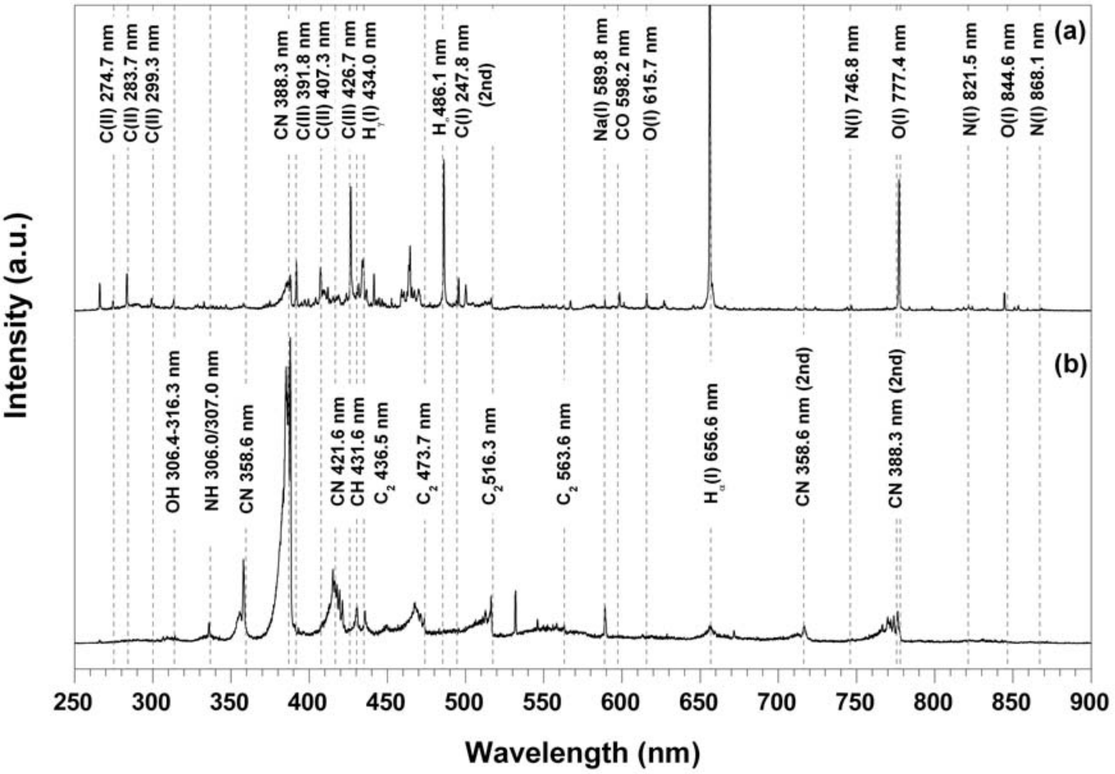

Figure 6.1. TNT LIBS broadband spectra acquired at two different pressures, (a) atmospheric pressure, (b) high vacuum regime (1.0 · 10^{-4} mb). UV pulse energy, 3.5 mJ. Fluence, 12.6 J /cm^2.

The relative abundance of the species present in the plasma under different vacuum levels exhibits a more complex behaviour. Figure 6.2 shows the net intensities of N, O, C, H, CN and C_2 for TNT as well as the corresponding LIBS spectra set normalized at their respective maximum intensity as a function of the pressure in the interval between 1000 and 10^{-4} mbar. Initially, the spectral windows for the different species were studied at 10^{-4} mbar. Once done, air was let to flow into the chamber by means of a needle valve until a desired pressure was reached. After pressure stabilization, a new set of spectra were acquired. The operation was repeated until reaching atmospheric pressure. As shown in the figures, CN and C_2 exhibit their larger intensities at the mid-high pressure range, dropping their values as soon as the pressure falls between 10 and 100 mbar. For pressure values lower than 0.1 mbar, their presence in the spectra is significantly reduced, but not completely extinguished. The presence of CN signals under high vacuum conditions may support the hypothesis of two CN contributions: one originated from the recombination of C atoms with N atoms dissociated from the organic molecule, and a second source of CN coming from the direct emission of native CN bonds, that become only noticeable under specific experimental conditions where atmospheric N has been completely removed. Some

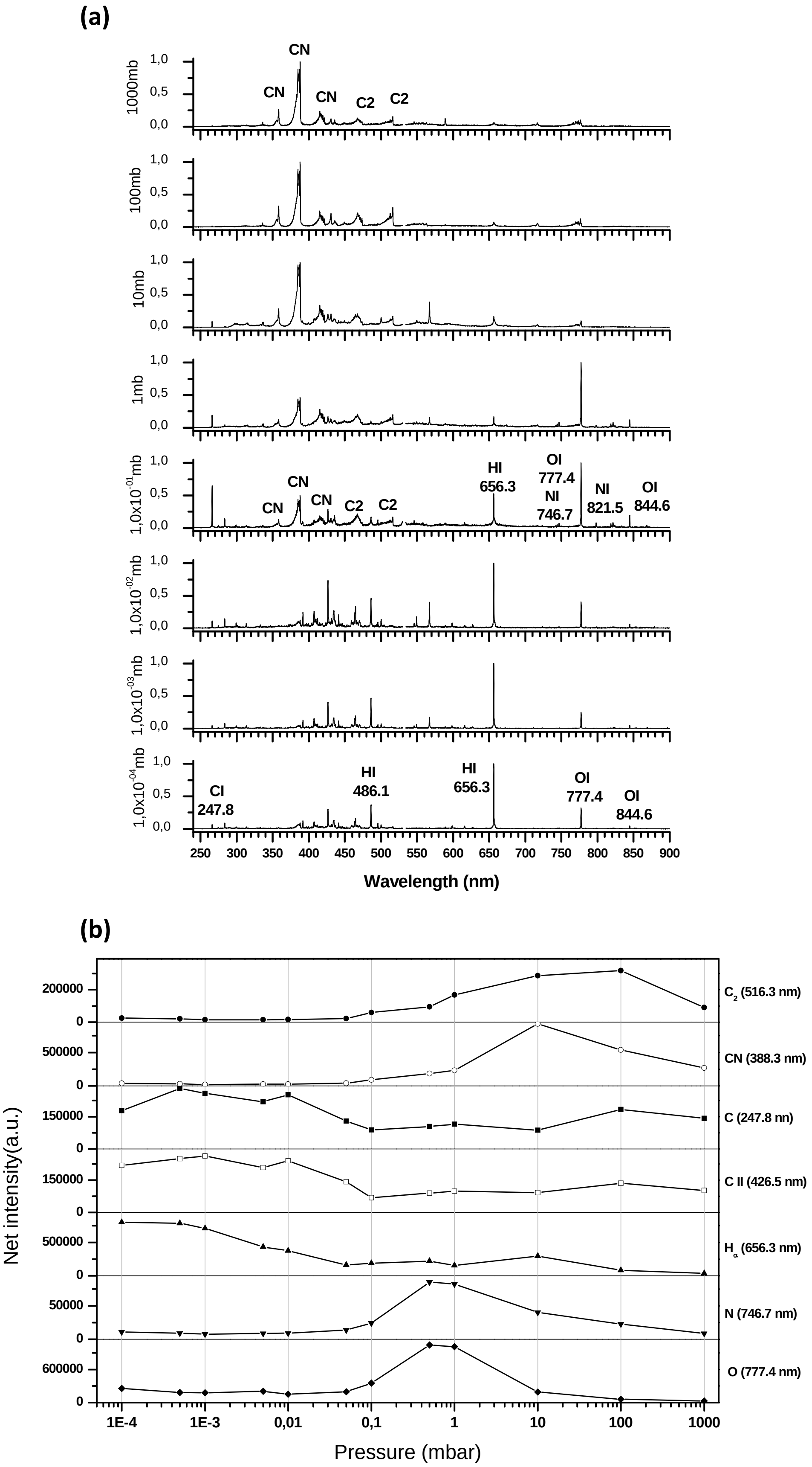

Figure 6.2. (a) Spectra set for TNT sample in the range 10^{-4} – 1000 mb. (b) Net intensities of main emitting species from respective emission spectra as a function of pressure level. UV pulse energy, 3.5 mJ. Fluence, 12.6 J /cm^2.

pathways for CN formation have been extensively reported in the literature **[Lucena, P. et al., 2011][St-Onge, L. et al., 1999][Portnov, A. et al., 2003 A][Baudelet, M. et al., 2007][Kushwaha, A. et al, 2008][Ma, Q. et al., 2011]** and can be summarized as follows:

$$C + N_2 \rightleftharpoons CN + N \tag{6.1}$$

$$C_2 + N_2 \rightleftharpoons 2CN \tag{6.2}$$

$$C_2H_n + N \rightleftharpoons CN + CH_n \tag{6.3}$$

$$[TNT] \longrightarrow nCN + mC_2 + \text{other prod.} \tag{6.4}$$

$$C + NO \rightleftharpoons CN + O \tag{6.5}$$

Besides reactions (6.1-6.3) with the intervention of nitrogen and direct molecular fragmentation (6.4), route (6.5) is probably also important in the formation of CN since NO is one of the main decomposition products of TNT **[Mullen, C. et al., 2006 B]**. The presence of C and NO in the plume has been probed by LIMS (see below) under the experimental conditions of these measurements.

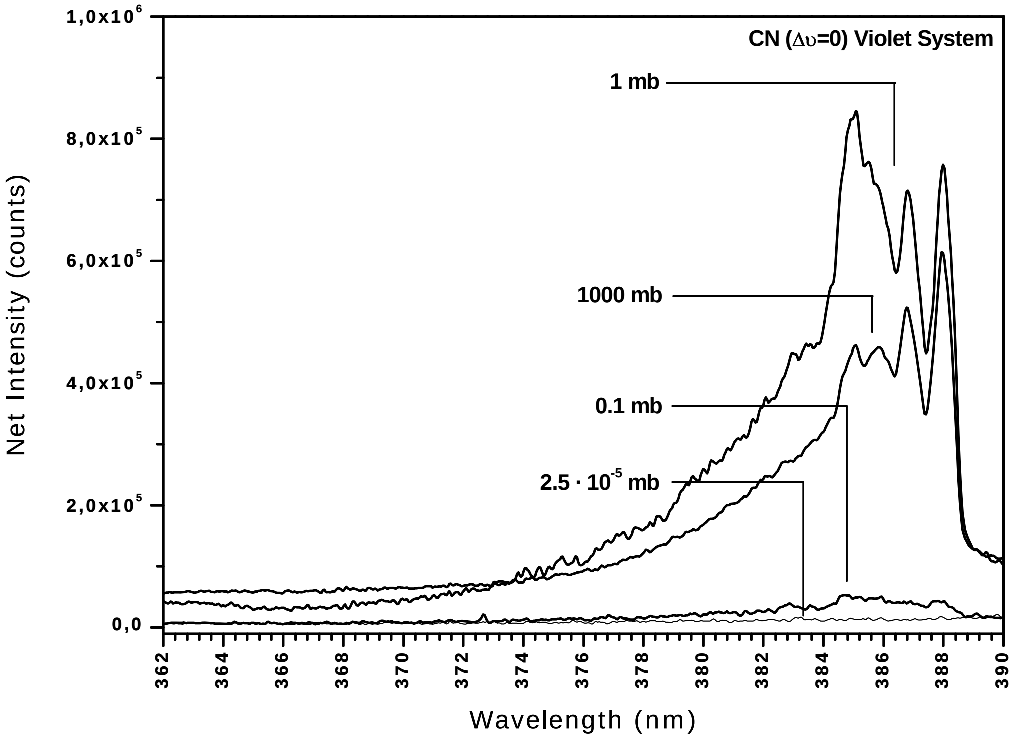

Figure 6.3. Detail of the CN emission spectra for pyrene sample at different base pressures. UV pulse energy, 3.5 mJ. Fluence, 12.6 J/cm^2.

In order to demonstrate the feasibility of reaction (6.4) in the plume chemistry of TNT, a trial with a pyrene sample was carried out. This polycyclic aromatic hydrocarbon molecule (PAH) was selected due to it does not contains nitrogen in its structure. Thus, the spectral emission of generated pyrene plasma at high vacuum pressure can elucidate suitable information on this issue. Figure 6.3 sketches the emission spectra corresponding to fundamental band ($\Delta\upsilon$=0) of CN Violet System for pyrene sample at different pressures in the interval between 1000 and $2.5 \cdot 10^{-5}$ mbar. Maximum intensity was observed at intermediate pressure of 1 mb. This experimental evidence is guessed to occur due to the presence of a significant number of N species that may interact effectively with C atoms in a non-dense medium. As long as the pressure decreases below a critic value, CN emission is reduced drastically (even disappearing completely in high vacuum conditions) due to the lack of the reactive species, unless it exists an internal source of N. Thus, we can assure with high confidence that pathway (6.4) occurs during laser ablation of TNT.

In the case of C_2 emissions, the presence of diatomic fragments with double or triple C-C bonds is required **[St-Onge, L. et al., 1999][Portnov, A. et al., 2003 B]**, and different formation pathways are also possible: either from direct fragmentation of the aromatic ring of the parent compound or from reaction between resulting hydrocarbon radicals present in the plasma **[Sovová, K. et al., 2010]**. Moreover, recombination of carbon atoms **[Zeinger, Z. et al., 2003][Kushwaha, A. et al., 2008]** besides carbon reaction with diatomic carbon species present in the hot plasma **[Ma, Q. et al., 2011]** are also possible**.** In any of the alternatives, ring opening and fragmentation is required, and reactions will be favoured only in specific plasma conditions. It is also known that any modification in the stability of the ring modifies the C_2 emission **[Portnov, A. et al., 2003].** This fact has been experimentally checked **[Moros, J. et al., unpublished results]** in the analysis of the C_2 emission in the homologous series of nitrotoluenes, where the C_2 emission decreases with the increase in the number of inductive and resonance electron-withdrawing NO_2 groups. As shown in Figure 6.2(b), C signals are very weak but detectable from atmospheric pressure to 0.1 mbar, in coincidence with the region were C_2 emission is larger. This fact could indicate that the ring has been not completely fragmented to atomic species, but to the generation of C_nH_m species, partly responsible of the C_2 emission. As long as a critical vacuum level pressure is reached, the diatomic fragments may exhibit an additional breakage, releasing C atoms that may explain the observed enhancement in their intensity at the lower pressures. At low pressure the longer lifetime of electrons in the plume would be responsible of the final atomization of the C_nH_m fragments. Direct electron impact ionization of organics by electrons released from solid surfaces or plasmas has been previously reported in photoelectron resonance capture ionization mass spectrometry **[LaFranchi, B. W. et al., 2006]** or in laser-ablation electron impact mass spectrometry **[Cheng, P. Y. et al., 1993]**. The concomitant release of H from dissociation of C_nH_m explains the increased abundance of H in the plasma with decreasing pressure noticed in Figure 6.2.

On the other hand, two-body reactions in the plume can be considered as well and may affect the presence of different species in the plasma. However, the extension of such reactions under vacuum or high pressure conditions is not clear. In principle, higher pressures should favour recombination of species as CN and C_2 that show up preferentially at pressures close to atmospheric (regardless its main source). However, at low pressures molecular emission tends to decrease. This fact can be explained by assuming that excited atomic species react with molecular species inside the plasma at high vacuum regime resulting in dissociation of such fragments. Thus, several side reactions **[Sovová, K. et al, 2010][Kruse, T. et al., 1999]** can be considered:

$$CH_n \longrightarrow CH_{n-1} + H \tag{6.6}$$

$$C_2 + H \rightleftharpoons CH + C \tag{6.7}$$

$$CH + CH \longrightarrow C_2H_2 \tag{6.8}$$

$$C_2 + O \rightleftharpoons CO + C \tag{6.9}$$

$$C_2 + NO \rightleftharpoons C_2N + O \tag{6.10}$$

$$CN + H_2 \rightleftharpoons HCN + H \tag{6.11}$$

Particularly interesting are reactions (6.7), (6.9) and (6.10), as seed the possibility of extinction of C_2 from the plasma by reaction with H, O, and NO, respectively. These reactions might be partially responsible of the absence of C_2 emissions observed in vacuum. The large abundance under vacuum conditions of H(I) and O(I), besides $^{30}NO^+$ species, may displace the reactions towards the formation of the products. In agreement with this fact is the presence of $^{13}CH^+$, $^{28}CO^+$ and $^{38}C_2N^+$ species observed in mass spectrum (Figure 6.4, bottom). An internal source of H would be the CH_n radical, which by ladder switching would free potential reactive atomic species involved in the reactions described.

As shown Figure 6.2, abundance of nitrogen and oxygen exhibited an increase from atmospheric pressure to a clear maximum at 1 mbar. The ample presence of N and O at medium-high pressure probably corresponds to dissociation from air. Based on the progressive removal of atmospheric N and O as the chamber is pumped down, a decrease in their intensities is observed. However, emission lines corresponding to such atomic species are also observed at high vacuum regime, which could be due to the dissociation of the NO_2 released from the aromatic ring. The clear intensity drop undergone by emission lines when atmospheric pressure is achieved could be explained by the fact that, at pressure values close to atmospheric, plasma generated with a nanosecond pulse is expanding in a denser atmosphere, which generates thicker plume. Therefore, fewer photons are allowed to reach the sample surface, which lead to a decreased ablation rate and a less intense emission signal **[Knight, A. K. et al., 2000]**.

Considering all the different reactions involved and the experimental evidences, the question arising is whether the laser performs an extensive and simultaneous fragmentation of the molecule, whose fragments exhibit subsequent reactions, or if there is a specific fragmentation pathway, dependent on the experimental conditions. The answering of this question was faced by simultaneous detection of the photons and ions generated in the laser interaction with the sample. The laser fluence was reduced to values close to the plasma formation threshold in order to avoid explosive ablation conditions that could mask the early-formed species in the expanding plume. In the high vacuum regime, the ablation environment was free to a large extent from any possible source of H, N or O other than the sample. Figure 6.4 presents the optical emission (top) and mass (bottom) averaged spectrum from TNT exposed to 100 laser pulses of 1.0 mJ/pulse (3.6 J/cm^2), slightly above the plasma formation threshold. Under these soft conditions, the LIBS spectrum (top) shows contributions from CN and C_2, and slight evidences of C, H and O. The presence of ions $^{12}C^+$, $^{13}CH^+$, $^{24}C_2^+$, $^{26}C_2H_2^+$, $^{28}HCNH^+$, and $^{38}C_2N^+$ supported the above reactions as possible routes of dissociation. Carbon signal is probably distributed in different carbonate fragments due to the break of the aromatic ring:

$$\Sigma C = {}^{12}C^+ + {}^{24}C_2^+ + \Sigma C_nH_m^+ \qquad (6.12)$$

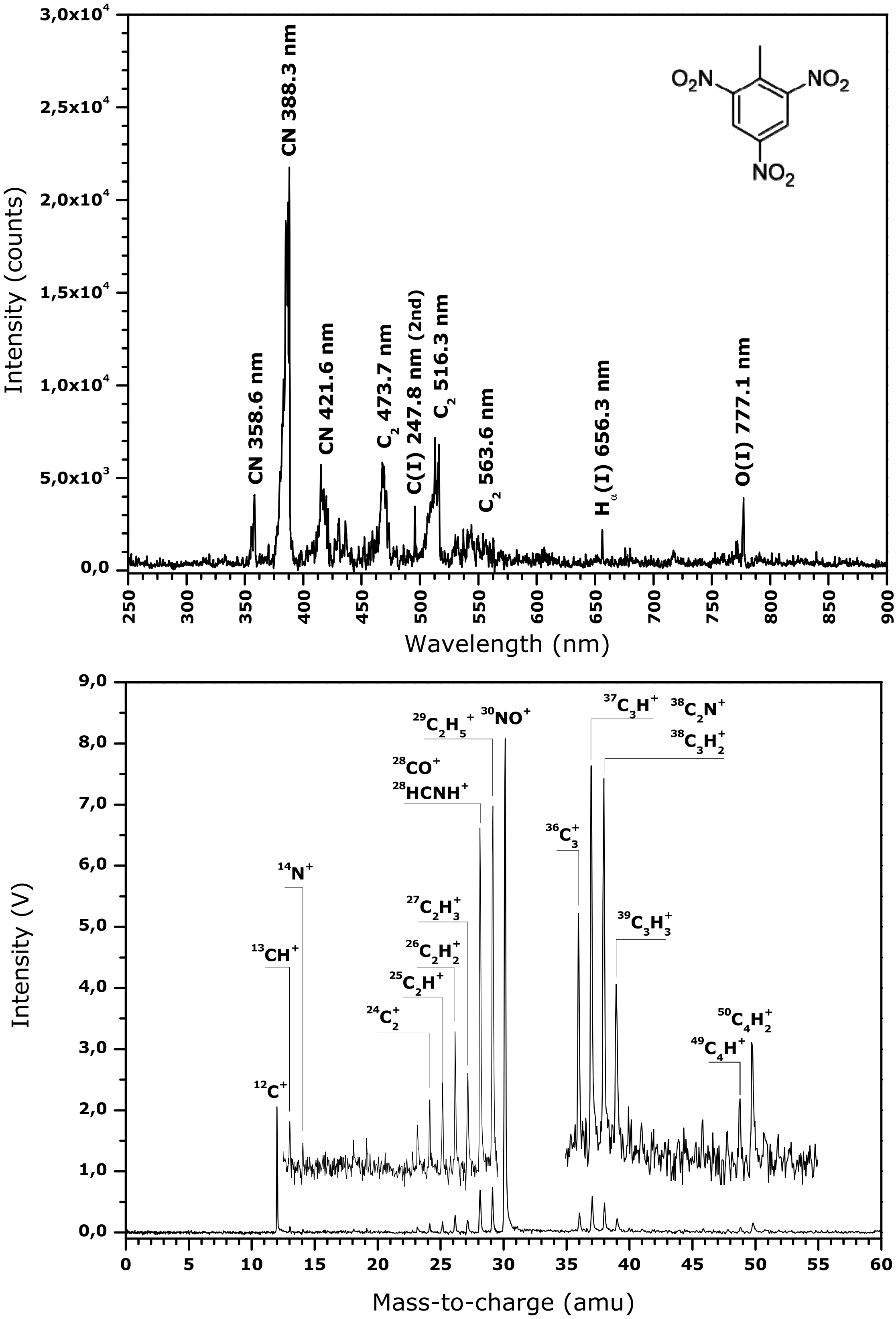

Figure 6.4. TNT LIMS spectrum (low mass range) acquired in coincidence with high vacuum LIBS spectrum. UV pulse energy, 1.0 mJ. Fluence, 3.6 J /cm^2.

Ring-opening is demonstrated based in the appearance in the mass spectrum of multiple signals associated to the ladder-switching process typically associated to the presence of aromatics, and compatible with reaction (6.6). As commented above, H and O present in the plume since the first nanoseconds of plasma lifetime could be responsible of avoiding the increase of molecular fragments signals according to reactions (6.7), (6.9) and (6.11) under vacuum conditions. On the contrary, at atmospheric pressure, reactions from (6.1) to (6.4) take place in a large extent and molecular bands from CN and C_2 fragments dominate the spectrum, losing prominence the atomic emission.

The mass spectrum was dominated by $^{30}NO^+$ ion from the immediate dissociation of NO_2 groups that were rapidly ejected from aromatic ring due to the stress of the molecule caused by the position of substituents in the space. The nitro explosives had a common feature, namely a relatively high degree of charge separation, and in this energetic molecule, the presence of NO_2 group introduced significant charge separation or local polarity. The nitro group is powerfully electron-attracting and this fact strongly conditioned the fragmentation routes followed by the molecules **[Murray, J. S. et al., 1998].**

With regard to PETN, the response obtained in the coincidental LIMS-LIBS analysis is showed in Figure 6.5. This explosive compound is an aliphatic molecule with four nitro groups in its structure. In the LIBS spectrum (top) is remarkable the absence of C_2 emission. These emissions are due to double C=C bonds in the molecule which are absent in this case. On the other hand, molecular CN fragments are formed mainly. Taking as reference the acquired LIMS spectrum (bottom), the main reactions suggested in the fragmentation of PETN at vacuum regime, in addition to those mentioned above namely (6.3), (6.5), (6.6) and (6.8), are presented below:

$$CN + H_2 \rightleftharpoons HCN + H \qquad (6.11)$$

$$CN + H_2O \rightleftharpoons HCN + OH \qquad (6.13)$$

$$C + NO \rightleftharpoons CO + N \qquad (6.14)$$

$$N + H_2 \rightleftharpoons NH + H \qquad (6.15)$$

In this case, direct fragmentation of CN radicals from the molecule is not possible since C-N bonds are inexistent in the structure. Thus, CN fragments are mostly formed in reactions of atomic nitrogen with carbon-containing species (6.3) or through

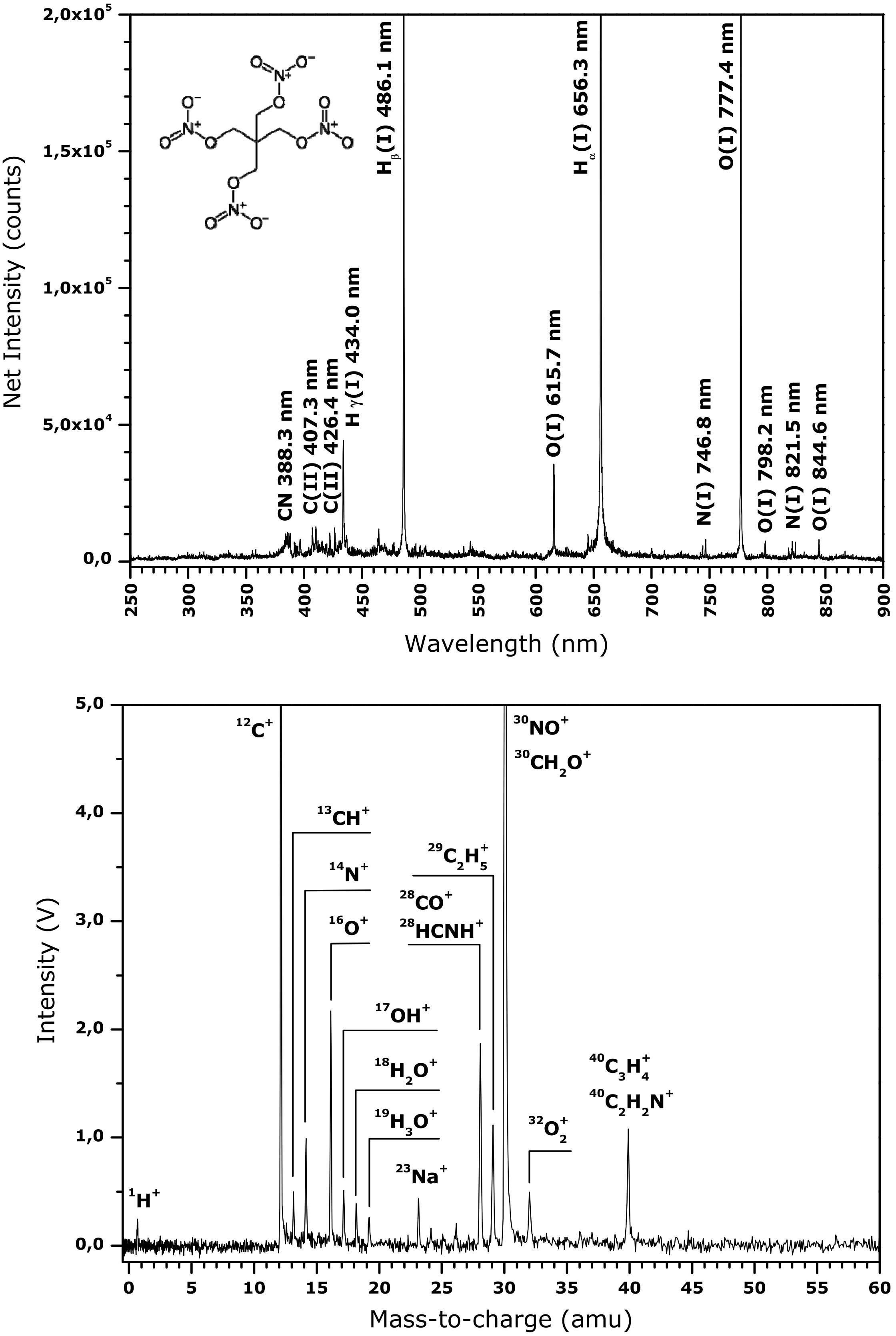

Figure 6.5. PETN LIMS spectrum (low mass range) acquired in coincidence with high vacuum LIBS spectrum. UV pulse energy, 2 mJ. Fluence, 7.2 J /cm^2.

secondary reactions as (6.5). On the other hand, CN radicals react with traces of hydrogen (6.11) and water (6.13) molecules present in the surrounding to result in a new dissociation, keeping CN balance in the plume.

The LIMS spectrum demonstrates the presence in the plasma of the species involved in the reactions (6.5), (6.8), and (6.11-6.15). These observations support the decomposition pathways proposed for this compound. However, characteristic hydrocarbon fragments from ladder-switching reaction associated to the presence of benzene cycles are absent. Mass spectrum was dominated by $^{12}C^{+}$ signal, and the absence of $^{24}C_2^{+}$ signal was checked. Moreover, total fragmentation or atomization of the PETN molecule was found to occur at a fluence level higher than the needed for TNT. This fact may be related to the molecular stability of PETN and, therefore, the spatial distribution of substituents that makes the structure to be less tensioned than in the case of TNT system.

6.4.2. Hydrogen and nitrogen atmospheres

The hypothesis of consumption of C_2 and CN species at vacuum ambient by hydrogen after reactions (6.7) and (6.11) is supported by an experiment carried out in hydrogen atmosphere. If such reactions would proceed to a significant extent in the plasma, an increase in the concentration of hydrogen in the atmosphere would result in an increase in the abundance of CH and a decrease of C_2 and CN emissions. In the experiment, pure hydrogen was provided as buffer gas into the vacuum chamber and plasma light was collected at different pressure levels from high vacuum to 3.5 mb (top pressure of the calibrated range for hydrogen gas). Figure 6.6 compares the TNT LIBS spectra acquired in nitrogen (top) and hydrogen (bottom) atmospheres at 1 mb. Both spectra are sketched in the same scale. In the case of nitrogen as buffer gas, CN and C_2 molecular bands appeared with marked intensity in the recorded spectrum, so it participates clearly in the mechanisms of reaction inside the plasma. Also notable is the presence of the emission system corresponding to the diatomic species NH at 336.0 and 337.0 nm. The increase of emission intensity for excited NH was appreciable compared to that obtained for other background atmospheres due to a larger rate of association between nitrogen from background gas and H atoms. In contrast, CH intensity increases using hydrogen as buffer gas, whereas the intensity of the CN and C_2 emission bands decrease drastically. This result was similar to that obtained in high vacuum pressure conditions. In vacuum, CN and C_2 species arise from the direct rupture of the aromatic ring since only a low degree of recombination was possible. The velocity of plasma expansion is quite high and this involves the virtual absence of

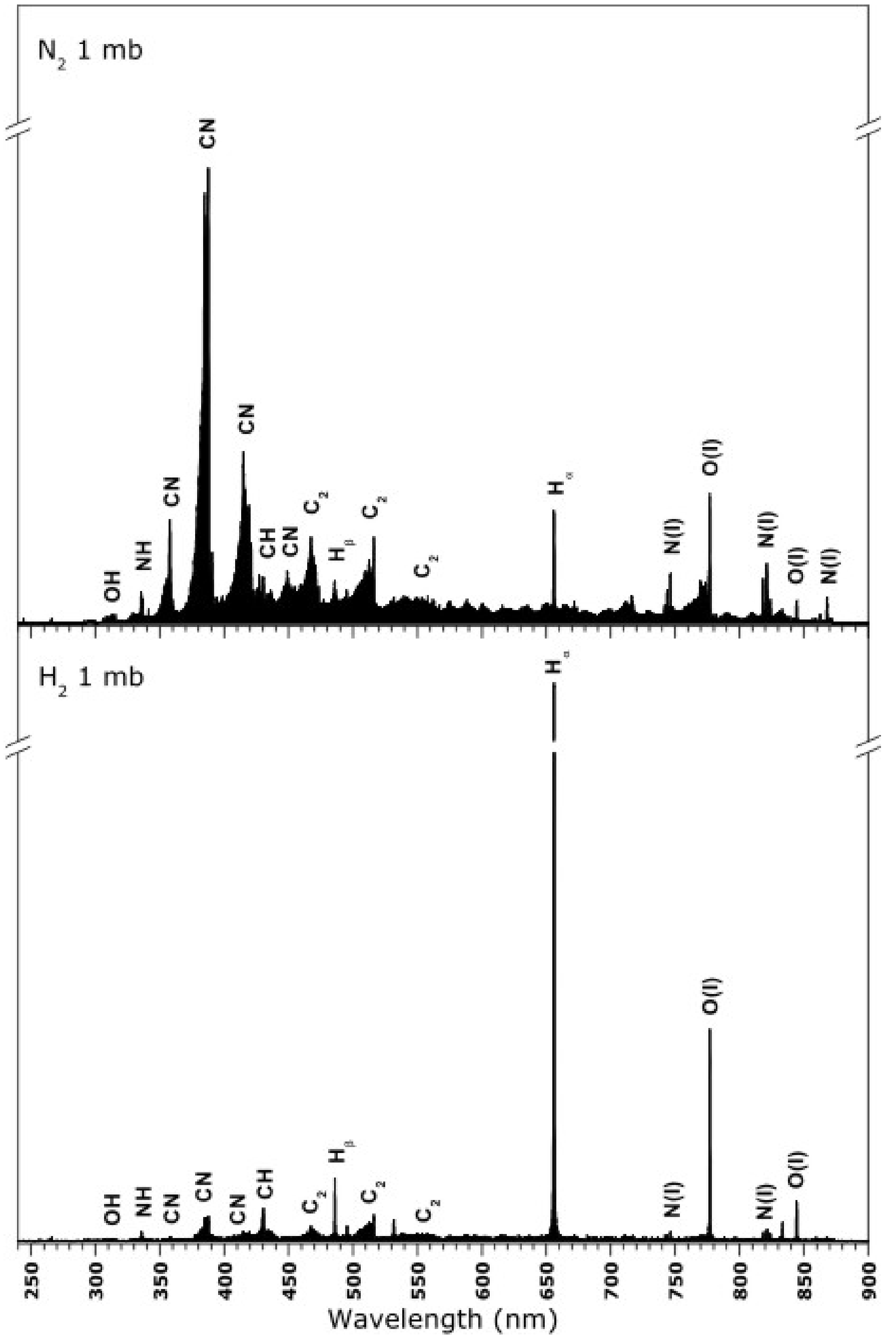

Figure 6.6. TNT LIBS spectra acquired in hydrogen and nitrogen atmospheres. UV pulse energy, 3.5 mJ. Fluence, 12.6 J /cm^2.

collisional processes in the plume. However, when hydrogen was present as background gas, the number of collisions inside the plasma increased gradually. In fact, a strong broadening effect was observed for emission lines of atomic H_α and H_β at pressures above 3.5 mb due to the higher electronic density of the plasma. Nevertheless, the intensity level of such molecular species was also very low compared

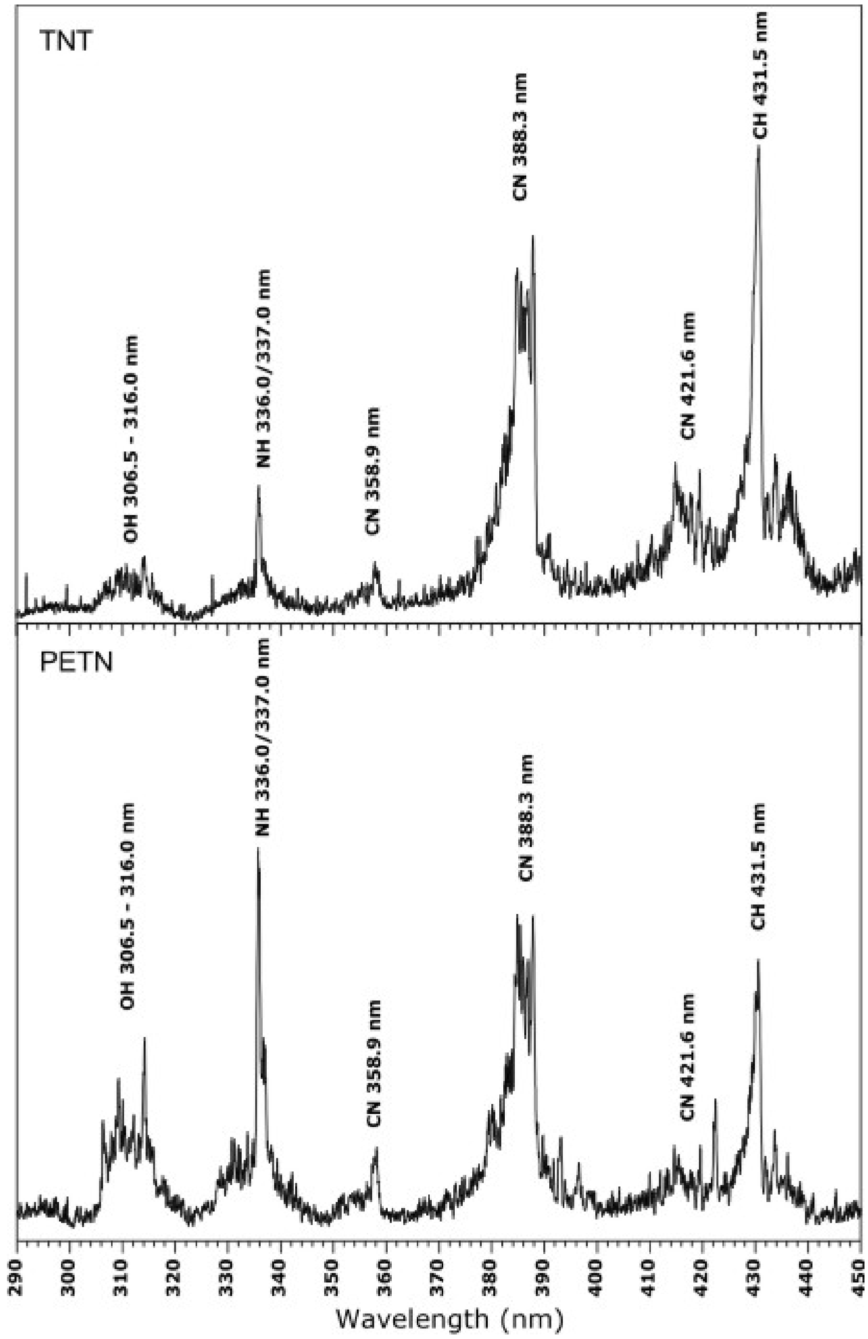

Figure 6.7. Detail of low-wavelength range of LIBS spectra acquired in hydrogen atmosphere at 3.5 mb for TNT (up) and PETN (bottom). UV pulse energy, 3.5 mJ. Fluence, 12.6 J/cm^2.

to other buffer gases. Therefore, it can be concluded that routes (6.7) and (6.11) play an important role in the chemistry of the plasma.

Within the studied pressure range from 0.1 mb to 3.5 mb for hydrogen atmosphere, different diatomic emitting species, namely CH, NH and OH, also appeared in spectra of analyzed compounds as commented before. Figure 6.7 shows a detail of LIBS spectra for TNT and PETN (spectral window between 290 and 450 nm) where such diatomic species are observable. Both spectra are sketched in the same scale. We can expect that hydrogen from buffer gas leads to the formation of these emitting species in a considerable extent. In this sense, the formation of CH mainly follows route (6.6) for both compounds according to the observed LIMS spectra. Moreover, in the case of TNT, routes (6.7) and (6.16) **[Wilson Jr., W. E., 1972]** are also probable since they involve C_2 consumption. On the other hand, recombination for NH formation follows route (6.15) in both cases. OH fragments mostly come from the intra-molecular reaction between a nitro group and a close hydrogen atom through the well-known *ortho-effect* in the case of TNT (see Figure 3.6 in Chapter 3) whereas pathway (6.13) likely occurs for PETN. In addition, pathway (6.17) is reported as an important oxidation processes of hydrocarbons **[Sicilia, E. et al., 1994]** so it becomes a possible route for the nitroaromatic molecule as well.

Finally, it is noteworthy in Figure 6.7 how such H-containing fragments (difficult to observe in typical LIBS spectra of organic compounds) present comparable intensities to those for CN emission bands in presence of hydrogen buffer gas.

$$C_2 + OH \rightleftharpoons CO + CH \qquad (6.16)$$

$$CH_3 + O_2 \rightleftharpoons CH_2O + OH \qquad (6.17)$$

6.5. CONCLUSIONS

In the present work we have collected and characterized LIBS spectra of TNT and PETN, two organic nitro-containing compounds. We have proposed probable fragmentation pathways for the compounds considering that same reactions prevail over others depending on experimental conditions: laser fluence, pressure level and type of atmosphere surrounding the plasma, mainly. The suggested routes are supported by LIMS measurements where many non-emitting reactive species in the plasma were identified.

Pressure becomes a critical parameter in LIBS trials affecting the dynamics of the plasma from values as little as 0.1 mbar. The presence of air influences on the specific emission of species due to interferences in the recombination pathways occurring in the plasma plume. Results obtained in N_2 and air atmospheres indicated that C_2 emission is strongly linked to molecular structure whereas CN is mostly produced by chemical recombination reactions. Results using H_2 as buffer gas suggested that hydrogen may alter the formation pathways for molecular species, thus reducing the CN and C_2 emission, while favouring the formation of NH, CH and OH species. We have verified this effect in absence of air (high vacuum regime), where molecular emission was also very weak. This is presumably caused by the reaction of hydrogen mostly and other atomic species with molecular species inside the plasma resulting in dissociation of such fragments (CN, C_2…).

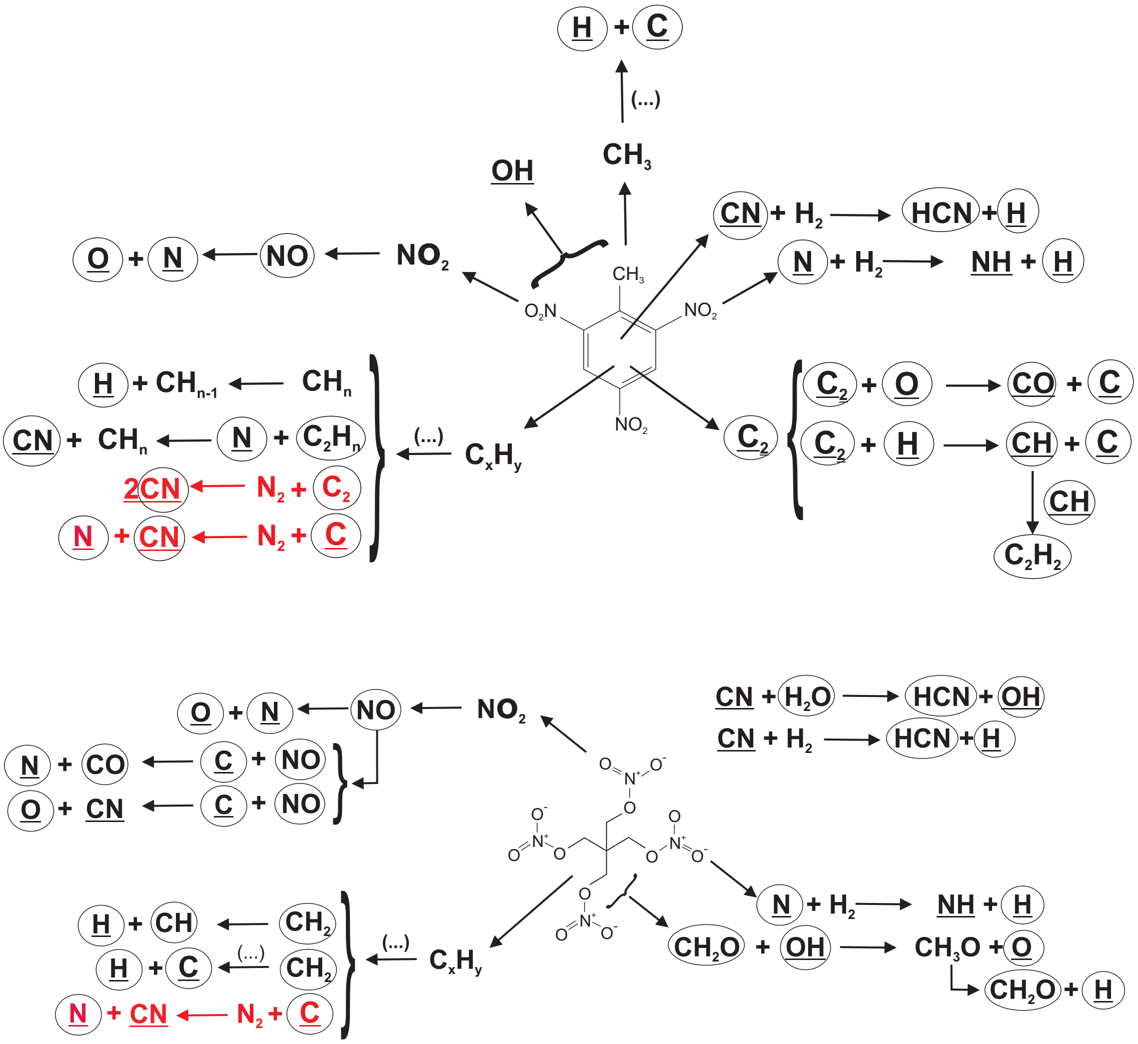

Underline: emitter species in LIBS spectra
In circle: species as ions in LIMS spectra
In red: reactions taking place preferentially at amospheric pressure

Figure 6.8. Summary of main fragmentation pathways followed by TNT (top) and PETN (bottom) molecules suggested from optical and mass spectroscopic studies.

CHAPTER 7

Analysis of Influence of Pressure on Dynamics of Laser-Induced Plasma Expansion for Nitro Aromatic Explosives by Time and Spatially-Resolved Studies

7.1. SUMMARY

The influence of pressure level of the ambient atmosphere on the dynamics of plasma expansion besides on the interaction between excited plasma and gas molecules have been studied for specific organic aromatic compounds.

The spectral emissions of TNT, a high energetic nitro organic compound (NC), and pyrene, an organic polycyclic hydrocarbon compound (PAH), were studied by laser-induced breakdown spectroscopy at different pressure environments, from high vacuum regime to atmospheric pressure, in order to analyze the influence of air on the formation pathways of atomic and molecular species inside the plasma plume. The solid samples were introduced in a vacuum chamber, and the fourth harmonic output of a Nd:YAG laser (λ 266 nm) was used as excitation source. The optical emission signal was collected with an optical fibre connected to a spectrograph with ICCD detector.

Results from LIBS spectra showed that changes in pressure level affect the kinetics of the characteristic excited species and their spatial distribution inside the plasma plume. Moreover, ablation rates of organic samples for nanosecond lasers are modified with pressure level due to the variation in the density of ambient in the surrounding of the sample.

7.2. INTRODUCTION

Laser-Induced Breakdown Spectroscopy (LIBS) has been widely used in the characterization of plasmas coming from samples of different nature, due to its many advantages as analytical technique. It involves a simple and rapid method for in situ and real-time multi-elemental analysis of solid, liquids, aerosols and gases. More specifically, an abundance of works regarding the influence of pressure and the nature of atmosphere in the dynamics of generation and evolution of plasma using emission spectroscopy are found in the literature in the last three decades, many of them based on LIBS technique. Kagawa *et al.* **[Kagawa, K. et al., 1982]** observed how the characteristics of plasma and the corresponding emission spectra in metallic samples depended markedly on pressure of environment. Moreover, they realized there were pressure values that benefited the quality of analytical signal. Iida **[Iida, Y., 1990]** studied the effects of pressure using different atmospheres. A strong dependence of plasma emission of metallic and ceramic samples with pressure level was observed for the different probed atmospheres, and how pressure affected the ablation rate of the material, which also depended on the nature of the sample and the properties of buffer gas. Some years later in 1997, Lee *et al.* **[Lee, Y. I. et al., 1997]** carried out measurements of time-integrated spatially resolved spectroscopy with different buffer gases and monitored different atomic and ionic emission lines from cupper plasma depending on the distance to the target at different pressure values. They observed differences in the spatial distribution of species in the plume and confirmed the importance of controlling this pressure setting. They also compared different laser wavelengths concluding that shorter wavelengths caused a more efficient excitation of species due to a lower reflectivity of the material and a lower absorption of radiation by the plasma compared to those for longer wavelengths. Knight **[Knight, A. K. et al., 2000]** also concluded from temporally and spectrally resolved imaging studies on aluminium plasmas that pressure parameter has a determining influence on the collision and excitation processes of species. This had an effect both in the quantity of ablated mass from the target and in net intensity of signals. On his behalf, Acquaviva *et al.* **[Acquaviva, S. et al., 2002 A][Acquaviva, S. et al., 2002 B]** studied the laser ablation of graphite in low-pressure nitrogen ambient following the kinetics of atomic carbon by time- and space-resolved emission spectroscopy. They analysed the expansion dynamics of plasma taking into account the interaction processes between ablated carbon and nitrogen molecules. A strong dependence on the ambient pressure was deduced from measurements of the emission intensity as a function of distances from the target and delay times. The increase of pressure implied a higher plasma plume confinement and a distribution of atomic and molecular species in the plume was found out. Two years later, Yalçin *et al.* **[Yalçin, S. et al., 2004]** with their results further fed this interesting area studying the variation in LIBS signal with pressure in metallic plasmas generated from femtosecond laser. A marked improvement in the characteristics of emission at relatively low pressures was verified and attributed to a slower cooling of the plasma. Moreover, they observed for femtosecond laser ablation a lower shielding effect that meant no variation of ablated mass with pressure changes.

The analysis of organics by emission spectroscopy has certain handicaps compared to samples of inorganic nature. It must be taken into account the interference effects involving recombination of species and interaction with the atmosphere. In addition, higher ablation rates are usually experimented by these compounds and tedious methods are sometimes required for its handling and preparation. Baudelet *et al.* in his work about interaction plasma-atmosphere for organic compounds **[Baudelet, M. et al., 2007]** probed how valuable the temporal resolved studies were in order to identify native species coming from organic sample or as a result of reactions between ambient air and excited material in the plasma. The different origins of emitters resulted in different kinetic behaviours. They emphasize the importance of controlling the laser fluence for identification of native molecular species vaporized from the organic sample.

Other studies concerning the influence of ambient pressure on the kinetics of excited species in laser-induced plasmas from ablation of carbons and organic compounds are emerging in recent years **[Kushwaha, A. et al., 2008][Baudelet, M. et al., 2008][Vors, E. et al., 2008][Ctvrtnickova, T. et al., 2009][Mercadier, L. et al., 2010][Choi, S. J. et al., 2011][Lei, W. Q. et al., 2012]**. Plasma is a spatially inhomogeneous and transient system, so temporally and spatially resolved spectroscopy stands as an efficient tool to carry out this type of researches in order to obtain a better knowledge of plasma expansion dynamics and to study the physical properties of its emission.

As noted earlier, control of pressure level is a crucial factor in the generation of plasma since it has a deciding effect on many areas of study of plasmas, from its reactivity and the rate of collisions inside the plume to the different expansion velocities, including the morphology of the plume and the spectral characteristics of the emitted light. The key of the alterations undergone by laser-induced plasmas is the interaction between plasma plume and the surrounding gas. In the case of ambient air, excitation of molecules of gas in the vicinity of irradiated organic sample by collision with excited species from ablated material inside the plasma leads to dissociation of O_2 and N_2 molecules from air and subsequent chemical reactions. These reactions lead to generation of new organic diatomic species in the plasma such as CN radicals **[Baudelet, M. et al., 2007].** The rate of collisions in the system depends directly on the density of species in the plume and, therefore, on the surrounding pressure. Atomic as well as molecular species produced after ablation due to interaction between plasma and ambient gas can additionally contribute to the total intensities of specific emission lines and bands **[Baudelet, M. et al., 2007].**

In this work, the main aim was to understand the way in that air pressure affects the kinetics of different excited and characteristic species of organic aromatic compounds within the generated plasma. A series of time- and spatially-resolved studies were performed in order to help us to have a better knowledge of the involved processes and the emission characteristics of plasmas. A high energetic nitro aromatic compound, 2,4,6-trinitrotoluene, and pyrene, a polycyclic aromatic hydrocarbon without oxygen or nitrogen content compound, were selected as samples for the comparative analysis because of its undeniable analytical interest and its suitable physical properties for plasma formation and emission signal acquisition.

7.3. EXPERIMENTAL

The scheme of the experimental set-up used in this work was shown in Fig. 2.18 in Chapter 2. The quadrupled Nd:YAG laser model Brio (266nm, 12 mJ, 4.4 ns pulse width) was used to irradiate the organic samples in solid phase placed into the stainless steel vacuum chamber previously described. The *bulk* samples were continuously moved during analysis in order to have a fresh surface for each laser shot. Laser pulse energy was controlled using a variable attenuator that allowed continuous variation of the energy per pulse without modifications in the beam spatial profile. The laser beam was focused approximately on the surface of the sample with a quartz plane-convex lens (200 mm) and the light emitted from the plasma plume was collected through the lateral quartz view port of the chamber by a 3” quartz plane-convex focal lens (150 mm) placed orthogonal to the plume expansion direction. After being reflected with a UV coated mirror placed at 45º to the collection path, the light was focused in the extreme of a quartz optical fibre (600 μm) connected to the entrance slit of the 500 mm focal-length imaging spectrograph, equipped with an intensified CCD as a detector (*iStar, Andor*). A dispersive grating of 599 lines/mm which let a spectral range of 45 nm was used to obtain high-resolution spectra from time-integrated plasma and for time-resolved and spatial-resolved analysis. Pressure into chamber was monitored at real-time by a single gauge *Pirani* system which allows a range control from 10^{-4} to 10^{3} mb. Specific pressure values were obtained by means of controlled air leaks through a needle valve in order to assure stability in the system for analysis.

Atomic and molecular species within the plasma plume were identified from LIBS spectra. Intensities of the emissions from the detected molecular species were recorded in the regions of the band heads, where the emission intensities were the strongest. In the case of emission lines from atomic and ionic species, peak intensities with background subtracted were taken for the study.

7.4. SAMPLES

Pyrene was acquired as small crystals to *Sigma-Aldrich* company whereas 2,4,6-TNT was obtained from National Department of Defence as small flakes**.** The bulk samples were prepared by compressing powders of pure compounds using a hydraulic press machine and the thickness of the resulting pellets was 2 mm. The samples then were fixed onto an aluminium holder and this was introduced into the auxiliary chamber for primary vacuum by means of an insertion probe equipped with a 3D micrometer for fine control of the position of the sample (see Figure 2.6). The handler was finally introduced in the main chamber through a lab-made load-lock device to allow fast sample changing without vacuum breakage.

7.5. RESULTS AND DISCUSSION

7.5.1. Effects of pressure on LIBS response

Fig. 7.1 shows a sequence of TNT and pyrene plasmas at different pressure values from 10^{3} mbar to 10^{-5} mbar at a fluence value of 12.7 J/cm^{2}. A grey rectangle showing the position and dimensions of the pellets in the sample holder and a scale has been inset to observe the expansion processes taking place. In general, it is observed a marked qualitative change in the morphology of plasma plume (colour, size and shape) with pressure variation, so dynamics and chemistry in the plume are changing considerably. As pressure becomes lower, the plasma presents a larger volume due to the obvious reduction of density of the surrounding media, so a gradual freer expansion is undergone by the plume. Finally, at high vacuum regime, the lack of gas density implies a not adequate confinement of plasma so the angle of expansion undergoes a marked increase since the excitation processes by collisions decrease in the plume. Moreover, it is well-known that the physical characteristics of plasmas change significantly with pressure: electronic density, abundance of excited species, absorption of laser radiation, etc **[Glumac, N. et al., 2007][Yalçin, S,. et al., 2004].** In addition, the figures reveal that the brighter portion of the plasma is located near the surface. However, as long as the pressure decreases, two well-defined regions appear: one close to the surface with little modification in its dimensions, and a second one that expands in axial and radial directions, in accordance with previous reports **[Glumac, N. et al., 2007]**.

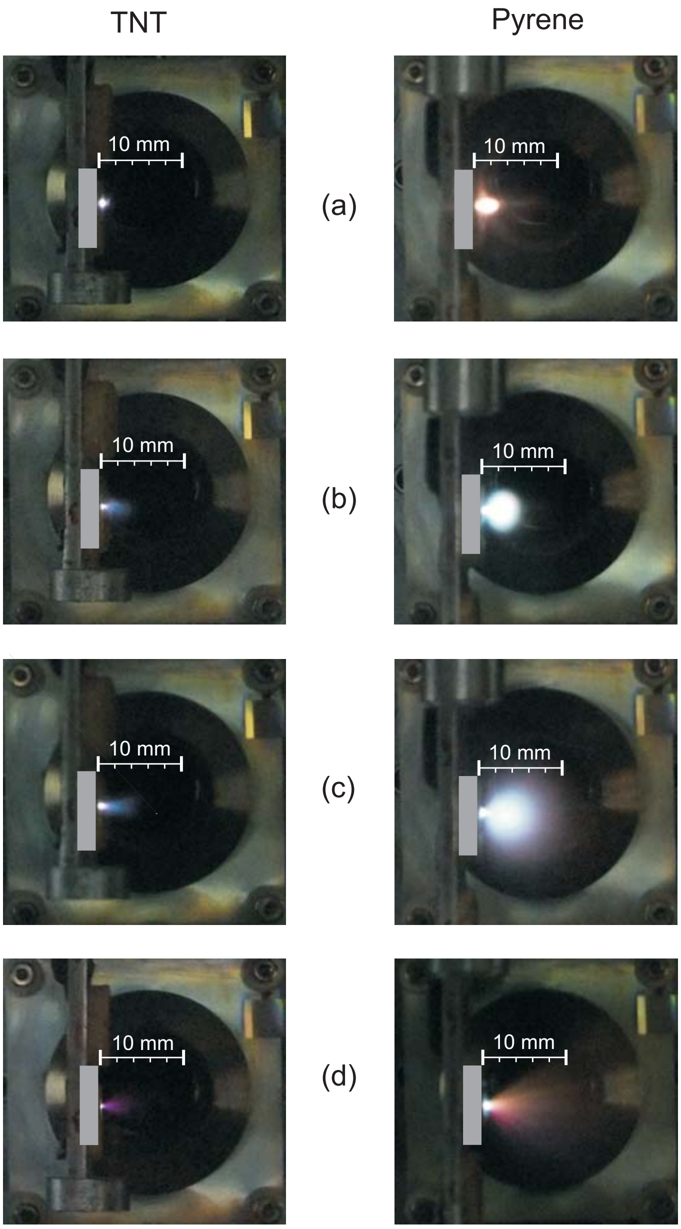

Figure 7.1. Images of trinitrotoluene and pyrene plasmas at different pressure levels, (a) 1000 mb; (b) 10 mb; (c) 1 mb; (d) 1 ·10^{-5} mb. Fluence, 12.7 J/cm^2.

The emission spectra are affected by the modification in the gas pressure. As a rule of thumb, atomic and ionic emitting species dominate the spectrum at high vacuum pressure whereas molecular emission is stronger for higher pressure levels. This fact is observable in Figure 7.2 for TNT and pyrene. At atmospheric pressure, the spectra show intense signals from molecular bands related to the presence of C=C bonds due to the breakage of the aromatic rings (C_2 bands). A comparison of the TNT and pyrene spectra reveals that the C_2 bands rises with the increasing number of aromatic rings. On the other hand, the CN bands may find its origin in the native presence of C-N in the molecule, or to the recombination of released C species with N_2 in the surrounding atmosphere. As the pressure is decreased, the number of collisions with the surrounding atmosphere decreases, yielding to an extinction of CN presence by recombination. However, even at 1 mbar, the media is dense enough to keep the C_2/CN ratio unaffected.

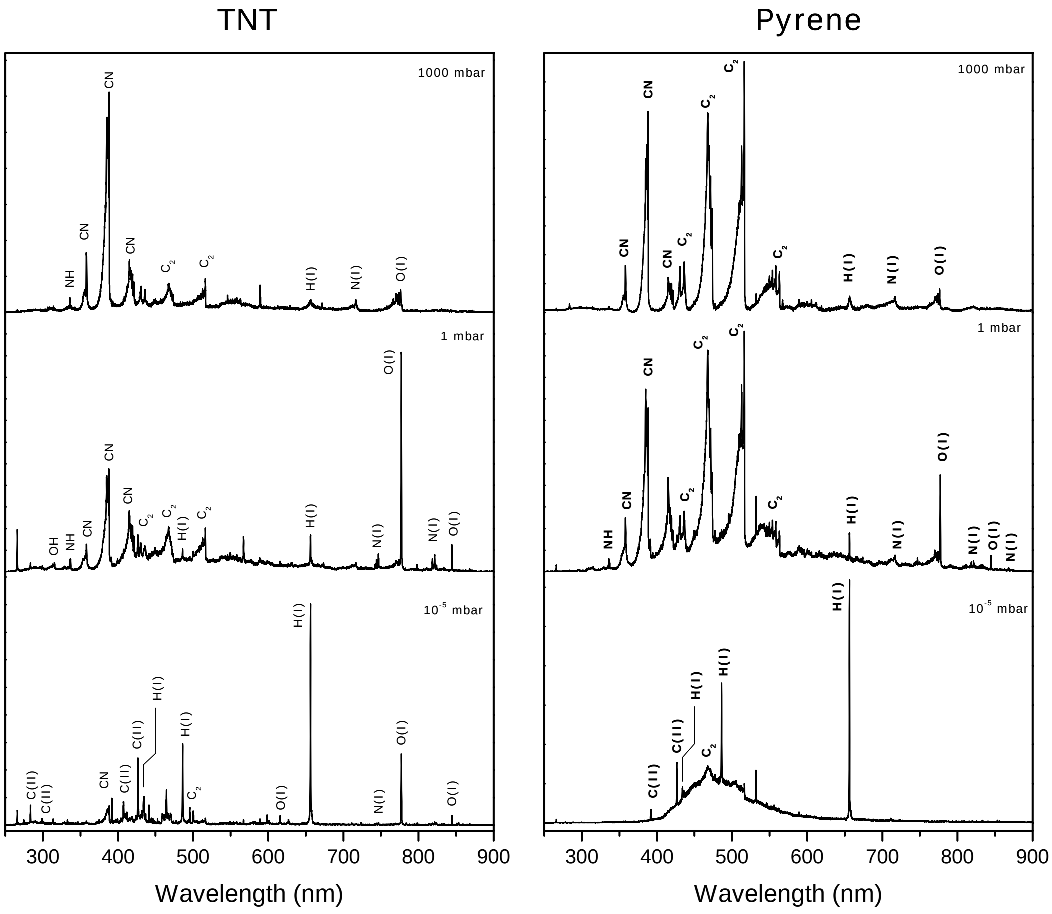

Figure 7.2. LIBS spectra of trinitrotoluene and pyrene plasmas at different pressure levels. Fluence, 12.7 J/cm^2.

At low vacuum conditions, where the media is free from molecules, no evidence of CN bands is observable in pyrene due to the absence of both gas nitrogen from air and nitrogen atoms in the molecular structure of the compound. The spectrum presents weak C_2 emission bands mainly from the rupture of aromatic ring of the molecule. The visualized atomic and ionic emission lines, namely H(I), C(I) and C(II), dominate the spectrum clearly and the FWHM values become very low. The very high peak resolution is probably due to the limited collision processes that implies an immediate relaxation and consequent emission that avoids the broadening effect.

Concerning atomic and ionic emissions, its presence in the spectra will be mainly related to the elemental composition of the sampled compounds (H, C, N and O in TNT, and H, C and O in pyrene). The significant presence of N emission in pyrene at 1 mbar is related to the free N atoms available after the recombination process to generate CN bands from N_2 dissociation. The broad signal centered at 480 nm corresponds to the fluorescence spectra of pyrene **[Ferguson, J., 1958][Schweitzer, D., 1976]**, visible as the low vacuum conditions and the lack of collision do not quench the fluorescence emission.

As shown the above figure, at low vacuum of 1 mb the generated spectra have higher richness of both atomic and molecular species with notable intensities. This is due to, on one hand, lower plasma shielding (i.e. a minimum laser absorption by plasma) compared to that occurring at atmospheric pressure and therefore, a higher ablation rate and, on the other hand, a higher plasma density compared to that at high vacuum regime. These factors imply an increase of volume of excited species at intermediate pressures by collision processes during the plasma plume expansion into the surrounding atmosphere**.**

Due to plasma contains different species as electrons, ions, and neutral atoms, the absorption of the laser radiation by such particles occurs by different mechanisms. While absorption of photons by free electrons in the plasma is described by inverse Bremsstrahlung (IB) mechanism **[Singh, R. K. et al., 1990 B]**, absorption by excited ions and neutral atoms is described by photoionization mechanism (PI) **[Neamtu, J. et al., 1999]**. Moreover, Mie absorption involves absorption in the case of clusters formation by condensation of supersaturated vapor inside the plasma **[Rozman, R. et al., 2008].** These have been reported as the dominant absorption mechanisms. However, the laser absorption due to IB mechanism is negligible at low laser wavelengths **[Fang, R. et al., 2007]** and hence, can be neglected in our experiments using UV laser pulses. Thus, PI and Mie mechanisms will be dominant in the present case.

As for TNT, the coupling between laser beam and sample surface was not so suitable and the ablation was not as efficient as in the case of pyrene. That resulted in smaller and less intense plasmas for this compound at energy setting conditions that could mean a problem for spatial resolution studies. However, the qualitative evolution of plasma as well as the associated spectra were successfully captured as shown Figures 7.1 and 7.2, respectively. Again, plume with the highest volume and superior richness of atomic and molecular species was observed for intermediate pressure level (1 mb), whereas the TNT plasma generated under high vacuum regime expanded and extinguished faster, and the corresponding spectrum presented weak C_2 and CN emission bands mainly from direct fragmentation of the molecule. In this case, the atomic and ionic emission lines mainly from H(I), O(I), C(I) and C(II) species dominated the LIBS spectrum. On the contrary, when acquisition was carried out in open air, intensity of molecular bands from CN and C_2 fragments increases due to reaction of C atoms with atmospheric nitrogen as in the previous case of PAH molecule.

At atmospheric air pressure, emission lines of atomic or ionic species appear highly attenuated in the spectra of both analysed compounds or even did not appear. Only main H(I) and O(I) lines were observed together with the characteristic molecular bands. The main reason of such observed effect is the high electronic density of plasma in air pressure that causes the broadening of the lines. In contrast, at vacuum regime, values for electron density are lower, so excited species relax rapidly due to lack of collisions as commented before.

Fig. 7.3 shows the variation in the intensity of main ionic (C(II) line at 426.5 nm), atomic (H_α(I) line at 656.3 nm; N(I) line at 746.7 nm; O(I) line at 777.4 nm) and molecular (CN($\Delta\upsilon$=0) band at 388.3 nm; C_2 ($\Delta\upsilon$=0) band at 516.3 nm) emission species with the increase of air pressure in TNT (Figure 7.3.a) and pyrene (Figure 7.3.b). The reported data correspond to integration times of 1 ms. Plasma light was entirely collected in the entrance of an optical fibre, so all the plasma image is part of the measurement. Intensity values are normalized to the maximum intensity for each data set so that we can notice which species are dominant and which ones are minority for each pressure level.

As a general trend, three conclusions may be extracted: a) molecular bands are mainly present in the pressure range between 10^3 - 0.1 mbar); b) N and O exhibit a maximum intensity at intermediate pressures, reaching a maximum at about 1 mbar; and c) C and H experience a clear cut-off at about 0.1 mbar, increasing its intensity as the pressure gets lower.

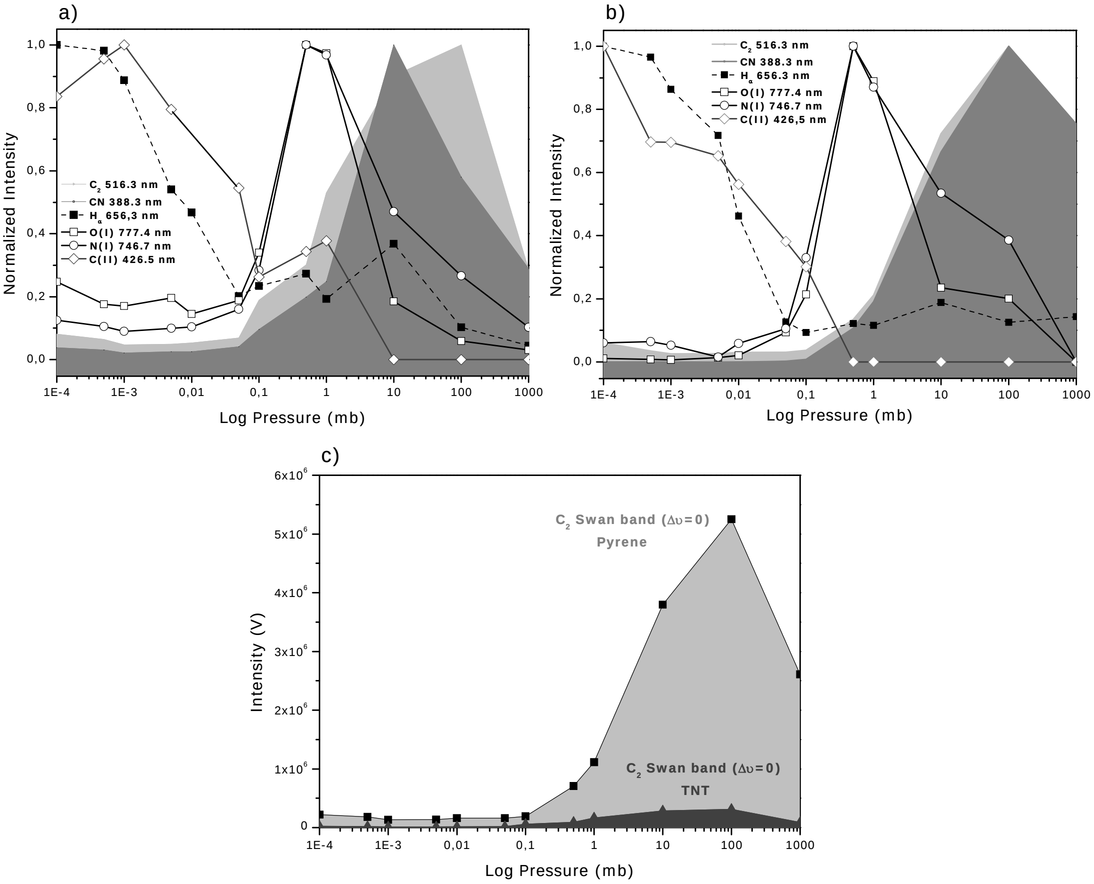

Figure 7.3. Normalized intensities of main emitting species depending on the air pressure level for (a) trinitrotoluene and (b) pyrene. (c) Comparative of net intensities of C_2 (Δυ=0) molecular band for both samples, depending on the air pressure level.

Since pyrene is a hydrocarbon aromatic molecule without neither O nor N atoms in its structure, LIBS measurements at vacuum pressures below 0.01 mbar only provides emission lines from ionic and atomic C, atomic H and weak molecular bands corresponding to C_2 fragments. As the pressure rises slightly, N_2 and O_2 presence becomes evident and the onset of N(I) and O(I) emission signals occurs due to their dissociation. The maximum emission is reached around 1 mb, coinciding with the greatest volume and the most intense expanding plasma plume. On the other hand, the notable presence of CN emission from 0.1 mb upward is in agreement with a number of recombination reactions in the plasma plume immediately after the increase of nitrogen emission. The rise of the population of excited CN fragments in the plume occurs in parallel to the increasing of C_2 molecules. Both molecular species follow an exponential decay fit so the main routes of formation of such species are directly related**.** Meanwhile, peak intensities of C(II) and H(I) lines drop continuously as the air pressure increases due to the progressive generation of continuum emission caused by the increase of electron number density in the plume thanks to the interaction of electrons with ionized and neutral atoms in the plasma after first nanoseconds of laser ablation process.

In the case of TNT molecule, at high vacuum we can observe emission signals corresponding to native N and O atoms coming from nitro substituents. Moreover, it is worth noting the relative maximum achieved by intensity of H(I) specie at 10 mb that breaks the general trend followed by this specie. This increase coincides with the maximum concentration of CN and C_2 molecular fragments in the plume, indicating a complete fragmentation of hydrocarbon radicals.

Apart from this fact, the behaviour of the emission species with the increase in air pressure is quite similar to that of pyrene, suggesting that the dynamics of expansion of plasma and the collision processes in the plume are mainly governed by the elemental composition of the molecule besides density and type of background gas.

All the signals fall down for pressures close to atmospheric precisely caused by a manifest plasma confinement, which in turn causes on the one hand, an intense continuum emission that overlap net signals and, on the other hand, a shielding effect that will be further bellow discussed.

Figure 7.3(c) provides evidence that, although molecular emission kinetics in laser ablation of both molecules followed similar trend with pressure variation, C_2 net signal was much greater for pyrene than for trinitrotoluene due to the direct dependence of this type of emission with the degree of aromaticity of the molecule **[Portnov, A. et al., 2003 A][Portnov, A. et al., 2003 B]**. In the case of molecules with similar structure and same degree of aromaticity, as the case of TNT and its precursors DNT and MNT compounds (with two and only one associated nitro groups, respectively), C_2 emission was observed to be proportional to the total number of nitro-substituents attached to the benzene ring **[Lucena, P. et al., 2011]**. The high electronegativity of nitro groups induce a decrease of the electron density in the ring, and as a consequence, the double bonds in the resonant structure become weakened, so lower amount of C_2 fragments is obtained in the rupture.

7.5.2. Time-resolved study for emission species

Time-resolved and spatially-resolved studies were carried out in order to analyze the variations undergone by plasma from its onset to its extinction and along the direction of expansion.

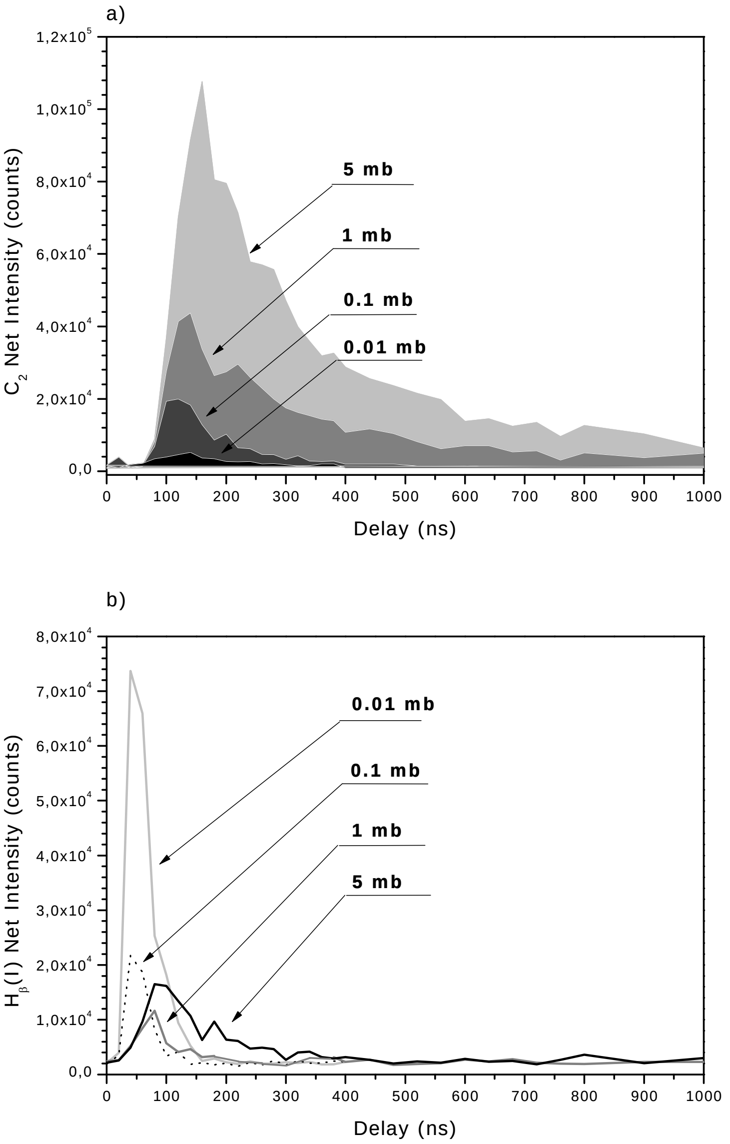

Figure 7.4. Time-resolved studies for (a) molecular C_2 band ($\Delta\upsilon$=0) and (b) atomic H_β emitting species with pressure variation for pyrene sample.

For time-resolved study we chose characteristic emission signals from pyrene LIBS spectrum, measuring their lifetimes at different pressure levels for later comparison. Figure 7.4 shows the temporal evolution of molecular band (C_2, $\Delta\upsilon$=0) and the atomic line H_β(I) in the pyrene expanding plasma. Gate widths of 10 ns and delay windows of 20 ns were used. As observed, the maximum intensity for atomic emissions occurs at earlier times than molecular one (between 50-100 ns), but their duration is significantly lower, with negligible signal beyond 300 ns in the pressure range plotted. Higher pressures provided longer lasting emissions, possibly due to the number of recombination effects occurring in the dense expanding plasma. Concerning molecular emission, the maximum intensity takes place 100-150 ns after the laser pulse, lasting for pressures above 1 mbar beyond 1 microsecond. In both atomic and molecular plotted emissions, the maximum of the curves moved to longer delay times as the pressure increases since higher pressure implies higher reactivity in the plume and therefore, longer lifetime of plasma.

On the other hand, the detection of ionic emission lines demands very low pressures (below 10^{-2} mbar) and short delay times due to their ephemeral cycle of excitation-ionization-relaxation in the emission process. This fact is quite evident in Figure 7.5, where the temporal evolution of C(I), C(II) and C_2 ($\Delta\upsilon=0$) at 10^{-3} mbar is shown as a function of plasma lifetime for pyrene. Similar results were obtained for TNT. At such pressure, all these emitting species coexist. Emission data are showed in net intensity values and time parameters (gate width and delay time) are as in Figure 7.4. As shown, there is a sequence in the appearance of the different species, where the C(II) emission shows up early, followed by C(I) and C_2. Ionic emission was quickly disabled and then vanished whereas atomic species were observed at short times and molecular band was the last to be generated by reaction with atmosphere and recombination processes at longer times. The extinction for every signal took place before than 250 ns as can be observed, so it evidences how ephemeral the plasma duration is at vacuum pressure regime. The obtained result will allow us to monitor different emission signals at their optimum temporal and pressure conditions in future LIBS experiments with organic materials.

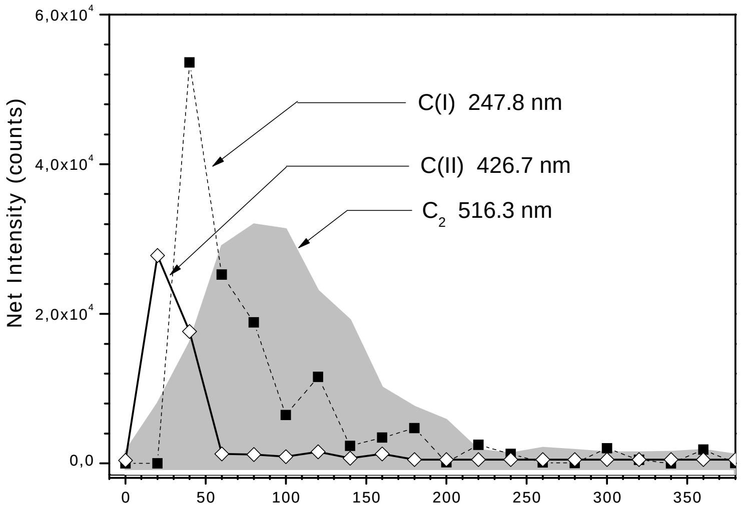

Figure 7.5. Time-resolved study for C_2 (molecular), C(I) (atomic) and C(II) (ionic) emitting species at 0.001 mb from pyrene sample.

Figure 7.6 shows the variation of the emission intensity with delay time (up to 1000 ns) for different species after laser irradiation of TNT sample at 10 mbar. As observed, the same sequence is also reproduced in the ablation of this compound, dominating ionic first and then atomic species at short times, and appearing the molecular bands at longer stages. The faster decrease in emission intensities of ionic and atomic species is assisted by the fact that the excitation energies for such species are substantially higher than those for molecular species. Even at low pressure conditions, the different dissociation and recombination pathways involved in the formation of diatomic species are significant to extend their lifetime way beyond the one for ionic and atomic species.

Fig. 7.6(b) shows the time-evolution of main CN ($\Delta\upsilon=0$) emission band at different pressure levels for TNT sample. It was noticed how CN species was more durable at intermediate pressures (1 – 10 mb), reaching the maximum intensity later than in the case of extreme pressures. Therefore, the influence of gas density in the dynamics of plasma plume is also evident for nitroaromatic compounds. When intermediate pressures are established in the system, the corresponding density value allows an optimum plasma confinement with minimized shielding effect in a greater volume as there is a slower heat transfer between the plasma and the air, which causes the longer plasma duration. Therefore, this result provides us another important key regarding the dynamics and plasma evolution. As can be noted, the drop of the curves following the kinetics of CN extinction for intermediate pressures, especially for 1 mb, present a weak rise after 250 ns approximately. This second slow component in the kinetics of CN generation suggests a late reaction stage in which other competitive and coexisting routes could get the maximum yield due to optimum conditions for such reactions (see also Figure 8.1 in Chapter 8). The highly endothermic reaction $C_2 + N_2 \rightleftharpoons 2CN$ can take place preferentially at earlier stages of plasma formation in presence of air since it requires extreme heating conditions **[Thareja R. K. et al., 2002][Baudelet, M. et al., 2006 B][Dong, M. et al., 2011]**. The electron density at the first stages of plasma formation is the largest and the collisional rate in the plume is decidedly affecting the excitation mechanisms compared to the conditions existing in the plasma at later stages in which both temperature and electron density decreases markedly and air molecules entrainment and diffusion within the plasma play a main role **[Fernández-Bravo, A. et al., in press]**. Therefore, for longer delay times, thermodynamic equilibrium in plasma is achieved and alternative reactions may become more significant as the recombination of atomic carbon with molecular or atomic N **[Ma, Q. et al., 2011][Zelinger, Z. et al., 2003][Abdelli-Mesaci, S. et al., 2002].**

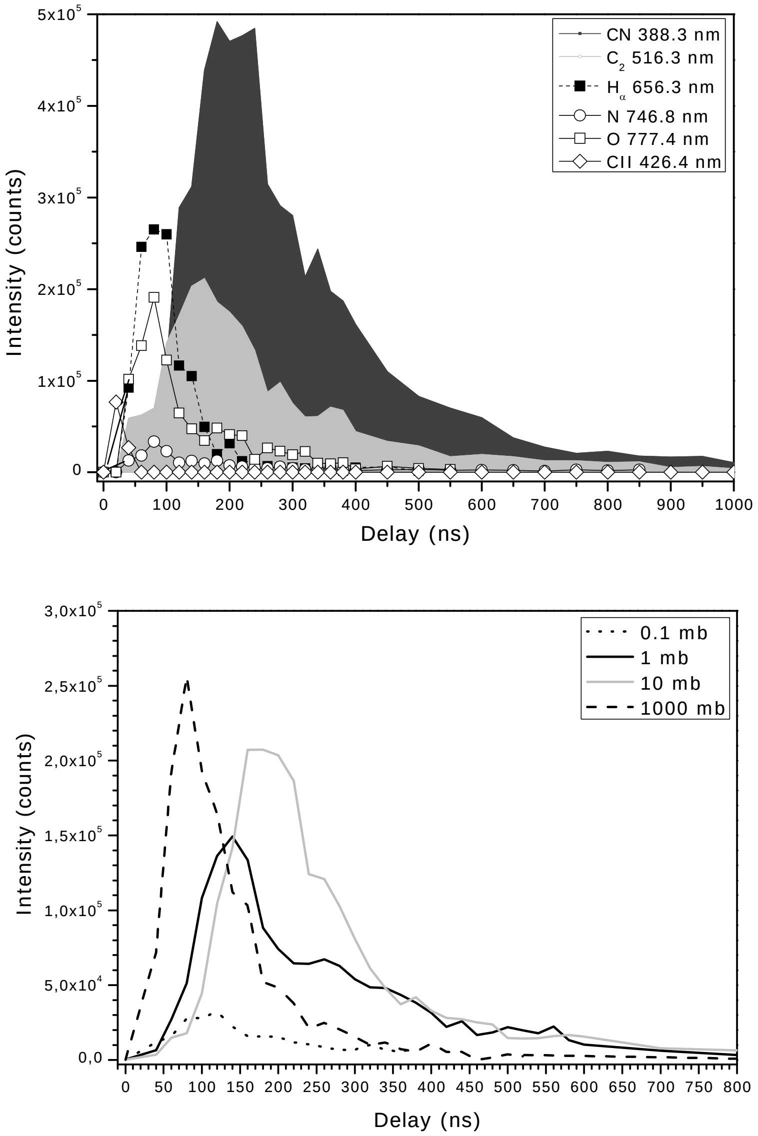

Figure 7.6. (a) Time-resolved evolution of main emitting species from TNT LIBS spectra (pressure 10 mb) (b) Time-resolved evolution of specific CN band (388.3 nm) from TNT LIBS spectra at different pressure levels. Gate width, 10 ns; Resolution, 20 ns.

All these possible routes for CN formation in ablation of organics have been thoroughly studied and deeply discussed in chapters 4 and 6 of the present memory.

7.5.3. Spatially-resolved study for emission species

In order to check the differences in the spectra as the plasma expands, a simple spatial distribution study of emitting species was performed. To get it, the collection fiber optic was attached to a three-dimensional micrometer stage to select the emission from specific zones of the plasma: next to sample surface area, plasma core and peripheral zone. The plasma image was slightly defocused on the plane of the fiber entrance. Thus, the distribution of species along the plume in the expansion direction was clearly observed using the orthogonal collection system. Selected pressure for study was 1 mb, as the size of generated plasma plume at such condition was the biggest (as showed Figure 7.1) so that we can evaluate properly the composition of plasma. However, it must be taken into account that, in these experimental conditions, the effect of air in both the kinetics of generation and dynamics of expansion of the plasma plume will be verifiable. The distribution of species along the plume in the expansion direction was clearly observed using the orthogonal collection system. Figure 7.7 shows the results obtained for pyrene and TNT at three different distances from the sample surface (0 mm, 2.5 mm, and 5 mm) in two selected regions of interest: 320-440 nm and 540-900 nm. Atomic species (H, N, O) were preferentially located near the target surface where the high electron density and electronic temperature allows full bond breakage, whereas excited molecules formed by reaction

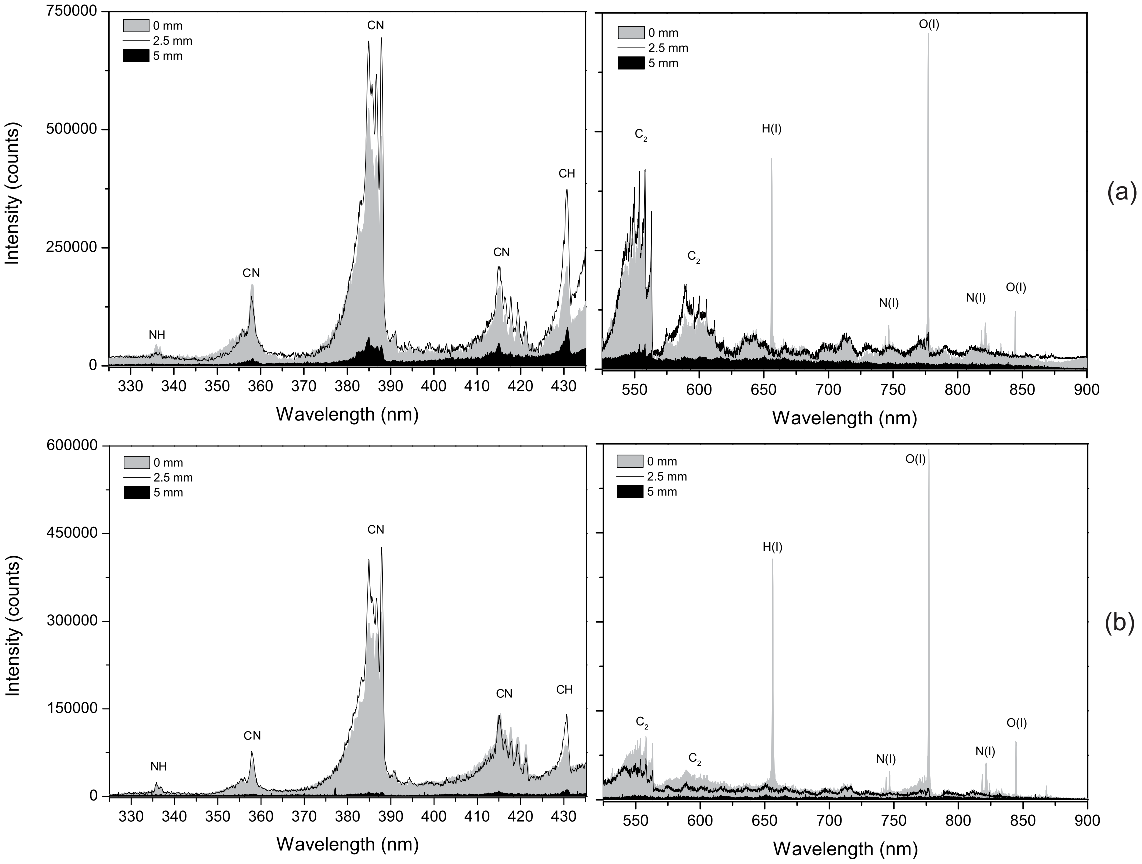

Figure 7.7. Spatially resolved LIBS spectra in the direction of expansion of (a) pyrene and (b) TNT. plasma plumes. Pressure, 1 mb. Each spectrum corresponds to the sum of 50 consecutive shots. Experimental conditions: λ, 266 nm; Fluence, 12.7 J/cm^2.

and recombination processes (CN, CH and C_2) were placed along the entire plume, decreasing their concentration only in the peripheral zone. Measurements beyond 10 mm length exhibited no trace of molecular emission bands.

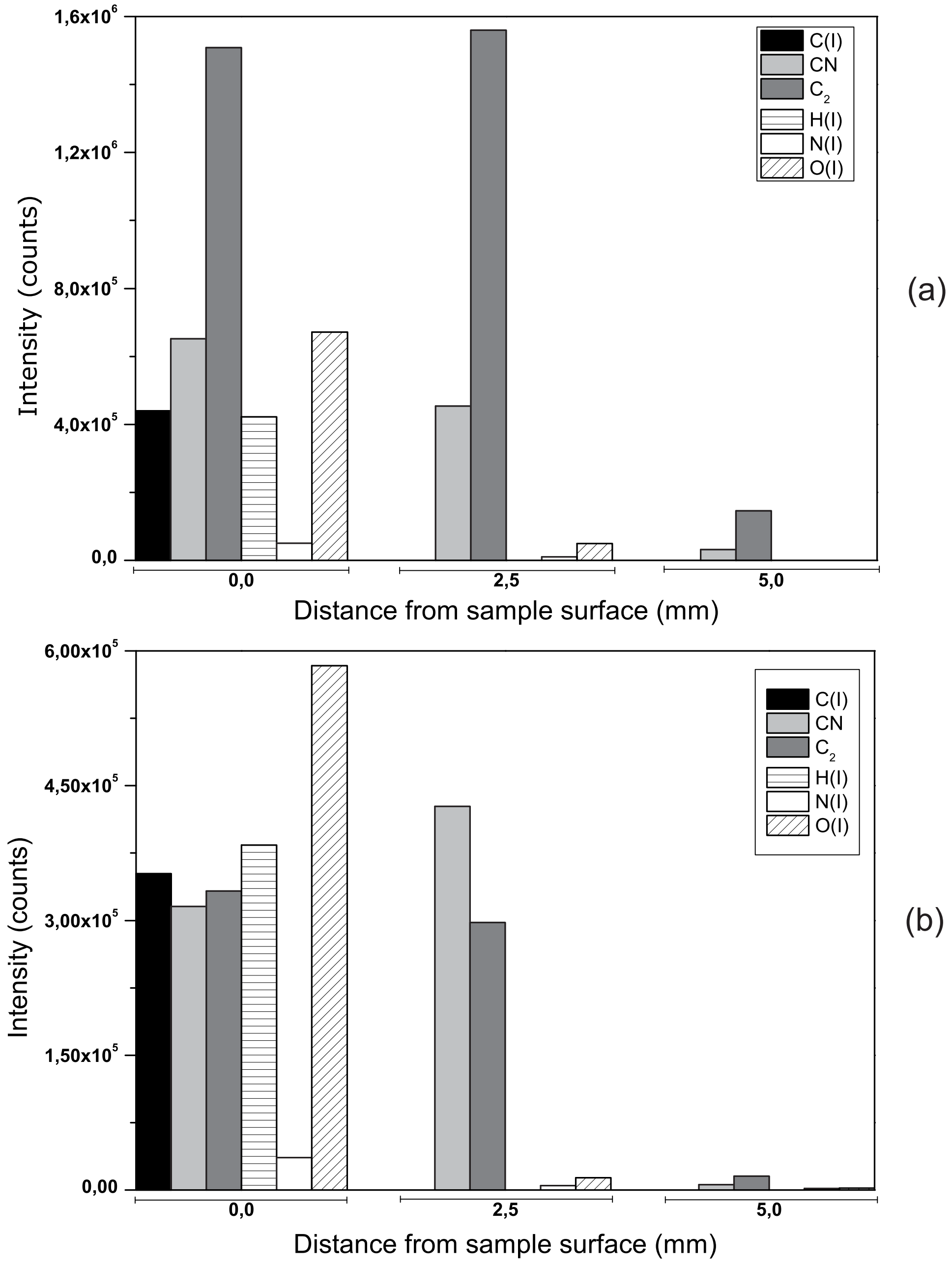

Figure 7.8. Spatial variation of signal intensity for C, N, O, H, CN and C_2 in (a) pyrene and (b) TNT. Experimental conditions: λ 266 nm; Fluence, 12.7 J/cm^2; Pressure, 1 mb; Sum of 50 consecutive shots. Intensity for C(I) emission line was multiplied by 10^2 factor for comparison.

From the spectra shown in Figure 7.7, it is possible to observe the selective presence of species along the propagation axis of the plasma. The results are summarized in Figure 7.8 for atomic (C, N, O and H) and molecular (CN and C_2) emissions. As shown, atomic emissions occur almost exclusively in the region closest to the sample surface. This fact is significant in hydrogen that is only visible near the surface, whereas N and O can be detected at a distance of 2.5 mm from the sample presumably due to the air interaction. In the same way, molecular bands are clearly detected at 2.5 mm at intensities almost identical that those at 0 mm, thus evidencing that the recombination process takes place during the expansion process.

On the other hand, the laser-induced plasma emission of pyrene at three selected pressure levels and at three different positions in the expansion direction of plasma were acquired. A sequence of time-evolution intensities for both C_2 ($\Delta\upsilon=0$) and CN ($\Delta\upsilon=0$) molecular emission signals are shown in Figure 7.9. For all measurements, the gate width for ICCD acquisition was set at 10 ns and delay steps of 20 ns were selected for time-resolution measurements. It was noticed, especially in the case of intermediate pressure (10 mb), a subtly displacement of the maximum in the intensity curves to longer times as the collection point moves in the direction of plume propagation for both molecular species, showing the dynamics followed by the excited fragments in the plume. At the same time, intensities of molecular emission signals vary with distance to sample surface. In the case of C_2 fragments, intensity decreases with distance for all tested pressures, suggesting that C_2 fragments come from direct fragmentation of the sample in a large extent during the laser ablation process. However, the highest intensity for CN emission takes place in the inner zone of plasma for the case of intermediate pressure of 10 mb. This is mostly due to reaction between ablated material and entrapped air into the plume. In the outer region of plasma (x = 6 mm) a remaining presence of CN fragments is still observed after several hundred of nanoseconds for intermediate and atmospheric pressures due to the effect itself of plume expansion besides reactions in the periphery of the plasma in contact with atmospheric nitrogen. However, there is no evidence of CN radicals at vacuum pressure as it results obvious due to the inexistence of nitrogen in the surrounding.

When high vacuum pressure is governing the system, velocity of escape of species is particularly high since there is no plasma confinement so interactions between species will be scarce. Therefore, the spatially-resolved study will be difficult and the lack of information becomes evident. On the other hand, if analysis is performed at atmospheric pressure, the size of plasma plume becomes smaller due to plasma propagation is slowed by impedance of the air during expansion, and part of

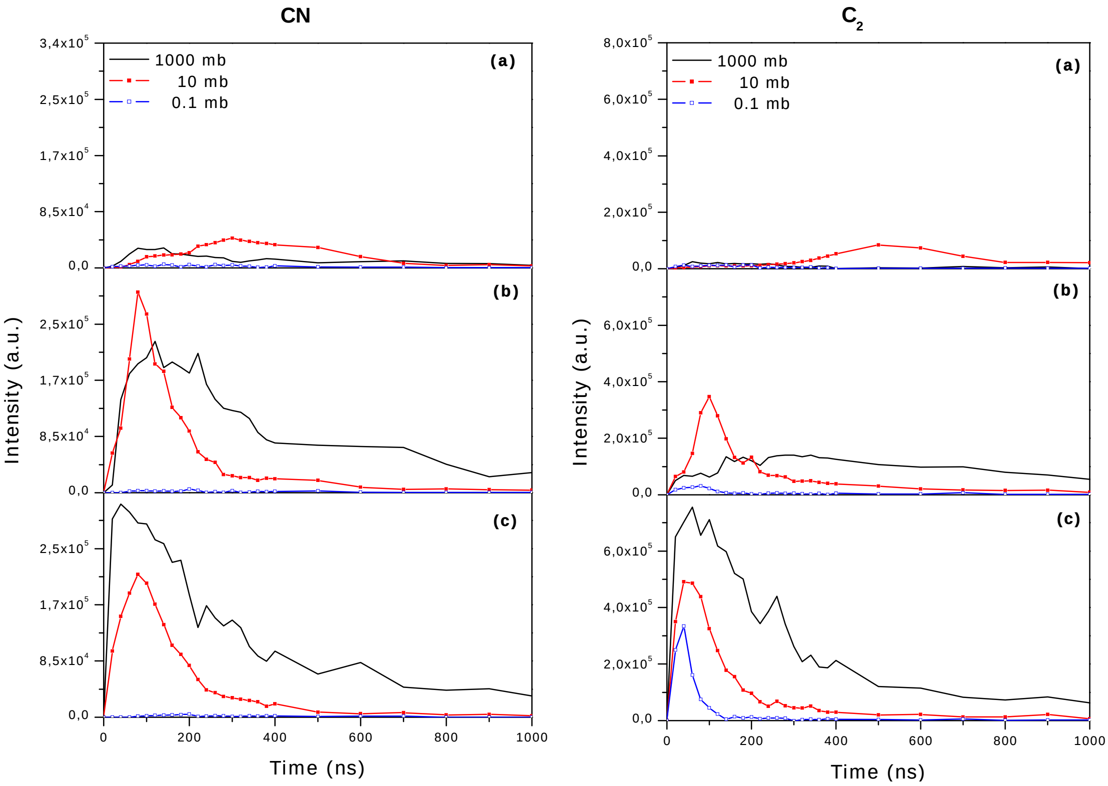

Figure 7.9. Spatially & time-resolved studies for molecular C_2 and CN species with pressure variation on pyrene sample. Data were acquired at different distances from the surface (a) 6 mm (b) 3 mm (c) 0 mm.

the radiation of laser pulse will be absorbed by the plume. Hence, these facts make the study complicated as well.

From obtained results, velocity of expansion of C_2 fragments in the plume was roughly estimated for the different pressure values in the system assuming that complete molecular emission comes from sample ablation. Thus, we estimated an average velocity of 32.5 μm/ns at 0.1 mb pressure measured at a distance of 3 mm, while at atmospheric pressure, the calculated value was reduced to 10 μm/ns at the same distance. In the case of 10 mbar, the calculated velocity was 21.4 μm/ns at 3 mm and it was reduced to 12 μm/ns when it was measured at a distance of 6 mm in the plume expansion. These values fit properly to the observed plasma lifetimes at each analysis pressure and the restrain effect produced by the air density.

7.5.4. Effects of pressure level on ablation rate

Emissions from laser induced-plasma are dependent on the ablation products and the plume chemistry, which is directly linked with the material composition. The ablation rate of organic samples is largely dependent on the amount of laser energy deposited in the sample as well as atmospheric conditions. Thus, to complete the study, measurements of the amount of ablated mass of TNT at different pressure levels and same energetic conditions were carried out. Each pellet was weighed before and after being subjected to 5000 laser shots (laser energy per pulse, 3 mJ). Results are showed in Fig. 7.10. Considerable changes in ablation rate of organic sample were detected as a consequence of changes in the physical characteristics of plasma due to the variation of pressure in the analysis. These changes lead to a shielding process at pressures next to atmospheric since the higher density and the excessive confinement of plasma avoided an effective absorption of energy by the sample since plasma itself worked as a barrier and the outer layers absorbed part of the laser beam energy. This effect became minimum at 10 mb, pressure at which the highest ablation rate was achieved. At such a pressure level, the most intense LIBS spectral emissions of molecular bands were also reached, indicating greater material available to react with surrounding air. At lower pressures, excessive unconfined plasma related to the collisionless free expansion in a laminar medium induced a poor molecular emission but intense atomic emission with high peak resolution. The ablation rate was, then, slightly lower due to high scape velocity of species from sample surface and less confined plasma.

Table 7.1 summarizes the effect of pressure on both the confinement of plasma and the ablation process for analyzed organic compounds.

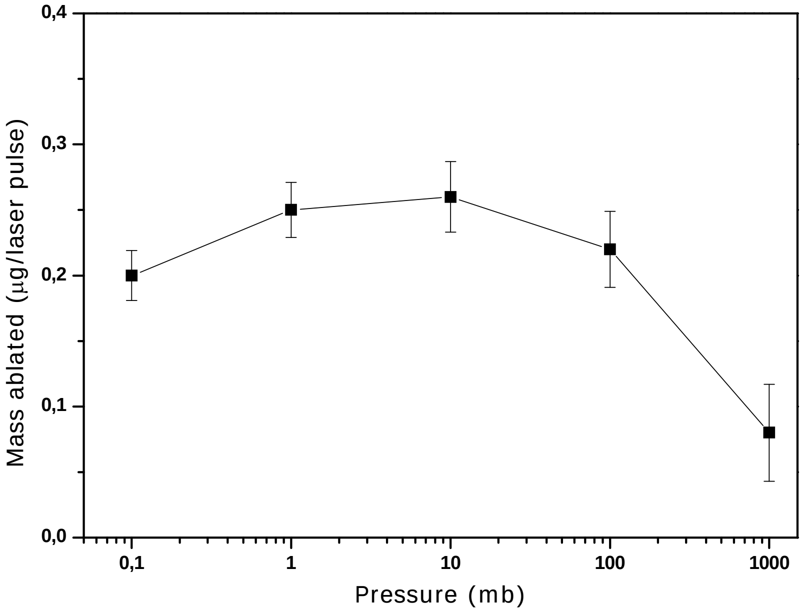

Figure 7.10. Evolution of mass ablated depending on analysis pressure for TNT sample. Laser wavelength, 266 nm. Energy pulse, 3 mJ.

Table 7.1. Effects of pressure level on ablation rate for organic compounds.

	Low pressure	***Moderate pressure***	***High pressure***
Density	Low	Moderate	High
Plasma expansion	Unconfined	Confined	Very confined
Absorption of laser energy by sample	High	High	Moderate
Absorption of energy by plasma (shielding)	Low	Low	Moderate
Ablation rate	Moderate	High	Low

7.6. CONCLUSIONS

In this work, truthful information about the influence of ambient pressure on the kinetics of excited atomic, ionic and molecular species in the laser ablation plasma as well as on the interaction between such species and surrounding air in the plume and, finally, on the dynamics of plasma expansion, have been obtained for selected organic aromatic compounds. Time and spatially resolved studies have been carried out as tool for characterization of dynamics and evolution of emission species in plasma. Finally, the importance of pressure on the ablation rate of organic samples under specific excitation conditions was shown.

Results have showed that pressure level becomes a critical parameter in LIBS trials so that the adequate control of this parameter can enhance to a large extent the features of generated emission signal applied in the analysis and distinction of organics materials. Therefore, changes in density of ambient atmosphere have a strong influence on dynamics of plasma expansion and the subsequent optical spectral information. Effect of air on LIBS signal began to be evident from 0.01 mb upward, whereas at 1 mbar pressure the plume reached the maximum volume and light intensity in the case of both NC and PAH analyzed samples. That was in agreement with the corresponding emission signals since at intermediate pressures the spectra showed great species richness and the highest intensity for atomic nitrogen and oxygen species, evidencing chemical activity between ablated material and excited air in the plume.

In time-resolved analysis, our LIBS system was able to measure the onset and extinction instants for ionic, atomic and molecular emission species resolved in a time-sequential process, by previous optimization of pressure conditions for each compound.

As for molecular fragments, results suggested that C_2 emission is strongly linked to molecular structure and come mainly from sample ablation, whereas CN radicals are mostly produced by chemical reactions and recombination processes. In fact, spatially-resolved studies of pyrene found out an appreciable CN emission in the core of plasma due to the interaction of native species with dissociated nitrogen molecules. LIBS spectrum of pyrene at high vacuum regime showed no evidence of CN emission. However, the presence of CN bands system for TNT at very low pressure suggested the production of excited molecular fragments by means of direct fragmentation and interaction between species from the organic molecule itself.

Changes in pressure level modified ablation rates in organic samples for UV nanosecond laser irradiation, achieving maximum values for intermediate pressure due to an optimum plasma confinement and to the absence of plasma shielding.

CHAPTER 8

Insights on the Acting Role of Background Gas in the Formation Pathways of Emitting Species in Laser-Induced Plasmas of High Energetic Nitro Compounds

8.1. SUMMARY

The aim of the present study was to analyze the influence of ambient air and other buffer gas environments (both reactive and inert atmospheres) on the characteristic emissions of excited atomic and molecular species coexisting in the laser-induced plasmas of ablated organic compounds. Solid samples were analyzed by LIBS at different pressure levels in diverse gas environments (air, N_2, O_2, H_2, He and Ar). This work completes the studies carried out in previous research (chapters 6 and 7) analyzing the behaviour of plasmas by using new background atmospheres in the surrounding of the irradiated samples.

Results from acquired emission spectra verified that molecular emission resulting after nanosecond laser ablation of organic samples depends not only on structural and chemical composition of the compound, but also on pressure level and nature of buffer gas present during the analysis, affecting the dynamics and composition of plasma by the direct interaction between ablated species in the plume and molecules from the background gas.

8.2. INTRODUCTION

Laser-Induced Breakdown Spectroscopy (LIBS) applications are tipically performed at ambient atmospheric conditions mainly due to operational reasons and flexibility. When analysis is performed over organic compounds in air atmosphere, it is well-accepted that the emission signals are clearly affected by the presence of aforesaid air in the vicinity of sample surface **[De Lucía Jr., F. C. et al., 2003][Baudelet M. et al., 2007][Lucena, P. et al., 2011]**. Even oxygen and nitrogen free-samples as PAHs or pyrolytic graphite have shown emission from air dissociation or the result of reactions between species in plasma plume and ambient air **[Portnov, A. et al., 2003 A][Baudelet, M. et al., 2007][[Park, H. S. et al., 2004].** However, interest in LIBS using other atmospheric conditions has increased in recent years, especially for use in space exploration **[Knight, A. K. et al., 2000]** (e.g., Lunar and Mars) or to improve resolution for isotopic signatures **[Mao, X. et al., 2011 A][Mao, X. et al., 2011 B]**. The phenomenon of interaction between plasma and excited ambient air also occurs with other buffer gases existing in the surrounding of the irradiated surface, and the degree of interference will depend on different variables such as those physical properties of the background gas, the nature of the analyzed material, the chemical composition of the ensuing plasma and finally, the pressure level established to carry out the measurements. Likewise, final emission intensity will primarily depend on parameters of laser source used in the ablation process as radiation wavelength, pulse duration and energy density, among others **[Fortes, F. J. et al., 2013]**.

In the case of air atmosphere, ambient pressure directly affects the plasma properties such as electron density and temperature, the dynamics of the plume expansion and the interactions between the rising species in the plasma (excited or ground-state neutrals, electrons and ions) and molecules of surrounding air. In this process, high energy density and temperature conditions favour the dissociation of N_2 molecules from air which can recombine or react with species from ablated material, mainly forming the characteristic CN fragments. The pressure level established in the system largely conditions the rate of interactions occurring within the plasma. Therefore, the final emission spectrum acquired from the plasma will be formed by a main contribution coming from native species corresponding to the elemental composition of the sample and another contribution relative to the interactions of such species with the surrounding air **[Baudelet, M. et al., 2008]**. From an analytical standpoint, it is crucial to be able to minimize atomic and molecular emission signals coming from interference with buffer gases, or to control this type of emissions so that the contribution can be separated from the total intensity recorded in the spectrum.

The study of the interaction between the plasma and the background gas becomes a fundamental aspect in the usage of optical emission techniques for a suitable identification and discrimination of organic compounds, so that interferences of surrounding in acquired signal can be identified and quantified properly. Furthermore, this type of study can shed light on the extent which gases of different nature can interfere in generation of excited species and fragmentation routes followed by organic compounds under laser ablation.

In-depth studies on the effect that the atmosphere has on emission intensity and plasma characteristics during LIBS measurements have been published **[Vadillo, J. M. et al., 1999]**. Iida studied the effect of Ar, He and air atmospheres on iron samples by laser excitation and the changes in plasma properties with pressure variation **[Iida Y., 1990]**. Aguilera *et al.*, in turn, did the same with laser-induced plasmas from steel samples and found important differences depending on the background atmosphere **[Aguilera, J. A. et al., 1999]**. Lee et al. studied the influence of different noble gases as surrounding atmospheres on pressure broadening and self-absorption in atomic cooper emission lines in order to improve intensity and resolution of spectral signals. Lee related these changes to differences in physical parameters of plasma depending on the nature of existing atmosphere **[Lee, Y. I., 1997]**. Other authors have researched about the potential use of LIBS for space exploration applications. That is the case of Salle *et al.* **[Salle, B. et al., 2005]** and Brennetot *et al.* **[Brennetot, R. et al., 2003]**, whose studies involved the analysis of soils and clays primarily in CO_2 and low air pressure environments simulating Mars and Lunar atmospheres. They found clear improvements in spectral features when they compared with emission acquired in atmospheric conditions. Recently, as the prime example of the application of emission spectroscopy in Martian atmospheres, the *Curiosity rover* was successfully launched to Mars surface as part of NASA's Mars Science Laboratory mission (MSL). The ChemCam instrument was integrated for chemical analysis of Martian rock and soil composition using LIBS technology.

The study presented below has focused on the analysis of the optical emission response obtained by LIBS from energetic nitro compounds sampled in atmospheres of different nature. Important pathways involved in the formation of atomic and molecular emission species by interaction of the vaporized sample with molecules present in the medium are thus revealed. For a given background gas, the pressure level into the ablation chamber was changed within a controlled range in order to modify the gas density and as consequence, the interaction plume-surrounding gas.

Firstly, reactive atmospheres of oxygen and nitrogen were used, and then hydrogen gas was tried as background gas. Finally, analysis with noble gases such as argon and helium were carried out, establishing a final discussion about emission features and plasma composition as a function of interactions with background gas in the laser ablation.

8.3. EXPERIMENTAL

The scheme of the experimental set-up is shown in Fig. 2.19 in Chapter 2 of the memory. Details on the laser excitation were described in previous chapters (266nm, 4.5 ns pulse width).

The chamber was equipped with a pumping system, an entry needle valve, gate valves and check gauges as well as gas inlets and an exhaust line to change the sampling buffer gas of analysis. The compressed gases used as buffer atmospheres were namely, air, N_2, O_2, H_2, He and Ar. Their main physical properties are summarized in Table 8.1. In the case of working with hydrogen gas, additional safety requirements were established in the experimental set-up. The chamber was completely isolated and a purge system with argon gas was installed to avoid the contact of H_2 with air and, therefore, the possible formation of explosive mixtures. Pressure into chamber was real-time monitored using a *pirani gauge TPR 280* which allowed checking pressure within a certain range depending on the type of atmosphere (interval 10^{-4} - 10^{3} mb in the case of air). The collection system was similar to that used in previous studies. A dispersive grating of 599 lines/mm which led a spectral range of 45 nm was used to obtain high-resolution spectra from time-integrated plasma composed of several overlapping spectral measurements (each one consisting of 30 accumulated spectra). The detection gate delay and the gate pulse width were set in 50 ns and 1 ms respectively for time-integrated measurements. The detected emission signal from molecular species was measured in the band heads, where the signal intensities were stronger. In the case of emission lines from atomic and ionic species, the peak intensities were taken for the study. In all cases background was subtracted from raw signal.

8.4. SAMPLES

Two aromatic compounds, 2,6-dinitrotoluene (2,6-DNT) and 2,4,6-trinitrotoluene (TNT) and an aliphatic compound, pentaerythritol tetranitrate (PETN), were selected as high energetic molecules. Pyrene, a polycyclic aromatic hydrocarbon

Table 8.1. Properties of background gases.

	Atomic number	Density (kg/m^3) 25ºC, 1 atm	Molecular weight	Thermal conductivity ($W \cdot m^{-1} \cdot K^{-1}$)	Binding Energy (kJ/mol)	Limit for pressure control (mb)
Hydrogen	1	0.09	2	0.175	432	3.5
Helium	2	0.17	-	0.147	-	4
Air	-	1.18	28.9	0.026	-	1000
Nitrogen	7	1.17	28	0.026	941.7	800
Oxygen	8	1.33	32	0.026	493.6	1000
Argon	18	1.66	-	0.017	-	50

compound (PAH), was also used for ulterior comparative analysis. TNT and PETN samples were acquired from National Department of Defence whereas 2,6-DNT and pyrene were purchased from Sigma-Aldrich company. Pellets preparation was made following the procedure described in previous chapters. The samples were fixed onto the aluminium holder that was introduced in the analysis chamber by means of a direct insertion probe and were moved continuously during analysis in order to have a fresh surface in each laser shot.

8.5. RESULTS AND DISCUSSION

8.5.1. Air as background gas

A thorough study on the influence of air pressure on the LIBS response of organics was carried out previously in Chapter 7 of the present memory. It was demonstrated how oxygen and nitrogen from ambient air contribute to the total emission intensities of those atomic species and, on the other hand, to the formation of characteristic molecular species in time-integrated LIBS spectra. That made difficult the application of spectral intensity ratios from integrated spectra as specific markers of organic compounds in open air.

As mentioned earlier, dissociation of air molecules and subsequent excitation in the vicinity of the irradiated area by the laser pulse alters the kinetics of plume expansion as well as the composition of plasma plume due to the chemical reactions between laser-induced plasma components and the surrounding gas. Therefore, when LIBS analysis is performed in air atmosphere, the observed emissions of specific components of the sample suffer interferences with emission from ambient air.

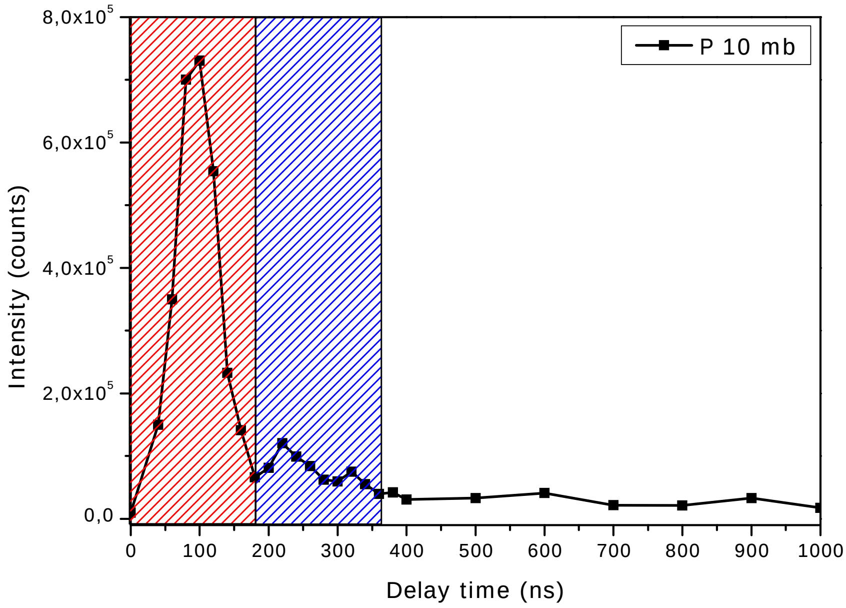

Figure 8.1. Time-resolved study of CN molecular emission band $\Delta\upsilon$=0 (388.3 nm) collecting the plasma core at 10 mb air pressure for TNT. Gate width pulse, 10 ns. Fluence, 12.5 J/cm^2.

As primary evidence, it was observed how CN bands presented a longer life-time compared to that showed by C_2 emission presumably due to recombination processes with atmospheric nitrogen. Another evidence of the kinetics of recombination in presence of air within the plasma is showed in Figure 8.1. At pressures between 1 and 10 mb and after the main prompt component of CN molecular emission (red pattern), it was subtly observed a delayed component around 250 ns after laser shot (blue pattern) presumably due to secondary reactions of recombination of atomic C with molecular or atomic nitrogen that assist CN formation **[Ma Q. et al., 2011][Zelinger, Z. et al., 2003][Abdelli-Mesaci, S., 2005].** Moreover, persistence of species was longer at low vacuum pressures as it was showed in Chapter 7, including CN fragments, so that the average duration of plasmas was also more lasting. The higher concentration of CN fragments implies a higher rate of collisions in the plume. Nevertheless, this rate reduced for lower pressures up to high vacuum. This effect is mainly due to both an overly large dispersion of particles and a low ablation rate by the lack of plume confinement. For higher pressures up to atmospheric, however, due to a greater density in the plasma plume, the collisional rate increases but in this case this means a lower ablation rate assisted by a rising shielding effect.

In Chapter 3, the influence of laser wavelength on organic desorption/ ionization process was studied. The ionization of 2,6-DNT was performed using 1064 nm, 532 nm and 266 nm radiations and the resulting mass spectra were compared. It was observed how IR laser sampling implied a less efficient ionization together with the ablation of larger amount of material and thus, an extensive fragmentation took place due to a higher contribution of electron-impact phenomena. However, for shorter wavelengths and especially for UV pulsed radiations, mass spectra presented a richer fragmentation pattern with high peak resolution. Moreover, a minimum amount of material was removed in ablation due to less thermal effects took place, increasing photo-ionization processes that led to a more efficient fragmentation of the organic sample.

In the present work, a similar study was carried out on the same organic sample (2,6-DNT) in order to compare the resulting emission signal when the sample was irradiated by laser pulses of different wavelength but using equal energy density (27 J/cm^2). Concretely, effects of 1064 nm versus 266 nm radiations were compared at three different pressure conditions, namely atmospheric, low vacuum (0.2 mb) and high vacuum ($4.0 \cdot 10^{-5}$ mb) regimes. As can be concluded from Figure 8.2, laser ablation using IR radiation resulted in stronger atomic emission than in the case of irradiation with UV laser pulses. The phenomenon occurs as pressure and subsequent plume confinement decreases. Moreover, the effect intensifies at low vacuum pressure (Figure 8.2(b)), a condition to which ablation process is highly favoured as it was concluded as well in Chapter 7 of this memory.

Once more, this behaviour could be related to the radiation nature and their photon energies. In the case of using infrared wavelength consisting of low energy photons (1.17 eV), the photo-thermal effects are predominant, whereas in the case of irradiating the sample with shorter ultraviolet radiation and higher energy photons (4.66 eV), the effects are based on photo-chemical processes. Thus, energy brought into play is used on different way in the excitation of atomic levels depending on this photon energy. For IR radiation, thermodynamic parameters as enthalpy and heat capacity of the material are directly involved in both the ionization and the ablation of the sample into plasma as thermodynamic open system. This is mainly due to the low energy absorption rate of IR radiation by these organic compounds and the high absorption of such laser radiation by the plasma that attenuates the laser energy reaching the sample surface and, subsequently, reducing the ablation rate, increasing at the same time the temperature of the plasma. **[Geertsen, C. et al., 1994]**. On the other hand, in the case of using UV radiation of 266 nm, the coefficient of energy absorption is greater and the plasma is generated by efficiently ionized species from a minimum amount of ablated material. In the specific case of aromatic compounds, the soft fragmentation process goes through the typical ladder-climbing reaction by means of reaction intermediates. Then, physical parameters related to heat effects are not as vastly involved in UV ablation as in the case of irradiation with IR wavelengths.

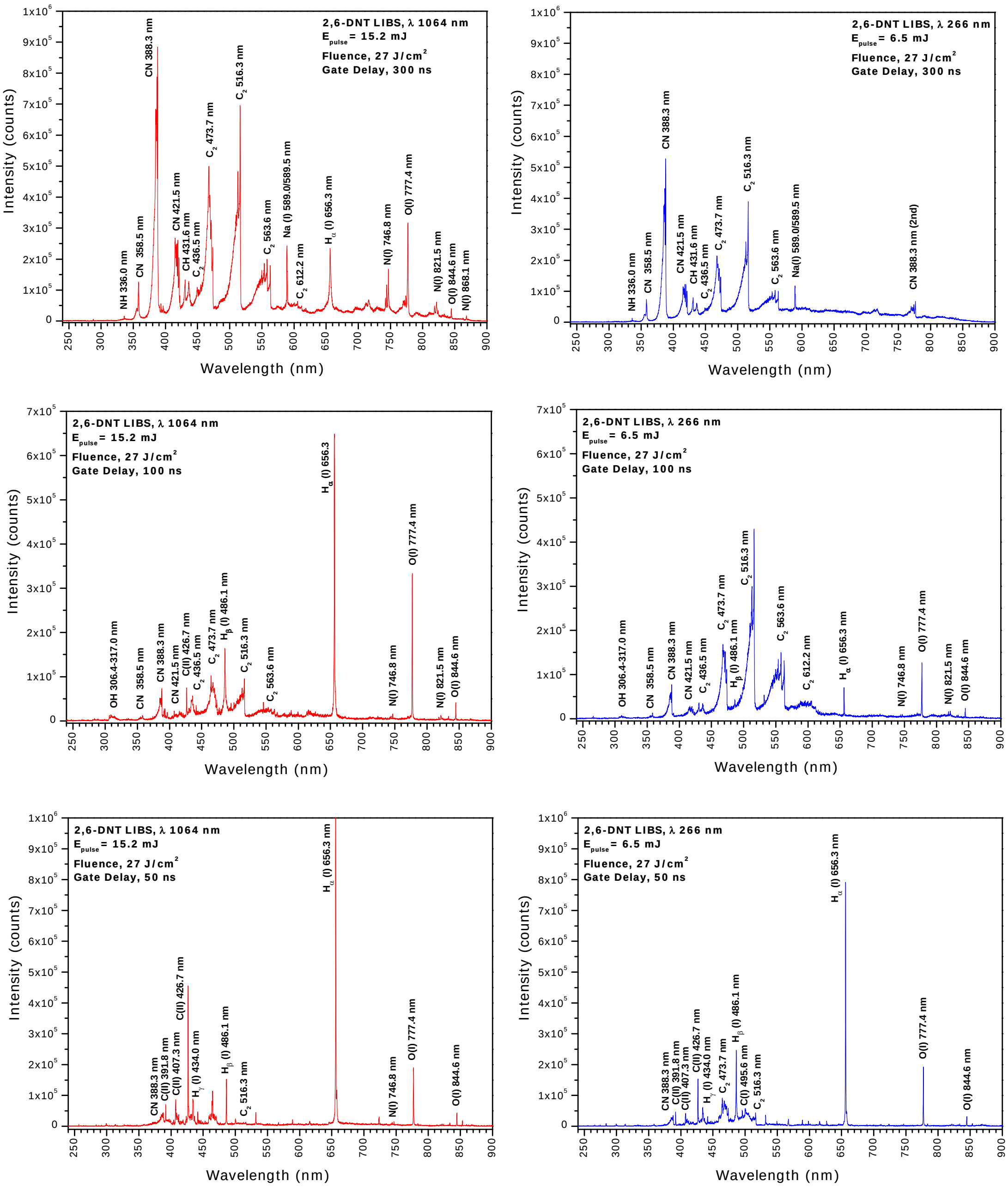

Figure 8.2. LIBS spectra for DNT using 266 nm and 1064 nm laser radiations and acquired at (a) air pressure, (b) low vacuum pressure, 0.2 mb, and (c) high vacuum pressure, $4.0{\cdot}10^{-5}$ mb.

In order to study in depth the molecular emission as a function of surrounding density, the relative intensities of emission lines in the CN ($\Delta\upsilon=0$) and C_2 ($\Delta\upsilon=0$) bands, generally known as *vibrational emission* and corresponding to transitions between different energy levels in the molecule, were studied. A previous work **[Fernández-Bravo, A. et al., submitted]** concluded that the response in vibrational band emission depends mainly on the structure of the organic material, but factors as irradiance level deposited on the surface or time evolution of plasma also influenced noticeably the internal distribution of the transitions. These parameters altered the excitation state of the levels related to the vibrational modes in the molecule. The Figure 8.3 shows the evolution of intensity ratio between the vibrational modes (0,0) and (1,1) for both C_2 ($\Delta\upsilon=0$) and CN ($\Delta\upsilon=0$) emission bands as pressure of the system increases in laser ablation of TNT. The experiment was carried out in both air and oxygen atmospheres.

As observed, CN emission presented subtly variations in both atmospheres, tending to equalize intensity values of both vibrational modes. This indicates a no dependence of CN internal distribution with the nature of the surrounding gas, and a slight influence of pressure level on the intensity ratio. However, variation of intensity ratio with pressure was more noticeable in the case of C_2 molecule, resulting in a trend opposite for each background gas. This fact suggests that both the density and the nature of the background gas existing in the surrounding of the ablation site affect somehow the distribution of vibrational modes of such molecular species.

When we repeat the study comparing TNT and pyrene in air, results indicated that pressure level influenced notably the distribution of the vibrational levels in the excitation of molecular species especially for PAH sample. In the case of the explosive molecule, subtle variations were observed in the distribution of energetic states. This effect is shown in Figure 8.4. This fact can be taken as a sign that influence of nitrogen and oxygen molecules in air on the recombination reactions leading to the formation of new C_2 and CN molecular species is crucial in the case of pyrene molecule (without N or O atoms in its structure). Regarding TNT, chemical pathways will be different considering that native nitrogen and oxygen in the molecule are also involved in the routes of formation of molecular species.

This is further evidence that the existing atmosphere has a basic contribution in the ablation process, as discussed in the following sections.

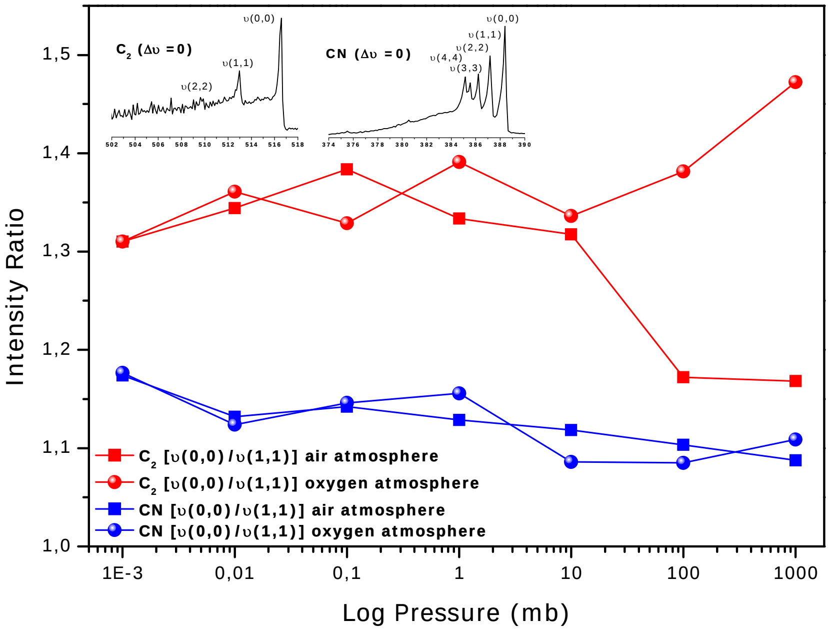

Figure 8.3. Intensity ratios between two transitions of both CN (Δυ=0) and C$_2$ (Δυ=0) emission bands as a function of air pressure and oxygen pressure for TNT.

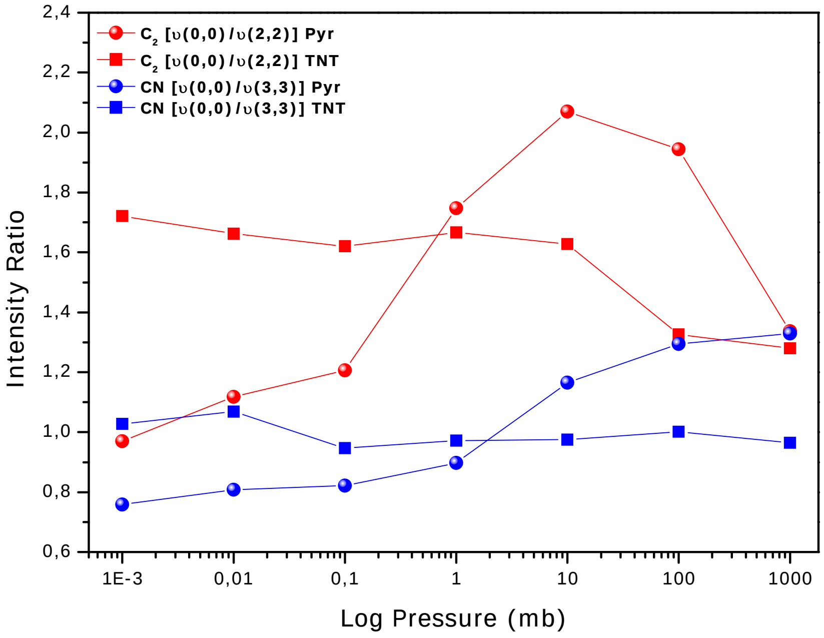

Figure 8.4. Intensity ratios between two transitions of both CN (Δυ=0) and C$_2$ (Δυ=0) emission bands as a function of air pressure for TNT and pyrene.

8.5.2. Nitrogen and oxygen as background gases

Nitrogen is considered as a reactive gas once the breaking of its strong triple covalent bond occurs during the laser ablation process. The binding energy for nitrogen molecule (9.8 eV) is higher than for oxygen molecule (5.2 eV). Energetic materials as TNT and PETN were examined in oxygen and nitrogen atmospheres as well as in the presence of air. Pyrene was also investigated to support some of our hypotheses.

Both broadband LIBS spectra and certain spectral regions (corresponding to the wavelength range where species of interest are emitting) were acquired as a function of pressure inside the ablation chamber. The minimum pressure value that could be stabilized into the chamber with a looped gas circuit for oxygen or nitrogen flow was 0.1 mb. In any case, below this pressure level, system can be considered traced with oxygen or nitrogen gas since gas density is not high enough to modify the emission signals or the characteristics of plasma in a substantial way. Spectra acquired below ca. 0.01 mbar are virtually identical to those obtained in high vacuum with no presence of the buffer gas.

Figure 8.5 shows emission spectra of TNT in air, nitrogen and oxygen acquired at a pressure of 100 mb. At first sight, we can observe a slight higher intensity of CN in the case of nitrogen atmosphere. This is due to the higher concentration of nitrogen available to react with ablated particles in the plume. The abundance of CN is lower in air as a consequence of a lower partial pressure of nitrogen in the mixture. The presence of C_2 emission in the three atmospheres indicates that this emission results from dicarbon fragments directly released from the aromatic ring. We were not able to detect atomic carbon in any of our measurements, at least with the settings used in the instrument.

Thus, it seems clear that when molecular nitrogen is available in the atmosphere, recombination of carbon species with nitrogen molecules to form CN fragments is the dominant process. Such a larger concentration of CN molecules is probably due to reactions (8.1) and (8.2) **[Vivien, C. et al., 1998][Dong, M. et al., 2011]**:

$$C_2 + N_2 \longrightarrow 2CN \qquad (8.1)$$

$$C + N_2 \rightleftharpoons CN + N \qquad (8.2)$$

In an atmosphere of oxygen, a drop in N and CN signals is expected due to the absence of nitrogen in the surroundings in comparison with spectra acquired in air or in nitrogen. In fact, Figure 8.5 shows that atomic nitrogen lines at ca. 750 nm are virtually absent in the oxygen ambient. However, the intensity for CN was similar to that in air. Another remarkable feature was the large abundance of CH (431.4 nm) existing in oxygen. These observations will be discussed below.

Figure 8.5 also shows that the abundance of C_2 is the largest in the nitrogen environment. On the other hand, ratio C_2/CN was found constant for all tested atmospheres, suggesting a possible interlink between C_2 and CN molecules during the ablation of nitro aromatic compounds. Therefore, an inter-crossing reaction (8.3) of CN and C_2 is thought to take place in plume chemistry **[Ma, Q. et al., 2011]**,

$$C_2 + N \rightleftharpoons CN + C \qquad (8.3)$$

In the atmosphere of oxygen, the CN emission exhibits a similar intensity to that found in air. CN fragments in this case must derive exclusively from reaction of native species from TNT, as no other source of nitrogen is available. Thus, the main route leading to CN formation will follow reaction (8.3). Dicarbon molecules necessary for this reaction result from ring opening, whereas nitrogen atoms are available via dissociation of NO, which in turn is released from nitro groups detached from the ring. Two additional paths could also take place **[Ma, Q. et al, 2011][Sovová, K. et al, 2010]**:

$$C + NO \rightleftharpoons CN + O \qquad (8.4)$$

$$C_2H_n + N \rightleftharpoons CN + CH_n \qquad (8.5)$$

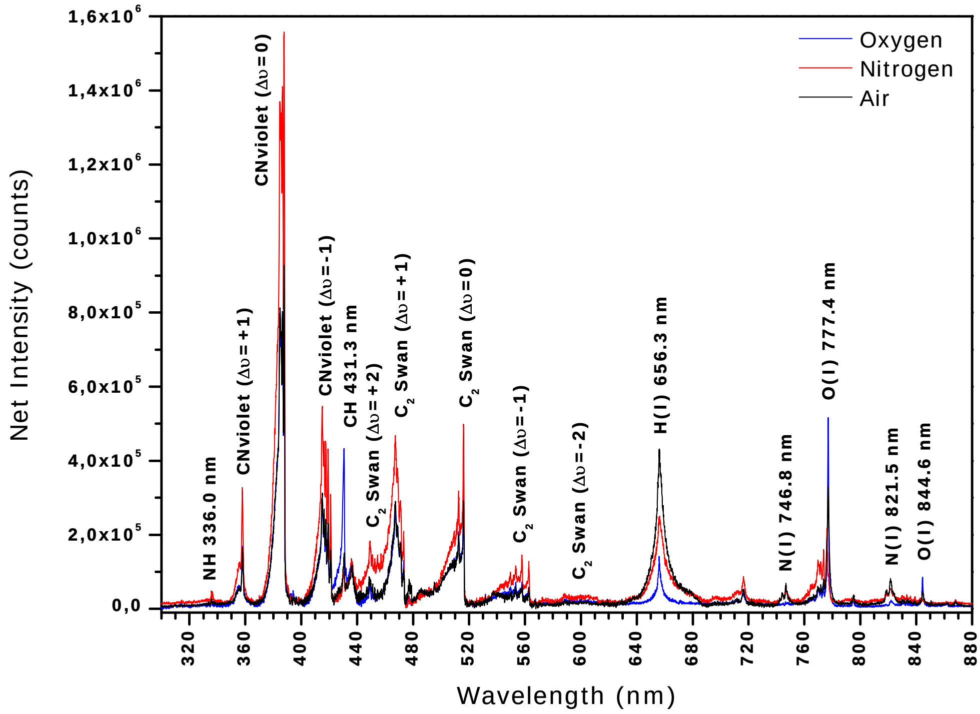

Figure 8.5. LIBS TNT spectra acquired in different atmospheres. Fluence, 12.5 J/cm^2. Pressure, 100 mb.

Hydrocarbon radicals (CH_n) can then lose hydrogen atoms leading to the formation of CH species via the route (8.6) indicated below. This fragmentation is thought to be favoured in oxygen atmosphere as an outstanding emission is observed for CH molecular system with the head band emitting at 431.4 nm in the TNT spectrum, indicating a high concentration in the plume. The reasons for this effect are not clear, but may be related to the high reactivity that atomic oxygen dissociated from O_2 molecules confers to the plasma.

$$CH_n \longrightarrow CH_{n-1} + H \qquad (8.6)$$

Pyrene also exhibits notable differences in the characteristic emitting species in different background atmospheres. Figure 8.6 shows the corresponding spectra. As oxygen and nitrogen are absent in this molecule, an analysis of pyrene spectra provides interesting insights into the processes occurring in the different atmospheres. As expected, O emission was only observed in oxygen, whereas CN fragments and N emissions were only seen in air or nitrogen atmospheres. Therefore, CN emission derives entirely from reaction with dissociated nitrogen from the buffer gas (as discussed in Chapter 7 of the memory). Following this premise, routes (8.1), (8.2), (8.3) and (8.5) are possible in CN formation. However, we believe that reaction (8.3) is the preferred pathway when the parent molecule is aromatic. As seen in Figure 8.6, the intensity of C_2 emission bands is by far the largest in oxygen, with progressive decreasing in air and nitrogen atmospheres. An almost opposite behaviour is exhibited by CN: absent in oxygen, and growing in nitrogen-containing atmospheres. Several authors claim that the four-center reaction (8.1) is not likely to occur due to its large activation energy **[Fuge, G. M. et al., 2006][De Lucía, F. C. et al., 2010]** and thus, C_2 species would be consumed mainly through route (8.3) to form CN species, thermodynamically more stable.

In summary, CN is not formed in oxygen atmosphere in the ablation of pyrene. In nitrogen or air atmospheres, CN is only formed from dissociation of nitrogen gas molecules that react with ablated carbon species. For TNT, however, there are alternative routes to form CN from native atomic nitrogen and other diatomic species, such as NO (reaction 8.4). Thus, the emission characteristics for both molecules are quite different in each case.

C_2 emission depends almost exclusively on the presence of carbon-carbon double bonds in the parent molecule. Routes leading to C_2 formation in oxygen atmosphere for pyrene, including direct fragmentation, are listed below **[Sovová, K. et al., 2010][Babushok V. I. et al., 2007]:**

$$[\mathrm{MOLEC}] \longrightarrow n\mathrm{C}_2 + \text{other prod.} \qquad (8.7)$$

$$\mathrm{CH}_n + \mathrm{CH}_m \longrightarrow \mathrm{C}_2 + (n+m)\mathrm{H} \qquad (8.8)$$

$$\mathrm{CO} + \mathrm{C} \rightleftharpoons \mathrm{C}_2 + \mathrm{O} \qquad (8.9)$$

However, reaction (8.9) towards right-side hand is unlikely in this case due to the large excess of oxygen in the medium and the presence of CO species is subjected to a previous recombination process in the plume.

On the other hand, interconversion reaction (8.10) must be a prevalent pathway for initial C_2 dissociation in oxygen atmosphere due to the intense emission band seen in the LIBS spectrum corresponding to the CH molecular system, with the head band emitting at 431.4 nm. Due to the initial high concentration of C_2 species, reaction favours to the right-hand side **[Babankova, D. et al., 2006]:**

$$\mathrm{C}_2 + \mathrm{H} \rightleftharpoons \mathrm{CH} + \mathrm{C} \qquad (8.10)$$

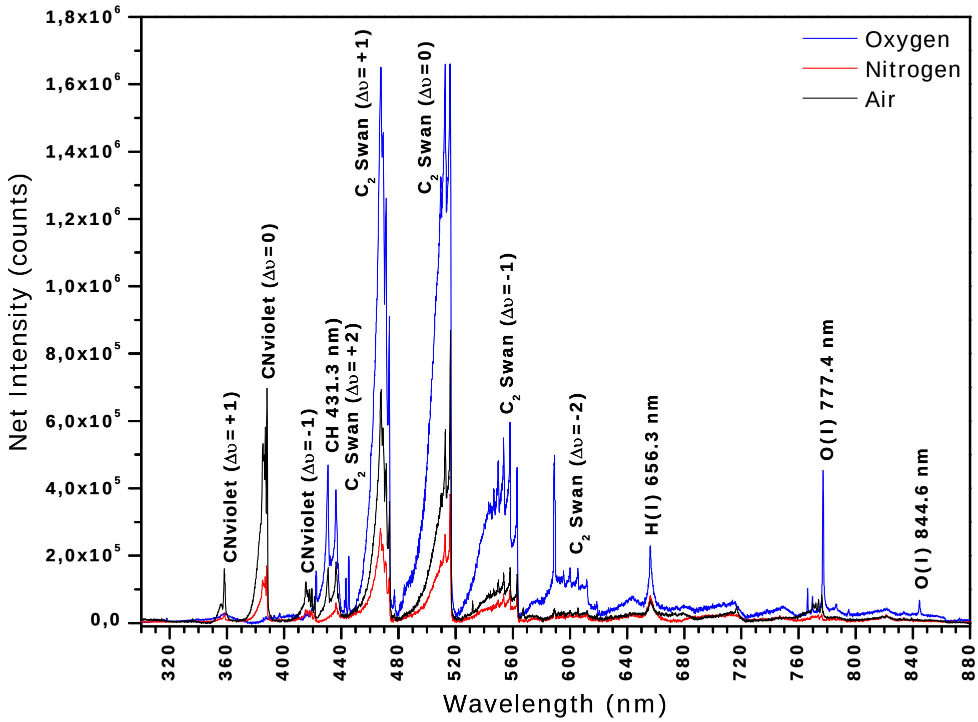

Figure 8.6. LIBS pyrene spectra acquired in different atmospheres. Fluence, 12.5 J/cm^2. Pressure, 100 mb.

Another possible route for CH formation is based on the loss of hydrogen atoms from hydrocarbon radicals previously indicated (8.6), but the lack of methyl radicals in pyrene probably implies a low extent for such reaction.

Reactions (8.7) and (8.8) could take place in nitrogen atmosphere as well. An alternative route in nitrogen atmosphere to form C_2 molecules would be reaction (8.3) towards the left-side hand, but in this case is clearly favourable the formation of CN fragments. Moreover, in presence of nitrogen gas, reaction (8.10) will not proceed to a significant extent due to the low CH concentration in the system. Reaction (8.5), meanwhile, will be also possible but is less probable due to the high degree of atomization occurring in plasmas within the first nanoseconds after laser pulse and at irradiances far from the onset of plasma emission, as is the case here.

In summary, it is worth noting that C_2 molecules are generated basically through the same pathways in nitrogen and in oxygen atmospheres. However, the key issue to understand the difference on the resulting molecular emission lies in interconversion C_2-CN reaction (8.3) that only takes place in the presence of nitrogen gas and favours the more stable CN formation and consequent consumption of C_2 radicals. In addition, CH higher emission observed in presence of oxygen gas probably has the same origin. Due to the absence of interconversion C_2-CN route in the oxygen atmosphere, a high concentration of C_2 species is generated in the plume, so route (8.10) will be favoured towards CH formation side. As discussed below, the observation that PETN exhibits no C_2 bands neither CH emissions is compatible with this explanation.

If analogous measurements are carried out on PETN, the observed behaviour could also give insight into the occurrence of certain pathways in the plume chemistry depending on background atmosphere. The influence of chemical structure of the ablated sample on emission signals is evident from the scrutiny of LIBS spectra shown in Figure 8.7. In general, the emissions observed are consistent with the structure of the molecule and the analysis presented above. As with TNT and pyrene, notable differences were found on signal intensities from O, N and CN depending on the buffer gas. CN emission becomes dominant in both nitrogen and air atmospheres. Since PETN has no carbon-carbon double bonds, C_2 fragments are absent as observed in the figure. Consequently, formation of CN must derive from reactions of atomic carbon with molecular nitrogen according to reaction (8.2). In the atmosphere of oxygen, the abundance of CN is much smaller. This molecule should be formed through reaction

(8.4) as nitrogen monoxide is one of the persistent molecules existing in the laser-induced plasmas of nitro compounds. Nitrogen monoxide can be further dissociated to produce atomic nitrogen, whose reaction with carbon could be an additional source of CN.

It is remarkable the higher emission intensities observed for atomic oxygen and hydrogen when using oxygen as buffer gas. In this case, the participation of diatomic species OH is crucial in the reactivity of the plume. CN molecules can react with water molecules present in the plume leading to OH formation **[Sovová, K. et al., 2010]**:

$$\mathrm{CN + H_2O \rightleftharpoons HCN + OH} \tag{8.11}$$

The presence of such species after laser irradiation has been confirmed by mass spectrometry studies performed on PETN (see Figure 6.5 in Chapter 6). Apart from the OH radical, generation of formaldehyde radicals (CH_2O) as a direct fragment from the rupture of the aliphatic molecule is also proposed. However, the unequivocal identification of this ionic species in the mass spectrum could not be confirmed since its mass was coincident with NO at *m/z* 30^+. Indeed, NO is one of the most abundant fragments derived from the rupture of nitroaromatic compounds. Nonetheless, route (8.12) was considered as feasible leading to high atomic oxygen and hydrogen concentration in the plume **[Sicilia, E. et al., 1994]**:

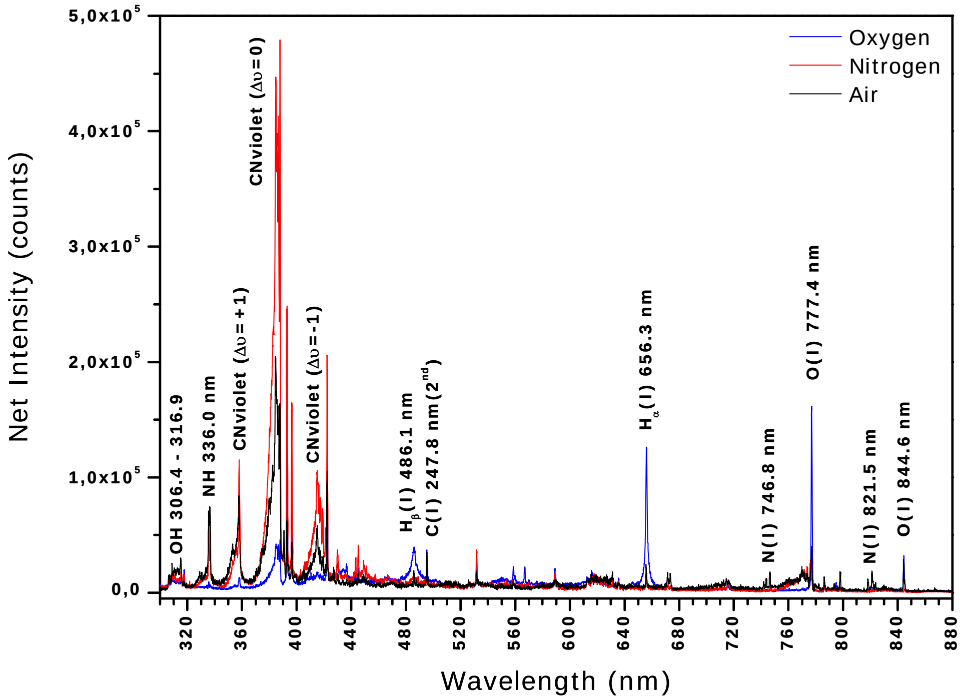

Figure 8.7. LIBS PETN spectra acquired in different atmospheres. Fluence, 12.5 J/cm^2. Pressure, 10 mb.

$$CH_2O + OH \rightleftharpoons CH_3O + O \qquad (8.12a)$$
$$CH_3O \rightleftharpoons CH_2O + H \qquad (8.12b)$$

Another interesting finding is the absence in PETN of CH emission in oxygen and nitrogen-containing atmospheres. This observation is consistent with the previous discussion as CH seems to be formed in organics mostly following reaction (8.10). Since in PETN emission C_2 is absent, no CH could be formed. Emission corresponding to NH appeared sharply at 336.0 nm both in nitrogen and in air atmospheres, likely as a result of the following reaction **[Civis, M. et al., 2011]:**

$$N + H_2 \rightleftharpoons NH + H \qquad (8.13)$$

Figure 8.8 shows the results of a comparative study that summarizes clearly the influence of buffer gas on emission response from plasmas of organic explosive compounds. Variations undergone by net intensities corresponding to emitting species of interest are sketched as a function of pressure level in the range between $1 \cdot 10^{-4}$ mb and 1000 mbar for each atmosphere. Intensity data correspond to the accumulated signal from a set of 100 laser pulses. It is noteworthy that, for a specific compound, the species present and their abundance at background pressures below 0.1 mb are equivalent in the three atmospheres tested. This means that the influence of the surrounding gas is only effective above a certain pressure, rated at ca. 0.1 mbar in our system. From this pressure onwards, collisions start to be effective both in the borders of expanding plume and conceivably inside the plume as a result of the entrainment of the buffer gas into the plasma.

Evolution of atomic emissions with pressure variation was found similar in all tested atmospheres and for both energetic compounds. However, as expected, a strong increase of O emission was observed when oxygen gas was used. In the same way, N and CN species underwent a visible increment in both nitrogen and air atmospheres. As discussed above, CN keeps a high intensity for oxygen atmosphere in the case of TNT unlike the case of PETN. This behaviour arises from the greater viability of pathways leading to CN formation in TNT due to the large concentration of C_2 molecules available to react in the plume.

The decreased intensities observed in atomic emission lines at pressures close to atmospheric was due to spectral broadening undergone by peaks under the effect of different mechanisms such as Stark effect and pressure broadening, principally.

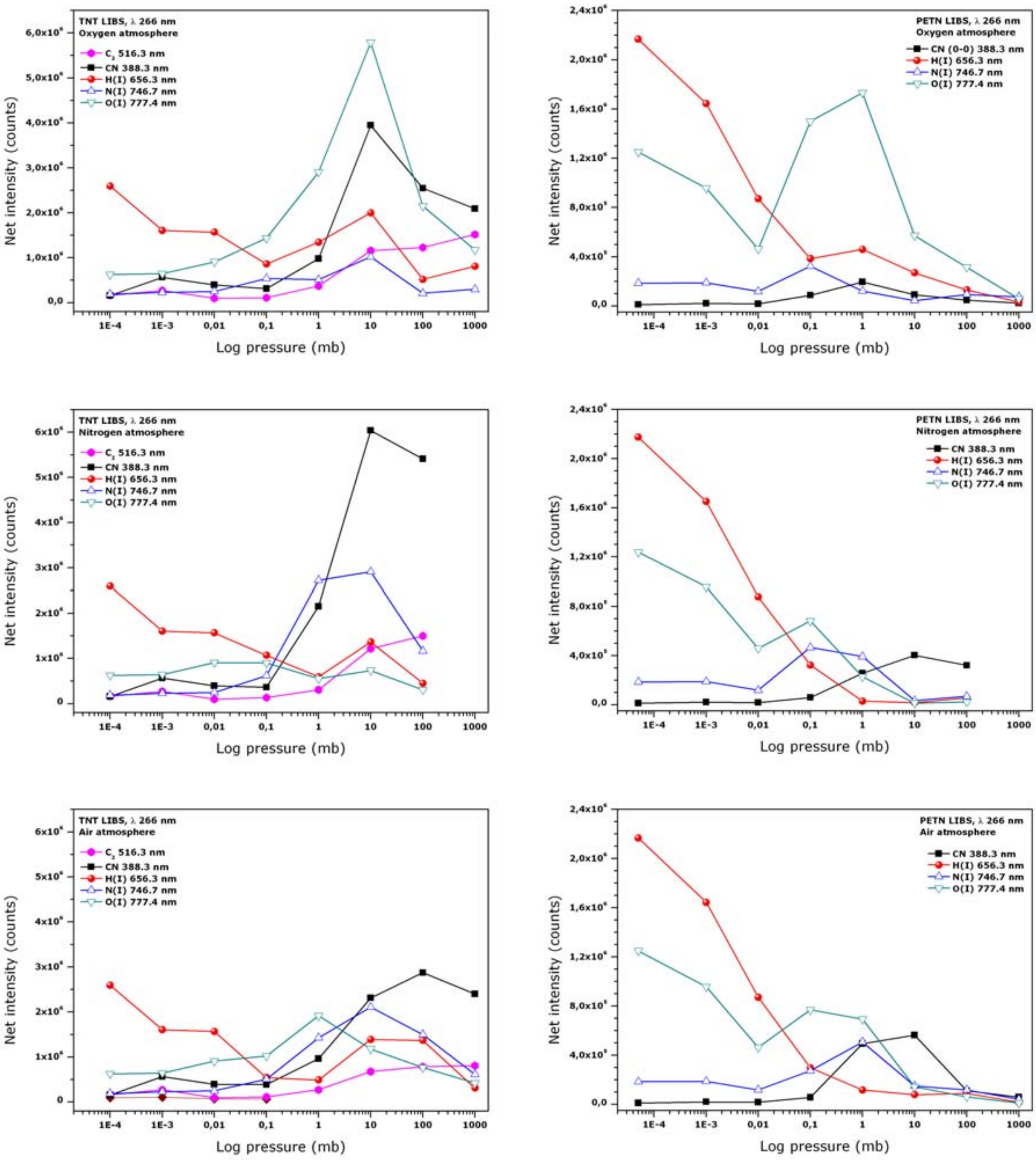

Figure 8.8. Net intensities of main atomic and molecular emission species of (left) TNT and (right) PETN as a function of pressure level in different atmospheres: (a) oxygen; (b) nitrogen; (c) air. Fluence, 12.5 J/cm^2. Nitrogen net intensities are multiplied by a x10 factor for a better comparison.

These mechanisms are due to both the progressive increasing of electron density in the plume and the consequent increment of number of electronic impacts within the plasma, respectively. As a sample, Figure 8.9 shows the broadening effect for H(I) emission line in oxygen atmosphere.

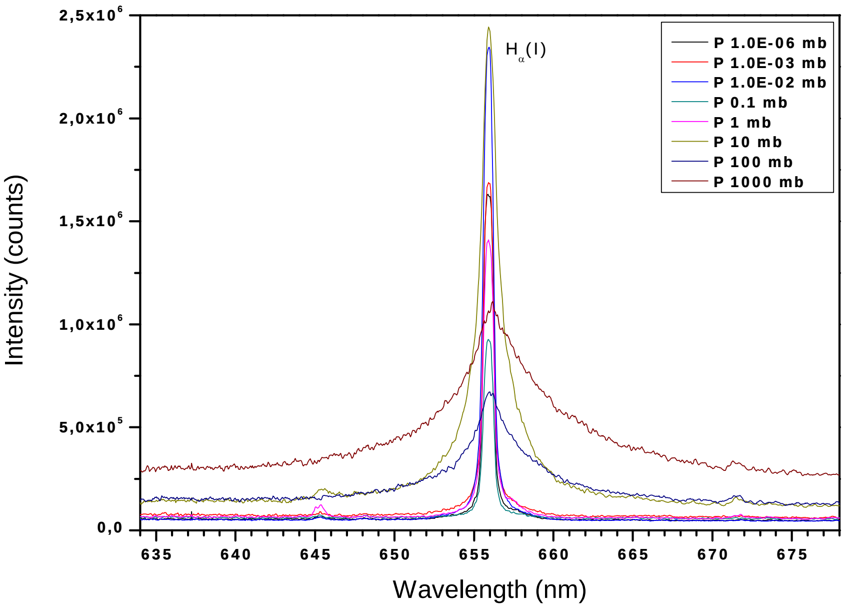

Figure 8.9. Detail of spectral widening of H(I) emission line (656.3 nm) as a function of oxygen pressure in UV-LIBS analysis of TNT. Fluence, 12.5 J/cm^2.

8.5.3. Hydrogen as background gas

In order to study possible changes in formation routes of neutral and excited species due to interferences with a reactive buffer gas, the same LIBS experiments were carried out in hydrogen atmosphere. Broadband emission spectra were acquired for both TNT and PETN. As hydrogen gas expands quickly, it was difficult to set pressure values into the analysis chamber. Due to safety issues, measurements were carried out in discontinuous mode so the inlet flow was cuff of when desired pressure value was reached.

Figure 8.10 shows a set of LIBS spectra acquired from TNT plasma at different hydrogen pressure values. It was only feasible to control the pressure up to 3.5 mb due to the internal calibration of the gauge for hydrogen gas. Pressure values above were estimated from the FWHM value for H_α(I) peak. As shown in the figure, a considerable reduction of molecular emissions from both CN and C_2 compared to previous tested atmospheres is the most noticeable feature. In the pressure range 10-50 mbar, molecular emissions are virtually absent. As expected, a marked rise of H(I) lines was observed. These observations are consistent with previous experimental results showed in Chapter 6 and the hypothesis according to which hydrogen reacts with the molecular species C_2 and CN thus hindering their appearance in the LIBS spectra. The reaction pathways are respectively (8.10) and (8.14):

$$CN + H_2 \rightleftharpoons HCN + H \qquad (8.14)$$

Reaction (8.14) has very low activation energy **[Spanel, P. et al., 2006]** so it is easily feasible at the high temperatures existing in the plasma. High concentration of hydrogen gas could favour the right-hand side in both routes, thus resulting in a low abundance of the carbon molecular forms in the plume. As a check of the above assumption, Figure 8.11 shows a comparison of the CN emission intensity for TNT and PETN in hydrogen and air atmospheres as a function of pressure. For two compounds, the abundance of CN grows sharply upon admittance of air in the chamber. However, as clearly seen, the growth of molecular emission is inhibited in the hydrogen atmosphere.

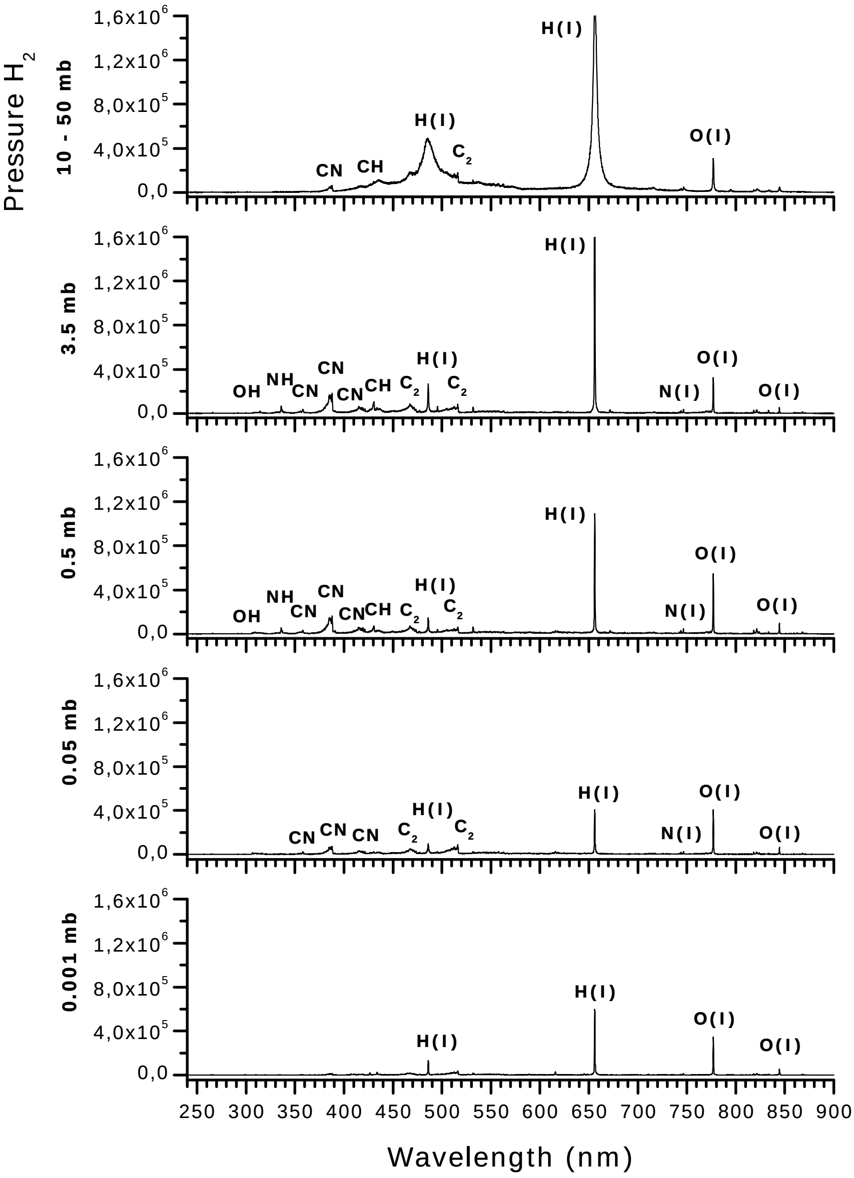

Figure 8.10. Set of LIBS TNT spectra for different H_2 pressure values. Top spectrum was taken at unknown H_2 pressure, but in the range between 10 – 50 mb. Fluence, 12.5 J/cm^2.

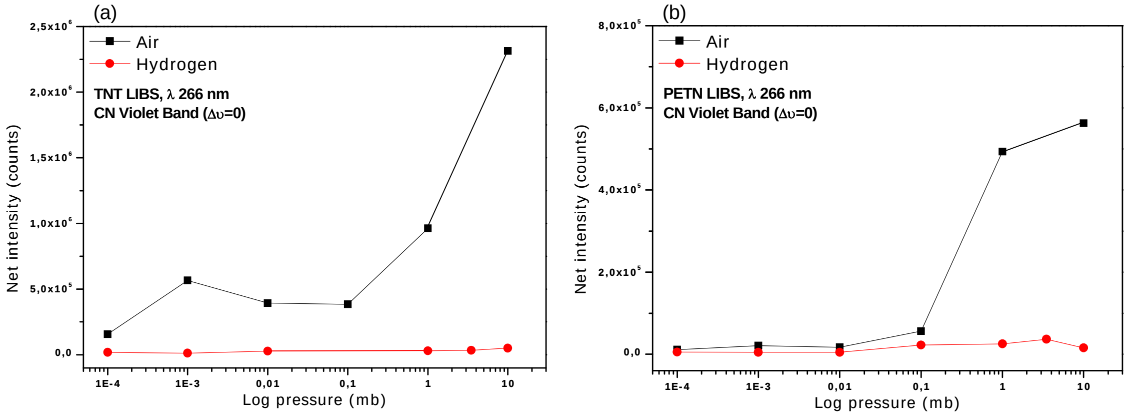

Figure 8.11. Comparative study concerning the variation of CN emission signal as a function of both air and hydrogen pressures for (a) TNT; (b) PETN. Fluence, 12.5 J/cm^2.

8.5.4. Argon and helium as background gases

Finally, the same experiment was carried out in presence of noble gases as argon and helium. Since these monoatomic gases have very low chemical reactivity, they will not participate actively in the chemistry of the plasma plume so we can assure that excited molecular fragments will be generated exclusively from reactions between native species from the ablated compound.

Figure 8.12 shows the changes in the emission signal of TNT in argon background as a function of pressure. The maximum pressure allowed by the gauge was 50 mb according to internal calibration of the instrument.

If we consider the buffer gas as ideal at a constant temperature, density will decrease proportionally with the pressure in the system. Argon has the highest density among buffer gases used in this work (see Table 8.1) and hence, for a specific pressure value, plasma confinement should be higher than that in the rest of buffer gases. Consequently, the collision rate will be also higher in this case. Moreover, the lifetime of plasma is related to thermal conductivity of the surrounding gas **[Lee, Y. I., 1997]**, so that higher values imply a faster cooling of plasma, and therefore, shorter lifetimes. Argon has the lowest thermal conductivity among the tested buffer gases (see Table 8.1), comparable to that for oxygen, nitrogen or air. Hence, lifetimes of plasmas in argon atmosphere become more lasting. All these features presented by the argon plasma could explain the significant production of molecular species in the pressure range between 1 and 50 mb as observed in the Figure 8.12. No measurements of plasma lifetime were conducted, but the larger background observed in the spectrum obtained at the highest Ar pressure indicates a larger plasma electron temperature, which is captured under the timing conditions used here. This excess temperature could result in dissociation of the molecules and the reduced intensities of CN and C_2

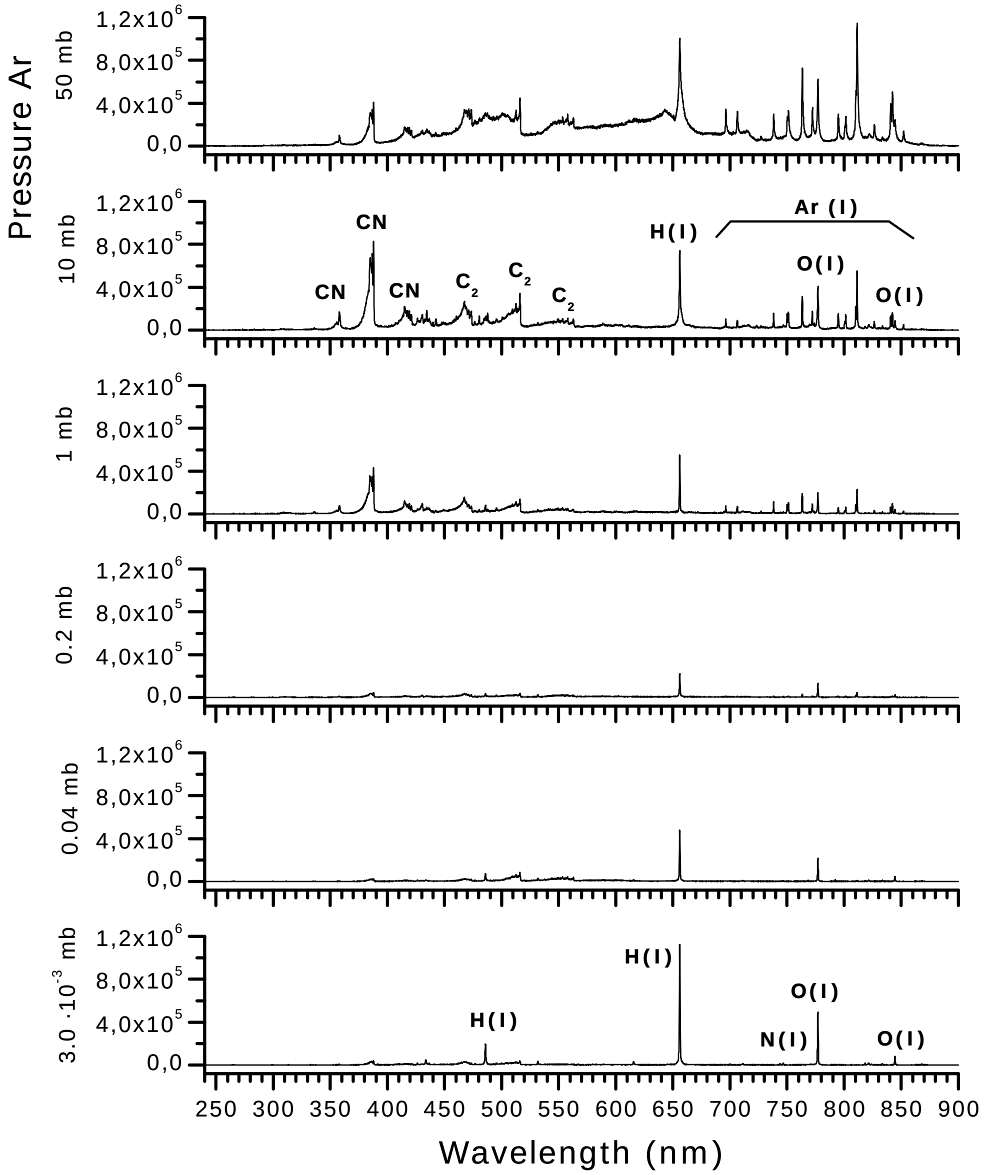

Figure 8.12. Set of LIBS TNT spectra for different Ar pressure values in the range between 5.0·10^{-5} mb and 50 mb. Fluence, 12.5 J/cm^2.

observed in the spectrum acquired at 50 mbar. The progressive increase of the characteristic emission of Ar (I) with the pressure confirms a high concentration of Ar atoms in the surroundings of the plasma.

Helium has certain similarities in physical properties with hydrogen, including density and thermal conductivity. Thus, the behaviour is expected to be similar regarding plume expansion and plasma lifetime. However, different from hydrogen but as argon, helium is essentially a non reacting gas due to the valence electrons. For all this, helium becomes a suitable candidate to carry out a comparison with hydrogen

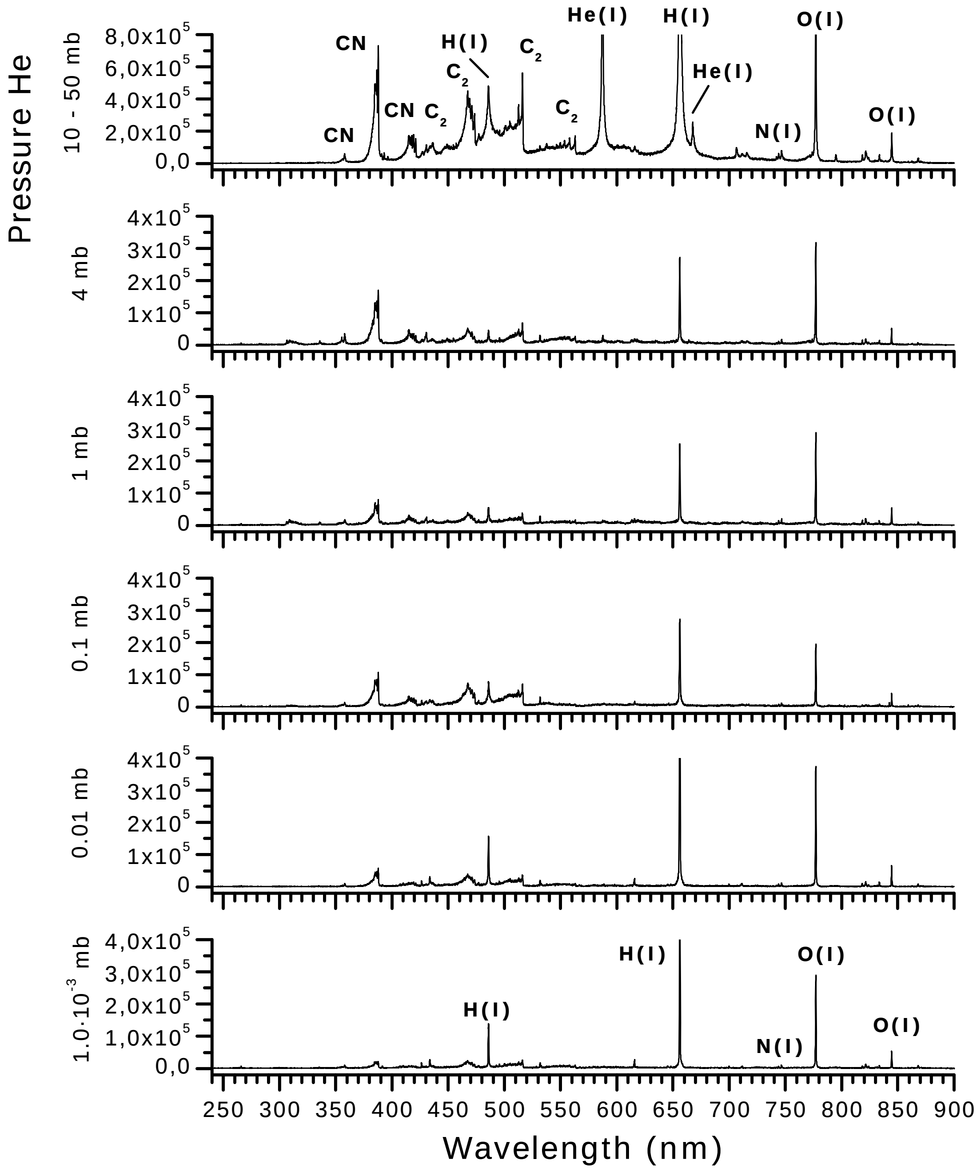

Figure 8.13. Set of LIBS TNT spectra for different He pressure values. Top spectrum was taken at unknown He pressure, but in the range between 10 – 50 mb. Fluence, 12.5 J/cm^2.

buffer gas concerning the evolution of emission signals in LIBS spectra with pressure level in order to confirm the interference of hydrogen in the pathways of molecular fragmentation previously discussed. Figure 8.13 sketches the evolution of LIBS spectra of TNT as a function of He pressure. This time the upper limit for pressure level allowed by the gauge calibration was 4 mb. As shown, apart from characteristic emission of atomic He from the own excited gas, the abundance of both CN and C_2 grows with the pressure, reaching a maximum at the largest pressure tested. This behaviour is similar to that observed in other atmospheres except in hydrogen. Thus, the presence of significant molecular emission in LIBS spectra acquired in presence of noble gases leads to the conclusion that hydrogen from the atmosphere has an active participation in the plume chemistry, the most important effect observed in LIBS being an almost complete suppression of the most common carbon molecular species existing in the plasmas.

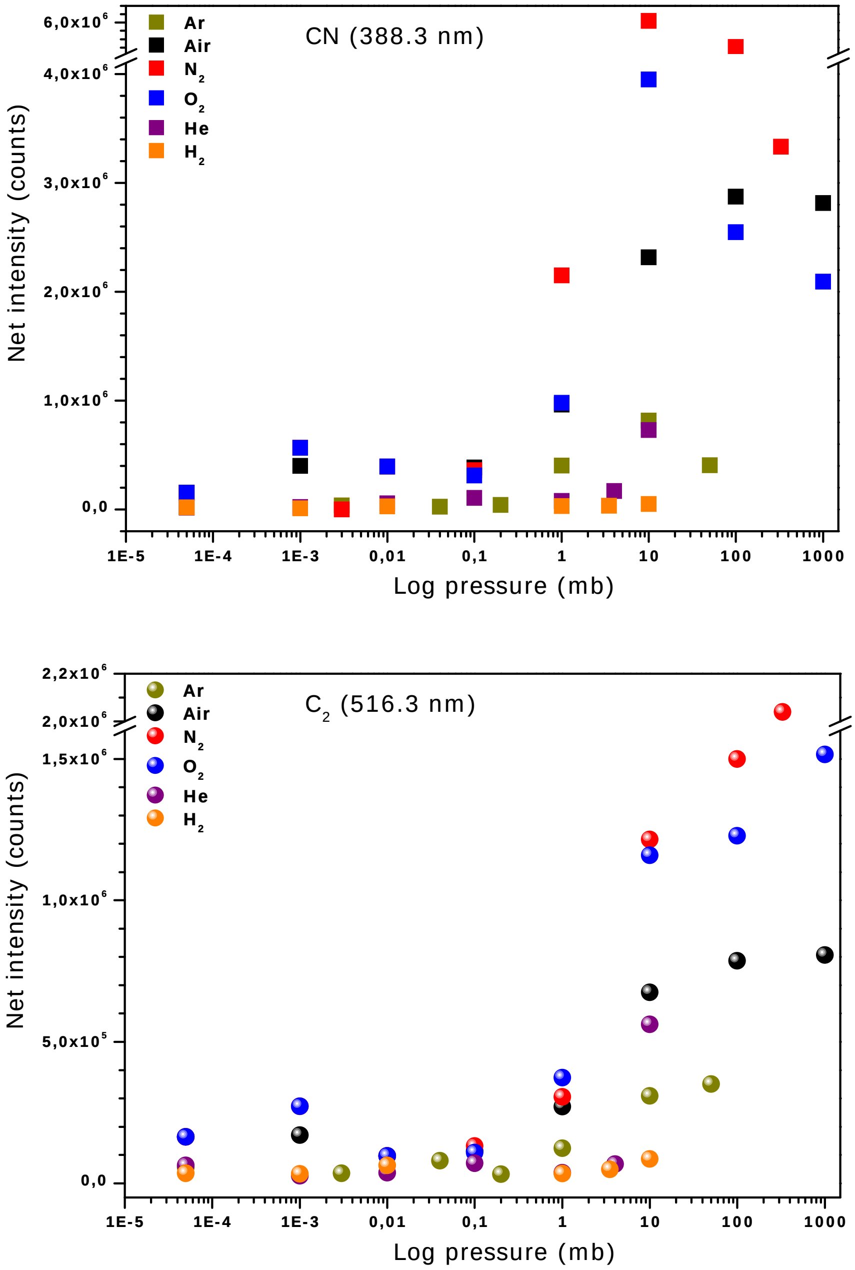

Figure 8.14. Net intensities of main emission bands corresponding to molecular species (top) CN and (bottom) C_2 from TNT LIBS spectra as a function of pressure level for different buffer gas. Laser wavelength, 266 nm Fluence, 12.5 J/cm^2.

In order to give an overview to the study of gas supply in the ablation of explosive organic compounds, Figure 8.14 summarizes the above results where conclusions of the experiment are evidenced. Net intensities for main emission bands of both CN Violet and C_2 Swan systems are presented as a function of pressure level in the chamber (in the pressure range that could be controlled in each case) for all the tested buffer gases for the laser ablation of TNT.

The growth of emission bands in both Ar and He atmospheres with increasing pressure is considerably lower than that in the case of atmospheric gases, but is significantly higher than in the case of H_2 gas.

The molecular emission generated in the case of noble gas atmospheres derive almost exclusively from the ablated material as commented above through both direct fragmentation and atomic recombination in the plume. For reactive gases such as N_2, O_2 and air, on the contrary, the recombination pathways with contribution of molecules from the atmosphere are greatly favoured. Nevertheless, very low intensity corresponding to a minimum presence of both type of molecular emission is observed in the H_2 atmosphere, so direct fragmentation was considered the source of such emission. In addition, the observed behaviour for C_2 (Figure 8.14, bottom), which at first could be thought to depended exclusively on the structure of ablated sample, was demonstrated to depend also on the nature of the buffer gas surrounding the plume.

8.6. CONCLUSIONS

In the present study, important differences in the features of emission spectra of laser induced plasmas from organic compounds were observed in different atmospheres. As a consequence, a number of pathways in the plume chemistry leading to the formation of emission species have been proposed for each background atmosphere.

Apart from nature of buffer gas, both pressure level in the system and laser wavelength have been demonstrated to have a significant effect in the plume composition and subsequent plasma emission.

A baseline survey about the influence of surrounding atmosphere in laser ablation analysis on the distribution of vibrational modes corresponding to energetic states in the molecule have been carried out for C_2 and CN emission bands. Results suggested that both the density and the nature of the background gas affect somehow the vibrational structure of such molecular species.

Regarding the comparative LIBS study carried out in different ablation atmospheres, it was found that, while CN is ubiquitous to spectra in nitrogen containing atmospheres, C_2 emission is undoubtedly associated to the presence of carbon-carbon double bonds in the parent molecule, irrespective of the composition of the buffer gas. The intense molecular emission observed in oxygen atmosphere suggests that atomic oxygen dissociated from O_2 (favoured by the low binding energy of the O_2 molecule) confers a large reactivity to the plume. Indirect pathways leading to C_2, CH and CN formation were consequently observed. Results using H_2 as buffer gas demonstrate that an excess of hydrogen in the environment prevents the formation of CN and C_2. A comparative study with buffer noble gases confirmed the occurrence of those inhibition routes since emission spectra for both argon gas and helium gases showed presence of such molecular species. PETN, a non-aromatic nitro compound, shows a remarkable participation of OH species in the plume reactions and an eloquent emission of the NH molecular system in both nitrogen and air, likely following reaction of H_2 dissociation from collisions with N atoms.

The routes studied here are only part of the many possible reactions occurring in a laser-induced plasma. We have focused on pathways leading to emitting species, but it seems that there are many more reactions involving non emitting intermediates and undetected final products, at least as LIBS in the UV and visible regions is concerned. Some important fragments have been identified in the past in laser ablation experiments in gas phase, and more recently, in condensed phase by means of mass spectrometry. It is clear that the surroundings of a plasma in vacuum are radically different of the environment at atmospheric pressure. The input laser energy, as responsible of the plasma temperature, constitutes an additional key experimental factor, whereas the emissions observed depend to a large extent on the time window examined during plasma evolution. The discovery of general rules in plasma chemistry is challenging since the phenomena observed are affected by many factors whose separate contributions are difficult to evaluate. Further research is underway to reach a deeper understanding of the combined effect of the involved variables, the chemical structure and the observed plasma spectra.

General Conclusions

In good agreement with the objectives exposed at the beginning of this memory and the conclusions extracted from each single chapter, a few general conclusions may be highlighted here, as follows:

1. The present work has demonstrated the ability of LI-TOF-MS as analytical microprobe technique based on nanosecond laser excitation to analyze directly molecular analytes in solid phase generating specific ionic fragments from one step desorption-ionization of the material. Acquired information is comparable to that obtained by Electron Impact Ionization technique.
2. The acquired mass spectra undergo important qualitative changes when extraction settings for ions are varied. This result allows a sort of modulation based on a simple modification in the extraction conditions, opening the possibility of acquiring quasi-simultaneous atomic/molecular modulated mass spectra at fixed excitation conditions.
3. Energy values corresponding to ionization thresholds were found for analyzed nitro aromatic compounds through a fine control on fluence regime.
4. Kinetic trend followed by main ionic species from ionization of nitro aromatic compound with the variation of laser pulse energy have been monitored, allowing the study of evolution and mechanisms involved in the fragmentation pathways of the molecule.

5. The optimization of the parameters for preferential acquisition of molecular information has allowed the identification of the organic compound from characteristic fragments in the corresponding mass spectrum.
6. A comparison of the analyzed nitro-aromatic compounds by high vacuum LIBS proved that this technique is suitable for identification and discrimination studies of organic molecules with similar chemical composition.
7. Studied nitro aromatic homologous series (MNT, DNT and TNT) presented similar fragmentation pattern in time-of-flight mass spectra in the low-mass region and analogous features in emission LIBS spectra. The fluence thresholds for both optical and ionic signals at high vacuum regime acquired with UV nanosecond pulses were found, so that desorption and generation of early ions required lower fluence dose than that for plasma formation. The latter implies a modification in the ablation regime that alters the plume expansion, decreasing the ion extraction efficiency (under our experimental conditions).
8. Fluence parameterization showed the evolution of the main optical-mass signals in the acquired spectra for a limited energetic range, showing the different stages of lifetime of plasma: the rising thresholds and extinction of the different atomic and molecular studied species, besides the breakage of the aromatic ring and the later excitation of ionic species at higher fluence level. Molecular species start to emit at lower fluence than atomic species.
9. A good agreement between the trends of the emission and mass atomic species (H, C, N and O) was found out, indicating a high correlation between both processes in time and energetic scales. As for molecular species, the observed trends were different for diatomic ion signal ($^{24}C_2^+$ and $^{26}CN^+$) and emission of molecular bands C_2 and CN mainly due to differences in the energetic regime of excitation and ionization processes.
10. Optical emission results for homologous series at high vacuum regime support those obtained in He atmosphere and suggest the use of CN/C_2 intensity ratio for nitro compounds identification.
11. It was found a relationship between the internal energy contained in the bonds of the different DNT isomers (associated to the spatial and symmetry characteristics of such molecules) and the response to ionization reflected in the information obtained from signal intensities in optical and mass spectra. This fact supports the capability of LIMS together with LIBS to discriminate between isomers from the analysis of the associated spectra.

12. Further statistic analysis of obtained spectral information could be taken as reference point for the search of discrimination criteria between organic nitro aromatic isomers but further optimization work has to be done before putting this analytical tool into practice for this application.
13. Results have proved the combined LIMS-LIBS analytical system becomes a good choice to understand the mechanisms involved in the decomposition pathways of organics and consequent formation of intermediate and final products in plasma chemistry.
14. Possible fragmentation and recombination routes have been proposed for tested organic compounds taking into account the fact that same reactions prevail over others depending on experimental conditions: laser fluence, pressure level and atmosphere surrounding the plasma, mainly. The suggested routes are supported by LIMS measurements where many non-emitting reactive species present in the plasma were identified on the acquired mass spectra: CO, C_nH_m, NO, HCN, among others**.**
15. Pressure becomes a critical parameter in LIBS trials affecting the dynamics of the plasma from values as little as 0.1 mbar for studied compounds. The presence of air influences on the specific emission of species due to interferences in the recombination pathways into the plasma plume. Regarding to molecular species, results from different atmospheric conditions indicated that C_2 emission is strongly linked to molecular structure whereas CN is mostly produced by chemical reactions.
16. Analysis of pyrene sample suggested that the supply of N_2 implies the loss of C_2 and CH excited species in the plasma, whereas results from H_2 as buffer gas suggested that the presence of hydrogen gas may alter the formation pathways of molecular species reducing the CN and C_2 emission. However, emission bands corresponding to NH, CH and OH species are observed whose intensities are usually weak but meaningful.
17. Results have verified that pressure becomes a decisive parameter in LIBS trials affecting the interaction between excited plasma and gas molecules besides the dynamics of the plasma plume in such a way that the morphology, chemical composition and distribution of species changes critically. This effect is probably related to the collision less expansion of plasma plume in a laminar medium.
18. Reduced pressures allow expansion of the plasma into a larger volume, the cooling of plasma is slower and the plasma lifetime is longer. On the other

hand, at higher pressures plasma shielding effect, higher absorption of laser energy by plasma and less efficient ablation were observed.

19. Changes in pressure level and ambient density were observed to modify ablation rates in organic aromatic compounds for nanosecond lasers.
20. Time and spatially resolved LIBS studies as tool for characterization of dynamics and evolution of plasmas were carried out. Mechanisms for generation of CN fragments in the plume during plasma lifetime were studied in air pressure. The presence (although very weak) of CN emission in absence of air (high vacuum regime) suggests the production of excited molecular fragments by means of direct fragmentation and interaction between species from the organic molecule itself.
21. At 1 mbar air pressure, the plasma plume reached the maximum volume and brightness level of measurements for analyzed organic samples. That was in agreement with the corresponding emission spectra with the most richness of species and signal intensity.
22. Results from spatially resolved study of organic samples showed inhomogeneous distribution of species in the plume along the plasma expansion axis, so that atomic species are located mainly in the zone close to sample surface whereas molecular fragments are distributed along the entire plume, but preferentially located in the inner core of plasma.
23. Atomic emission in LIBS spectra using UV laser radiation in the excitation of the organic compound showed attenuation in comparison with the strong intensity of atomic emission found in the case of IR excitation. This effect was observed for all tested pressure levels and it is probably linked to the different energetic mechanisms involved in the excitation of species in the plume using different wavelength as laser source.
24. It was demonstrated how the kinetics and the formation channels of excited species in the laser ablation of organic compounds were affected by the direct interaction of the ensuing plasma with the buffer gas present in the surrounding.
25. In the case of time-resolved study of nitro aromatic compounds in air atmosphere, after the main prompt component of CN molecular emission system, a delayed component was observed presumably due to secondary reactions of recombination of atomic C with dissociated N_2 molecules that assist CN formation. This is an evidence of the kinetics of recombination in presence of air within the plasma.

26. Intense molecular emission was found in oxygen atmosphere for organic aromatic compounds. This fact suggests that the presence of oxygen atoms in the plume implied high reactivity in the plume, favouring indirect pathways leading to C_2, CH and CN formation.
27. Pyrene analysis in presence of nitrogen atmosphere showed a fall in C_2 emission signal compared to such intensity for oxygen atmosphere. Moreover, CN emission only appears for the case of presence of nitrogen in the surrounding gas. These facts probe the recombination pathway for CN with nitrogen molecules and that part of such recombination come from C_2 fragments consumption.
28. From analysis of monocyclic, polycyclic and aliphatic organic molecules, the direct dependence of C_2 molecular emission with the aromaticity was demonstrated.
29. The very low intensity of molecular bands emission in spectra acquired in presence of H_2 as buffer gas suggests that hydrogen may alter the CN and C_2 formation pathways favouring its dissociation toward other species. This conclusion is supported by results from emission intensity measurements of excited molecular species in presence of noble gases as argon and helium since considerable emission from CN and C_2 fragments are found when plasma is formed in presence of such inert atmospheres.
30. Results showed that molecular emission of C_2 fragments depends not only on molecular composition of ablated sample, but also on pressure level and type of background gas present in the surrounding at the time of analysis.

Finally, it should be stressed that those chemical reactions taking place within laser induced plasmas govern decisively the observed emission spectra. This fact has been systematically studied and demonstrated in the present doctoral thesis. Contrary to the widespread belief that the atomic emission spectrum should respond exclusively to the elemental composition of the organic compound, this thesis demonstrates that the atomic emission spectrum also contains a great deal of information about the molecular structure of the compound. Most of the molecular species involved in these reactions are small molecules and not appear in the emission spectra. However, such molecules and reactions in which they are directly involved define the resulting emission spectrum in a decisive way.

References

A

Abdelli-Messaci, S., Kerdja, T., Bendib, A. and Malek, S. Emission study of C2 and CN in laser-created carbon plasma under nitrogen environment. *Journal of Physics D: Applied Physics*, 35:2772-2778, 2002.

Abdelli-Messaci, S., Kerdja, T., Bendib, A. and Malek, S. CN emission spectroscopy study of carbon plasma in nitrogen environment. *Spectrochimica Acta Part B*, 60:955-959, 2005.

Acquaviva, S. and De Giorgi, M. L. Study of kinetics of atomic carbon during laser ablation of graphite in nitrogen by time- and space-resolved emission spectroscopy. *Applied Surface Science*, 186:329-334, 2002 **A**.

Acquaviva, S. and De Giorgi, M. L. Temporal and spatial analysis of plasmas during graphite laser ablation in low-pressure N2. *Applied Surface Science*, 197–198:21-26, 2002 **B**.

Adams, G. F. and Shaw, R. W. Chemical reactions in energetic materials. *Annual Review of Physical Chemistry*, 43:311-340, 1992.

Aghaei, M., Mehrabian, S. and Tavassoli, S. H. Simulation of nanosecond pulsed laser ablation of copper samples: A focus on laser induced plasma radiation. *Journal of Applied Physics*, 104:053303-053312, 2008.

Aguilera, J. A. and Aragon, C. A comparison of the temperatures and electron densities of laser-produced plasmas obtained in air, argon, and helium at atmospheric pressure. *Applied Physics A*, 69, S475-S478, 1999.

Aguilera, J. A. and Aragon, C. Temperature and electron density distributions of laser-induce plasmas generated with an iron sample at different ambient gas pressures. *Applied Surface Science*, 197-198:273-280, 2002.

Aguilera, J. A. and Aragon, C. Characterization of a laser-induced plasma by spatially resolved spectroscopy of neutral atom and ion emissions. Comparison of local and spatially integrated measurements. *Spectrochimica Acta Part B*, 59:1861-1876, 2004.

Aguilera, J. A., Aragon, C., Madurga, V. and Manrique, J. Study of matrix effects in laser induced breakdown spectroscopy on metallic samples using plasma characterization by emission spectroscopy. *Spectrochimica Acta, Part B*, 64:993–998, 2009.

Akhavan, J. The chemistry of explosives*, Royal Society of Chemistry*, Manchester, 2004.

Alcántara, J. F., Vadillo, J. M. and Laserna, J. J. Subthreshold two-pulse time-delayed laser ionization of Cu. *Applied Physics A*, 92:963-967, 2008 **A**.

Alcántara, J. F., Vadillo, J. M. and Laserna, J. J. Two-pulse delayed 532-nm laser ionization of metals using collinear sub-threshold beams. *Rapid Communications in Mass Spectrometry*, 22:1999-2005, 2008 **B**.

Alcántara, J. F. Time-of-Flight mass spectrometry experimental studies on the onset of laser-generated ins under subthreshold plasma formation regime*. PhD Thesis, University of Málaga*, 2010.

Amoruso S., Bruzzese, R., Spinelli, N. and Velotta, R. Characterization of laser-ablation plasmas. *Journal of Physics B: Atomic, Molecular and Optical Physics,* 32:R131-R172, 1999.

Anisimov, S. I., Kapaliovich, B. L. and Perel'man, T. L. *Sov. Phys. JETP,* 39, 375, 1974.

Anisimov, S. I., Bauerle, D. and Luk'yanchuk, B. S. Gas dynamics and film profiles in pulsed-laser deposition of materials. *Physical Review B,* 48:12076-12081, 1993.

Anzano, J. M., Gornushkin, I. B., Smith, B. W. and Winefordner, J. D. Laser-induced breakdown spectroscopy for plastic identification. *Polymer Engineering & Science*, 40:2423–2429, 2000.

Appleton, E. V. Wireless studies of the ionosphere, *Journal of the Institute of Electronic Engineers,* 71, 642, 1932.

Aragon, C., Peñalba, F. and Aguilera, J. A. Spatial characterization of laser-induced plasmas: distributions of neutral atom and ion densities. *Applied Physics A*, 79:1145-1148, 2004.

Aragon, C. and Aguilera, J. A. Characterization of laser induced plasmas by optical emission spectroscopy: A review of experiments and methods. *Spectrochimica Acta, Part B*, 63:893−916, 2008.

Arp, Z. A., Cremers, D. A., Harris, R. D., Oschwald, D. M., Parker, G. R. and Wayne, D. M. Feasibility of generating a useful laser-induced breakdown spectroscopy plasma on rocks at high pressure: Preliminary study for a Venus mission. *Spectrochimica Acta Part B: Atomic Spectroscopy,* 59:987-999, 2004.

B

Babankova, D., Civis, S. and Juha, L. Chemical Consequences of laser-induced breakdown in molecular gases. *Progress in Quantum Electronics*, 30:75-88, 2006.

Babushok, V. I., De Lucia, F. C., Dagdigian, P. J., Gottfried, J. L., Munson, M. J. and Miziolek, A. W. Kinectic modeling study of the laser-induced plasma plume of cyclotrimethyl-enetrinitramine (RDX). *Spectrochimica Acta Part B*, 62:1321-1328, 2007.

Baeri, P., Campisano, S. U., Foti, G. and Rimini, E. A melting model for pulsing-laser annealing of implanted semiconductors. *Journal of Applied Physics*, 50:788-798, 1979.

Baiocchi, C., Giacosa, D., Saini, G., Cavalli, P., Omenetto, N., Passarella, R., Polettini, A. and Trincherini, P. R. Determination of thallium in Antarctic snow by means of laser induced atomic fluorescence and high resolution inductively coupled plasma mass spectrometry. *Int. J. Environmental Analytical Chemistry,* 55:211–218, 1994.

Barkan, A., D’Angelo, N. and Merlino, R. L. Experiments on ion-acoustic waves in dusty plasmas, *Planetary and Space Science,* 44:239-242, 1996.

Baudelet, M., Guyon, L., Yu, J., Wolf, J. P., Amodeo, T., Frejafon, E. and Laloi, P. Femtosecond time-resolved laser-induced breakdown spectroscopy for detection and identification of bacteria: A comparison to the nanosecond regime. *Journal of Applied Physics*, 99, 084701, 2006 **A**.

Baudelet, M., Guyon, L., Yu, J., Wolf, J. P., Amodeo, T., Frejafon, E. and Laloi, P. Spectral signature of native CN bonds for bacterium detection and identification using femtosecond laser-induced breakdown spectroscopy. *Applied Physics Letters,* 88, 063901, 2006 **B**.

Baudelet, M., Boueri, M., Yu, J., Mao, S. S., Piscitelli, V., Mao, X. and Russo, R. E. Time-resolved ultraviolet laser-induced breakdown spectroscopy for organic material analysis. *Spectrochimica Acta Part B*, 62:1329-1334, 2007.

Baudelet, M., Boueri, M., Yu, J., Mao, S. S., Mao, X. and Russo, R. E. Correlation between early-stage expansion and spectral emission of a nanosecond laser-induced plasma from organic material. *Proceedings of SPIE. The International Society for Optical Engineering*, 7005, 2008.

Becker, J. S. and Dietze, H. J. Laser ionization mass spectrometry in inorganic trace analysis. *Fresenius Journal Analytical Chemestry*, 344:69–86, 1992.

Becker, J. S., Dietze, H. J. Inorganic mass spectrometric methods for trace, ultratrace, isotope, and surface analysis. *International Journal of Mass Spectrometry*, 197:1-35, 2000.

Becker, J. S. and Dietze, H. J. State-of-the-art in inorganic mass spectrometry for analysis of high-purity materials. *International Journal of Mass Spectrometry*, 228:127-150, 2003. Special Issue: In honour of Helmut Schwarz.

Bellan, P. M. A model for the condensation of a dusty plasma, *Physics of Plasmas* 11, 3368, 1996.

Beenen, G. J. and Piepmeier, E. H. Chemical dynamics of a laser microprobe vapour plume in a controlled atmosphere. *Applied Spectroscopy*, 38:851-857, 1984.

Berkowitz, J. Heat of formation of the CN radical. *The Journal of Chemical Physics*, 36:2533-2539, 1962.

Bhasu, V. C. J. and Chaudhri, M. M. Rapid mass spectrometric analysis of fragments of trinitrotoluene, picric acid and tetryl generated by laser irradiation. *Journal of Materials Science,* 26:2100-2207, 1991.

Bleiner, D., Bogaerts, A., Belloni, F. and Nassisi, V. Laser-induced plasmas from the ablation of metallic targets: the problem of the onset temperature, and insights on the expansion dynamics, *Journal of Applied Physics*, 101:1-5, 2007.

Boels, U. Laser mass spectrometry for environmental and industrial chemical trace analysis. *Journal of Mass Spectrometry*, 35:289-304, 2000.

Bogaerts, A., Chen, Z., Gijbels, R. and Vertes, A. Laser ablation for analytical sampling: what can we learn from modeling? *Spectrochimica Acta, Part B,* 58:1867-1893, 2003.

Bogaerts, A. and Chen, Z. Y. Nanosecond laser ablation of Cu: modeling of the expansion in He background gas, and comparison with expansion in vacuum, *Journal of Analytical Atomic Spectrometry,* 19:1169–1176, 2004.

Bogaerts, A. and Chen, Z. Y. Effect of laser parameters on laser ablation and laser induced plasma formation: A numerical modeling investigation. *Spectrochimica Acta Part B*, 60:1280-1307, 2005.

Bogaerts, A., Chen, Z. Y. and Bleiner, D. Laser ablation of copper in different background gases: comparative study by numerical modeling and experiments, *Journal of Analytical Atomic Spectrometry,* 21:384-395, 2006.

Bogaerts, A., Chen, Z. Y., Gijbels, R., and Vertes, A. Laser ablation for analytical sampling: what can we learn from modeling? *Spectrochimica Acta Part B*, 58:1867-1893, 2003.

Borchert, H., Dare´e, K. and Hugenschmidt, M. Plasma formation during the interaction of picosecond and nanosecond laser pulses with BK7 glass. *Journal of Physics D: Applied Physics,* 38:300-305, 2005.

Bouchonnet, S., Denhez, J., Hoppilliard, Y. and Mauriac, C. Is plasma desorption mass spectrometry useful for small-molecule analysis? Fragmentations of the natural amino acids. *Analytical Chemistry*, 64:743-754, 1992.

Braams, C. M. and Stott, P. E. Nuclear Fusion: Half a Century of Magnetic Confinement Research. *Institute of Physics Publishing*, 2002.

Brech, F. and Cross, L. Optical microemission stimulated by a ruby maser. *Applied Spectroscopy*, 16:59-63, 1962.

Brennetot, R., Lacour, J. L., Vors, E., Rivoallan, A., Vaihen, D. and Maurice, S. Mars analysis by laser-induced breakdown spectroscopy (MALIS): Influence of Mars atmosphere on plasma emission and study of factors influencing plasma emission with the use of doehlert designs. *Applied Spectroscopy*, 57:744-752, 2003.

Brinckerhoff, W. B., Cornish, T. J., McEntire, R. W., Cheng, A. F. and Benson, R. C. Miniature time-of-flight mass spectrometers for in situ composition studies. *Acta Astronautica*, 52:397-404, 2003.

Brinckerhoff, W. B. On the possible in situ elemental analysis of small bodies with laser ablation tof-ms. *Planetary and Space Science*, 53:817-838, 2005.

Broekaert, J. A. C. Analytical Atomic Spectrometry with Flames and Plasmas. *Wiley-VCH Verlag*, Weinheim, 2002.

Buchsbaum A., Rauchbauer, G., Varga, P., Schmid, M., Time-of-flight spectroscopy of the energy distribution of laser-ablated atoms and ions. *Review of Scientific Instruments*, 79:1-8, 2008.

Bulgakova, N. M., Bulgakov, A. V. and Babich, L. P. *Applied Physics A: Materials Science Processing*, 79, 1323, 2004.

Butcher, D. J. Advances in laser-excited atomic fluorescence and ionization. *Applied Spectroscopy Reviews,* 40:147–164, 2005.

C

Callies, G., Schittenhelm, H., Berger, P. and Hugel, H. Two-wavelength interferometry on excimer laser induced vapour/plasma plumes during the laser pulse. *Applied Surface Science*, 127–129:922-927, 1998.

Campos, D., Harilal, S. S. and Hassanein, A. The effect of laser wavelength on emission and particle dynamics of Sn plasma. *Journal of Applied Physics*, 108:113305-1−113305-7, 2010.

Chen, J. K., Beraun, J. E. and Tham, C. L. Investigation of thermal response caused by pulse laser heating. *Numerical Heat Transfer, Part A,* 44:705-722, 2003.

Chen, P. C, Chieh, Y. C. and Tzeng, S. C. Density functional calculations of the heats of formation for various aromatic nitro compounds. *Journal of Molecular Structure (Theochem)*, 634:215-224, 2003.

Chen, Z. Y. and Bogaerts, A. Laser ablation of Cu and plume expansion into 1 atm ambient gas. *Journal of Applied Physics*, 97, 1, 2005.

Cheng, P. Y. and Dai, H. L. A photoemitted electron-impact ionization method for time-of-flight mass spectrometers. *Review of Scientific Instruments*, 64:2211-2214, 1993.

Choi, S. J. and Yoh, J. J. Laser-induced plasma peculiarity at low pressures from the elemental lifetime perspective. *Optics Express*, 19:23097-23103, 2011.

Cirisan, M., Jouvard, J. M., Lavisse, L., Hallo, L. and Oltra, R. J. Laser plasma plume structure and dynamics in the ambient air: The early stage of expansion. *Applied Physics*, 109:103301-1–103301-17, 2011.

Civis, M., Civis, S., Sovová, K., Dryahina, K., Spanel, P. and Kyncl, M. Laser ablation of FOX-7: Proposed Mechanism of Decomposition. *Analytical Chemistry*, 82:1069-1077, 2011.

Cohen, R., Zeiri, Y., Wurzberg, E. and Kosloff, R. Mechanism of Thermal Unimolecular Decomposition of TNT (2,4,6-Trinitrotoluene): A DFT Study. *The Journal of Physical Chemistry A*, 111:11074-11083, 2007.

Cooks, R. G., Ouyang, Z., Takats, Z. and Wiseman, J. M. Ambient mass spectrometry. *Science*, 311:1566-1570, 2006.

Coons, R. W., Harilal, S. S., Hassan, S. M. and Hassanein, A. The importance of longer wavelength reheating in dual-pulse laser-induced breakdown spectroscopy. *Applied Physics B: Laser Optics*, 107:873−880, 2012.

Costache, F., Ratzke, M., Wolfframm, D. and Reif, J. Femtosecond laser ionization mass spectrometric analysis of layers grown by pulsed laser deposition Original Research Article. *Applied Surface Science,* 247:249-255, 2005.

Cremers, D. A. and Knight, A. K. Laser-induced breakdown spectroscopy. In Encyclopedia of Analytical Chemistry Vol. 11*. John Wiley & Sons*, Chichester, 2000.

Cremers, D. A. and Radziemski, L. J. Handbook of Laser-Induced Breakdown Spectroscopy*. John Wiley & Sons, West Sussex*, 2006.

Cremers, D. A., Beddingfield, A., Smithwick, R., Chinni, R. C., Jones, C. R., Beardsley, B. and Karch, L. Monitoring uranium, hydrogen, and lithium and their isotopes using a compact Laser-Induced Breakdown Spectroscopy probe and high resolution spec-trometer. *Applied Spectroscopy*, 66:250-261, 2012.

Csele, M. Fundamentals of Light Sources and Lasers*. John Wiley & Sons,* New Jersey, 2004.

Ctvrtnickova, T., Mateo, M. P., Yañez, A., Nicolas, G. Characterization of coal fly ash components by laser-induced breakdown spectroscopy. *Spectroschimica Acta Part B: Atomic Spectroscopy*, 64:1093-1097, 2009.

Ctvrtnickova, T., Mateo, M. P., Yañez, A. and Nicolas, G. Laser Induced Breakdown Spectroscopy application for ash characterisation for a coal fired power plant. *Spectrochimica Acta Part B*, 65:734-737, 2010.

D

Dahotre, N. B. and Harimkar, S. P. Laser Fabrication and Machining of Material. *Springer*, New York, 2007.

Dale, M. J., Jones, A. C., Pollard, S. J. T. and Langridge-Smith, P. R. R. Direct determination of polycyclic aromatic hydrocarbons in environmental matrices using laser desorption laser photoionization time-of-flight mass spectrometry. *The Analyst*, 119:571-578, 1994.

Davies, C. M., Telle, H. H., Montgomery, D. J. and Corbett, R. E. Quantitative analysis using remote laser-induced breakdown spectroscopy (libs). *Spectrochimica Acta Part B: Atomic Spectroscopy*, 50:1059-1075, 1995.

De Giacomo, A., Dell'Aglio, M., Gaudiuso, R., Cristoforetti, G., Legnaioli, S., Palleschi, V. and Tognoni, E. Spatial distribution of hydrogen and other emitters in aluminum laser-induced plasma in air and consequences on spatially integrated Laser-Induced Breakdown Spectroscopy measurements. *Spectrochimica Acta Part B*, 63:980-987, 2008.

Delgado, T., Vadillo, J. M. and Laserna, J. J. Analysis of the influence of pressure on the dynamics of laser-induced plasma expansion for trinitrotoluene by time and spatially-resolved studies. Submitted for publication **A**.

Delgado, T., Vadillo, J. M. and Laserna, J. J. Insights on the acting role of background gas in the formation pathways of emitting species in laser-induced plasmas of high energetic nitro compounds. Submitted for publication **B**.

Delgado, T., Vadillo, J. M. and Laserna, J. J. Pathways for production of emitting species in the laser-induced plasma of organic compounds. Submitted for publication **C**.

Delgado, T., Alcántara, J. F., Vallido, J. M. and Laserna, J. J. Condensed-phase laser ionization time-of-flight mass spectrometry of highly energetic nitroaromatic compounds. *Rapid Communications in Mass Spectrometry*, 27:1-7, 2013 **D**.

Delgado, T., Vadillo, J. M. and Laserna, J. J. Laser-induced plasma spectroscopy of organic compounds. Understanding fragmentation processes using ion-photon coincidence measurements. *Journal of Analytical Atomic Spectroscopy*, Article in press, 2013 **E**.

De Lucia Jr., F. C., Harmon, R. S., McNesby, K. L., Winkel, R. J. and Miziolek, A. W. Laser-induced breakdown spectroscopy analysis of energetic materials. *Applied Optics*, 42:6148-6152, 2003.

De Lucia Jr., F. C., Gottfried, J. L., Munson, C. A. and Miziolek, A. W. Double pulse laser-induced breakdown spectroscopy of explosives: Initial study towards improved discrimination. *Spectrochimica Acta Part B: Atomic Spectroscopy*, 62:1399-1404, 2007.

De Lucia, F. C. and Gottfried, J. L. Characterization of a series of nitrogen-rich molecules using laser-induced breakdown spectroscopy. *Propellants, Explosives, Pyrotechnics,* 35:268-277, 2010.

De Lucia Jr., F. C. and Gottfried, J. L. Rapid analysis of energetic and geo-materials using LIBS. *Materials Today*, 14:274-281, 2011.

Demeure, K., Quinton, L., Gabelica, V. and De Pauw, E. Rational selection of the optimum maldi matrix for top-down proteomics by in-source decay. *Analytical Chemistry*, 79:8678-8685, 2007.

Demtroder, W. Molecular Physics. Theoretical Principles and Experimental Methods. *WILEY-VCH Verlag GmbH & Co. KGaA*, Berlin 2005.

Dimov, S. S. and Chryssoulis, S. L. Standardization of time-of-flight laser ionization mass spectrometry analysis of minerals. *Spectrochimica Acta Part B*, 53:399-406, 1998.

Dingus, R. S. and Scammon, R. J. Grüneisen-stress-induced ablation of biological tissue. *Proc. SPIE* 1427, 45, 1991.

Dong, M., Lu, J., Yao, S., Zhong, Z., Li, J., Li, J. and Lu, W. Experimental study on the characteristics of molecular emission spectroscopy for the analysis of solid materials containing C and N. *Optics Express,* 19:17021-17028, 2011.

Dolan, T. J. Fusion Research, Volume 1 - Principles. *Pergamon Press*, New York, 1982.

Dreisewerd, K. The desorption process in MALDI. *Chemical Reviews*, 103:395-425, 2003.

Durrant, S. F. and Ward, N. I. Recent biological and environmental applications of laser ablation inductively coupled plasma mass spectrometry (la-icp-ms). *Journal of Analytical Atomic Spectrometry*, 20:821:829, 2005.

E

Effenberger Jr., A. J. and Scott, J. R. Effect of Atmospheric Conditions on LIBS Spectra. *Sensors*, 10:4907-4925, 2010.

Eggins, S. M., Kinsle, L. P. J. and Shelley, J.M.G. Deposition and element fractionation processes during atmospheric pressure laser sampling for analysis by ICP-MS. *Applied Surface Science,* 127-129:278-286, 1998.

European Commission, Scientific Committee on Food. Polycyclic Aromatic Hydrocarbons – Occurrence in foods, dietary exposure and health effects. December 4, 2002.

F

Fabbro, R., Fabre, E., Amiranoff, F., Garban-Labaune, G., Virmont, J., Weinfeld, M. and Max, C. E. Laser wavelength dependence of mass-ablation rate and heat-flux inhibition in laser-produced plasmas. *Physical Reviews A*, 26, 2289–2292, 1982.

Fang, R., Zhang, D., Li, Z., Li, L., Tan, X. and Yang, F. Laser-target interaction during high-power pulsed laser deposition of superconducting thin films. *Physica Status Solidi A*, 204:4241-4248, 2007.

Fang, R., Zhang, D., Li, Z., Yang, F., Li, L., Tan, X. and Sun, M. Improved thermal model and its application in UV high-power pulsed laser ablation of metal target. *Solid State Communications*, 145:556-560, 2008.

Fardel, R., Nagel, M., Nuesch, F., Lippert, T. and Wokaun, A. Fabrication of organic light-emitting diode pixels by laser-assisted forward transfer. *Applied Physics Letters*, 91:061103-1-061103-2, 2007.

Ferguson, J. Absorption and Fluorescence Spectra of Crystalline Pyrene. *Journal of Chemical Physics*, 28:765-768, 1958.

Fernández-Bravo, A., Lucena, P. and Laserna, J. J. Selective sampling and laser-induced breakdown spectroscopy (LIBS) analysis of organic explosive residues on polymer surfaces. *Applied Spectroscopy*, 66:1197−1203, 2012.

Fernández-Bravo, A., Delgado, T., Lucena, P. and Laserna, J. J. Vibrational emission analysis of the CN molecules in laser-induced breakdown spectroscopy of organic compounds, 2013. Submitted for publication.

Fetzer, J. C. The Chemistry and Analysis of the Large Polycyclic Aromatic Hydrocarbons. *Polycyclic Aromatic Compounds*, 27:143, 2000.

Fisch, N. Confining a tokamak plasma with rf-driven currents, *Physical Review Letters,* 41, 873, 1978.

Fortes, F. J. and Laserna, J. J. The development of fieldable LIBS instrumentation: No limits on the horizon. *Spectrochimica Acta B*, 65: 975-990, 2010.

Fortes, F. J., Moros, J., Lucena, P., Cabalín, L. M. and Laserna, J. J. Laser-induced breakdown spectroscopy. *Analytical Chemistry*, 85:640−669, 2013.

Frank, M. Mass spectrometry with cryogenic detectors. *Nuclear Instruments and Methods in Physics Research A*, 444:375-384, 2000.

Fuge, G. M., Ashfold, M. N. R. and Henley, S. J. Studies of the plume emission during the femtosecond and nanosecond ablation of graphite in nitrogen. *Journal of Applied Physics*, 99:014309(1)–014309(12), 2006.

G

Galbács, G., Jedlinszki, N., Herrera, K., Omenetto, N., Smith, B. W. and Winefordner, J. D. A study of Ablation, Spatial, and Temporal Characteristics of Laser-Induced Plasmas Generated by Multiple Collinear Pulses. *Applied Spectroscopy,* 64:161-172, 2010.

Galloway, D. B., Bartz, J. A., Huey, L. G. and Crim, F. F. Pathways and kinetic energy disposal in the photodissociation of nitrobenzene. *The Journal of Chemical Physics*, 98:2107-2114, 1993.

Garcia, C. C., Vadillo, J. M., Palanco, S. and Laserna, J. J. Comparative analysis of layered materials using laser-induced plasma spectrometry and laser-ionization time-of-flight mass spectrometry. *Spectrochimica Acta Part B*, 56:923-931, 2001.

Garcia, C. C., Vadillo, J. M., Ruiz, J. and Laserna, J. J. Nanometric in-depth characterization of P diffusion and TiO2 anti-reflective coatings in solar cells by laser ionization time of flight mass spectrometry. *Journal of Analytical Atomic Spectrometry,* 18:779-782, 2003.

Garcia, C. C., Lindner, H., Von Bohlen, A., Vadla, C. and Niemax, K. Elemental fractionation and stoichiometric sampling in femtosecond laser ablation. *Journal of Analytical Atomic Spectrometry*, 23:470-478, 2008.

Garcia, C. C., Lindner, H. and Niemax, K. Laser ablation inductively coupled plasma mass spectrometry - current shortcomings, practical suggestions for improving performance, and experiments to guide future development. *Journal of Analytical Atomic Spectrometry*, 24:14-26, 2009.

Garcia-Reyes, J. F., Harper, J. D., Salazar, G. A., Charipar, N. A., Ouyang, Z. and Cooks, R. G. Detection of Explosives and Related Compounds by Low-Temperature Plasma Ambient Ionization Mass Spectrometry. *Analytical Chemistry*, 83:1084–1092, 2011.

Gaudiuso, R., Dell'Aglio, M., de Pascale, O., Senesi, G. S. and de Giacomo, A. Laser induced breakdown spectroscopy for elemental analysis in environmental, cultural heritage and space applications: A review of methods and results. *Sensors*, 10:7434-7468, 2010.

Geertsen, C., Briand, A., Chartier, F., Lacour, J. L., Mauchien, P., Siöström, S. and Mermet, J. M. Comparison between infrared and ultraviolet laser ablation at atmospheric pressure-implications for solid sampling inductively coupled plasma spectrometry. *Journal of Analytical Atomic Spectrometry*, 9:17-22, 1994.

Globig, D. and Weickhardt, C. Rapid analysis of aromatic contaminants in water samples by means of laser ionization mass spectrometry. *Analytical and Bioanalytical Chemistry*, 377:1124-1132, 2003.

Glumac, N and Elliott, G. The effect of ambient pressure on laser-induced plasmas in air. *Optics and Lasers in Engineering*, 45:27-35, 2007.

Gondal, M. A., Hussain, T., Yamani, Z. H. and Baig, M. A. On-line monitoring of remediation process of chromium polluted soil using LIBS. *Journal of Hazardous Materials*, 163:1265-1271, 2009.

Gordillo, F. J. Plasmas fríos. *Investigación y Ciencia*, june, 70-79, 2008.

Gornushkin, I. and Panne, U. Radiative models of laser-induced plasma and pump-probe diagnostics relevant to laser-induced breakdown spectroscopy. *Spectrochimica Acta, Part B*, 65:345−359, 2010.

Gottfried, J. L., De Lucia Jr, F. C., Munson, C. A. and Miziolek, A. W. Strategies for residue explosives detection using laser-induced breakdown spectroscopy. *Journal of Analytical Atomic Spectrometry*, 23:205–216, 2008.

Gottfried, J. L., De Lucia Jr, F. C., Munson, C. A. and Miziolek, A. W. Laser-induced breakdown spectroscopy for detection of explosives residues: a review of recent advances, challenges, and future prospects. *Analytical and Bioanalytical Chemistry*, 395:283-300, 2009.

Günther, D., Hattendorf, B. and Latkoczy, C. LA-ICP-MS – it´s particle size that really matters. *Analytical Chemistry*, 75:341A-347A, 2003.

Günther, D. and Hattendorf, B. Solid sample analysis using laser-ablation-inductively coupled plasma mass spectrometry. *Trends in Analytical Chemistry,* 24:255-265, 2005.

Gusarov, A. V., Gnedovets, A. G., Smurov, I. and Flamant, G. Simulation of nanoscale particles elaboration in laser-produced erosive flow. *Applied Surface Science*, 154–155, 331-336, 2000.

H

Hang, W. Laser ionization time-of-flight mass spectrometer with an ion guide collision cell for elemental analysis of solids. *Journal of Analytical Atomic Spectrometry*, 20:301-307, 2005.

Hanif, M., Salik, M. and Baig, M. A. Quantitative studies of copper plasma using laser induced breakdown spectroscopy. *Optics and Laser in Engineering*, 49:1456−1461, 2011.

Hankin, S. M., Tastker, A. D., Robson, L., Ledingham, K. W. D., Fang, X., McKenna, P., Mc Canny, T., Singhal, R. P., Kosmidis, C., Tzallas, P., Jaroszynski, D. A., Jones, D. R., Issac, R. C. and Jamison, S. Femtosecond laser time of flight mass spectrometry of labile molecular analytes: laser-desorbed nitro-aromatic molecules. *Rapid Communication in Mass Spectrometry,* 16:111-116, 2002.

Hardman, M. and Makarov, A. Interfacing the orbitrap mass analyzer an electrostatic ion source. *Analytical Chemistry,* 75:1699-1701, 2003.

Harilal, S. S., Bindhu, C. V., Tillack, M. S., Najmabadi, F. and Gaeris, A. C. Internal structure and expansion dynamics of laser ablation plumes into ambient gases. *Journal of Applied Physics*, 93:2380-2389, 2003.

Harilal, S. S., Sizyuk, T., Hassanein, A., Campos, D., Hough, P. and Sizyuk, V. The effect of excitation wavelength on dynamics of laser-produced tin plasma. *Journal of Applied Physics,* 109:063306-1–063306-9, 2011.

Harmon, R. S., De Lucia Jr., F.C., LaPointe, A., Winkel Jr., R.J. and Miziolek, A.W. LIBS for landmine detection and discrimination, *Analytical and Bioanaytical Chemistry*, 385:1140–1148, 2006.

He, J., Zhong, W., Mahan, C. and Hang, W. Laser ablation and ionization time-of-flight mass spectrometer with orthogonal sample introduction and axial field rf-only quadrupole cooling. *Spectrochimica Acta Part B*, 61:220-224, 2006.

He, X. N., Xie, Z. Q., Gao, Y., Hu, W., Guo, L. B., Jiang, L. and Lu, Y. F. Mass spectrometry of solid samples in open air using combined laser ionization and ambient metastable ionization. *Spectrochimica Acta Part B*, 67:64-73, 2012.

Hillenkamp, F. and Katalinic, J. P. MALDI MS: A Practical Guide to Instrumentation, Methods and Applications. *Wiley-VCH Verlag GmbH & Co. KGaA,* Weinheim (Germany), 2007.

Hollas, J. M. Modern spectroscopy. *John Wiley & Sons ltd*, Chichester, 1987.

Huang, R., Yu, Q., Tong, Q., Hang, W., He, J. and Huang, B. Influence of wavelength, irradiance, and the buffer gas pressure on high irradiance laser ablation and ionization source coupled with an orthogonal Time of Flight Mass Spectrometer. *Spectrochimica Acta Part B*, 64:255-261, 2009.

Huang, R., Lin, Y., Li, L., Hang, W., He, J. and Huang, B. Two-Dimensional Separation in Laser Ionization Orthogonal Time-of-Flight Mass Spectrometry. *Analytical Chemistry*, 82:3077-3080, 2010.

Huang, R., Yu, Q., Li, L., Lin, Y., Hang, W., He, J. and Huang, B. High irradiance laser ionization orthogonal time of flight mass spectrometry: A versatile tool for solid analysis. *Mass Spectrometry Reviews*, 30:1256-1268, 2011.

Huestis, D. L., Mullen, C., Coggiola, M. J. and Oser, H. Laser-ionization mass spectrometry of explosives and chemical warfare simulants. *Intenational Journal of High Speed Electronics and Systems*, 18:159-166, 2008.

I

Ibdzig, A. A. and Smimow, B. M. Reference Data on Atoms, Molecules and Ions, *Springer Verlag*, Berlin, 1983.

Iida, Y. Effects of atmosphere on laser vaporization and excitation processes of solid samples. *Spectrochimica Acta Part B: Atomic Spectroscopy*, 45:1353-1367, 1990.

Itina, T. E., Hermann, J., Delaporte, P. and Sentis, M. Laser-generated plasma plume expansion: combined continuous-microscopic modeling. *Physical Reviews,* E66: 066406(1)-066406(12), 2002.

Itina, T. E., Hermann, J., Delaporte, P. and Sentis, M. Combined continuous-microscopic moleling of laser plume expansion. *Applied Surface Science*, 208–209:27-32, 2003.

Itzkan, I., Albagli, D., Banish, B. J., Dark, M., von Rosenberg, C., Perelman, L. T., Janes, G. S. and Feld, M. S. The thermoelastic basis of short pulsed laser ablation of biological tissue. AIP Conference Proceedings, 288, 491, 1994.

J

Johnson, R. C. The Structure and Origin of the Swan Band Spectrum of Carbon. *Philosophical Transactions of the Royal Society of London. Ser. A.*, 226:157-230, 1927.

Joseph, D. D. and Preziosi, L. Heat waves. *Reviews of Modern Physics*, 61:41-74, 1989.

K

Kagawa, K. and Yokoi, S. Application of the N_2 laser to laser microprobe spectrochemical analysis. *Spectrochimicas Acta Part B*, 37:789-795, 1982.

Kelly, R. and Miotello, A. Contribution of vaporization and boiling to thermal-spike sputtering by ions or laser pulses. *Physical Review E*, 60:2616-2625, 1999.

Kim, W. S., Hector, L. G. and Ozisik, M. N. Hyperbolic heat conduction due to axisymmetric continuous or pulsed surface heat sources. *Journal of Applied Physics*, 68, 5478-5486, 1990.

Kivelson, M. G. and Russell, C. T. Introduction to space physics. *Cambridge University Press,* Cambridge (England), 1995.

Knight, A. K., Scherbarth, N. L., Cremers, D. A. and Ferris, M. J. Characterization of Laser-Induced Breakdown Spectroscopy (LIBS) for Application to Space Exploration. *Applied Spectroscopy*, 54:331-340, 2000.

Knochenmuss, R. A quantitative model of ultraviolet matrix-assisted laser desorption/ionization including analyte ion generation. *Analytical Chemistry*, 75:2199-2207, 2003 **A**.

Knochenmuss, R. and Zenobi, R. MALDI ionization: The role of in-plume processes. *Chemical Reviews*, 103:441-452, 2003 **B**.

Konjević, N., Ivković, M. and Jovićević, S. Spectroscopic diagnostics of laser-induced plasmas. *Spectrochimica Acta, Part B*, 65:593−602, 2010.

Kordás, K., Békési, J., Vajtai, R., Nánai, L., Leppävuori, S., Uusimäki, A., Bali, K., K. George, T.F., Galbács, G., Ignácz, F. and Moilanen P. Laser-assisted metal deposition from liquid-phase precursors on polymers. *Applied Surface Science*, 172:178-189, 2001.

Kosmidis, C., Ledingham, K. W. D., Clark, A., Marshall, A., Jennings, R., Sander, J. and Singhal, R. P. On the dissociation pathways of nitrobenzene. *International Journal of Mass Spectrometry and Ion Processes*, 135:229-242, 1994.

Kovacs, I. Rotational structure in the spectra of Diatomic Molecules. *Adam Hilger Ltd*., London, 1969.

Kruse, T. and Roth, P. High-temperature reaction of C2 with NO including product channel measurements. *International Journal of Chemical Kinetics*, 31:11-21, 1999.

Kushwaha, A. and Thareja, R. K. Dynamics of laser-ablated carbon plasma: formation of C2 and CN. *Applied Optics*, 47:G65-G71, 2008.

L

Labutin, T. A., Popov, A. M., Lednev, V. N., Zorov, N. B. Correlation between properties of a solid sample and laser-induced plasma parameters. *Spectrochimica Acta, Part B*, 64:938−949, 2009.

LaFranchi, B. W. and Petrucci, G. A. A comprehensive characterization of photoelectron resonance capture ionization aerosol mass spectrometry for the quantitative and qualitative analysis of organic particulate matter. *International Journal of Mass Spectrometry,* 258:120-133, 2006.

Laska L., Jungwirth, K., Kralikova, B., Krasa, J., Pfeifer, M., Rohlena, K., Skala, J., Ullschmied, J., Badziak, J., Parys, P., Wolowski, J., Woryna E., Gammino, S., Torrisi, L., Boody, F. P. and Hora, H. Generation of multiply charged ions at low and high laser-power densities, *Plasma Physics and Controlled Fusion*, 45:585–599, 2003.

Lazic, V., Palucci, A., Jovicevic, S., Poggi, C. and Buono, E. Analysis of explosive and other organic residues by laser induced breakdown spectroscopy. *Spectrochimica Acta Part B*, 64:1028-1039, 2009.

Lazic, V., Palucci, A., Jovicevic, S. and Carpanese, M. Detection of explosives in traces by laser induced breakdown spectroscopy: Differences from organic interferents and conditions for a correct classification. *Spectrochimica Acta Part B: Atomic Spectroscopy,* 66:644-655, 2011.

Le Drogoff, B., Margot, J., Vidal, F., Laville, S., Chaker, M., Sabsabi, M., Johnston, T. W. and Barthe´lemy, O. Influence of the laser pulse duration on laser-produced plasma properties, *Plasma Sources Science and Technology,* 13:223-230, 2004.

Ledingham, K. W. D., Kilic, H. S., Kosmidis, C., Deas, R. M., Marshall, A., McCanny, T., Singhal, I. R. P., Langley, A. J. and Shaikh, W. A Comparison of Femtosecond and Nanosecond Multiphoton Ionization and Dissociation for Some nitro-molecules. *Rapid Communications in Mass Spectrometry*, 9:1522-1527, 1995.

Lee, Y. I., Song, K., Cha, H. K., Lee, J. M., Park, M. C., Lee, G. H. and Sneddon, J. Influence of atmosphere and irradiation wavelength on copper plasma emission induced by excimer and Q-switched Nd:YAG laser ablation. *Applied Spectroscopy,* 51:959-964, 1997.

Lee, W., Wu, J., Lee, Y. and Sneddon, J. Recent applications of laser-induced breakdown spectrometry: A review of material approaches. *Applied Spectroscopy Reviews*, 39:27-97, 2004.

Lei, W. Q., Ma, Q. L., Motto-Ros, V., Bai, X. S., Zheng, L. J., Zeng, H. P., Yu, J. Effect of ablation photon energy on the distribution of molecular species in laser-induced plasma from polymer in air. *Spectrochimica Acta Part B*, 73:7-12, 2012.

Lewis, A. L. and Piepmeier, E. H. Chemical and physical influences of the atmosphere upon the spatial and temporal characteristics of atomic fluorescence in a laser microprobe plume. *Applied Spectroscopy*, 37:523-530, 1983.

Lin, Y., Yu, Q., Hang, W., He, J. and Huang, B. Characterization of laser ablation and ionization in helium and argon: a comparative study by time-of-flight mass spectrometry. *Spectrochimica Acta Part B*, 64:1204-1211, 2009.

Lin, Y., Yu, Q., Hang, W. and Huang, B. Progress of laser ionization mass spectrometry for elemental analysis - A review of the past decade. *Spectrochimica Acta Part B,* 65:871-883, 2010.

Loewen, E. and Popov, E. Diffraction Gratings and Applications. *Optical Engineering, Marcel Dekker Inc*, New York, 1997.

López-Moreno, C., Palanco, S., Laserna, J. J., DeLucia Jr., F., Miziolek, A. W., Rose, J., Walters, R. A. and Whitehouse, A. I. Test of a stand-off laser-induced breakdown spectroscopy sensor for the detection of explosive residues on solid surfaces. *Journal of Analytical Atomic Spectrometry*, 21:55-60, 2006.

Lubman, D. M. Lasers and mass spectrometry. *Oxford University Press*, New York, 1990.

Lucena, P., Doña, A., Tobaria, L. M. and Laserna, J. J. New challenges and insights in the detection and spectral identification of organic explosives by laser induced breakdown spectroscopy. *Spectrochimica Acta Part B*, 66:12-20, 2011.

Luo, W. F., Zhao, X. X., Sun, Q. B., Gao, C. X., Tang, J., Wang, H. J. and Zhao, W. Characteristics of the aluminum alloy plasma produced by a 1064 nm Nd:YAG laser with different irradiances. *Pramana - Journal of Physics*, 74:945–959, 2010.

M

Ma, Q. and Dagdigian, P. J. Kinetic model of atomic and molecular emissions in laser-induced breakdown spectroscopy of organic compounds. *Analytical and Bioanalytical Chemistry*, 400:3193-3205, 2011.

Ma, Q., Motto-Ros, V., Laye, F., Yu, J., Lei, W., Bai, X., Zheng, L. and Zeng, H. Ultraviolet versus infrared: Effects of ablation laser wavelength on the expansion of laser-induced plasma into one-atmosphere argon gas. *Journal of Applied Physics*, 111:053301-1–053301-11, 2012.

Makarov, A. Electrostatic axially harmonic orbital trapping: a high performance technique of mass analysis. *Analytical Chemistry,* 72:1156-1162, 2000.

Makarov, A., Denisov, E., Kholomeev, A., Balschun, W., Lange, O., Strupat, K. and Horning, S. Performance evaluation of a hybrid linear ion trap/orbitrap mass spectrometer. *Analytical Chemistry,* 78:2113-2120, 2006.

Mamyrin, B. A., Karataev, V. I., Shmikk, D. V. and Zagulin V. A. Mass-reflectron, a new nonmagnetic time-of-flight high-resolution mass-spectrometer. *Sovietic Physics JETP,* 37:45-48, 1973.

Mao, X. L., Chan, W. T., Shannon, M. A. and Russo, R. E. Plasma shielding during picosecond laser sampling of solid materials by ablation in He *versus* Ar atmosphere. *Journal of Applied Physics,* 74:4915-4922, 1993.

Mao, X. L., Borisov, O. V. and Russo, R. E. Enhancements in laser ablation inductively coupled plasma-atomic emission spectrometry based on laser properties and ambient environment. *Spectrochimica Acta, Part B: Atomic Spectroscopy*, 53:731-739, 1998 **A**.

Mao, X. L., Ciocan, A. C., Borisov, O. V. and Russo, R. E. Laser ablation processes investigated using ICP-AES. *Applied Surface Science,* 127-129:262-268, 1998 **B**.

Mao, X., Bol'shakov, A. A., Perry, D. L., Sorkhabi, O. and Russo, R. E. Laser ablation molecular isotopic spectrometry: parameter influence on boron isotope measurements. *Spectrochimica Acta Part B*, 66:604–609, 2011 **A**.

Mao, X., Bol'shakov, A. A., Choi, I., McKay, C. P., Perry, D. L., Sorkhabi, O. and Russo, R. E. Laser Ablation Molecular Isotopic Spectrometry: Strontium and its isotopes. *Spectrochimica Acta Part B*, 66:767-775, 2011 **B**.

March, R. E. and Hughes, R. J. Quadrupole Ion Storage Mass Spectrometry, *Wiley Interscience.* New York, 1989.

March, R. E. and Todd, J. F. J. Practical Aspects of Ion Trap Mass Spectrometry. *CRC Press: Boca Raton*, New York, 1995.

Margetic, V., Pakulev, A., Stockhaus, A., Bolshov, M., Niemax, K. and Hergenroder, R. A comparison of nanosecond and femtosecond laser-induced plasma spectroscopy of brass samples. *Spectrochimica Acta Part B: Atomic Spectroscopy*, 55:1771-1785, 2000.

Marshall, A., Clark, A., Ledingham, K. W. D., Sander, J., Singhal, R. P., Kosmidis, C. and Deas, R. M. Detection and identification of explosives compounds using laser ionization time-of-flight techniques. *Rapid Communications in Mass Spectrometry*, 7:521-526, 2005.

Marshall, M. and Oxley, J. C. Aspects of explosives detection. *Elsevier*, Amsterdam, 2009.

Martin, A. N., Farquar, G. R., Gard, E. E., Frank, M. and Fergenson, D. P. Identification of High Explosives Using Single-Particle Aerosol Mass Spectrometry. *Analytical Chemistry*, 79:1918-1925, 2007.

McDonnell, L. A. and Heerem, R. M. A. Imaging Mass Spectrometry. *Mass Spectrometry Reviews,* 26:606-643, 2007.

McMillen, D. F., Erlich, D. C., He, C., Becker, C. H. and Shockey, D. A. Fracture-induced and thermal decomposition of NTO using laser ionization mass spectrometry. *Combustion and Flame*, 111:133-160, 1997.

Melrose, D. B. Instabilities in space and laboratory plasmas. *Cambridge University Press Cambridge* (England), New York, 1986.

Mercadier, L., Hermann, J., Grisolia, C. and Semerok, A. Plume segregation observed in hydrogen and deuterium containing plasmas produced by laser ablation of carbon fiber tiles from a fusion reactor. *Spectroschimica Acta Part B: Atomic Spectroscopy,* 65:715-720, 2010.

Minsek, D. W., Chen, P. Photoelectron spectrum of the propargyl radical in a supersonic beam. *Journal of Physical Chemistry*, 94:8399-8401, 1990.

Miotello, A. and Kelly, R. Laser-induced phase explosion: New physical problems when a condensed phase approaches the thermodynamic critical temperature. *Applied Physics A: Materials Science and Processes*, 69:S67-S73, 1999.

Miziolek, A. W., Palleschi, A. and Schechter, I. Laser Induced Breakdown Spectroscopy. *Cambridge University Press*, Cambridge, 2006.

Moench, I., Sattmann, R. and Noll, R. High-speed identification of polymers by laser-induced breakdown spectroscopy. *Proceedings of SPIE,* 3100:64–74, 1997.

Mominuzzaman, S. M., Chandrasekaran, N., Soga, T. and Jimbo, T. Polymeric semiconducting carbon from fullerene by pulsed laser ablation. *Diamond and Related Materials*, 17:641-645, 2008.

Moore, D. S. Recent Advances in Trace Explosives Detection Instrumentation. *Sensing and Imaging*, 8:9-38, 2007.

Moros, J., Lorenzo, J. A., Lucena, P., Tobaria, L. M. and Laserna, J. J. Simultaneous Raman-LIBS for the standoff analysis of explosive materials. *Spectroscopy Europe*, 22:18-22, 2010 **A**.

Moros, J., Lorenzo, J. A., Lucena, P., Tobaria, L. M. and Laserna, J. J. Simultaneous Raman spectroscopy-laser induced breakdown spectroscopy for instant standoff analysis of explosives using a mobile integrated sensor platform. *Analytical Chemistry*, 82:1389-1400, 2010 **B**.

Moros, J. and Laserna, J. J., unpublished results.

Mullen, C., Huestis, D. L., Coggiola, M. J. and Oser, H. Laser photoionization of triacetone triperoxide (TATP) by femtosecond and nanosecond laser pulses. *International Journal of Mass Spectrometry*, 252:69-72, 2006 **A**.

Mullen, C., Irwin, A., Pond, B. V., Huestis, D. L., Coggiola, M. J. and Oser. H. Detection of explosives and explosives-related compounds by single photon laser ionization time-of-flight mass spectrometry. *Analytical Chemistry*, 78:3807-3814, 2006 **B**.

Mullen, C., Coggiola, M. J. and Oser, H. Femtosecond Laser Photoionization Time-of-Flight Mass Spectrometry of Nitro-aromatic Explosives and Explosives Related Compounds. *Journal of the American Society of Mass Spectrometry*, 20:419-429, 2009.

Murray, J. S., Lane, P. and Politzer, P. Effects of strongly electron-attracting components on molecular surface electrostatic potentials: application to predicting impact sensitivities of energetic molecules. *Molecular Physics,* 93:187-194, 1998.

N

Nakayama, T., Kitamura, M. Y. and Watanabe, K. Ionization Potential and Absorption Coefficients of Nitrogen Dioxide. *Journal of Chemistry and Physics*, 30:1180-1186, 1959.

Nefedov, A., Morfill, G., Fortov, V., Thomas, H., Rothermel, H., Hagl, T., Ivlev, A., Zuzic, M., Klumov, B., Lipaev, A., Molotkov, V., Petrov, O., Gidzenko, Y., Krikalev, S., Shepherd, W., Ivanov, A., Roth, M., Binnenbruck, H., Goree, J. and Semenov, Y. PKE-Nefedov: plasma crystal experiments on the International Space Station. *New Journal of Physics*, 5:33.1-33.10, 2003.

Neamtu, J., Mihailescu, I. N., Ristoscu, C. and Hermann, J. Theoretical modelling of phenomena in the pulsed-laser deposition process: Application to Ti targets ablation in low-pressure N_2. *Journal of Applied Physics*, 86:6096-6107, 1999.

O

Osticioli, I., Wolf, M. and Anglos, D. An optimization of parameters for application of a laser-induced breakdown spectroscopy microprobe for the analysis of works of art. *Applied Spectroscopy*, 62:1242-1249, 2008.

P

Park, H. S., Nam, S. H. and Par, S. M. Optical emission studies of a plume produced by laser ablation of a graphite target in a nitrogen atmosphere. *Bulletin of the Korean Chemical Society*, 25:620-624, 2004.

Pasquini, C., Cortez, J., Silva, L.M.C. and Gonzaga, F.B. Laser Induced Breakdown Spectroscopy. *Journal of the Brazilian Chemical Society,* 18:463–512, 2007.

Pearse, R. W. B. and Gaydon, A. G. The identification of molecular spectra, *Chapman and Hall*, London, 1976.

Peterlongo, A., Miotello, A. and Kelly, R. Laser-pulse sputtering of aluminum: vaporization, boiling, superheating and gas-dynamic effects. *Physical Review E,* 50:4716-4727, 1994.

Pisonero, J., Koch, J., Wäle, M., Hartung, W., Spencer, N. D. and Günther, D. Capabilities of femtosecond laser ablation inductively coupled plasma mass spectrometry for depth profiling of thin metal coatings. *Analytical Chemistry*, 79:2325-2333, 2007.

Pond, B. V., Mullen, C., Suarez, I., Kessler, J., Briggs, K., Young, S. E., Coggiola, M. J., Crosley, D. R. and Oser, H. Detection of explosive-related compounds by laser photoionization time-of-flight mass spectrometry. *Applied Physics A,* 86:735-742, 2007.

Portnov, A., Rosenwaks, S. and Bar, I. Emission following laser-induced breakdown spectroscopy of organic compounds in ambient air. *Applied Optics*, 42:2835-2842, 2003 **A**.

Portnov, A., Rosenwaks, S. and Bar, I. Identification of organic compounds in ambient air via characteristic emission following laser ablation. *Journal of Luminiscence*, 102-103:408-413, 2003 **B**.

Pradhan, A. D., Partridge, H. and Bauschlicher Jr., C. W. The dissociation energy of CN and C2. *Journal of Chemistry and Physics*, 101:3857-3861, 1994.

Q

Qiu, T. Q. and Tien, C. L. Femtosecond laser heating of multi-layer metals—I. Analysis. *International Journal of Heat and Mass Transfer*, 37:2789-2797, 1994.

R

Radziemski, L. J. and Cremers, D. A. Laser-induced Plasmas and Applications. *Marcel Dekker*, New York, 1989.

Radziemski, L. J. Review of selected analytical applications of laser plasmas and laser ablation, 1987-1994. *Microchemical Journal*, 50:218:234, 1994.

Ralchenko, Y., Kramida, A. and Reader, J. NIST ASD Team, Nist atomic spectra database (version 3.1.5), [Online]. Available: http://physics.nist.gov/asd3 [2008, July 24]. *National Institute of Standards and Technology*, Gaithersburg, MD.

Ratcliffe, J. A. An Introduction to the Ionosphere and Magnetosphere, *Cambridge University Press Cambridge* (England), New York 1972.

Rieger, G. W., Taschuk, M., Tsui, Y. Y. and Fedosejevs, R. Comparative study of laser-induced plasma emission from microjoule picosecond and nanosecond KrF-laser pulses, *Spectrochimica Acta, Part B: Atomic Spectroscopy,* 58:497-510, 2003.

Rios Castro, A., Moreno Bondi, M. C., Simonet Suau, B. M. Técnicas espectroscópicas en química analítica. Vol. I. *Ed. Síntesis*, Madrid, 2013.

Rodriguez-Celis, E. M., Gornushkin, I. B., Heitmann, U. M., Almirall, J. R., Smith, B. W., Winefordner, J. D. and Omenetto, N. Laser induced breakdown spectroscopy as a tool for discrimination of glass for forensic applications. *Analytical and Bioanalytical Chemistry*, 391:1961-1968, 2008.

Rozman, R., Grabec, I. and Govekar, E. Influence of absorption mechanisms on laser- induced plasma plume. *Applied Surface Science*, 254:3295-3305, 2008.

Rusak, D. A., Castle, B. C., Smith, B. W., Winefordner, J. D. Recent trends and the future of laser-induced plasma spectroscopy. *Trac-Trends in Analytical Chemistry,* 17:453–461, 1998.

Russo, R. E. Laser ablation. *Applied Spectroscopy*, 49:14A–28A, 1995.

Russo R. E., Mao X. L. and Borisov O. V. Laser ablation sampling. *Trac-Trends Analytical Chemistry*, 17:461–469, 1998.

Russo R. E., Mao X. L., Borisov O. V. and Liu, H. Influence of wavelength on fractionation in laser ablation icp-ms. *Journal of Analytical Atomic Spectrometry*, 15: 1115-1120, 2000.

Russo, R. E., Mao, X. L., Borisov, O. V., and Liu, H. Influence of wavelength on fractionation in laser ablation ICP-MS, *Journal of Analytical Atomic Spectrometry,* 15:1115–1120, 2000.

Russo, R. E., Bol'shakov, A. A., Mao, X., McKay, C. P., Perry, D. L. and Sorkhabi, O. Laser Ablation Molecular Isotopic Spectrometry. *Spectrochimica Acta Part B*, 66:99-104, 2011.

S

Sakka, T., Masai, S., Fukami, K., Ogata, Y. H. *Spectrochimica Acta Part B*, 64:981-985, 2009.

Salle, B., Cremers, D. A., Maurice, S. and Wiens, R. C. Influence of the ambient pressure on the calibration curves prepared from soil and clay samples. *Spectrochimica Acta Part B - Atomic Spectroscopy*, 60:479-490, 2005.

Schweitzer, D., Hausser, K. H., Kirrstetter, R. G. H. and Staab, H. A. Transanular Interaction in [2.2]Phanes: [2.2](2,7)Pyrenophane. *Z. Naturforsch*, 31a:1189-1192, 1976.

Schramm, E., Mühlberger, F., Mitschke, S., Reichardt, G., Schultze-Ladbeck, R., Pütz, M. and Zimmermann, R. Determination of the ionization potentials of security-relevant substances with single photon ionization mass spectrometry using synchrotron radiation. *Applied Spectroscopy*, 62:238-247, 2008.

Shafranov, V. D. Plasma equilibrium in a magnetic field. *Reviews of Plasma Physics, Vol. 2*, Consultants Bureau, New York, p. 103, 1966.

Sheaff, C. N., Eastwood, D., Wai, C. M. and Addleman, R. S. Fluorescence Detection and Identification of Tagging Agents and Impurities Found in Explosives. *Applied Spectroscopy,* 62:739-746, 2008.

Schmitz, T. A., Koch, J., Günther, D. and Zenobi, R. Characterization of aerosol plumes in nanosecond laser ablation of molecular solids at atmospheric pressure. *Applied Physics B: Laser Optics*, 100:521–533, 2010.

Schmitz, T. A., Koch, J., Günther, D. and Zenobi, R. Early plume and shock wave dynamics in atmospheric-pressure ultraviolet-laser ablation of different matrix-assisted laser ablation matrices. *Journal of Applied Physics*, 109:123106-1−123106-15, 2011.

Shukla, P. K. and Mamun, A. A. Introduction to dusty plasma physics. *Institute of Physics Publishing Bristol*, 2002.

Sicilia, E., Di Maio, F. P. and Russo, N. Features of the potential energy surface for the $CH_3 + O_2$ reaction channels. *Chemical Physics Letters*, 225:208-212, 1994.

Siegman, A. E. Lasers. *University Science Books*, USA 1986.

Silfvast, W. T. Laser Fundamentals. *Cambridge University Press*, New York, 1996.

Singh, R. K. and Narayan, J. Pulsed-laser evaporation technique for deposition of thin films: Physics and theoretical model. *Physics Reviews B* 41:8843-8854, 1990 **A**.

Singh, R. K., Holland, W., and Narayan, J. Theoretical model for deposition of superconducting thin films using pulsed laser evaporation technique. *Journal of Applied Physics*, 68:233-248, 1990 **B**.

Smith, C. A., Martinez, M. A., Veirs, D. K. and Cremers, D. A. Pu-239/Pu-240 isotope ratios determined using high resolution emission spectroscopy in a laser-induced plasma. *Spectrochimica Acta Part B*, 57: 929-937, 2002.

Smith, R. M. Understanding mass spectra: a basic approach. John *Wiley & Sons,* Inc., Hoboken, NJ, USA, 2004.

Sneddon, J. and Yi, L. Novel and recent applications of elemental determination by laser-induced breakdown spectrometry. *Analytical Letters,* 32:2143–2162, 1999.

Song, K., Lee, Y. I. and Sneddon, J. Applications of laser induced breakdown spectrometry. *Applied Spectroscopy Reviews*, 32:183–235, 1997.

Song, K., Kim, D., Cha, H., Kim, Y., Chang Jung E., Choi, I., Yoo, H. and Oh, S. Characterization of laser-induced plasma in a vacuum using laser ablation mass spectrometry and laser-induced breakdown spectrometry. *Microchemical Journal*, 76:95-103, 2004.

Sovová, K., Dryahina, K., Spanel, P., Kyncl, M. and Civis, S. A study of the composition of the products of laser-induced breakdown of hexogen, octogen, pentrite and trinitrotoluene using selected ion flow tube mass spectrometry and UV-Vis Spectrometry. *Analyst,* 135:1106-1114, 2010.

Spanel, P., Dryahina, K. and Smith, D. A general method for the calculation of absolute trace gas concentrations in air and breath from selected ion flow tube mass spectrometry data. *International Journal of Mass Spectrometry,* 249:230-239, 2006.

Stafe, M, Negutu, C. and Popescu, I. M. Theoretical determination of the ablation rate of metals in multiple-nanosecond laser pulses irradiation regime. *Applied Surface Science*, 253:6353-6358, 2007.

Stchur, P., Yang, K. X., Hou, X. D., Sun, T. and Michel, R. G. Laser excited atomic fluorescence spectrometry - a review. *Spectrochimica Acta Part B,* 56:1565–1592, 2001.

Steinfeld, J. I. and Wormhoudt, J. Explosives Detection: A Challenge for Physical Chemistry. *Annual Review of Physical Chemistry,* 49:203-232, 1998.

Stephens, W. E. A Pulsed Mass Spectrometer with Time Dispersion, *Phys. Rev.*, 69:691, 1946.

St-Onge, L., Sing, R., Béchard, S. and Sabsabi, M. Carbon emissions following 1064 μm laser ablation of graphite and organic samples in ambient air. *Applied Physics A*, 69:913-916, 1999.

St-Onge, L., Kwong, E., Sabsabi, M. and Vadas, E. B. Quantitative analysis of pharmaceutical products by laser-induced breakdown spectroscopy. *Spectrochimica Acta Part B*, 57:1131–1140, 2002.

Surko, C., Leventhal, M. and Passner, A. Positron plasma in the laboratory, *Physical Review Letters* 62, 8:901-904, 1989.

Svelto, O. Principles of Lasers. *Springer*, 1998.

Sysoev, A. and Sysoev, A. Can laser-ionisation time-of-flight mass spectrometry be a promising alternative to laser ablation/inductively-coupled plasma mass spectrometry and glow discharge mass spectrometry for the elemental analysis of solids? *European Journal of Mass Spectrometry*, 8:213-232, 2002.

T

Takats, Z., Wiseman, J. M., Gologan, B. and Cooks, R. G. Mass Spectrometry sampling under ambient conditions with desorption electrospray ionization. *Science*, 306:471-473, 2004.

Tanaka, G. and Weatherford, C. Decomposition mechanisms of dinitrotoluene. *International Journal of Quantum Chemistry*, 108:2924-2934, 2008.

Tellez, H., Vadillo, J. M., Chater, R. J., Laserna, J. J. and McPhail, D. S. Focused ion beam imaging of laser ablation sub-surface effects on layered materials. *Applied Surface Science*, 255:2265-2269, 2008.

Téllez, H. Secondary ion mass spectrometry characterization of surface and interfaces in nanolayered structures. *PhD Thesis, University of Málaga*, 2010.

Tellez, H., Vadillo, J. M., Laserna, J. J. Secondary ion mass spectrometry of powdered explosive compounds for forensic evidence analysis. *Rapid Communications in Mass Spectrometry*, 26:1203-1207, 2012.

Thareja, R. K., Dwivedi, R. K. and Ebihara, K. Interaction of ambient nitrogen gas and laser ablated carbon plume: Formation of CN. *Nuclear Instruments and Methods in Physics Research B,* 192:301-310, 2002.

Tielens, A. G. G. M. Interstellar Polycyclic Aromatic Hydrocarbon Molecules**.** *Annual Review of Astronomy and Astrophysics*, 46:289–337, 2008.

Tönnies, K., Schmid, R. P., Weickhardt, C., Reif, J. and Grotemeyer, J. Multiphoton ionization of nitrotoluenes by means of ultrashort laser pulses. *International Journal of Mass Spectrometry*, 206:245–250, 2001.

Torrisi, L., Ando, L., Ciavola, G., Gammino, S. and Barna, A. Angular distribution of ejected atoms from Nd:YAG laser irradiating metals. *Review of Scientific Instrument,* 72:68-72, 2001.

Torrisi, L. Fractional ionization in plasmas produced by pulsed laser ablation. *Radiation Effects and Defects in Solids*, 157:347-356, 2002.

Tsuboi, Y., Hatanaka, K., Fukumura, H. and Masuhara, H. The 248 nm Excimer Laser Ablation Mechanism of Liquid Benzene Derivatives: Photochemical Formation of Benzyl Radical Leads to Ablation*.* *The Journal of Physical Chemistry A*, 102:1661-1665, 1998.

V

Vadillo, J. M., Romero, J. M. F., Rodríguez, C. and Laserna, J. J. Effect of plasma shielding on laser ablation rate of pure metals at reduced pressure. *Surface and Interface Analysis*, 27:1009-1015, 1999.

Vadillo, J. M. and Laserna, J. J. Laser-induced plasma spectrometry: truly a surface analytical tool. *Spectrochimica Acta Part B: Atomic Spectroscopy*, 59:147-161, 2004.

Vadillo, J. M., García, C. C., Alcántara, J. F. and Laserna, J. J. Thermal-to-plasma transitions and energy thresholds in laser ablated metals monitored by atomic emission/mass spectrometry coincidence analysis. *Spectrochimica Acta Part B*, 60:948-954, 2005.

Vastola, F. J. and Pirone, A. Journal of Ionization of Organic Solids by Laser Irradiation. *Advances in Mass Spectrometry,* 4:107-111, 1968.

Vastola, F. J., Mumma, R. O. and Pirone, A. J. Analysis of Organic Salts by Laser Ionization. *Organic Mass Spectrometry*, 3:101-104, 1970.

Venugopalan, V. Pulsed laser ablation of tissue: surface vaporization or thermal explosion? *Proceeding SPIE* 2391, 184, 1995.

Vertes, A., Juhasz, P., Balazs, L. and Gijbels, R. Target heating, plasma formation and expansion processes during laser ionization. *E. Russell (Ed.), Microbeam Analysis, San Francisco Press,* 273-276, 1989.

Vertes, A., Gijbels, R. and Adams, F. Laser ionization mass analysis. *John Wiley & Sons*, New York, 1993.

Viskup, R., Praher, B., Stehrer, T., Jasik, J., Wolfmeir, H., Arenholz, E., Pedarnig, J. D. and Heitz, J. Plasma plume photography and spectroscopy of Fe-Oxide materials. *Journal of Applied Surface Science,* 255:5215–5219, 2009.

Vivien, C., Hermann, J., Perrone, A., Boulmer-Leborgne, C. and Luches, A. A study of molecule formation during laser ablation of graphite in low-pressure nitrogen. *Journal of Physics D: Applied Physics*, 31:1263-1272, 1998.

Volkov, A. N., Lukianov, G. A. and O'Connor, G. M. *Proceeding SPIE* 6985, 69850P, 2008.

Vors, E., Gallou, C. and Salmon, L. Laser-induced breakdown spectroscopy of carbon in helium and nitrogen at high pressure. *Spectrochimica Acta Part B: Atomic Spectroscopy*, 63:1198-1204, 2008.

W

Wang, X., Amoruso, S., Armenante, M., Boselli, A., Bruzzese, R., Spinelli, N. and Velotta, R. *Optics and Lasers in Engineering*, 39:179-190, 2003.

Watanabe, K., Hattori, K. and Kawarabayashi, J. Improvement of resonant laser ablation mass spectrometry using high-repetition-rate and short-pulse tunable laser system. *Spectrochimica Acta Part B*, 58:1163-1169, 2003.

Weber, I.T., Rousseau, A., Guilloux-Viry, M., Bouquet, V. and Perrin, A. Microstructure comparison between $KNbO_3$ thin films grown by polymeric precursors and PLD methods. *Solid State Sciences*, 7:1317-1323, 2005.

Webb, R. L., Dickinson, J. T. and Exarhos, G. J. Characterization of Particulates Accompanying Laser Ablation of NaNO3. *Applied Spectroscopy*, 51:707-717, 1997.

Weickhardt, C., Tönnies, K. and Globig, D. Detection and Quantification of Aromatic Contaminants in Water and Soil Samples by Means of Laser Desorption Laser Mass Spectrometry. *Analytical Chemistry*, 74:4861-4867, 2002.

Wen, S. B., Mao, X. L., Greif, R. and Russo, R. E. Expansion of the laser ablation vapor plume into a background gas. *Journal of Applied Physics*, 101:1–13, 2007.

Wenzel, R. J., Matter, U., Schultheis, L. and Zenobi, R. Analysis of megadalton ions using cryodetection maldi time-of-flight mass spectrometry. *Analytical Chemistry*, 77:4329-4337, 2005.

Winefordner, J.D., Gornushkin, I.B., Correll, T., Gibb, E., Smith, B.W., Omenetto, N. Comparing several atomic spectrometric methods to the super stars: special emphasis on laser induced breakdown spectrometry, LIBS, a future super star. *Journal of Analytical Aomict Spectrometry,* 19:1061–1083, 2004.

Wiley, W. C. and McLaren, I. H. Time-of-flight mass spectrometer with improved resolution. *Review of Scientific Instruments*, 26:1150-1157, 1955.

Willmott, P. R. and Huber, J. R. Pulsed laser vaporization and deposition. *Reviews of Modern Physics*, 72:315-328, 2000.

Wilson Jr., W. E. A critical review of the gas-phase reaction kinetics of the hydroxyl radical. *Journal of Physical and Chemical Reference Data*, 1, 535-573, 1972.

Wood, R. F. and Giles, G. E. Macroscopic theory of pulsed-laser annealing I. Thermal transport and melting. *Physical Revies B,* 23:2923-2942, 1981.

Y

Yalçin, S., Tsui, Y. Y. and Fedosejevs, R. Pressure dependence of emission intensity in femtosecond laser-induced breakdown spectroscopy. *Journal of Analytical Atomic Spectrometry*, 19:1295-1301, 2004.

Yinon, J. Advances in Forensic Applications of Mass Spectrometry. *CRC Press*, London, 2004.

Yinon, J. Counterterrorist detection techniques of explosives. *Elsevier*, Amsterdam, 2007.

Yu, Q., Chen, L., Huang, R., Hang, W., He, J. and Huang, B. Laser ionization time-of-flight mass spectrometry for direct elemental analysis. *Trends in Analytical Chemistry*, 28:1174-1185, 2009.

Z

Zelinger, Z., Novotny, M., Bulir, J., Lancok, J., Kubat, P. and Jelinek, M. Laser plasma plume kinetic spectroscopy of the nitrogen and carbon species, *Contributions to Plasma Physics,* 43:426-432, 2003.

Zenobi, R. Advances in surface analysis and mass spectrometry using laser desorption methods. *Chimia*, 48:64-71, 1994.

Zhang, D., Liu, D., Li, Z., Hou, S., Yu, B., Guan, L., Tan, X. and Li, L. A new model of pulsed laser ablation and plasma shielding. *Physica B,* 362:82-87, 2005.

Zhigilei, L. V., P. B. S. Kodali, P. B. S. and Garrison, B. J. On the Threshold Behavior in the Laser Ablation of Organic Solids, *Chemical Physics Letters,* 276:269-273, 1997.

Zhigilei, L. V. and Garrison, B. J. Molecular dynamics simulation study of the fluence dependence of particle yield and plume composition in laser desorption and ablation of organic solids. *Applied Physics Letters*, 74:1341-1344, 1999.

Zhigilei, L. V. and Garrison, B. J. Microscopic mechanisms of laser ablation of organic solids in the thermal and stress confinement irradiation regimes. *Journal of Applied Physics*, 88:1281-1299, 2000.

Zoriy. M. V., Kayser, M. and Becker, J. S. Possibility of nano-local element analysis by near-field laser ablation inductively coupled plasma mass spectrometry: New experimental arrangement and first application. *International Journal of Mass Spectrometry*, 273:151-155, 2008.

APPENDIX 1

LIMS Spectral Library

Melamine $C_3H_6N_6$

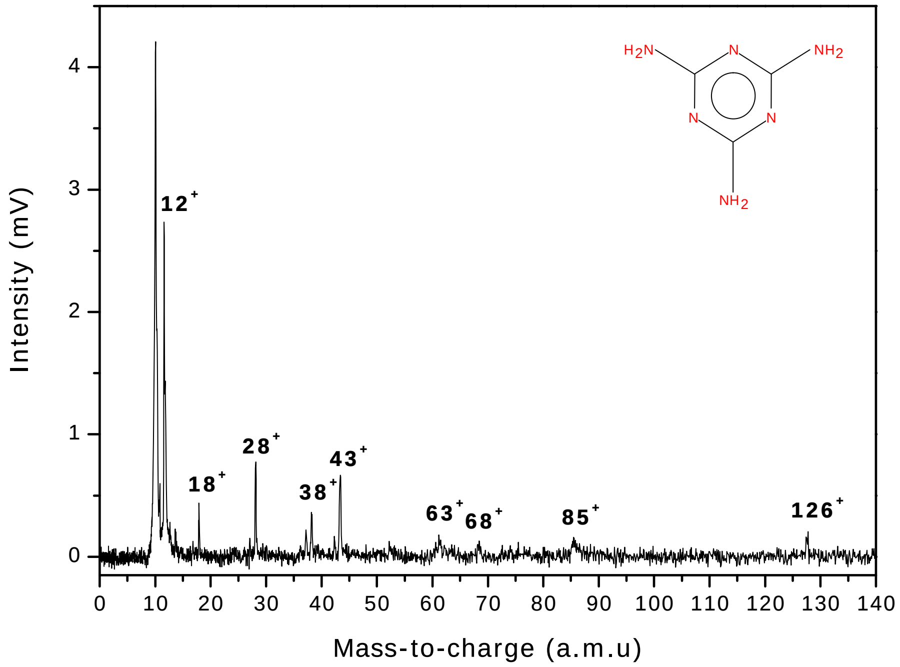

Name	**Melamine**	**Wavelength (nm)**	**266**	**Pulse Width (ns)**	**800**
Formula	**$C_3H_6N_6$**	**Pressure (mb)**	**$< 10^{-5}$**	**Pulse Delay (ns)**	**0**
Mw	**126**	**Energy (mJ)**	**1.8**	**Ext. Voltage (V)**	**-1280**

Melamine $C_3H_6N_6$

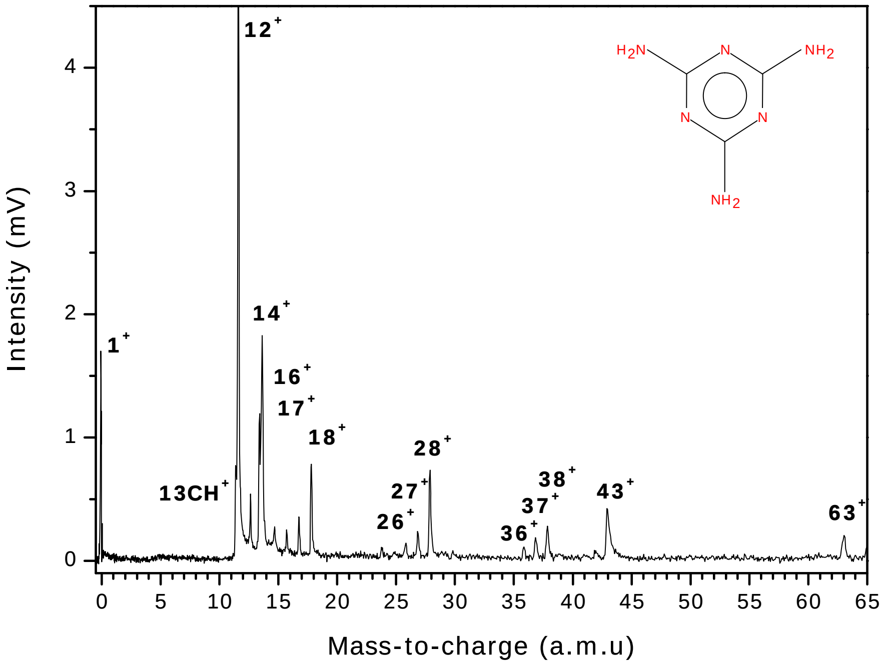

Name	**Melamine**	**Wavelength (nm)**	**266**	**Pulse Width (ns)**	**400**
Formula	**$C_3H_6N_6$**	**Pressure (mb)**	**< 10^{-5}**	**Pulse Delay (ns)**	**0**
Mw	**126**	**Energy (mJ)**	**1.8**	**Ext. Voltage (V)**	**-1280**

Ferulic Acid $C_{10}H_{10}O_4$

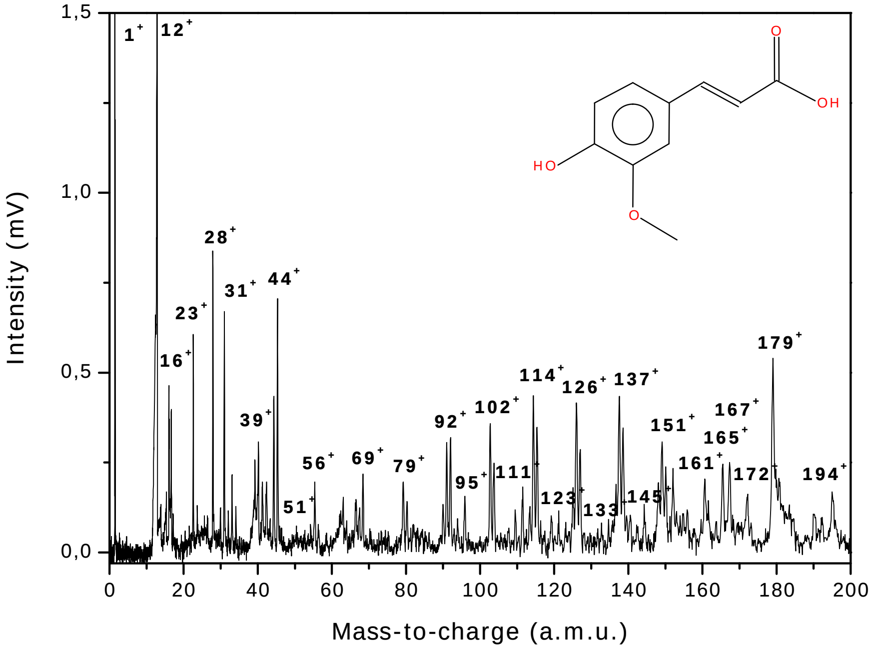

Name	Ferulic Acid	Wavelength (nm)	266	Pulse Width (ns)	2000
Formula	$C_{10}H_{10}O_4$	Pressure (mb)	$< 10^{-5}$	Pulse Delay (ns)	0
Mw	194	Energy (mJ)	1.5	Ext. Voltage (V)	-1290

4-Mononitrotoluene $C_7H_7NO_2$

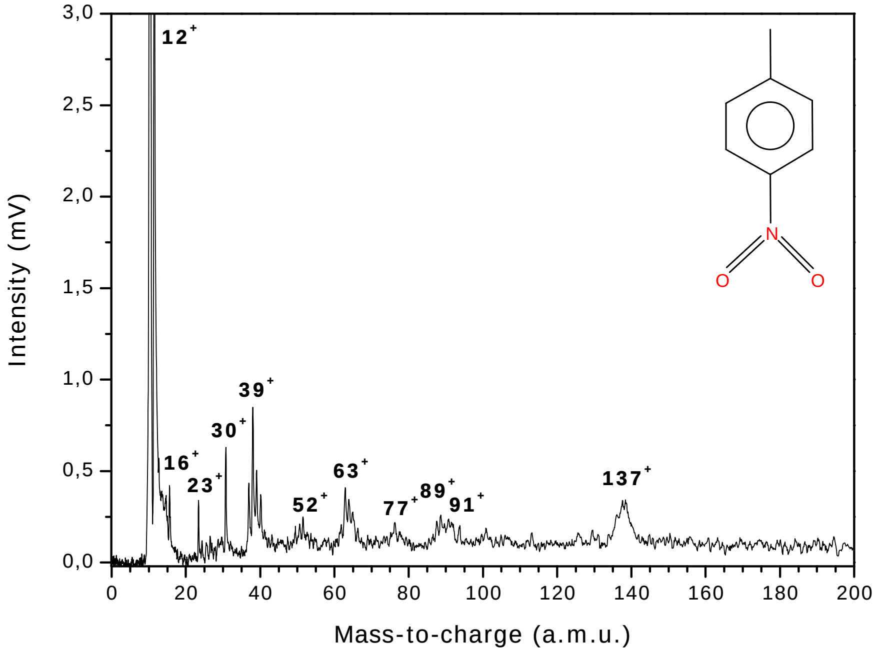

Name	4-MNT	Wavelength (nm)	266	Pulse Width (ns)	800
Formula	$C_7H_7NO_2$	Pressure (mb)	$1.0x10^{-5}$	Pulse Delay (ns)	200
Mw	137	Energy (mJ)	0.8	Ext. Voltage (V)	-1280

2,3-Dinitrotoluene $C_7H_6N_2O_4$

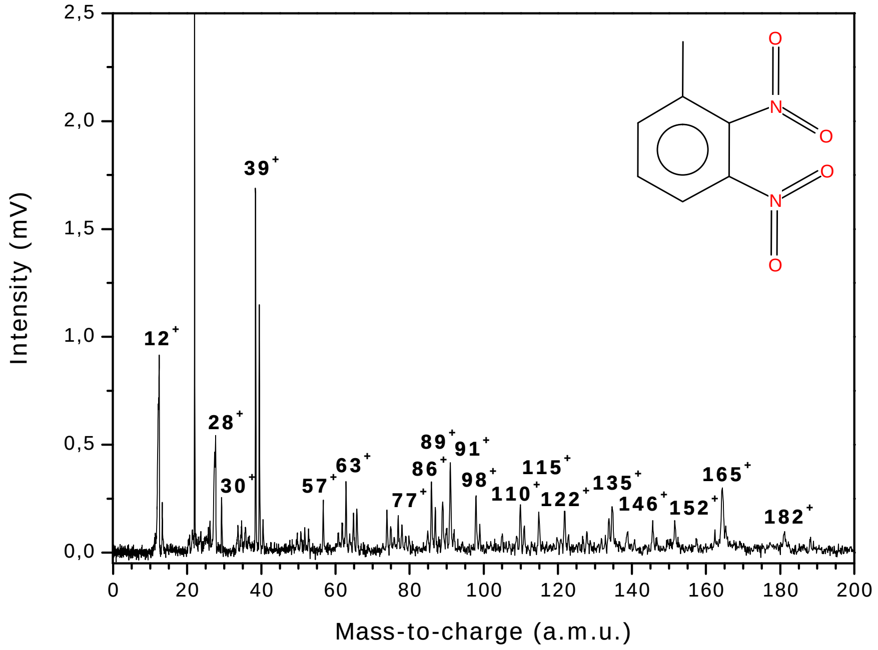

Name	**2,3-DNT**	**Wavelength (nm)**	**266**	**Pulse Width (ns)**	**800**
Formula	**$C_7H_6N_2O_4$**	**Pressure (mb)**	**$< 10^{-5}$**	**Pulse Delay (ns)**	**500**
Mw	**182**	**Energy (mJ)**	**0.7**	**Ext. Voltage (V)**	**-1280**

2,4,6-Trinitrotoluene $C_7H_5N_3O_6$

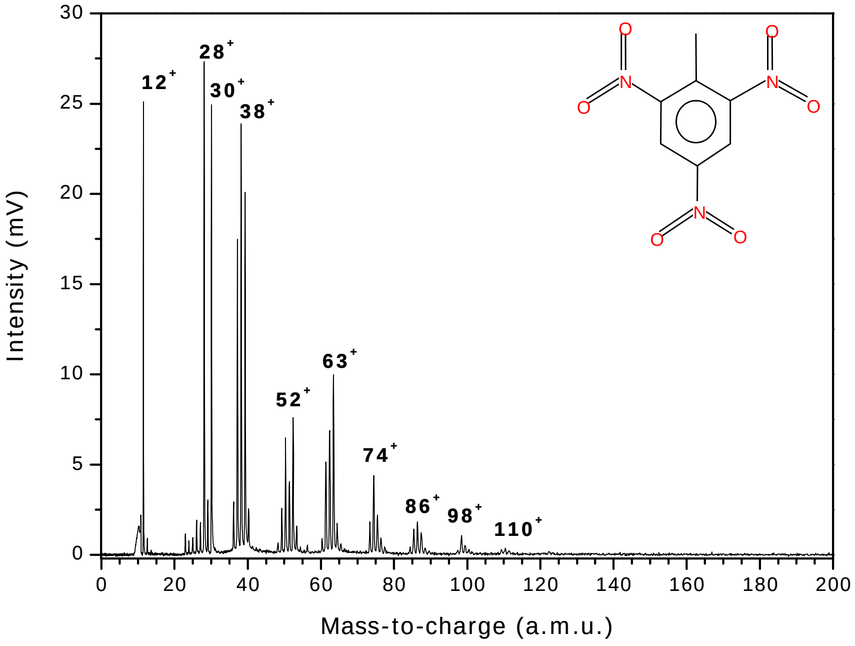

Name	2,4,6-TNT	Wavelength (nm)	213	Pulse Width (ns)	800
Formula	$C_7H_5N_3O_6$	Pressure (mb)	$< 10^{-5}$	Pulse Delay (ns)	0
Mw	227	Energy (mJ)	4.0	Ext. Voltage (V)	-1290

2,4,6-Trinitrotoluene $C_7H_5N_3O_6$

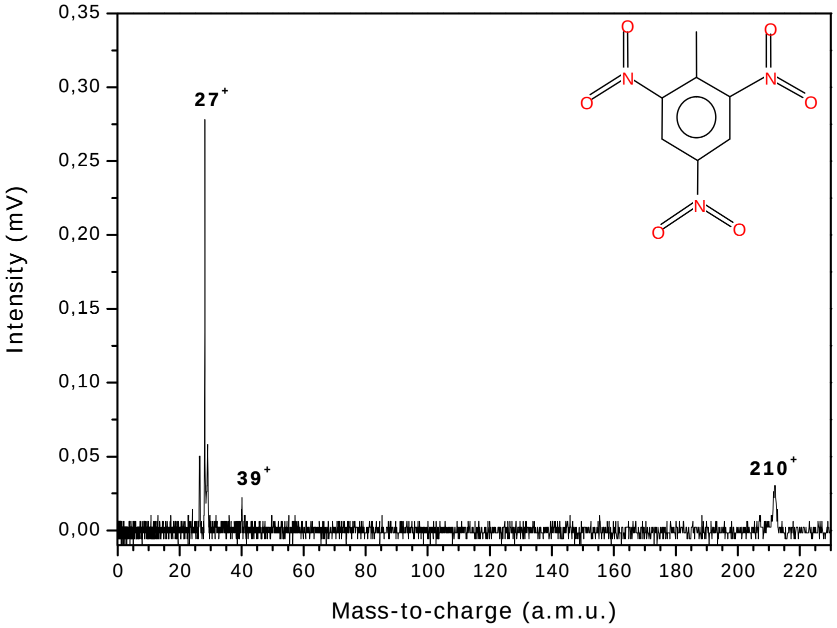

Name	**2,4,6-TNT**	**Wavelength (nm)**	**213**	**Pulse Width (ns)**	**800**
Formula	**$C_7H_5N_3O_6$**	**Pressure (mb)**	**< 10^{-5}**	**Pulse Delay (ns)**	**0**
Mw	**227**	**Energy (mJ)**	**0.5**	**Ext. Voltage (V)**	**-1290**

Chloratite

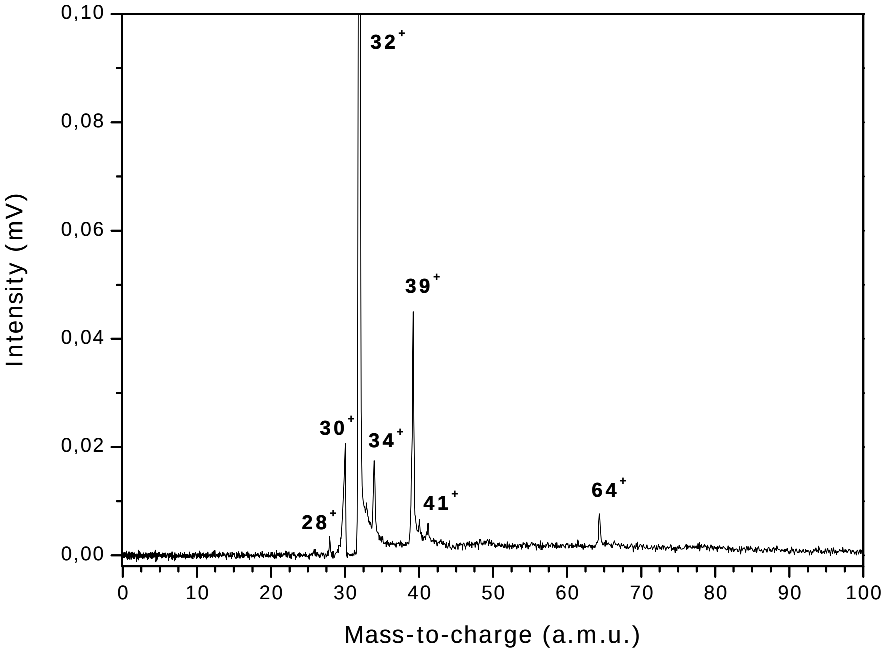

Name	**Chloratite**	**Wavelength (nm)**	**266**	**Pulse Width (ns)**	**800**
Formula	**S_2 / $KClO_3$ / $C_6H_{12}O_6$**	**Pressure (mb)**	**< 10^{-5}**	**Pulse Delay (ns)**	**0**
Mw	**-**	**Energy (mJ)**	**0.2**	**Ext. Voltage (V)**	**-1290**

Chloratite

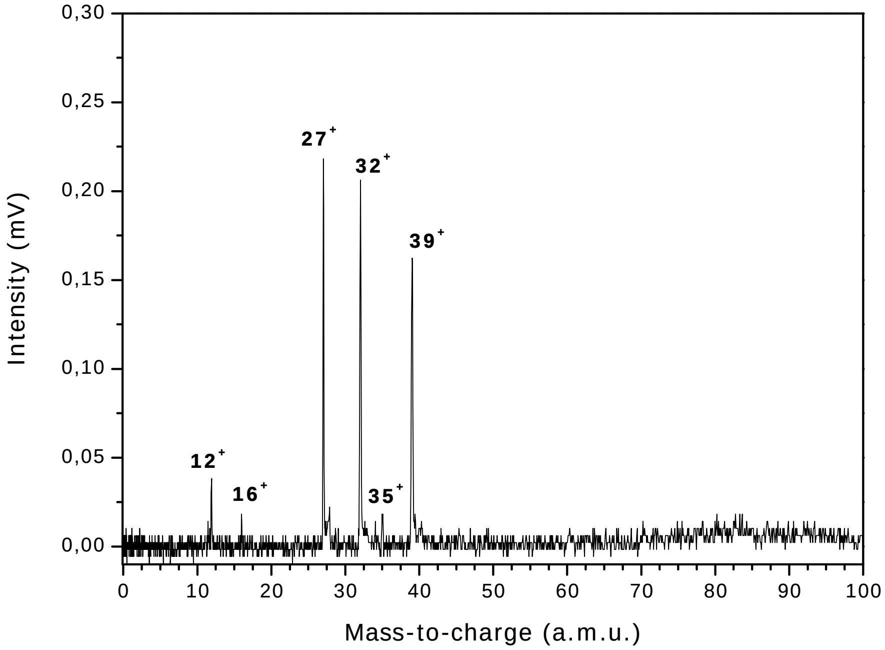

Name	**Chloratite**	**Wavelength (nm)**	**213**	**Pulse Width (ns)**	**400**
Formula	**S_2 / $KClO_3$ / $C_6H_{12}O_6$**	**Pressure (mb)**	**< 10^{-5}**	**Pulse Delay (ns)**	**0**
Mw	**-**	**Energy (mJ)**	**0.5**	**Ext. Voltage (V)**	**-1290**

Pentaerythritol tetranitrate $C_5H_8N_4O_{12}$

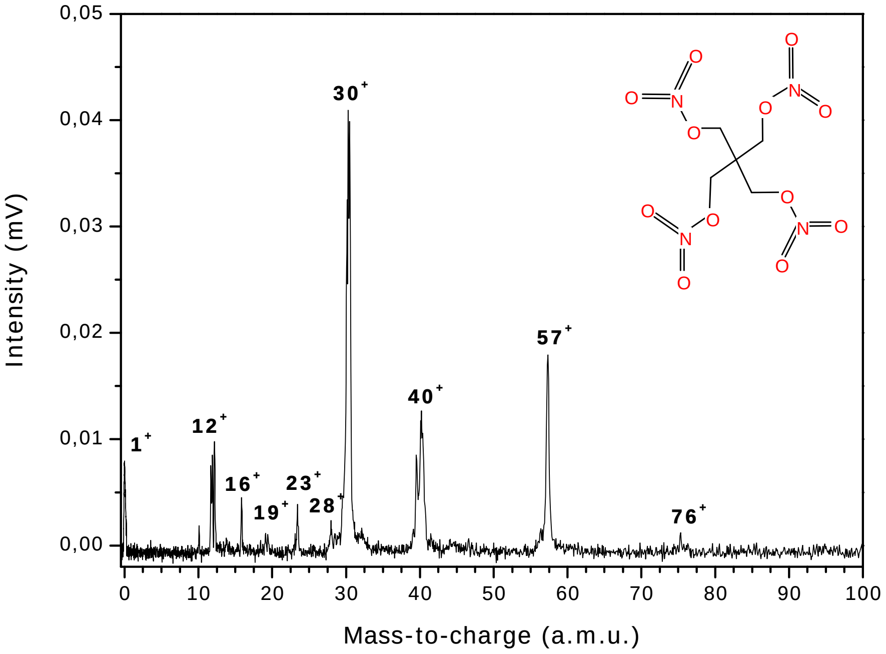

Name	PETN	Wavelength (nm)	266	Pulse Width (ns)	400
Formula	$C_5H_8N_4O_{12}$	Pressure (mb)	$< 10^{-5}$	Pulse Delay (ns)	1200
Mw	316	Energy (mJ)	0.54	Ext. Voltage (V)	-1290

Pentaerythritol tetranitrate $C_5H_8N_4O_{12}$

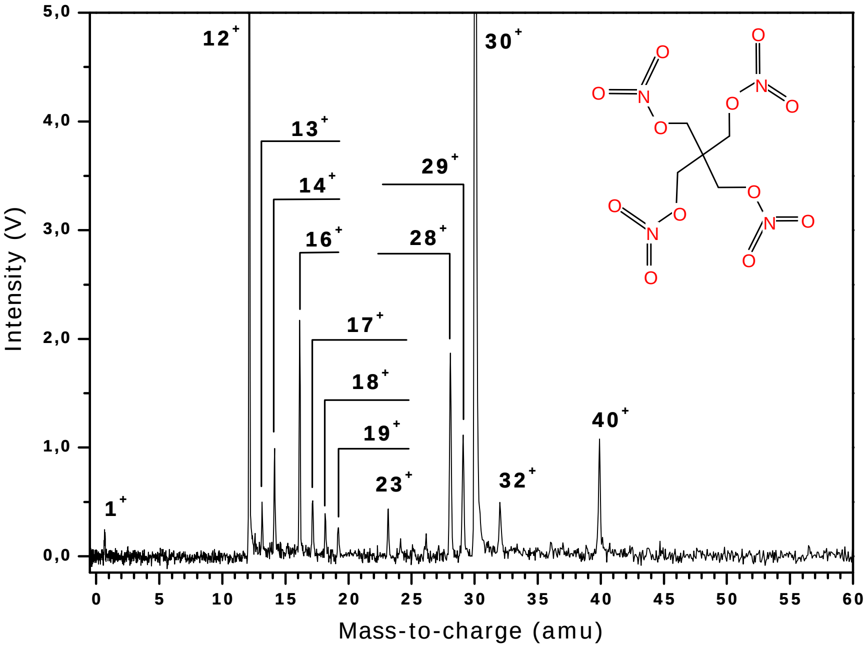

Name	PETN	Wavelength (nm)	266	Pulse Width (ns)	400
Formula	$C_5H_8N_4O_{12}$	Pressure (mb)	< 10^{-5}	Pulse Delay (ns)	0
Mw	316	Energy (mJ)	2.0	Ext. Voltage (V)	-1290

Sodium Citrate $C_6H_7O_7Na$

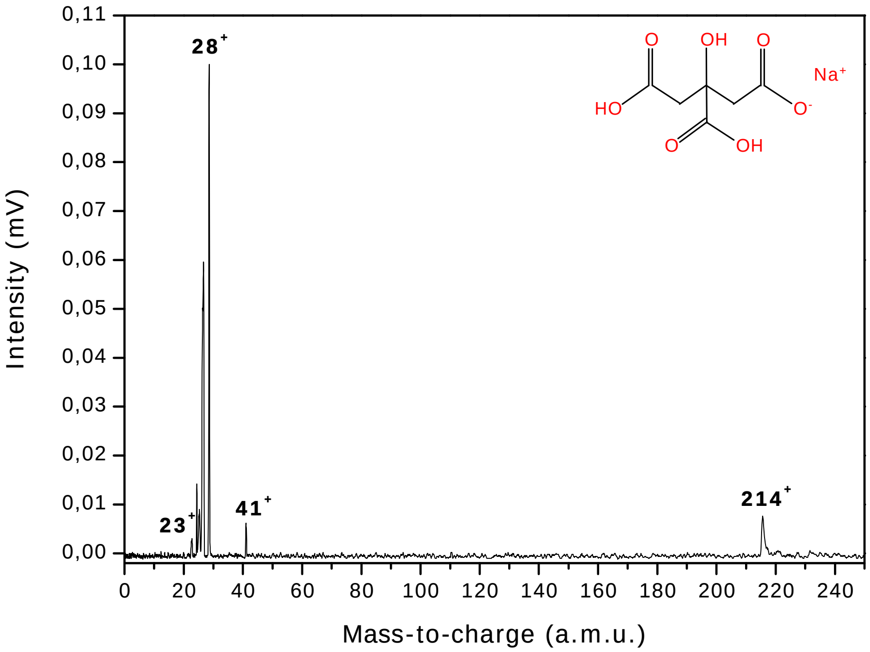

Name	**Monosodium citrate**	**Wavelength (nm)**	**266**	**Pulse Width (ns)**	**800**
Formula	**$C_6H_7O_7Na$**	**Pressure (mb)**	**$< 10^{-5}$**	**Pulse Delay (ns)**	**0**
Mw	**214**	**Energy (mJ)**	**0.2**	**Ext. Voltage (V)**	**-1280**

2,3Dimethyl, 3Dinitrobutane $C_6H_{12}N_2O_4$

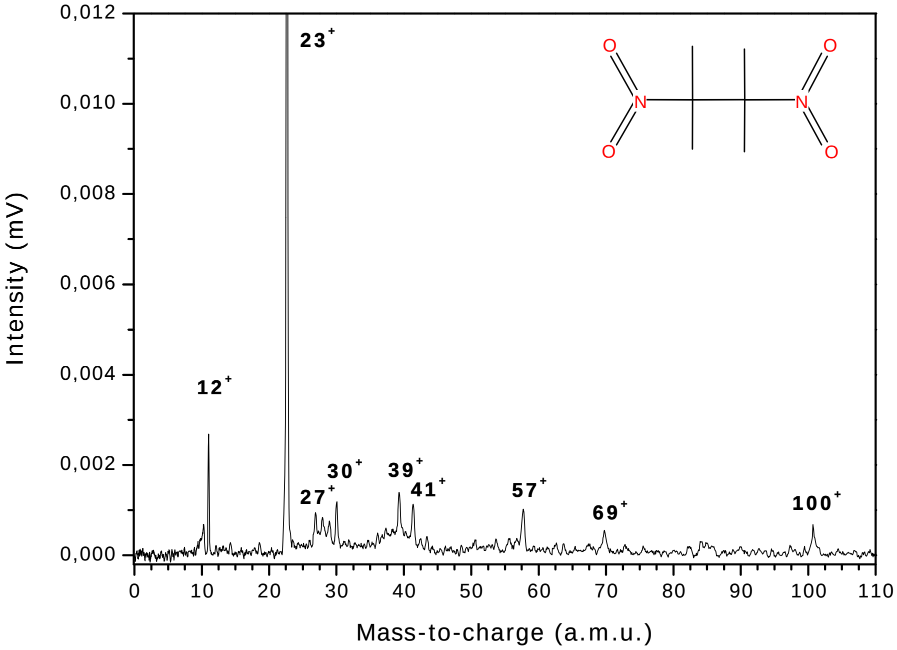

Name	**2,3-DM-2,3-DNB**	**Wavelength (nm)**	**266**	**Pulse Width (ns)**	**1200**
Formula	**$C_6H_{12}N_2O_4$**	**Pressure (mb)**	**$< 10^{-5}$**	**Pulse Delay (ns)**	**0**
Mw	**176**	**Energy (mJ)**	**0.6**	**Ext. Voltage (V)**	**-1290**

Hexamethyl Bencene $C_{12}H_{18}$

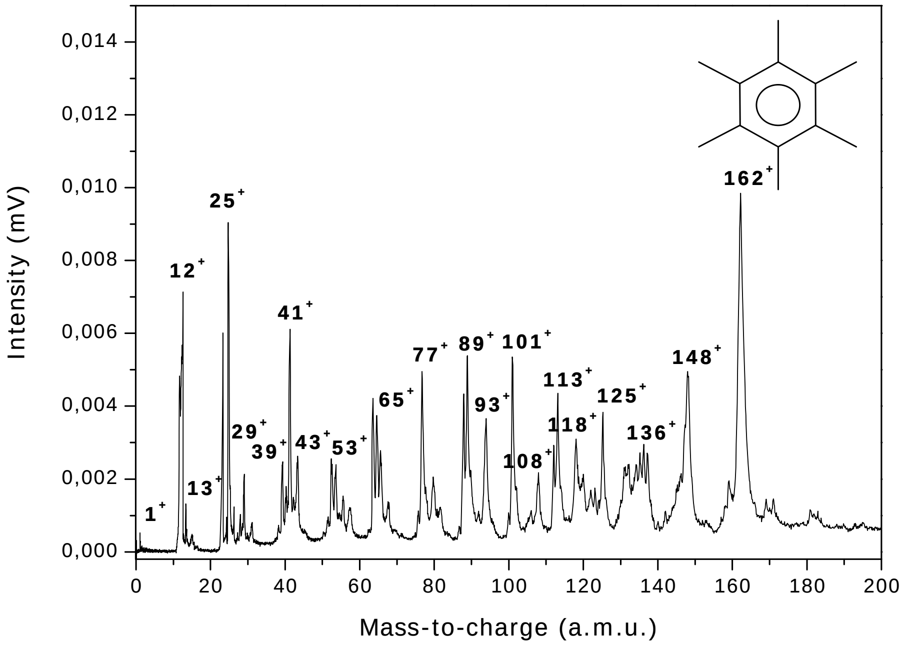

Name	**Hexamethyl bencene**	**Wavelength (nm)**	**266**	**Pulse Width (ns)**	**800**
Formula	**$C_{12}H_{18}$**	**Pressure (mb)**	**< 10^{-5}**	**Pulse Delay (ns)**	**0**
Mw	**162**	**Energy (mJ)**	**0.6**	**Ext. Voltage (V)**	**-1280**

Anthracene $C_{14}H_{10}$

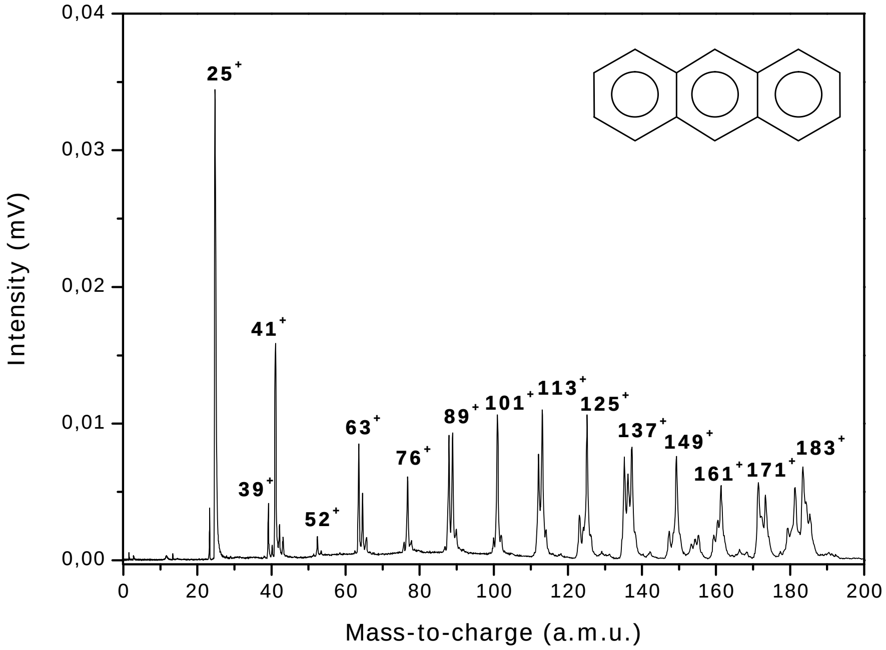

Name	Anthracene	Wavelength (nm)	266	Pulse Width (ns)	800
Formula	$C_{14}H_{10}$	Pressure (mb)	$< 10^{-5}$	Pulse Delay (ns)	0
Mw	178	Energy (mJ)	1.60	Ext. Voltage (V)	-1280

PolyStyrene $(C_8H_8)_n$

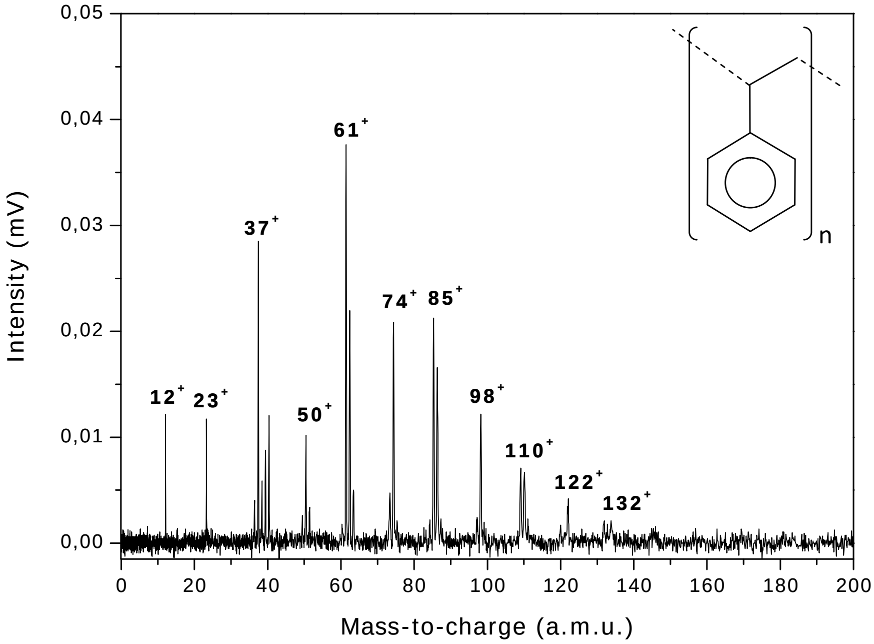

Name	Polystyrene	Wavelength (nm)	213	Pulse Width (ns)	800
Formula	$(C_8H_8)n$	Pressure (mb)	$< 10^{-6}$	Pulse Delay (ns)	0
Mw	104	Energy (mJ)	0.7	Ext. Voltage (V)	-1290

PolyStyrene $(C_8H_8)_n$

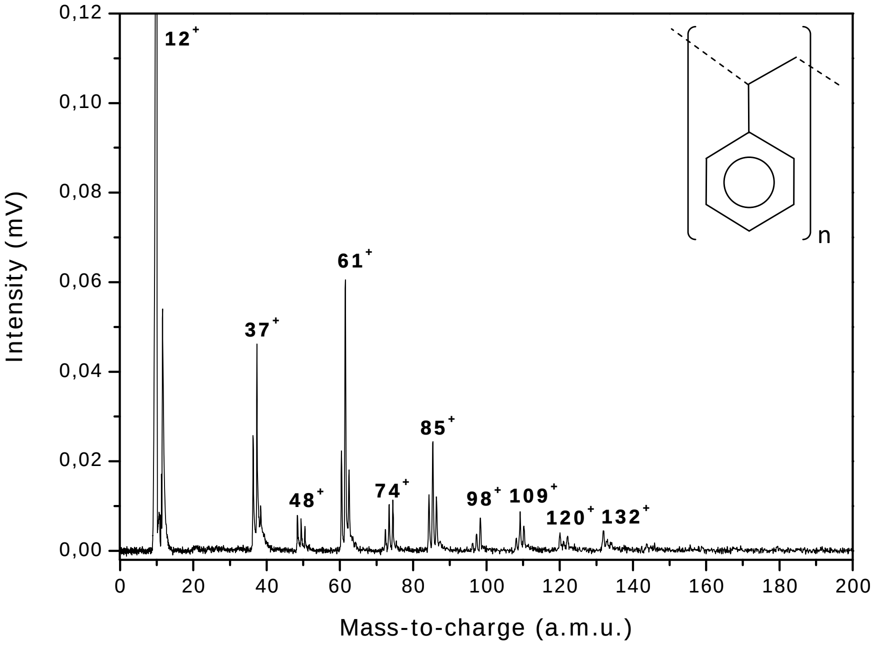

Name	Polystyrene	Wavelength (nm)	266	Pulse Width (ns)	800
Formula	$(C_8H_8)n$	Pressure (mb)	$< 10^{-6}$	Pulse Delay (ns)	0
Mw	104	Energy (mJ)	1.5	Ext. Voltage (V)	-1290

Teflon $(C_2F_2)n$

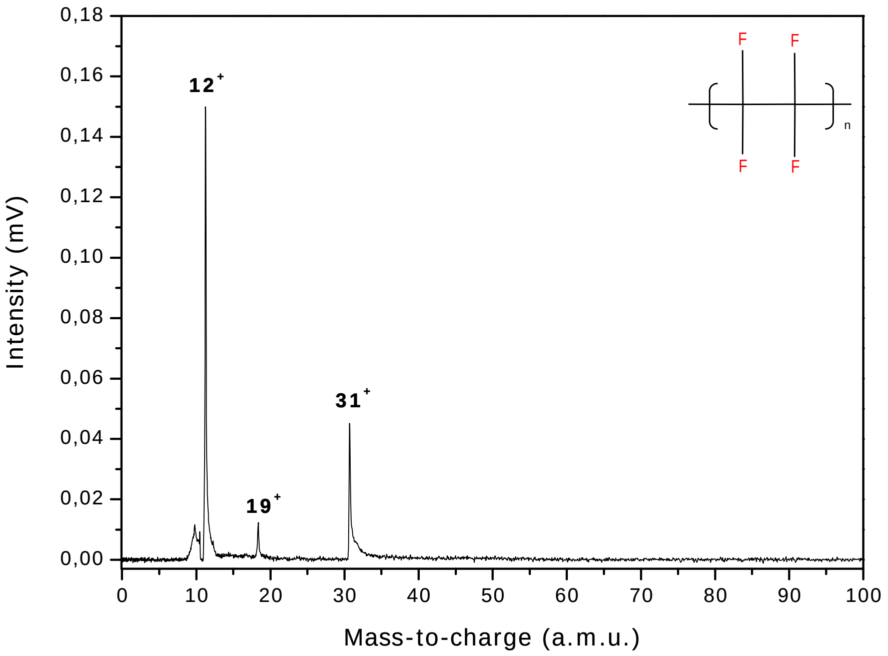

Name	**Teflon**	**Wavelength (nm)**	**266**	**Pulse Width (ns)**	**1000**
Formula	**$(C_2F_4)n$**	**Pressure (mb)**	**$< 10^{-6}$**	**Pulse Delay (ns)**	**0**
Mw	**100**	**Energy (mJ)**	**2.0**	**Ext. Voltage (V)**	**-1280**